

Final Report

EcoGlide
DSE Group 04

Technische Universiteit Delft



(This page was intentionally left blank.)

DELFT UNIVERSITY OF TECHNOLOGY

DESIGN SYNTHESIS EXERCISE

FINAL REPORT

SPRING 2019-2020

EcoGlide

Authors (group 04):

J. BERTHOLDT	4557794
J. BOURGOIS	4667565
G. DEN BUTTER	4659457
A. CHATTERJEE	4662881
V. CONINGS	4664345
S. MCGINLEY	4670957
B. ODINOT	4497368
R. SMITS	4653319
D. TÓTH	4460375
D. VAN DER WERFF	4662512
M. VERKAMMEN	4650468

Supervisor:

Prof. C.A. DRANSFELD

Coaches:

V. DHANISSETY
J. SUN

June 30, 2020



Executive Overview

Overview: Mission Overview

The use case from the Dutch military was at the centre of the EcoGlide project. It starts with the need of Dutch army medics to receive a near-daily supply of blood to their field hospitals. These field hospitals need a stock of approximately 6 litres, have limited capability of storing and cooling the blood and are located some 100 to 150 kilometres from main hospitals. The reliability of the transportation method should be insensitive to the environment of the trip to the field hospitals, which might even be an active combat zone. The transportation method should also be semi-agile as the location of field hospitals is dynamic. The EcoGlide project aims to provide a solution to these needs.

Overview: Project vision

The EcoGlide project was initiated by our principal tutor Prof. C.A. Dransfeld, who gave the first set of requirements for the design. The underlying assignment has been captured in the mission need statement: *Deliver small cargo to areas with limited on-ground accessibility with high precision, large deployment capacity and constant mission readiness, while minimising life-cycle costing.*

The team of 11 aerospace engineering bachelor students also decided to involve third party stakeholders. From all the stakeholders, the use case proposed by the Dutch military was chosen, resulting in the project objective statement: *Design a biodegradable glider, by 11 students in 10 weeks, that autonomously delivers blood to military field hospitals on a near-daily basis.*

To design a product that would successfully complete the mission, a persona analysis was made. This fit in with our design thinking philosophy, where the input of potential users is analysed to generate requirements. Finally, the EcoGlide team put focus on sustainability by adopting the lean management philosophy.

Overview: Design overview

The EcoGlide solution to the proposed mission is a single-use glider as shown in Figure 1. The glider will be launched using a tethered helium balloon, which allows for multiple launches without having to be lowered. The glider has a wingspan of nearly 5 metres and is almost exclusively produced using biodegradable materials. Despite its single use nature, the glider is high performance with a wind-corrected range of 125 kilometres and a cruise speed of 100 [km/h]. This performance is made possible by clever structural solutions, such as the egg-carton inspires ribs. It can carry a total payload of 11.6 [kg], or 6 litres of blood using our in-house developed cooling containers. After its flight, the payload compartment and electronics can be removed and reused for subsequent missions, while the structure of the glider is left to biodegrade.

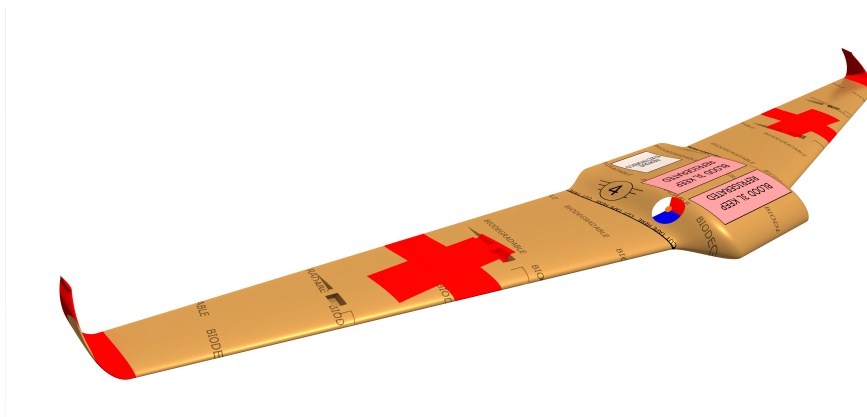


Figure 1: EcoGlide glider

Overview: Design outline

The starting point for the detailed design presented in this report comes from previous design phases. These design phases will be summarised to show the origin of the current design. The start was a requirement specification that followed from requirement discovery, based on user requirements, functional analysis, market study, regulations, risk

analysis and sustainability analysis. Based on the requirements a concept exploration was performed for deployment methods and glider configurations.

A total of 10 deployment methods were weighed against each other in a qualitative trade-off. Based on this trade-off, the multi use tethered helium balloon was selected as the concept that would be further designed in this report.

Initially, there were also 10 concepts for possible glider configurations. After a first concept selection and a functional forecast, 4 concepts remained. Those concepts were the high wing, low wing, blended wing-body and Prandtl wing configuration. These configuration concepts were then rated against each other on their potential in a quantitative trade-off. Based on the scores of this trade-off, the blended wing-body configuration was selected as the best concept. A sensitivity analysis of both trade-offs proved that the chosen concepts for deployment and configuration were the best for almost all combinations of weights and scores. This proved that the chosen concepts were a robust entry point for the next design phase.

Overview: Subsystems

This section provides an overview of the design of the different subsystems integrated in the EcoGlide system.

Aerodynamics & Performance

For the aerodynamic design of the glider, an innovative approach was taken. Since the selected configuration concept was a tailless blended wing-body, design challenges to create a stable design became apparent. Rather than creating a stable configuration with the wing planform alone, the body section of the glider was shaped such that it provided a large stabilising contribution. This stabilising body was created by shaping a new airfoil capable of generating a lifting force in front and a down-force behind the centre of gravity, resulting in a stabilising pitch up moment. This meant that the wings did not have to be swept backwards as much for stability, favouring the lifting capabilities of the wing. This however also meant that almost no overall lift was generated by the body itself. The wings were therefore responsible for carrying the weight of the glider using the HS 522 airfoil. This reflex airfoil was found to favour the stability characteristics of the glider.

This resulted in a aerodynamic design that cruises at a trim angle of 4.4 [*deg*] with a lift coefficient of 0.33 creating 250 [*N*] of lift. Hence, it is capable of carrying the weight of the glider. Additionally, at this trim condition, the design provides a glide ratio of 31.4. With the inclusion of winglets to the wing tips of the glider, this means that, when deployed from 5 [*km*] altitude, a range of 125 [*km*] can be achieved during 80% of the year at the two proposed mission locations, Timbuktu and Kabul.

Structures & Materials

With the requirements in mind a simple and biodegradable structural buildup was chosen. Several structural configurations were taken into account. In order to keep the structure as simple as possible it was determined that the spar shall take a majority of the load and the skin will provide a aerodynamic shape. A configurations with 2 spars was chosen due to its capability to provide torsional stiffness.

The spar will be made out of plywood and the skin out of paper pulp, to increase the surface quality and to waterproof the wing, a PLA film will be wrapped around the final assembly. The materials were chosen because of their low cost, bio biodegradability and their widely availability.

Finally the structure was modelled to assure its structural integrity. A load distribution along the quarter chord line with a load case of 3.8 was chosen to deduce stresses and deformations. The bending was assumed to be purely taken by the spars, reaching stresses up to 50% of the ultimate strength. The maximum wing deflection was determined to be 28 [*cm*]. Shear forces and torque were assumed to be carried by the spars and the upper and lower skin connecting the two. The shear stresses reaches 11% of the skins maximum shear strength and 6% of the maximum shear strength of the spar. The wing twist was determined to be 3.3 degrees. After a buckling analysis it 2 ribs were added.

Guidance, Navigation Control

Guidance, Navigation and Control (GNC) consist of the determination of the glider's current state, the determination of its desired state and the use of its control surfaces to change its state. Therefore, the GNC preliminary design presented in this report is mainly focused on the design of the control surfaces as well as on the choice of flight controller and sensors.

Before being able to size the control surfaces, one must first define the full mission, that is the deployment, the cruise and the landing. Deployment consists of a dive before a pull-up manoeuvre is executed, while staying at a safe distance from the balloon tether. Then, during cruise, the glider follows point-to-point navigation and is able to detect thermals and sinks, to recover some altitude if needed. The landing approach itself is a stall landing from a height of 20 [*m*], which greatly reduces the landing area required. If the glider would arrive too high close to the landing area, it would perform a corkscrew manoeuvre to descent without going too far away from the landing zone.

With this defined, one can now size the control surfaces. It was decided to use only elevons, two control surfaces combining the effect of ailerons and elevators, for the full flight. Analytical methods found in literature are used for

the aileron's effect while statistical data from similar UAV and human piloted airplanes is used for the elevator effect. In the end, the elevons are found to span from 70% to 90% of the half-wingspan. Their chord is 45% of the local wing chord over the whole elevon span. This assumes a maximum deflection of 35° up and down.

With the surfaces sized, the actuation mechanism can be sized. For this, the *ANNIMOS 25kg RC Digital Servo* is chosen as the actuator. The mechanism itself consists of a biodegradable torque rod made out of *Hachiku* bamboo, connected to the servo via a control rod.

In terms of flight controller and sensors required, it was soon decided that open source and common flight controls and software would be beneficial for EcoGlide for time and cost saving purposes. A number of flight controllers were looked at and the Pixhawk 4 Mini with its GPS receiver was chosen. It is a very small, lightweight and quite renowned flight controller with the open source Px4 software which has a large community base.

Payload

The payload compartment is responsible for protecting the blood during the mission. It consists of two identical payload boxes. The two main threats to protect against are temperatures and the blood bags bursting.

In order to keep the blood in its safe temperature range, the boxes are insulated with an expanded cork layer and phase change elements are added as a thermal buffer. To protect the bags against bursting, a cork filler is used to keep the bags under constant pressure. To ensure the boxes can carry their own weight, it is reinforced with a plywood outer layer.

The boxes are sized and optimised for empty weight using a thermal analysis tool. This optimisation is done to increase the sustainability of the box. An attempt is made to verify and validate the thermal analysis model and the results are promising. However, a prototype should be built to fully validate the box. Through a sensitivity analysis the design is found to be robust.

The boxes and phase change elements are fully biodegradable, but should be reused when possible.

Electrical Power Subsystem

The Electrical Power Subsystem (EPS) is sized such that the electrical power source can provide enough energy during the whole mission to satisfy the electronics' needs. The mission is defined for the EPS as 1.75 [h] of flight time and 1.75 hours of non-flight time, including the loading, hoisting time and the time to find the glider after landing. The electronics' power needs is found based on manufacturers' data or UAV online community forums' information.

It was found that a 2700 [mAh] battery at a nominal voltage of 7.4 [V] in conjunction with a 5.5 [V] voltage regulator is sufficient for the flight. Since it is preferred to use off-the-shelf components, it was found that the commercially available *ZIPPY Compact 2700mAh 2S 25C Lipo Pack* battery and *Jeti Voltage Regulator SBEC 5-8V/12A* would be suitable for EcoGlide's mission

This leads to a wiring such as the one shown in Figure 2, where the battery's voltage is reduced by the voltage regulator. This then goes to the flight controller and from there also to the remaining electronics.

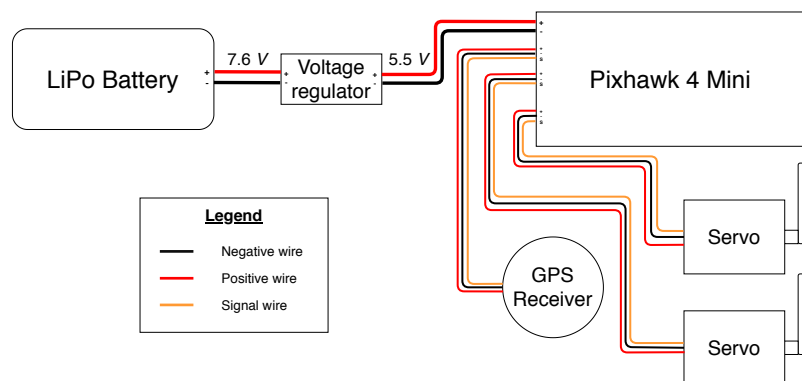


Figure 2: EPS Electric Diagram

Overview: Deployment, Logistics & Operation

This section will provide an overview of the deployment, logistic and operational aspect of the EcoGlide system.

Deployment

No tethered balloon that meets EcoGlide specifications is available commercially, so one needs to be designed specifically for the deployment of EcoGlide gliders. The payload of this tethered balloon consists of a radiosonde (Vaisala RS41-SG), communication system, as well as the "flying" segment of hoisting and launch mechanism, responsible for lifting the glider to the desired altitude, then release it in a safe manner. It consists of a hoisting rope (Tech-12 aramid fibre rope), three three pulleys, and a spacer beam, to keep them apart. The later is 5.8 [m] long rectangular

hollow 7075 aluminium tube, with even width and height of 5 [cm], and thickness of 1 [cm]. Ground segment of the hoisting system consists of two reels and a driving motor. The total mass of the balloon payload was limited to 180 [kg]. Then the dimensions of a US Navy C-type balloon were established such that is capable of lifting this payload, in winds as high as 21.6 [m/s], and maintain its maximum altitude of 500 [m] for 140 hours. The balloon of this design is 37.6[m] long, has a maximum dimension of 11.8[m], and a volume of 2760.8[m³]. The flight time was calculated by assuming a permeability of $6.599 \times 10^{-5} \left[\frac{m^3}{hr \times m^2} \right]$, based on the AB-20 tethered balloon. The sustainability analysis of the deployment system found that the air winch (Ingersoll Rand Infinity Guidline) and the air compressor required to power it (Ingersoll Rand Sierra SL132) are estimated to have a yearly energy consumption of 28.720 [MWh], and the balloon has a yearly helium consumption of 16374.4 [m³]. The sensitivity analysis found that the balloon design is only marginally sensitive to changes in payload mass, however changes in maximum wind speed greatly affects its performance. When the tethered balloon sizing tool was applied to reference tethered balloons, it was found to be inaccurate, and so its validation was deemed inconclusive.

Logistics

The two most critical links of the logistics chain are the transport of the gliders from the production plants in the Netherlands and the transport of the reusable components back from the field to the main hospital.

For the first link, driving factors are that the whole EcoGlide system has to fit in 20ft shipping containers and that transport efficiency should be increased even if that comes at the cost of having to assemble the gliders on-site. These requirements on logistics mean that the glider has to be shipped as a kit, as this is the most efficient way of fitting them in the limited volume of a container. Optimising the assembly for efficient transport resulted in the capability of fitting up to 64 gliders in a single container.

For the second link the key factor is that the land connection between the two hospitals is only sporadically available and does not allow for the transport of large items. This means that the reusing of components had to be limited to the electronics and PCM elements. These are transported back to the main hospital on the return leg of occasional supply missions to the field hospital, when the situation allows for this.

Operations

In order to comply with the operating constraints of the payload box, the payload loading, glider hoisting, and payload recovering times are limited to 15, 30, and 30 minutes respectively.

A mission operations diagram was created for the chronological presentation of actions in a mission cycle. The interactions of personas with the EcoGlide system, and sub-system level communication are also shown in this diagram.

The environmental conditions for long term storage were limited to a maximum temperature of 10 [°C] and relative humidity of 88% for the plywood spars, and 20 [°C] and 45% relative humidity for the paper pulp skin. The maximum time a glider may spend at the main hospital in inventory is 4 months, during which all components must be stored such that they are protected from the weather, and are kept as cold as possible.

Overview: Production & Assembly

Production and assembly are strongly influenced by the logistical need to optimise the glider for transport. The glider components and sub-assemblies will be manufactured at the EcoGlide plant or by external suppliers in the Netherlands. These components will then be shipped to the deployment location, where the gliders can be assembled by the customer.

The paper pulp skin panels will be produced by a packaging manufacturer, the PLA film and the electronic components are commercially available items and will be purchased from the manufacturers. The spars will be manufactured in-house as will the payload box components. The electronics compartment will be assembled by integrating and wiring the modules in the compartment.

The assembly process involves five main steps. The spars and lower fuselage section are joined to form the base of the assembly. This is followed by the joining of the wing panels, which are then added to the existing structure. The payload boxes and their content is installed and finally the addition of the top fuselage section completes the assembly.

Overview: Reliability, Availability, Maintainability and Safety

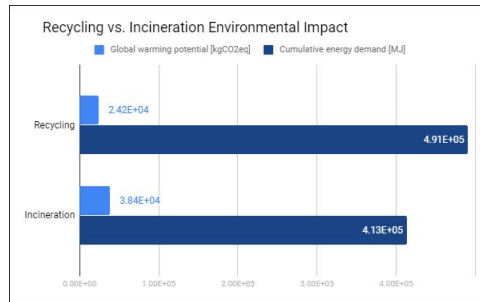
To assess the performance of the EcoGlide system, a RAMS analysis was done. It was found that the system was very reliable, as the glider is designed to perform its mission 80% of the time. This takes the weather conditions into account, so even with headwind the glider will still succeed most of the time. The system is also very available: the gliders are shipped in containers, where 64 gliders can be stored. This means that the client will always have a large number of gliders at their disposal. The maintainability of the system is limited, considering that the gliders are single-use. The deployment system however does need some maintaining, such as the occasional helium refill. Finally, the system is also considered safe, as its meant for medical aid and lacks any means to actively harm people.

Overview: Sustainability

Life-Cycle Assessment

The main goal of addressing sustainability in the final stages of the design period was to quantify the environmental impact of the glider. The starting point was to make a conclusion on what the optimal method of disposal for the glider would be. It should be noted that, in the case where the gliders are used in conflict areas, the likely method of disposal will simply be degradation as the area of operations may not have proper existing waste disposal infrastructure but the comparison pertains to an idealistic situation where recycling and incineration are the more sustainable alternatives. The results of the LCA for both of the scenarios are shown in Figure 3, and are presented in terms of the carbon dioxide emission shown using the global warming potential (GWP) and the cumulative energy demand (CED), and are shown for a 1000 gliders produced in a single year.

Figure 3: End-of-life scenario impact comparison



Based on the results, recycling was ultimately ruled as the more sustainable method due to following reasons: first and foremost, as stated, the GWP is lower for recycling, more specifically 1.6 times lower. More importantly, the impact from recycling can be reduced much further and this is because the LCA was modelled with only 30% of recycled material being redirected to the manufacturing facilities. Cellulose based materials like wood and paper result in up to 90% of recovered material from recycling and hence the potential to reduce the impact is quite a lot which led to the conclusion that recycling is the preferred end-of-life scenario.

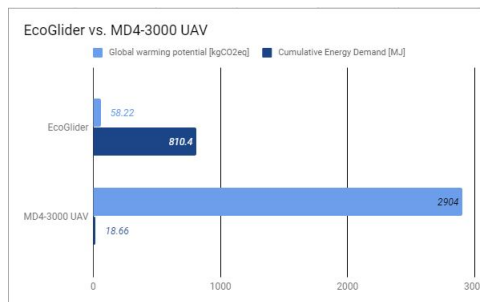
The next step was to conduct the LCA of the manufacturing process. The main idea behind conducting a LCA for the manufacturing process was to compare the environmental impact of the glider to that of a reusable, commercially used drone. Since the glider is primarily manufactured out of paper pulp and plywood, these were the two materials for which the LCA was done. The results are shown in Table 1.

Table 1: Aggregate GWP and CED: EcoGlide

Global warming potential (GWP) [kgCO2eq]	Cumulative energy demand (CED) [MJ]
5.822E+4	8.104E+5

As stated, these results were then compared to the impact of a conventional drone, in this case the MD4-3000 drone. The results of course had to be first normalised in terms of the payload capability and the range as the glider and the drone have different characteristics. The results of the comparison are shown in Figure 4.

Figure 4: Comparison of the impact of the MD4-3000 drone against the EcoGlide glider



Based on the comparison, it was concluded that while the global warming impact was of an acceptable magnitude, the energy consumption was not. Although ways of reducing this have not been looked into in detail, a definitive way of reducing the consumption would be to increase the amount of recycled content used in manufacturing. Additionally, the most energy intensive processes, i.e. the pulping step itself followed by the bleaching process, were identified. Of course pulping is an essential step in the process and so it cannot be eliminated but bleaching can potentially be

removed. Although it hasn't been extensively looked into, bleaching only serves to preserve the color of paper over a longer period of time, and hence not an essential step in the context of the mission. The preliminary estimate of the energy saved or reduced by the elimination of bleaching is approximately 14400[MJ]. While this needs to be investigated further, it is a good start towards designing an even more sustainable product.

Life-Cycle Costing

In addition to conducting a life-cycle assessment of the glider, a preliminary cost estimate of manufacturing the glider was also done. This included the cost of obtaining raw materials and processing the materials such that they can be used in manufacturing and manufacturing the glider parts, in addition to accounting for transport of the materials to the manufacturing facility. The costs were quantified based on the labour hours and the amount of electricity used. In the case of obtaining the raw materials and processing them, the estimated cost is €47.63 . The cost associated with the transportation of the materials is approximately €0.08 per glider, based on the fact that up to 20,000 [kg]. of raw material may be transported at a single time. Finally, the labour costs associated with manufacturing the parts of the glider are approximately €240 based on a total manufacturing time of 12 hours for a single glider, with an hourly wage of €20. This resulted in a preliminary cost estimate of €309 for the finished glider, in a disassembled form.

Overview: Market Analysis

The majority of the price of the EcoGlide system comes from the price of the deployment system. The gliders themselves are relatively inexpensive. A possible business model that the EcoGlide system could use to take advantage of this would be the razor blade business model, where the more expensive product, the deployment system, is sold at a loss while the dependent product, the individual gliders are sold at a profit. It was also found that the EcoGlide system could be easily adapted to fulfil other markets such as humanitarian aid. For the military mission use case the team decided to not settle on a final livery as this can be easily adapted to where the glider is being used by printing on the PLA film. Finally the EcoGlide system was found to be competitive in the market with drawbacks such as the large initial investment required for the deployment system.

Overview: Future Planning

The final step in the design cycle is to create a future planning of the EcoGlide project. This is to ensure it can be continued after the Design Synthesis Exercise. The first step in the continuation of the project would be to create a functional prototype together with a simplified glider code for the onboard systems. This is to validate the design of the different subsystems separately as well as their integration. After this, the design presented in this report will be revisited and updated where necessary. Then the glider code will be fully worked out such that a test mission can be performed. When this is successful, the required certifications can be obtained and manufacturing will be set-up. During this period, other customers than the army can be contacted to potentially increase profitability of the EcoGlide product.

Contents

Executive Overview	ii	7 Guidance, Navigation & Control	50
Nomenclature	xi	7.1 Functional Analysis	50
Introduction	xii	7.2 Design Approach	56
1 Mission Overview	1	7.3 GNC Software and Hardware	60
1.1 Mission Description	1	7.4 Design Overview	64
1.2 Mission Flow Diagram	1	7.5 Verification & Validation	65
2 Project Vision	3	7.6 Risk Assessment	66
2.1 History & Future	3	7.7 Sustainability Analysis	67
2.2 The EcoGlide Project	3	8 Payload Box	68
2.3 Persona Analysis	4	8.1 Functions and requirements	68
2.4 Design Thinking Philosophy	4	8.2 Design Approach	69
2.5 Sustainable Development Strategy	5	8.3 Design Overview	77
3 Design Overview	6	8.4 Materials	77
3.1 Final Concept	6	8.5 Thermal analysis model.	78
3.2 Layout	7	8.6 Structural Analysis Model	81
3.3 Operational Envelope	8	8.7 Verification & Validation	81
3.4 EcoGlide Specifications	9	8.8 Sensitivity Analysis	83
3.5 Product journey map	9	8.9 Risk Assessment	84
3.6 Budget Breakdown	11	8.10 Sustainability Analysis	84
4 Design Outline	13	9 Electrical Power Subsystem	85
4.1 User Requirements	13	9.1 Functional Analysis	85
4.2 Concept Selection.	14	9.2 Design Approach	85
4.3 Risk Assessment	15	9.3 Power source sizing	85
4.4 Functional Analysis	15	9.4 Electric system	87
5 Aerodynamics & Performance	19	9.5 Design Overview	87
5.1 Functional Analysis	19	9.6 Verification & Validation	88
5.2 Design Approach	20	9.7 Risk Assessment	88
5.3 Aerodynamic models	21	9.8 Sustainability Analysis	88
5.4 Wing Planform Design	24	10 Deployment	89
5.5 Airfoil Selection	25	10.1 Functional Analysis and Requirements	89
5.6 Integrated Wingbody Design	27	10.2 Balloon System Description and Design Approach	90
5.7 Stability Analysis	28	10.3 Description of Balloon Payload	92
5.8 Design Overview	29	10.4 Sizing of the hoisting system	93
5.9 Performance Analysis	30	10.5 Balloon sizing for payload.	94
5.10 Verification & Validation	34	10.6 Balloon sizing for flight time	95
5.11 Sensitivity Analysis	37	10.7 Sustainability Analysis	96
5.12 Risk Assessment	38	10.8 Sensitivity Analysis	97
6 Structures & Materials	39	10.9 Recommendations	97
6.1 Functional Analysis	39	10.10 Validation	98
6.2 Design Approach	39	10.11 Risk Assessment	98
6.3 Design Subsystem.	40	11 Production and Assembly	100
6.4 Design Overview	45	11.1 Functional Analysis	100
6.5 Verification & Validation	45	11.2 Design Approach	100
6.6 Sensitivity Analysis	47	11.3 Production Plan and Methods	101
6.7 Risk Assessment	48	11.4 Proof of Concept and Future Steps	104
6.8 Sustainability Analysis	49	11.5 Risk Assessment	104
		11.6 Sustainability Analysis	105

12 Logistics	106
12.1 Functions and Requirements	106
12.2 Logistics Overview	106
12.3 Detailed Logistical Aspects	108
12.4 Risk Assessment	108
12.5 Sustainability Analysis	109
13 Operations	110
13.1 Functions and Requirements	110
13.2 Design Approach	110
13.3 Design Overview	110
13.4 Procedures	111
14 Life-Cycle Assessment	114
14.1 End-of-Life Analysis.	114
14.2 Life-Cycle Assessment: Manufacturing . . .	117
14.3 Life-Cycle Costing.	121
15 Reliability, Availability, Maintainability & Safety	123
16 Market Analysis	125
16.1 Cost Estimation and Business Model	125
16.2 Adaptability.	126
16.3 Reflection on Aesthetics.	127
16.4 Market Competitiveness	128
17 Future Planning	129
17.1 Project Design & Development Logic Dia- gram	129
17.2 Post-DSE Gantt chart	129
Conclusion & Recommendations	132
Bibliography	134

Nomenclature

List of Abbreviations

AoA	Angle of Attack
BEC	Battery Elimination Circuit
CED	Cumulative Energy Demand
DOD	Depth of Discharge of the battery
EKF	Extended Kalman Filter
FS	Factor of Safety
GNC	Guidance, navigation and control
GPS	Global Positioning System
GR	Glide ratio
GWP	Global Warming Potential
ISA	International Standard Atmosphere
KF	Kalman Filter
MAC	Mean aerodynamic chord
MOTW	Maximum Take-off Weight
PCM	Phase Change Material
PLA	Poly Lactic Acid
SBEC	Smart Battery Elimination Circuit
SM	Stability margin
TBD	To Be Determined
UV	Ultra Violet

List of Symbols

α	Angle of attack
χ	Point thermal transmittance
δ	Wing deflection
ϵ	emissivity
η_{BAT}	Efficiency of the battery
Γ	Circulation
Λ	Sweep angle
λ	Taper ratio
λ	Thermal conductivity
μ	Poisson ratio
ω	distributed load
ψ	Linear thermal transmittance

ρ	Density
σ	Boltzmann constant
σ	Tensile stress
σ_{cr}	Yield stress
θ	Wing twist
A	Crosssectional area
A	Wall area
AR	Aspect ratio
b	Wing span
C	Boundary condition parameter
c	Wing chord
C_D	Drag coefficient
C_L	Lift coefficient
C_M	Pitching moment coefficient
C_{BAT}	Capacity of the battery
C_{D_0}	Zero lift drag coefficient
C_{fe}	Friction coefficient
$C_{L\beta}$	Stability lateral stability coefficient
C_{M_0}	Zero lift pitching moment coefficient
$C_{M\alpha}$	Static longitudinal stability coefficient
$C_{N\beta}$	Static directional stability coefficient
c_p	Specific heat at constant pressure
c_v	Specific heat at constant volume
E	Youngs modulus
e	Span efficiency factor
F_g	Maximum force on the hoisting rope
F_m	Net force acting
h_c	Convective coefficient
h_r	Radiation coefficient
i	Unit imaginary number
I_{xx}	Second moment of inertia
K_0	Tethered balloon altitude coefficient
K_1	Tethered balloon sizing coefficient
K_b	Buckling stress parameter

L	Length
L	Lift force
M	Internal moment
m_B	Mass of balloon envelope with rigging
m_{total}	Mass of the flying section of the balloon system
M_{eq}	Equilibrium Moisture Content
n	Load factor
P_{BAT}	Power delivered by the battery
q	Heat flow
q	Shear flow
R	Thermal resistance
R_{He}	Individual gas constant of helium
R_s	Thermal surface resistance
S	Surface area
S	Wing surface area
S_{wet}	Wetted area
T	Internal torque
$t_{discharge}$	Battery discharge time
U	Thermal wall transmittance
V	Internal shear force
V	Volume
V_∞	Freestream velocity
W	Weight
w	Downwash velocity
$x_{n.p.}$	Neutral point x-position

Introduction

Imagine being a field medic working for the military, just like Pete Mitchell, a Dutch soldier stationed in Afghanistan. At his field hospital, the infrastructure was limited however the injuries were severe. One of the key missing pieces of infrastructure was a large blood cooler to store sufficient blood required for healing injured soldiers. Therefore, to remain capable of saving lives, a frequent blood supply from a main hospital was required. This supply run was however irresponsible as it endangered the lives of military personnel travelling through an active combat zone. Hence a safer logistic solution had to be found. This solution is provided by the EcoGlide project.

The EcoGlide project identified the need for methods of transporting relatively small packages with vital supplies such as blood over large distances and with high precision in a sustainable manner. The transportation of supplies can get complicated in hostile areas or areas lacking infrastructure, where near-daily supply might be required. EcoGlide aims to solve this problem by autonomously transporting the cargo through the air by means of deploying dedicated single-use gliders. This mission will be performed while minimising life-cycle costing. The EcoGlide system has been designed specifically to deliver blood from hospitals to smaller field hospitals for the military to allow people like Pete to do what they do best: saving lives. This report provides a detailed design of the EcoGlide system and all its various subsystems.

Chapter 1 marks the start of this report and gives a detailed description of the exact use case and mission the EcoGlide system is being designed for. Chapter 2 covers the project vision and mission objective of the EcoGlide system, explains the need for the project and the design approach taken by the team. An overview of the design presented in this report will be presented in chapter 3, including all technical specifications, operational limits and the mass and power budgets of the design.

The following part of the report is a substantiation of the design and aims to give an in-depth description of the technical design that has been performed. It starts with chapter 4, which briefly summarises the design stages that took place in the first half of the Design Synthesis Exercise and presents the functional analysis, the start of every subsystem design. In the chapters that follow, the different subsystems of the glider are covered. Chapter 5 covers the aerodynamic design of the glider and analyses of its aerodynamic performance. Chapter 6 covers the structure and materials that will support the other subsystems and bear the loads. Chapter 7 covers the guidance, navigation and control systems that help the glider fly to its destination in a controlled manner. Chapter 8 covers the protection and thermal control of the payload. Chapter 9 covers the electrical power system that will provide power to the glider. The method that will be used to deploy the glider is described in chapter 10. The production method and production plan for construction of the glider is then presented in chapter 11. Leaving the logistics and operations of the glider to be treated in chapter 12 and chapter 13 respectively.

With all the subsystems covered, some analysis of the design as a whole will be presented. Chapter 14 presents the life cycle analysis of the EcoGlide system and assesses the sustainability of the design. Chapter 15 covers the reliability, availability, maintainability and safety of the glider throughout its life. Chapter 16 covers the market analysis which discusses the costs of the glider and how it fits into the market. Afterwards, the plan for the future is given in chapter 17. The report ends with the conclusions of the paper as well as recommendations for anyone who would like to further develop the EcoGlide concept.

Mission Overview

Early on in the design process [25], the team chose a specific use case for EcoGlide. It is that of the fictional Dutch army medic, Pete Mitchell, who needs blood on a near-daily basis to treat his patients in the field hospital at 10 [km] from the front line. This selection was made based on interactions with the Dutch army from the very early stages of the project. It gives more insight into the real potential for the EcoGlide project and highlights its importance in modern society. A description of the mission that provided the use case for the EcoGlide project can be found in section 1.1. The interaction of the people with the EcoGlide system throughout this mission is given in section 1.2.

1.1. Mission Description

In order to allow Pete to perform his job, a stock of approximately 6 [L] of blood should be present at his field hospital. Blood is however a sensitive liquid with a limited lifetime if not properly cooled. This provides an issue at the field hospitals as their infrastructure is limited and no large capacity cooling unit can be placed on site. Therefore a near-daily delivery of blood from a main hospital is required. The distance from the field hospital to the main hospital is however in the range of 100 to 150 [km], with an active combat zone in between. Therefore it is irresponsible to initiate a supply run through the combat zone between the two hospitals, endangering the lives of military personnel. Hence a new logistical solution had to be found that allows for a safe and reliable resupply of military field hospitals. The aim of EcoGlide project is to provide this solution. In order to do so, a system capable of regularly delivering a small amount of blood to the field hospital has to be designed. Additionally, this system has to be semi-agile as combat situations are dynamic and the location of both the main hospital and field hospital might change over time. This provides requirements that tailor the design of EcoGlide for this specific mission. It should however be noted that from time to time a traditional logistic solution is used for the field hospital in order to restock its supplies such as food. This provides an opportunity for the EcoGlide system to retrieve useful components from the glider and transport them back to the launch site allowing for them to be reused and thereby increasing sustainability.

1.2. Mission Flow Diagram

To better understand the mission from the perspective of the people that will interact with the system, personas were created. These personas are introduced for each general step of the mission and can be seen in the mission flow diagram given in Figure 1.1. Additionally, the steps each persona will perform are discussed below. This way of understanding the mission highlights the human-centred design philosophy followed by the project team.

The mission flow diagram presents these steps in a visual way and provides a brief overview of the function of the different personas. A more detailed analysis of the interaction between the different personas will be presented in chapter 3 through the use of a product journey map

The different steps that are included in the mission flow diagram are elaborated below.

- The first step involves the manufacturing of the system and is carried out by Mike Metcalf. He is also responsible of checking verifying the quality of the manufactured products, after production.
- The second step sees Carol Bradshaw, who is in charge of logistics and transportation of the system to the main hospital, i.e. the launch location.
- After the system's delivery, the aircraft is assembled by Perry Siedenthal who is a technician at the main hospital.
- Once the aircraft has been assembled, the deployment system is set up by Tom Kazansky. Simultaneously, Sam Wells, a doctor at the main hospital loads the system with the blood.
- The weather conditions are monitored by Monica Barbaro, who is a meteorologist and ensures that the weather conditions are suitable for launch based on data from weather satellites.
- Once the system has been loaded with blood and weather conditions have been deemed suitable for flight, Tom uses the deployment system for launch.
- Bill Cortez is an army personnel operating in the mission area. He is might be unaware of the fact that EcoGlide launched a new aircraft in the air. Therefore, if he sees it, he must not identify it as hostile. Bill Cortez's persona therefore is added to ensure that EcoGlide's aircraft will be perceived as friendly by nearby soldiers.

- The next step sees the collection of the blood with the cool boxes, by Pete Mitchell who is a medic at the field hospital. He will also collect the reusable items and store them.
- Once a certain minimum number of reusable items have been stored by Pete, they are retrieved by Penny Benjamin. She is responsible for the retrieval and transportation of the useful parts back to the field hospital.
- The final step involves Marcus Williams who is a resident in the vicinity of the mission location. He does not want to be bothered by a potential pile of Ecoglide aircraft, when the military moves to another location. The inclusion of his persona therefore ensures that Ecoglide should limit minimise any waste to the bare minimum and prioritise means of decomposing the aircrafts.

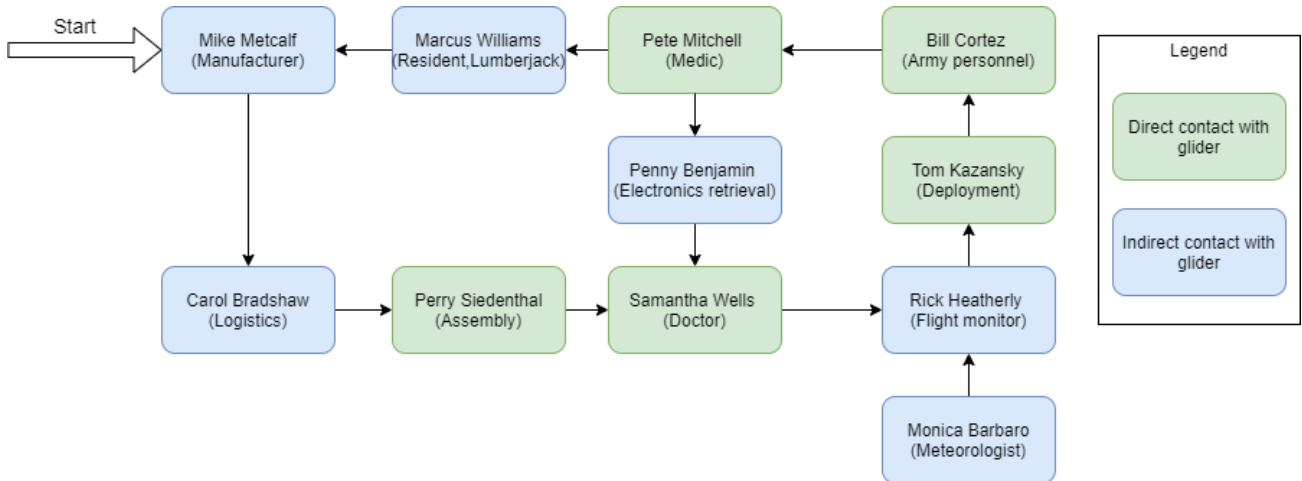


Figure 1.1: Mission flow diagram

From analysing the interaction of personas with the EcoGlide system, a new insight into its use case was provided. This insight gave an idea of what the people find important when interacting with the system, resulting in additional requirements or constraints which will be treated in the next chapter.

2

Project Vision

This chapter elaborates the vision that will be implemented to execute the project successfully. In section 2.1, the past and the future of single-use gliders is investigated as they provide a promising solution for the mission described before. From this investigation, an opportunity arose leading to the mission need statement and project objective statement as given in section 2.2. An analysis of the personas interacting with the system is provided in section 2.3 giving the requirements these personas impose on the design. The chapter concludes with section 2.4 which provides the design thinking philosophy adopted by the project team followed by section 2.5 giving the sustainability strategy implemented in the project.

2.1. History & Future

In the second world war, the issue of delivering payload to hard-to-reach areas was partly addressed with the introduction of single-use gliders. These gliders were capable of delivering cargo and soldiers to the battlefield. More recently however, companies like *Logistic Gliders Inc* were experimenting with this technology to create a single-use cargo glider capable of delivering payloads weighing a few hundreds of kilos. [25]

The future must however also be considered. Awareness about our impact on nature grows quickly and this is reflected in the current engineering industry. There is a clear trend towards sustainability, that is not limited to the environmental impact of the created products, but implemented throughout all aspects in the engineering process. The industry reduces its life-cycle costing hence becoming more financially, ecologically and socially sustainable. This is done by implementing methods such as lean manufacturing and proper system engineering approaches. [25]

From the discussion above, the past, present and future indicate an opportunity for single-use cargo gliders providing small payloads such as 6 [L] of blood to locations with limited on-ground accessibility, as long as this glider is sustainable in a cradle-to-grave scenario. The latter would make this system unique in its market. In order to analyse the feasibility of such a system, the EcoGlide project was initiated. [26]

2.2. The EcoGlide Project

Initiated by Prof. C.A. Dransfeld, the EcoGlide project aims to address the feasibility analysis introduced in Section 2.1 through a preliminary design. The project was handed over by Prof. Dransfeld to a team of students, with a set of user requirements and constraints to which the design needs to adhere. In order to condense the assignment, a mission need statement is derived. This mission need statement is given below. [25]

MNS: *Deliver small cargo to areas with limited on-ground accessibility with high precision, large deployment capacity and constant mission readiness, while minimising life-cycle costing.*

The team consists of 11 aerospace engineering bachelor students. The project serves as a ten week Design Synthesis Exercise where the students can apply the theoretical knowledge gained during their bachelor to a design project. Although the project is mainly focused on designing a glider that meets the user requirement set by the professor, the team decided that the project would benefit from the involvement of third party stakeholder setting additional requirements. The military was chosen as the most suitable commercial stakeholder for this project resulting in clearly defined mission profile, as was given in chapter 1. [25]

Focusing on the military mission profile, and adding the constraints of the project, the following Project Objective Statement was created and given below.

POS: *Design a biodegradable glider, by 11 students in 10 weeks, that autonomously delivers blood to military field hospitals on a near-daily basis.*

Additionally, a visualisation of this statement is shown in Figure 2.1.



Figure 2.1: Visual representation of the Project Objective Statement.

2.3. Persona Analysis

When analysing the interaction of the personas with the system in section 1.2, it became apparent that these interactions impose additional requirements on the system. These additional requirements are elaborated below.

- When considering the interaction of Mike Metcalf with the system, it is apparent that the manufacturer requires an easy to manufacture system. Especially since it is single-use product and manufacturing cost should be as low as possible.
- The logistics aspect of the system is covered by Carol Bradshaw. She requires the system to be compact for logistics such that a large number can be shipped at once reducing operational cost. This means that in case of a large system, it should be packaged in kit form rather than fully assembled.
- In order to allow for a reliable operation of the glider, Perry Siedenthal and Samantha Wells require that the system allows for a straightforward assembly at the mission location.
- To plan out the mission, Rick Heatherly requires up to date weather conditions from Monica Barbaro. However a limit on operational conditions in which the system will operate have to be defined and analysed.
- Tom Kazansky, the deployment operator, evidently requires that the deployment is easy and fully integratable with the rest of the system.
- As mentioned before, Bill Cortez requires that the functional aspect of the aesthetics of the system are considered during the design of the system.
- Both Pete Mitchell and Penny Benjamin require an easy and quick retrieval of the cargo and electronics of the system respectively. As they are in a combat zone and have other things on their mind, they do not want to move the EcoGlide system around unless absolutely necessary as they have more urgent things to do. This is however in contrast to Marcus Williams, a local resident that requires no waste of the army to remain when they leave the location. Therefore the only solution is to create a biodegradable product that can be left in the environment without causing harm to it. This imposes requirements mostly focused on the material choice for the EcoGlide system.

The requirements given above will be summarised in the functional analysis, given in section 4.4.

2.4. Design Thinking Philosophy

The team used a design thinking philosophy during this project, which focuses on the user [15]. This approach is based on five steps that aim to understand the users and use that information as input to the ideation phase. [26]

The first step is to empathise with the users that interact with the design. Four categories can be defined for the EcoGlide project. There are people who design the product, people who manufacture the product, the operators and the customers who receive the glider with its cargo. The team has created personas in order to empathise with all the people that are involved, they are introduced in Chapter 1. [26]

The second step is definition, where requirements on the product are defined by the people that interact with it. The aim of this step is to ensure that all needs from the people who interact with the product are taken into account. [26]

Once the user wishes are properly understood, the ideation phase starts. During ideation, multiple rounds of design and concept creation are organised. At the start of each round, the problem and constraint space are reassessed and redefined to ensure that a successful design remains feasible. Sketching is a valuable tool in this phase especially. [26]

The next phase is the prototyping phase. This phase is limited by the fact that the Design Synthesis Exercise cannot be held on campus. However, prototypes will be made using the computer aided design software CATIA. Some small scale physical prototyping, in the order of one > 1 [m], will be done using the faculty's 3-D printers. These prototypes can be used to assess feasibility of concepts that can only be analysed from visualisation. The team has also received some material samples which will be used to make a prototype part. [26]

The final phase of the design thinking process is testing of the product. The testing will be performed with the final end-user of the product. Due to the current COVID-19 measures and the limited time available in this project, it is assumed to be unfeasible to create a product that can be tested by its end-user during the DSE project. However, this approach still facilitates the execution of a successful project by creating the preliminary design based on requirements from users. [26]

2.5. Sustainable Development Strategy

Since sustainability is of growing importance in our modern society, where resources have become scarcer than ever, a sustainable development strategy has to be implemented in this project. Within this strategy, not only the way the system contributes to sustainability is considered, but also the way the sustainability is implemented throughout the design process of the system.

In the initial stages of the project, the focus was put on organisational sustainability in order to ensure proper functioning of the team such that deadlines were met on time and to the stakeholders' satisfaction. In order to do this, the philosophy of 'lean management' was used. This ensured that stakeholder requirements and needs were always prioritised with respect to design choices. Since environmental sustainability was one of the primary stakeholder requirements, the use of the 'lean management' philosophy also made sure that sustainability played a key role when making important design choices, for example, in the case of selecting materials for the structure of the glider or selecting a deployment system that would have minimal impact on the environment.

Following this, sustainability was incorporated into the technical design of the system. First of all, a number of general sustainability requirements were initiated for the system. Compliance with these requirements ensures that the final product has a minimal environmental impact. The clearest example of such a requirement is that the glider should be biodegradable, as also stated in the project objective statement. Additionally, since the final product is a glider and therefore lacks a propulsion system, no harmful gasses are emitted by the glider during its mission. Along with this, sustainability requirements were formulated for individual subsystems. Finally, in order to fully assess the glider's impact on the environment and quantify this impact, a life-cycle assessment is performed and given in chapter 14.

Sustainability is also incorporated during the design process as the team decided to perform concurrent engineering. This means that the mutually dependent subsystems are designed simultaneously. This is done to speed up the design process and therefore reduce the amount of resources used. Additionally, sustainability is one of the key aspects considered when making design decisions and a trade-off between performance and sustainability will be performed before a decision is made. Finally, all the work is performed from home thereby limiting the need for transportation of people or equipment and thus increasing sustainability.

3

Design Overview

This chapter presents a summary of the outcome of the EcoGlide project. Section 3.1 contains the final concept of the EcoGlide system, containing the glider and its corresponding deployment system. In section 3.2, a graphical representation of the final glider design can be found. The operational envelope within which the glider is capable to operate is given in section 3.3. After this, the most important specifications for a customer are given in section 3.4. The chapter is concluded with providing the mass and power budget to which the glider is designed, given in section 3.6.

3.1. Final Concept

The final concept can be split in two major parts. Firstly, the concept for the glider itself is presented after which the deployment system of the glider is given. These two concepts are given below. It should be noted that the system as a whole complies to the user requirements set out by the principal tutor and that each subsystem additionally complies to subsystem specific requirements.

Glider

The EcoGlide glider configuration is a blended wing-body design. The main structural elements are the two spars and its skin. The spars form the load carrying structure of the glider and are made out of plywood. Their cross-section varies along the span to allow for the wing to taper and to accommodate for the lift distribution. The skin meanwhile provides the aerodynamic shape and transfers the loads to the spars. To simplify the production and assembly process, the ribs are directly integrated into the wing. This is made possible by the choice of a suitable material and manufacturing process, paper pulp moulding. To maintain the airfoil shape at the ribs, and to improve the overall smoothness of the skin surface, the pulp mouldings are wrapped in thin biodegradable PLA film.

The blood payload is contained in two separate cool boxes located in the body, in front of and between the spars. The cool boxes are custom made biodegradable containers made out of a plywood outside layer for structural integrity and an inner cork layer for good insulating properties. They contain phase change material bags to keep the temperature within the required boundaries, as well as cork filler, to further insulate the blood and absorb impacts.

Aerodynamically, the glider is designed for high performance and achieves a predicted glide ratio of 33.5. This makes it capable of reaching its destination even against headwind conditions during 80 % of the year at the two sample mission locations, Timbuktu and Kabul. To make this possible, the wing features a slender reflex airfoil to ensure both low drag and good stability and the wing has a high aspect ratio of over 10. Additionally, the wings are tapered and its tips are fitted with winglets, to further improve its efficiency. For the body, a sleek aerodynamic shape was created to encapsulate the payload entirely. Additionally, the body airfoil provides stability for the glider by creating a positive moment without producing significant lift. Finally, the glider has a slightly swept back wing with washout, allowing it to remain controllable even during stall conditions.

The autonomy of the EcoGlide gliders comes from the guidance, navigation and control subsystem. As soon as the glider is released from the deployment system the GNC subsystem will ensure that the glider enters a dive to gain speed while avoiding any collisions with the deployment system. The glider will then fly between way-points inputted into the flight controller until it reaches the landing location. At this point it will spiral downwards to bleed altitude until it can enter into a controlled stall to land. All of these functions will be the responsibility of the GNC, which consists of two elevons, an actuation mechanism, an off-the-shelf flight controller with various built in sensors, an external off-the-shelf GPS and two off-the-shelf servos. This will all be powered by a single 2700 [mAh] battery.

The gliders are designed to be delivered in kit form to the customer, to allow for efficient packaging for transport. This means that about 80 gliders fit inside a 20 [ft] shipping container, which is the standard method of transportation for the military. The paper pulp wing and fuselage panels will be produced by an external supplier that specialises in paper pulp products. For the spars, the plywood will be cut and glued before being shipped. The reusable electronics will be wired and assembled inside of the removable electronics compartment. Upon delivery of the gliders at the field hospital, the customer can assemble the prefabricated components by gluing and shrink-wrapping them according to the included manual. When a delivery needs to be done with a glider, the blood bags and PCM bags can be secured in the cool boxes and the top fuselage panel attached such that the glider is ready to be deployed.

Deployment System

The gliders will be deployed using a multi-use tethered balloon system. The balloon will use helium gas to stay in the air. The whole system can be set up in a few hours. Once set up, it can stay inflated for several days before it needs to be refilled. Attached to the balloon is a beam with a pulley system. This allows the glider to be towed up to the balloon for deployment. The tether of the balloon is connected to a winch to heighten or lower it. The same pulley system that is used to tow the glider up, ensures that the glider is always released in tailwind. After deployment, the glider will first gain speed, regardless of the direction it is headed. Once cruise speed has been reached, the glider will navigate itself toward its goal and begin its flight. Overall the total time spent on deployment phase is estimated to be 30 minutes.

This deployment system allows gliders to be deployed on a daily basis. As mentioned before, the balloon needs some occasional refills due to helium leakage. This however causes no limitation for the required daily delivery. Since winching down, refilling, and winching the balloon back up takes less than a day, this can simply be done after a daily delivery has been sent and is ready before the following delivery is required.

3.2. Layout

In order to visualise the design presented above, a number of renderings were created. Firstly, the glider itself is treated. The glider as it will look in operation is shown in Figure 3.1. In Figure 3.2 and Figure 3.3 a mixed view of the glider's internal and external layout is provided. In these figures one can clearly distinguish the skin made out of paper pulp with included ribs from the external view. Additionally, from the internal view one can see the spars of glider running from tip to tip and the payload boxes included in the body. Secondly, a rendering of the deployment system is provided in Figure 3.4. Finally, a technical drawing containing the dimensions of the glider is included at the end of this chapter. The glider is shown from several angles and sectional views are included to highlight design details.

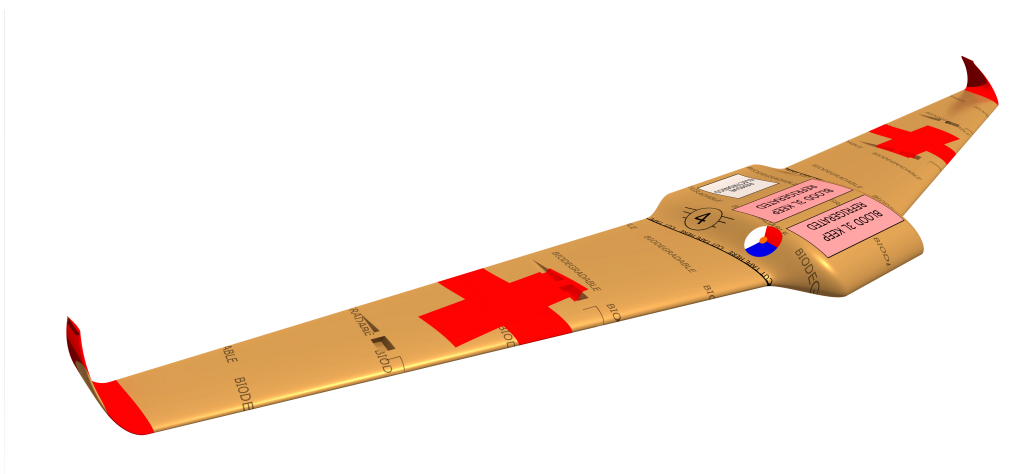


Figure 3.1: Render of the glider

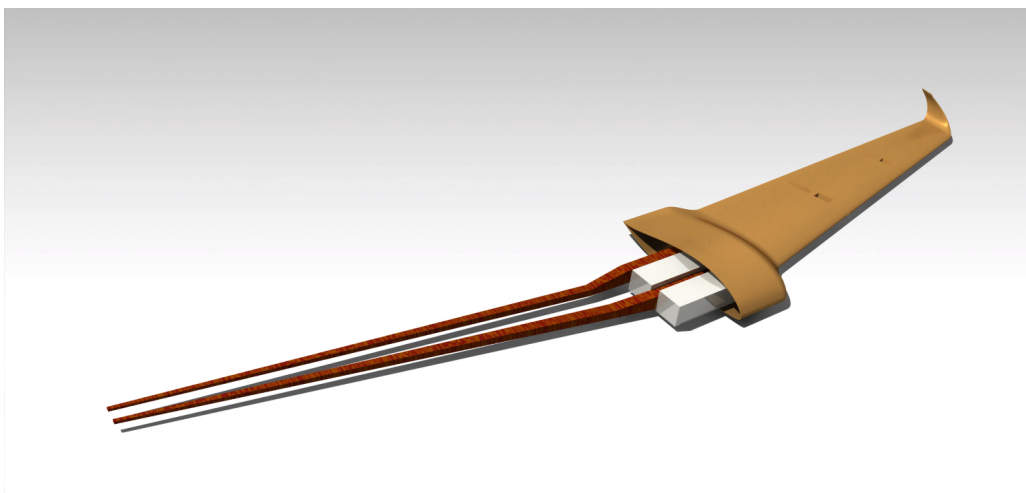


Figure 3.2: Render of the glider showing only one half of the skin to make the cool boxes and spars visible

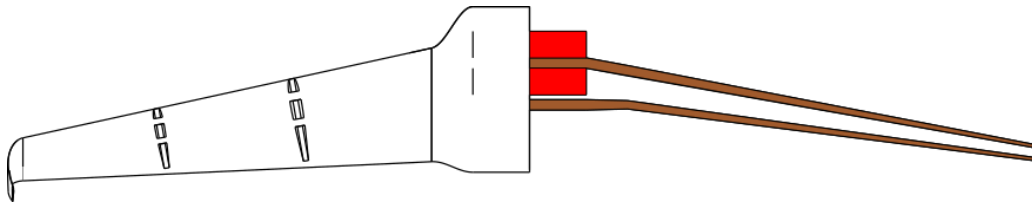


Figure 3.3: Top view of the glider showing only one half of the skin to make the cool boxes and spars visible



Figure 3.4: Render of the EcoGlide balloon design

3.3. Operational Envelope

The operational envelope of the glider is limited by 4 main things. Firstly, the environmental conditions in which the system can operate are quantified by the maximum allowable wind conditions that results in safe and successful operation. This is done for both the glider itself as well as for the deployment system. Additionally, the temperature range encountered by the glider during its mission is provided Secondly, the maximum loads that the structure of the glider can withstand are provided in the form of a flight envelope diagram. It should be noted that the glider must remain within the flight envelope during its entire mission to ensure safe operation. Thirdly, the operation of the glider is limited by the free area at the landing location as sufficient free landing area should be provided. Finally, glider operations are limited by the amount and size of payload that can be carried on board of the glider.

For both the deployment system and the glider, the maximum allowable wind velocity is set at $77 [km/h]$. It should however be noted that wind velocity increases with altitude and therefore this limit is imposed at deployment altitude. This results in a maximum wind velocity of $50 [km/h]$ imposed at ground level. Additionally, the temperature range in which the glider will have to operate is from -4 to $44 [^{\circ}C]$.

The flight envelope in which the glider can withstand the imposed loads is given in Figure 3.5. It shows the maximum load factor for a range of equivalent airspeeds. The maximum load factors have an upper limit of 3.8 and a lower limit of -1.52 . Four velocities are indicated in the diagram, where V_S is stall speed, V_C is cruise speed, V_M is the design maneuvering speed and V_D is the dive speed. The maneuvering loads start from $n = 0$ and increases along the lines of positive and negative stall until the limit load factor is reached. The gust loads start from $n = 1$ and are taken from literature for two speeds, cruise speed and dive speed [13][46].

When considering the free area at the landing site, it is required that within $200 [m]$ of the landing target there are no obstacles higher than $20 [m]$ and that the maximum obstacle height decrease linearly the closer you get to the target. This $200 [m]$ strip of land should also be at least $50 [m]$ wide. When such an area is unavailable at the landing location, a safe landing of the glider and its cargo cannot be assured.

Finally, when considering the payload, a maximum of two payload containers with a size of $12.96 \times 54.92 \times 10.92 [cm^3]$ and loaded maximum mass of $5.38 [kg]$ each can be carried on board of the glider.

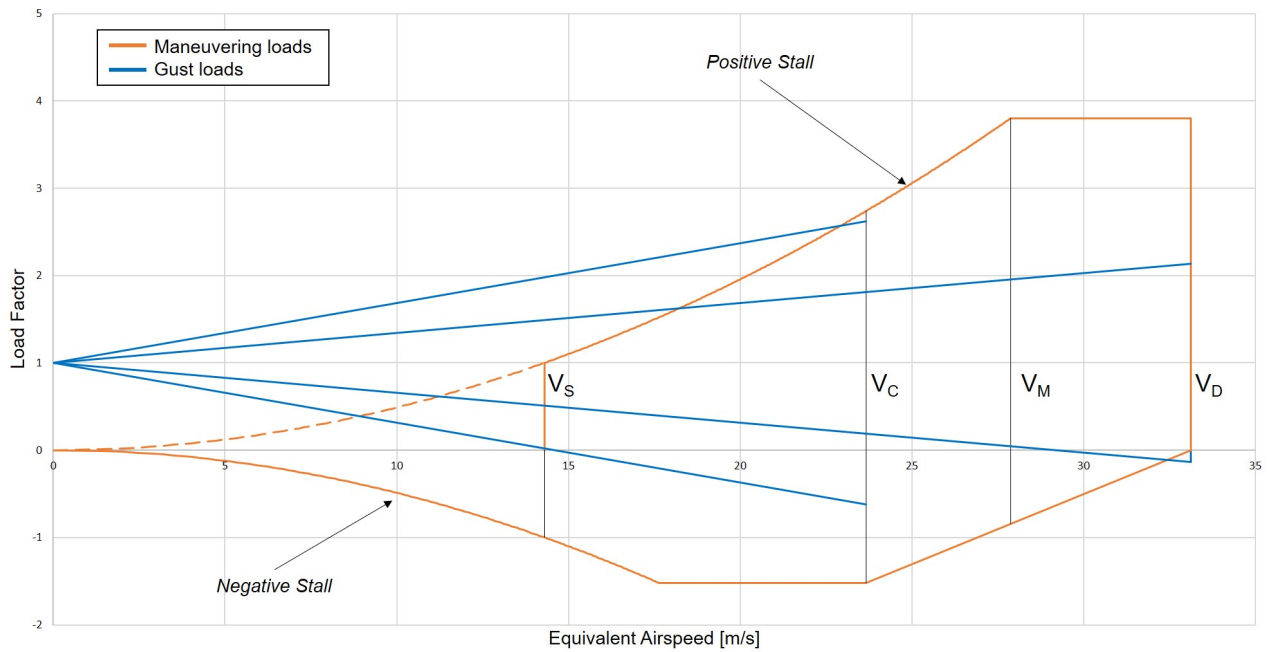


Figure 3.5: Flight envelope of the EcoGlide glider

3.4. EcoGlide Specifications

The Ecoglide glider is capable of transporting 6 [L] of blood in a 125 [km] radius around the launch site during 80% of the year for both reference mission locations, Kabul and Timbuktu. This range is provided by a glider with a wingspan of 4.91 [m] reaching a glide ratio of 33.5 at a cruise velocity of 100 [km/h]. The expected time required to hoist the glider to the balloon is 30 minutes whilst the flight time will be 105 minutes, leading to a whole mission time of 135 minutes. The payload container is guaranteed to keep the blood in between 2 and 6 [°C] for at least 3 hours and therefore the blood will not be spoiled during the mission. The empty glider will weigh approximately 13 [kg] whereas the payload weighs 11 [kg], leading to a total weight of 24 [kg]. These specifications of the glider are summarised in Table 3.1.

Table 3.1: Summary table of EcoGlide specifications

Parameter	Value	Unit	Parameter	Value	Unit
Payload	6	[L]	Hoisting time	30	[min]
Range	125	[km]	Flight time	105	[min]
Availability	80	[%]	Empty weight	13	[kg]
Wing span	4.91	[m]	Payload weight	11	[kg]
Glide ratio	33.5	[-]	Total weight	24	[kg]

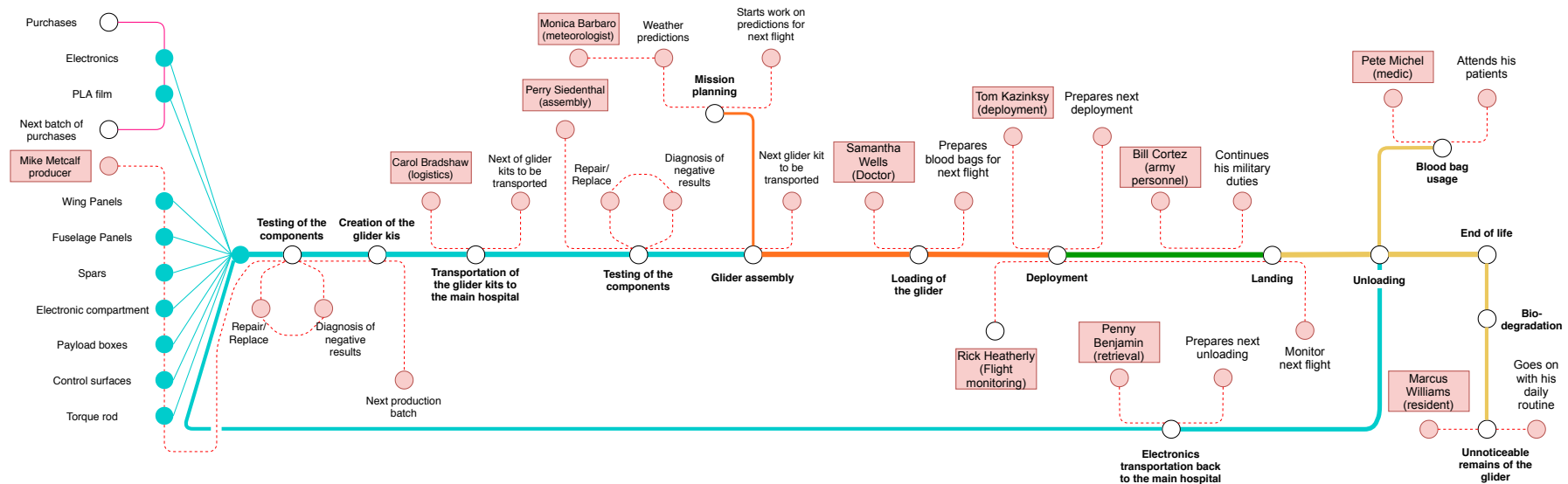
3.5. Product journey map

The product journey map allows easy visualisation of all the stages of the Ecoglide glider's life. It is a diagram which must be read from left to right and shows the different phases the product will follow. It is quite comparable to metro line mass transit maps in the sense that one could follow the different lines to see where the product will stop, and thus which steps it will undergo.

Besides the thick line representing the glider's journey, the dotted lines represent the journey the personas go through. They sometimes cross the same steps as the glider, representing their interaction with it. When a persona's journey is only parallel to the glider's journey, no direct physical interaction occurs, however, the persona might see or hear the glider, either directly or indirectly.

Product Journey Map

10



Legend

Product phases

- Non-mission phase
- Pre-flight phase
- Flight phase
- Post-flight phase

External phases

- Purchases steps
- Persona steps

Person name and function

Tom Kazinsky (deployment)

Main steps

- Main glider steps
- Components production steps
- Additional persona steps

3.6. Budget Breakdown

The mass and power budget of the glider are presented in this section. First the mass budget is covered followed by an elaboration of the power budget. It should be noted that contingency margins are considered when creating these budgets.

Mass Budget

The mass is subdivided in structural mass, the electronic mass and the payload mass. All the sub elements and its individual mass are shown in Table 3.2. The filler material mass can vary, depending on the ambient temperatures. The maximum value of 0.138 kg is used here in the mass budget.

Further are there still uncertainties in these budgets, which are taken in to account in the contingency margins. It was deemed that the accuracy of the design for the electronic and the payload was higher than the rest of the design. A contingency margin of 10% was deemed suitable to covers the uncertainty. A higher margin of 20% was selected to cover the uncertainties in the structural mass.

From the budgets we can concluded at 97.5% of the mass of the glider is biodegradable, after the payload is taken out. But the payload box and the phase changes materials are also biodegrade, so they could be also left to biodegrade. The electronics are positioned in the glider in such a way that they can be taken out and be reused. This means that the glider will be 100% biodegradable.

Power Budget

Power is consumed by the 3 main electronic components. In the power budget is the average power used, which the battery should be able to deliver through the mission. This, together with the peak power requirement of 11 W for the servos dictate the selection criteria for the battery. For the power is a contingency margin of 10% selected, due to the uncertainty in the power budget. This is shown in Table 3.3.

Table 3.2: Mass budget

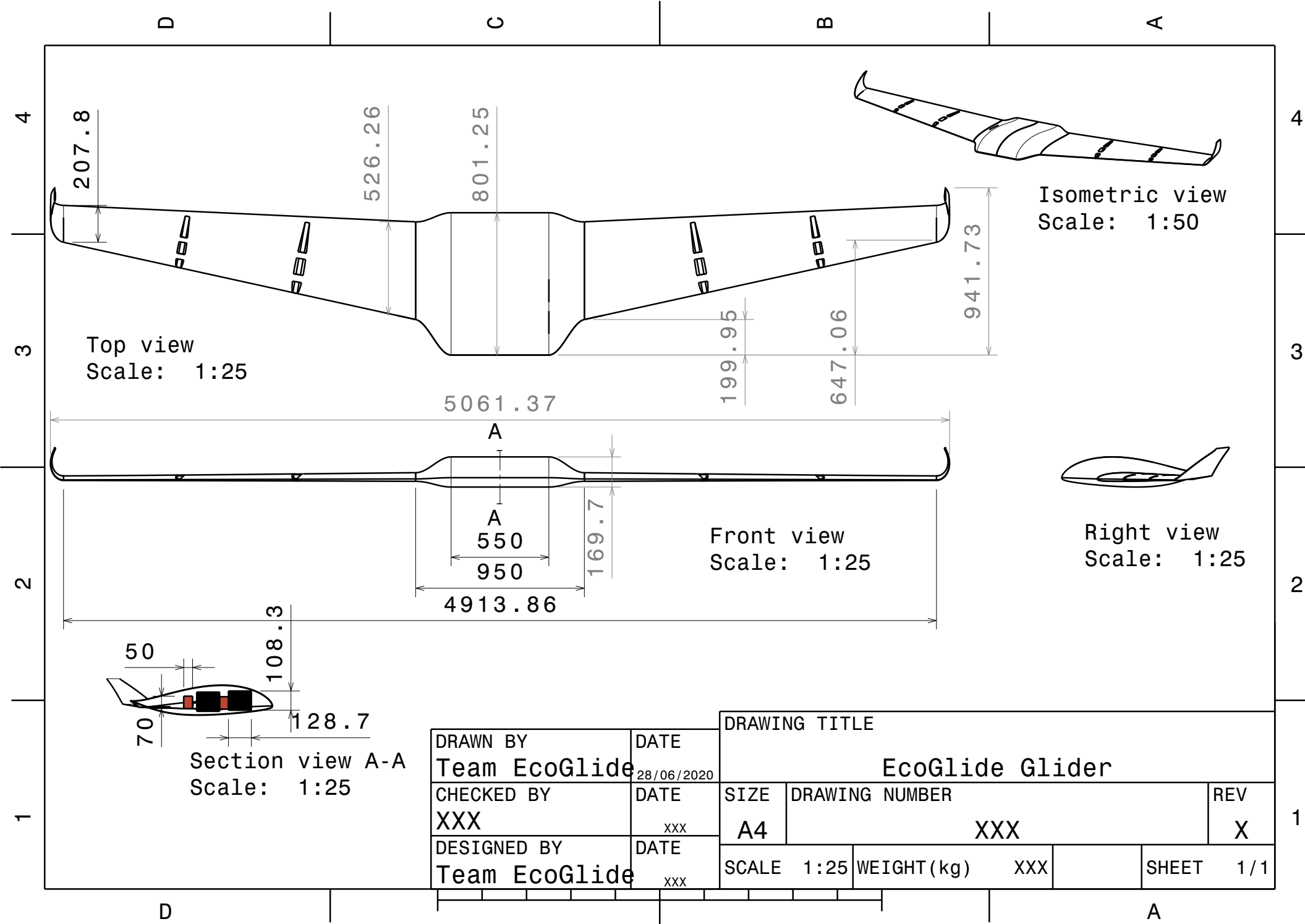
Item	weight
Leading edge spar	5.085 kg
Trailing edge spar	4.092 kg
Skin cardboard	3.204 kg
Skin PLA film	0.32 kg
Total structural mass	12.70 kg
Contingency margin (20%)	2.54 kg
Battery	0.101 kg
Servos (2x)	0.15 kg
Voltage regulator (SBEC)	0.029 kg
Flight controller	0.0372 kg
Total electronics mass	0.32 kg
Contingency margin (10%)	0.032 kg
Blood (6L)	6.36 kg
Phase change material	3.5 kg
Expanded cork	0.34 kg
Plywood	0.42 kg
Filler material	0.116 or 0.138 kg
Total payload mass	10.76 kg
Contingency margin (10%)	1.076 kg
Total mass	23.78 kg
Maximum total mass	27.43 kg

Table 3.3: Power budget

Item	Avg. power
Servos (2x)	3.85 W
GPS receiver	0.3025 W
Flight controller	0.9625 W
Total power	5.12 W
Contingency margin (10%)	0.512 W
Maximum total average power	5.63 W

Cost breakdown

A preliminary cost estimate of the glider was made, based primarily on the manufacturing steps. The costs included in the breakdown are the obtainment of the raw materials, processing of these materials, and then ultimately manufacturing the parts of the glider. More specifically, the costs include the electricity cost, specific raw materials, and the labour costs associated with the complete manufacturing process. The total estimated cost is e309 and a more detailed breakdown is presented in Chapter 16 and Chapter 14.



DRAWN BY Team EcoGlide		DATE 28/06/2020		DRAWING TITLE EcoGlide Glider			
CHECKED BY XXX		DATE XXX		SIZE A4	DRAWING NUMBER XXX		REV X
DESIGNED BY Team EcoGlide		DATE XXX		SCALE 1:25	WEIGHT (kg) XXX	SHEET 1/1	

4

Design Outline

The design presented in this report is a continuation of the work performed during the first phase of the Design Synthesis Exercise. This chapter serves as an introduction to the current design phase by briefly summarising the work done in previous design phases. Firstly, user requirements are discussed in section 4.1. These requirements functioned as the starting point for the design since they provide the basis to which the glider concept was tailored. Secondly, a summary of the previously performed trade-offs is given in section 4.2. The section considers both the trade-off for the deployment method as well as the glider configuration. The concepts selected during those trade-offs are the basis on the design as it is presented in chapter 3. Finally, a risk assessment and a functional analysis is presented in section 4.3 and section 4.4 and serves as the common start to every subsystem design.

4.1. User Requirements

Preceding the start of this project, a number of requirements and constraints were established by the principal tutor. These requirements provided the outline for the EcoGlide project and are therefore summarised below in Table 4.1.

Table 4.1: User requirements

Identifier	Requirement statement
R_EG_PERF_01	The glider shall have a maximum flight altitude of 5000 [m].
R_EG_PERF_02	The glider shall have a maximum launch altitude of 5000 [m].
R_EG_PERF_03	The glider shall have a minimum range of 125 [km] when launched from its maximum launch altitude.
R_EG_PERF_04	The glider shall have a maximum operational lifetime of 3.5 hours.
R_EG_PERF_05	The glider shall be able to navigate autonomously to its designated landing area upon launch.
R_EG_PERF_06	The glider shall be able to land autonomously at its designated landing area.
R_EG_SFRL_01	The glider shall have an on ground shelf life of at least 10 years.
R_EG_SFRL_02	The glider shall comply with the current drone regulations, EU Regulations 2019/947, with respect to safety and reliability.
R_OP_SFRL_01	During operation the drone shall be supervised in accordance with the rules of the EU Regulations 2019/947.
R_EG_ENBD_01	The maximum total mass of the glider including cargo shall be 25 [kg].
R_EG_ENBD_02	The glider shall be able to transport a payload of at least 6 [L] of blood.
R_EG_SUST_01	The glider shall be made out of renewable materials.
R_PO_SUST_01	The production of the glider shall use renewable resources.
R_OP_SUST_01	The operation of the glider shall use renewable resources.
R_EG_SUST_02	The environmental impact of the glider shall be minimal in a cradle to grave scenario.
R_EG_SUST_03	The glider shall decompose upon landing.
R_EG_SUST_03	The glider shall decompose in three model climates (Trondheim-NOR, Fukushima-JPN, Timbuktu-MLI).
R_EG_SUST_01	The design concepts shall be evaluated by means of life cycle assessment.
R_EG_COST_01	The Life Cycle Cost (financial, environmental and social) of the glider shall be minimal for a yearly production of 1000 gliders.
R_DS_AEST_01	The glider shall be aesthetically pleasing in the opinion of Prof. C.A. Dransfeld.

This list of requirements clearly indicated the direction that the user had in mind for the EcoGlide project, namely to develop an autonomous, biodegradable glider. After performing a functional analysis, market study and requirement discovery of the glider project, the list of requirements was elaborated with system and subsystem level requirements. These requirements are omitted here for brevity, but summarised per system in the subsequent chapters. Additionally, it should be noted that some of these user requirements are relevant for a large number of subsystems. Therefore

they are omitted in the tables of those specific subsystem chapters. The design is however also specified to these requirements such that their compliance checks out.

4.2. Concept Selection

Once a complete list of requirements was established, two major design choices had to be made. Both the deployment concept and glider configuration concept were selected since they were considered fundamental for the continuation of the design, influencing all subsystems on-board the glider. A trade-off was performed for both topics such that the most suitable solution could be found. The concepts are briefly discussed below, together with a summary of the results obtained from the trade-offs.

Deployment concept

For the deployment, three main types were considered: aerotowing, airdropping, and ballooning. For aerotowing and airdropping, several types of carrying aircraft were considered. For balloons, both single-use balloons and tethered balloons were considered, as well as different types of lifting gas. The concepts were judged based on various criteria, each with a corresponding weight indicating the relative importance. These criteria and weights are omitted for brevity, however the main conclusion of the trade-off is provided.

After performing the trade-off, it was concluded that aerotowing and airdropping are unsuitable for this project due to poor reliability and safety performance while requiring high expertise and excessive initial cost. Hence only the ballooning options remained, where the single-use balloons were discarded due to poor sustainability, safety and reliability performance. Tethered balloons are more reliable due to not drifting away in wind, and are not suffering from low sustainability due to their reusable nature. The most suitable lifting gas for tethered balloons was found to be helium, slightly outperforming hydrogen as a lifting gas based on the safety and expertise level criteria. Although hydrogen obtained a higher sustainability score, this could not outbalance the two drawbacks previously mentioned. Therefore the final deployment concept chosen is a multi-use tethered helium balloon. [26]

Configuration concept

During the trade-off, five configuration concepts were generated: a biplane configuration, a blended wing-body configuration, a Prandtl wing configuration, a high-wing configuration and a low-wing configuration. The biplane concept was eliminated by way of a functional forecast analysis. Its elimination was mainly caused by poor aerodynamic characteristics inherent to the biplane configuration. It was also decided that the low-wing and high-wing concepts would be treated as one during the trade-off due to the many similarities. The remaining four concepts were rated on their potential of a total of 11 criteria, using the AHP method. The trade-off of the different configurations will be summarised for each concept. [26]

The conventional concepts, as presented in Figure 4.1, were certainly the safe choice. Due to the many already existing gliders with this configuration, development risk was expected to be low and the reliability was rated highly. The traditional configuration also resulted in good stability characteristics and was easy to store. However, the configuration was structurally most challenging and was likely to have the lowest payload-to-weight ratio. [26]

The trade-off summary of the Prandtl wing is shown in Figure 4.2. The innovative wing design benefits aerodynamics and structures at the same time, all while having the smallest overall dimensions. However, this configuration is very hard to manufacture compared to the other concepts. The development risk is also very high for the Prandtl wing, as little research has been done on aircraft with this configuration. [26]

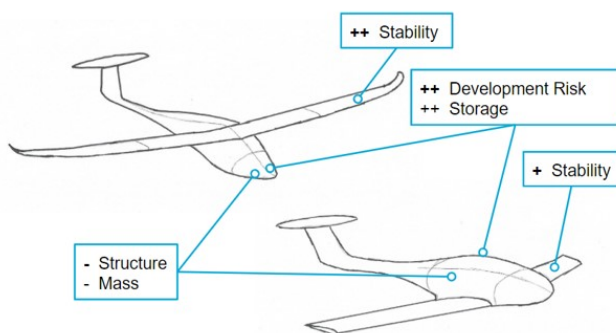


Figure 4.1: High-wing & Low-wing concepts

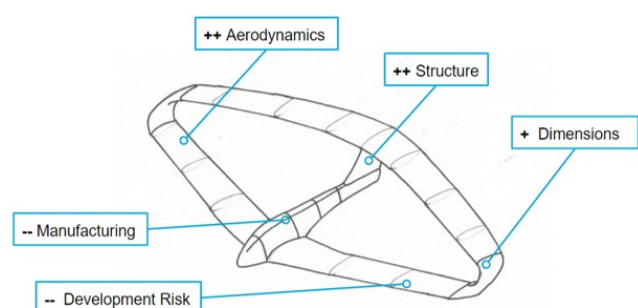


Figure 4.2: Prandtl wing concept

The configuration concept that won the trade-off was the blended wing-body, presented in Figure 4.3. The simplicity of the design looks good, performs well aerodynamically and is much easier to produce than any of the other concepts. The stability of a tailless aircraft can be a problem, but a good design can help to overcome that. This will in turn also increase the reliability of the glider. Overall, the blended wing body concept was found to be about 10% better on all

criteria combined than any of the other concepts. A sensitivity analysis confirmed that this conclusion was robust. [26]

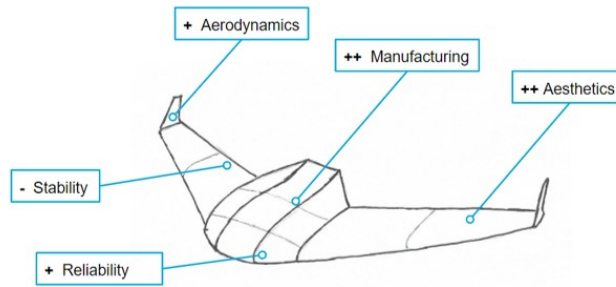


Figure 4.3: Blended wing-body concept

4.3. Risk Assessment

Risk assessment is an important part of the EcoGlide, as it ensures that the end product can work safely and reliably. The first step of this process is to identify the risks related to each subsystem or operation. Next their level needs to be assessed, by estimating both the probability of occurrence and the severity of the consequences and combining both aspects by using a risk matrix. The descriptive scales used for this process are shown in Table 4.2. These scales serve as an indication when assessing the risks, but cannot always be strictly applied, depending on the aspect that is being considered. The risk matrix with the different risk levels and their abbreviations is shown in Table 4.3.

Table 4.2: Risk probability and severity scales

Probability	
negligible (n)	will most likely not happen throughout deployment of glider fleet
improbable (i)	will possibly happen once throughout deployment of glider fleet
probable (p)	will happen at least once throughout deployment of glider fleet
highly probable (h)	will happen multiple times throughout deployment of glider fleet
Severity	
negligible (n)	does not influence mission success
marginal (m)	mission is only partially successful
critical (c)	mission is not fulfilled at all
catastrophic (ca)	mission failure and harm to people

Table 4.3: Risk matrix with risk levels and their abbreviations

(Unmitigated) / Mitigated	Highly probable (h)	Probable (p)	Improbable (i)	Negligible (n)
Catastrophic (ca)	Very high (vh)	High (h)	Moderate (m)	Low (l)
Critical (c)	High (h)	Moderately high (m)	Moderate (m)	Low (l)
Marginal (m)	Moderate (m)	Moderate (m)	Low (l)	Low (l)
Negligible (n)	Low (l)	Low (l)	Low (l)	Low (l)

To reduce the risk level, mitigation methods can be applied. Typical mitigation methods are the implementation of additional requirements or taking risk reducing design decisions. These usually decrease either the probability or severity of a given risk, so after mitigation the risks need to be reevaluated. To help identify particularly risk-prone areas and assess the effectiveness of the mitigation process risk maps can also be constructed. The risk maps in this report show both the risks before and after mitigation in the same map. The unmitigated risks are written between brackets. Each chapter where it is deemed necessary contains its own brief risk assessment.

4.4. Functional Analysis

A second, more detailed functional analysis was performed after the concepts were selected. The outcome of this analysis served as the starting point for every subsystem design. The specifics of the functional analysis itself and the requirements that follow from it are listed at the start of every subsequent subsystem chapter. The functional analysis of all subsystems combined results in two diagrams, a functional flow diagram and a functional breakdown diagram. These diagrams are explained and presented in this section.

Functional Flow Diagram

The Functional Flow diagram orders the functions of the system in a chronological way. The described functions are detailed up until 3 levels deep. [25]

The red boxes describe the highest level functions which are divided into the preparatory phase, execution phase and the end-of-life phase. Note that for this specific project, end-of-life is considered as one of the high level functions as it contributes largely to the sustainability of the project. The light red boxes represent the sub-level functions, one level deeper than the red boxes. The yellow boxes describe the lowest level functions, one level deeper than the light red boxes, and represent all the functions that have to be performed per highest level function.

When all of these lowest level functions are provided by the product, it can be considered successful. Therefore a functional flow diagram is used to think about the different functions the product has to fulfil and what that means in terms of requirements. [25]

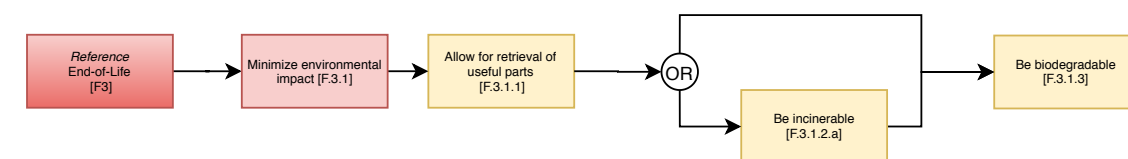
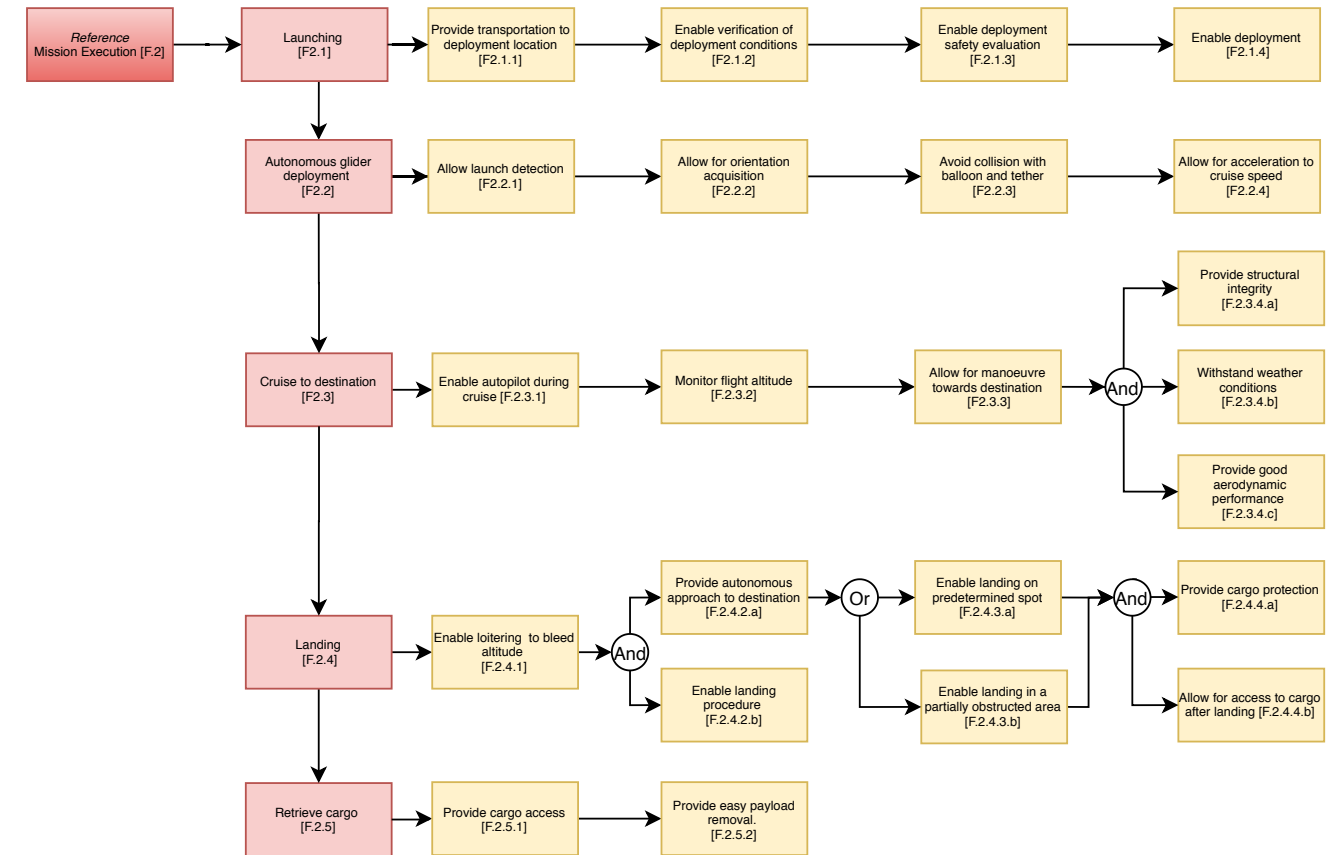
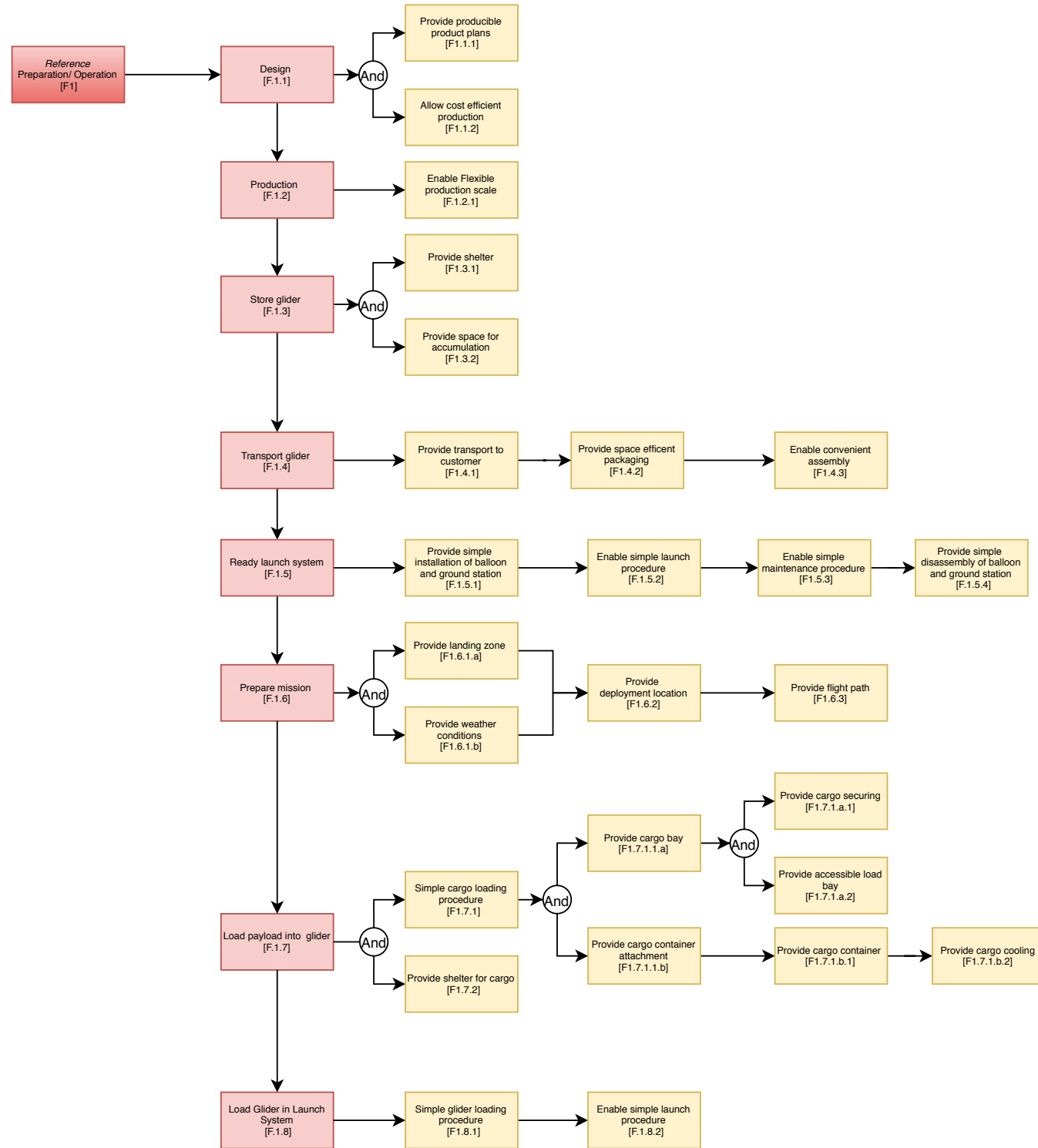
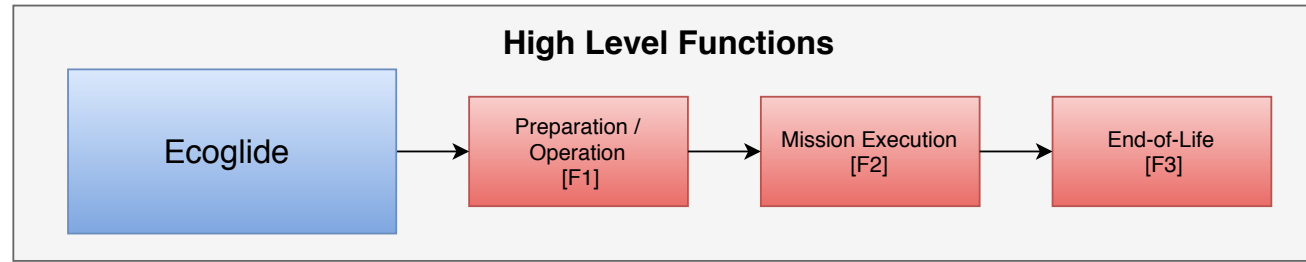
Functional Breakdown Diagram

The Functional Breakdown diagram divides the functions per subsystem, identifiable by the orange boxes, and orders them to show their hierarchy. This diagram is an "AND-tree" meaning that all of these functions have to be performed per subsystem. [25]

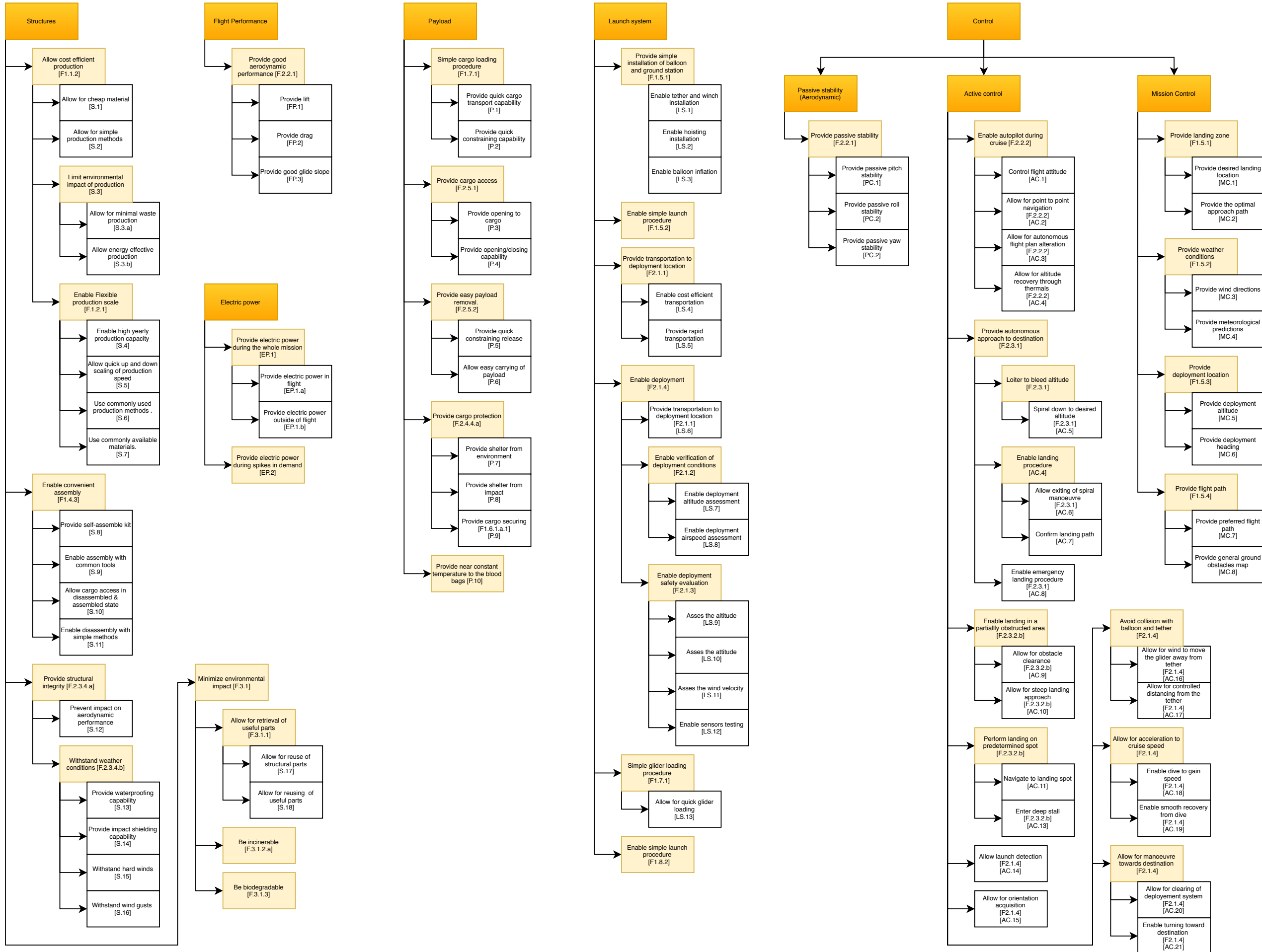
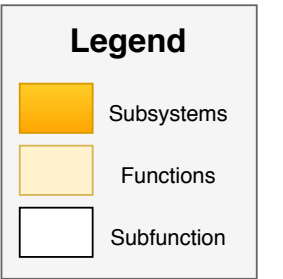
The yellow boxes represent the higher level functions, as taken from the Functional Flow Diagram. Finally, the white boxes describe the lower level functions and flow directly from the yellow boxes. [25]

Once again, the Ecoglide system must provide all of these lowest level functions for it to be successful. Therefore the functional breakdown is a different approach than the functional flow diagram to analyse the functions the Ecoglide system has to fulfil and what impact those functions have on requirements. [25]

Functional Flow Diagram



Functional Breakdown Diagram



5

Aerodynamics & Performance

Gliders are characterised as aircraft without propulsion. They rely exclusively on aerodynamic efficiency to have good range performance. For the EcoGlide glider, a blended wing-body configuration concept was selected. However, an additional design challenge occurs for tailless gliders in specific due to the intrinsic stability issues. Hence the aerodynamic design of the EcoGlide project is not as straightforward as for traditional aircraft.

This chapter starts with a functional analysis, where the requirements for the aerodynamic design are discovered. This is given in section 5.1. The design approach, taken to ensure a successful design is created, can be found in section 5.2. Section 5.3 explains the lifting-line and lifting-surface models used when designing the wing planform. The results obtained from following the design approach are given in section 5.4 to section 5.7 and these results are summarised in section 5.8. The performance that can be obtained with this aerodynamic design is given in section 5.9. Finally, the chapter is concluded with a section on verification and validation of the models used, given in section 5.10, a sensitivity analysis of the design in section 5.11 and a risk assessment of the design in section 5.12.

5.1. Functional Analysis

The aerodynamic subsystem is very important because it is solely responsible for the range performance of a glider. This section describes the most important functions of the aerodynamic subsystem and lists all the subsystem requirements. The compliance with each requirement is described in the indicated section. This can be found in Table 5.1. The requirements are derived from customer needs, regulations, previously performed market analyses and the functional analysis.

Table 5.1: Aerodynamics & Performance requirements

Identifier	Requirement statement	Compliance
R_EG_PERF_01	The glider shall have a maximum flight altitude of 5000 [m].	section 5.9
R_EG_PERF_02	The glider shall have a maximum launch altitude of 5000 [m].	section 5.9
R_EG_PERF_03	The glider shall have a minimum ideal range of 125 [km] when launched from its maximum launch altitude.	section 5.9
R_EG_ENBD_01	The maximum total mass of the glider including cargo shall be 25 [kg].	section 5.4
R_EG_ENBD_03	The fuselage shall fully enclose the payload subsystem.	section 5.5
R_EG_PERF_07	The glider shall be able to reach the ideal range in all directions for at least 80% of the time at the two mission locations, Timbuktu & Kabul.	section 5.9
R_EG_REG_01	The wingspan of the UAV shall be no more than 8 [m].	section 5.4
R_EG_REG_02	The kinetic energy of the UAV shall not exceed 1084 [kJ] at any point during flight.	section 5.10
R_EG_AED_01	The glider shall be able to provide a lifting force of minimum 250 [N] for a minimum flight velocity of 15 [m/s].	section 5.6
R_EG_REG_16	The UAS manufacturer shall either conduct flight tests or perform simulations that cover the complete flight envelope to validate the UAS.	section 5.9
R_EG_CON_01	The glider shall be statically stable along all axes.	section 5.7
R_EG_CON_02	The glider shall be dynamically stable along the longitudinal axis.	section 5.7
R_EG_CON_03	The outboard sections of the wings of the glider should stall last.	section 5.6

For the functional analysis, the mission has two parts that are important for the design of the aerodynamic subsystem. These are; the cruise phase and the landing phase. For each phase, several important functions can be determined.

The aerodynamic subsystem of the EcoGlide design serves three main purposes during cruise. Firstly, the lifting surfaces of the glider should provide sufficient lift to carry the weight of the glider, approximately 25 [kg]. Secondly, the glider should be able to reach a 125 [km] range from its deployment altitude. The customer also specified that the glider should be able to reach this range in all directions for at least 80% of the year. This availability requirement

means that the wind conditions at the proposed mission locations have to be accounted for in a performance analysis. Thirdly, the glider should be statically stable along all axes and, as a minimum, should also be dynamically stable in the longitudinal direction. Because the philosophy of the EcoGlide project is to have a cheap and disposable glider, the control system should be kept minimalistic. To that end, the glider should be as inherently stable as possible.

During the landing phase, the aerodynamic design serves two main purposes. Firstly, the lifting surfaces still need to provide sufficient lift to carry the weight. However, the velocity at which the glider flies during landing is much lower than during cruise, as the allowable impact at landing limits the landing velocity to 15 [m/s]. Secondly, the glider will make use of a stall landing and therefore the stall behaviour of the glider should be predictable and gradual. This can be achieved by letting the outboard section of the wing stall last.

5.2. Design Approach

This section explains the approach that was taken to ensure the aerodynamic subsystem is able to fulfil all requirements set in section 5.1. The approach can be split into three major phases. Firstly, a design of only the wing was performed using numerical tools built by the team. This was done because the design of the cargo holding body is dependent on payload dimensions which were not finalised until late in the design. In the second phase an airfoil trade-off was performed. Airfoils for both the wing and body were selected. In the third and final phase, an integrated design of body and wing planform was performed using XFLR5.

Wing Planform Design

The wing planform is the basis of the aerodynamic design. It should provide excellent gliding capabilities whilst having good inherent stability. For longitudinal stability it is required that the derivative of the pitching moment coefficient is negative to ensure the glider converges back to equilibrium after a disturbance. Additionally, it is required that the zero lift pitching moment coefficient is positive, such that the glider can have longitudinal moment equilibrium while generating positive lift. These two conditions are summarised in Equation 5.1 and Equation 5.2.

$$\frac{\delta C_m}{\delta \alpha} < 0 \quad (5.1) \quad C_{m_0} > 0 \quad (5.2)$$

A wing planform can be characterised by a certain set of parameters describing its shape. These parameters are summarised as: surface area, aspect ratio, span, average chord, taper ratio, sweep angle, twist and dihedral. The values of these parameters can be derived using some basic equations or numerical models. Since both the numerical models and basic equations do not take the wing profile into account, a first wing planform was designed before the airfoil selection was performed. This allowed the team to get a feel for the shape and dimensions of the wing after which it was easier to select suitable airfoils.

In order to find the surface area of the wing, landing conditions were considered. Landing is critical as it occurs at minimum velocity, which makes it more difficult to generate the required lift. This results in a constraining condition for wing area¹. After rearranging Equation 5.3 and using landing conditions as input, the required wing area was calculated by equating lift to weight. A safety factor of $n = 1.1$ was used to account for manoeuvring loads during landing. In this equation, L represents lift force, W is the glider landing weight, C_{Lmax} is the maximum lift coefficient of the wing, ρ is the freestream density, V_∞ is the freestream velocity and S is the wing surface area. This equation was the start of every design iteration, as data on glider weight, maximum lift coefficient and landing velocity became more accurate after every iteration.

$$L = n \cdot W = n \cdot C_{Lmax} \frac{1}{2} \rho V_\infty^2 S \quad (5.3)$$

The wing's aspect ratio was then calculated as a function of the required glide ratio. Glide ratio is defined as the horizontal distance per vertical distance travelled and equivalent to the lift over the drag ratio [1]. A parabolic drag polar was used, shown in Equation 5.4, where C_{D0} is the zero lift drag coefficient, AR the aspect ratio and e the span efficiency factor [51]. The optimum lift coefficient resulting in maximum $\frac{C_L}{C_D}$ was calculated using Equation 5.5 [46]. The zero lift drag coefficient that appears in both equations can be estimated using Equation 5.6². A typical friction coefficient for sailplanes is 0.003 [45].

$$C_D = C_{D0} + \frac{C_L^2}{\pi A R e} \quad (5.4) \quad C_L = \sqrt{C_{D0} \pi A R e} \quad (5.5) \quad C_{d0} = C_{fe} \frac{S_{wet}}{S} \quad (5.6)$$

Combining these equations, the required aspect ratio was calculated using Equation 5.7 after selecting a glide ratio based on the required availability of the glider as calculated in section 5.9. From this it was straightforward to find the corresponding wingspan b using Equation 5.8, and average chord c_{avg} using Equation 5.9.

$$GR_{max} = \frac{\sqrt{C_{D0} \pi A R e}}{C_D} = \frac{\sqrt{\pi A R e}}{2\sqrt{C_{D0}}} \quad (5.7) \quad b = \sqrt{S \cdot A R} \quad (5.8) \quad c_{avg} = \frac{S}{b} \quad (5.9)$$

¹URL: <https://www.grc.nasa.gov/WWW/K-12/airplane/size.html> [cited 16 June 2020]

²URL https://www.fzt.haw-hamburg.de/pers/Scholz/H00U/AircraftDesign_13_Drag.pdf [cite 10 Jun 2020]

The values of the required taper ratio and sweep angle followed from analysis using the aerodynamic models described in section 5.3. For the preliminary planform design, the twist and dihedral angle were kept at zero for simplicity. Their final values will be established during the third phase.

Airfoil Selection

The wing planform can now be expanded by adding airfoil sections to it. From the functional analysis it is required that the wing is inherently stable. This poses limits on possible airfoils that can be used for the glider. As explained in the previous section, the wing planform had to be designed before much was known about the body. Therefore, it was decided that the wing would generate almost all lift, whereas the body section would be designed for minimum drag whilst giving a high, positive pitch moment coefficient. This required the selection of two completely different airfoils for the wing and the body of the glider.

The main wing should have an airfoil with a small inherent pitch moment. The optimum value for the moment coefficient has a positive sign, but it can also be negative as long as it is small compared to the mid-section airfoil. Furthermore, it is important for the glider to obtain a high glide ratio, which is fully determined by the $\frac{C_L}{C_D}$ ratio. It is therefore beneficial that the 2D airfoil obtains a high value for $\frac{C_l}{C_d}$, preferably at a lift coefficient close to the design point. In order to achieve good drag characteristics at a large operating range, the C_{dmin} should be small and the drag bucket as wide as possible. Finally, the airfoil should have a high maximum lift coefficient, which has traditionally been a problem for reflex airfoils [5].

The airfoil used for the body should have different characteristics, as it is not intended to generate much lift. First, it should have high thickness-to-chord ratio to be able to fit the payload inside. Secondly, the body should have minimum drag for a wide range of angles of attack. To ensure the glider does not stall in an unstable manner, the airfoil of the body needs to stall before the airfoil of the wing and therefore it can be expected that the body airfoil often operates at relatively high angles of attack. Finally, it should have a large inherent pitch up moment, so that the overall moment coefficient of the whole glider is positive and satisfies Equation 5.2.

Integrated Wingbody Design

After selecting an appropriate airfoil for the body and finalising the sizing of the payload, the dimensions of the body were defined. This was done by fitting the body airfoil around the payload box, encapsulating it entirely. Subsequently, the wing planform design from phase 1 was attached to the body and analyses of the integrated wingbody were performed in XFLR5. XFLR5 is an airfoil and wing analysis software specifically created for the design of model aircraft. Due to the limited wingspan of 8 [m] given in R_EG_REG_01, the software is particularly appropriate for the design of the EcoGlide glider. The results should, however, be interpreted with care and validated as soon as a physical model of the glider can be built. This is currently outside the scope of the report. The planform obtained in phase 1 was used as a baseline for the integrated wingbody from which iterations were performed. During these iterations, the parameters that define the geometry were optimised to obtain a high-performance glider. Additionally, the static stability was analysed by inspecting the stability derivatives. Finally, the dynamic stability was also analysed by inspecting the eigenvalues of the symmetric and asymmetric state matrices generated by the software.

The numerical aerodynamic models that were used for this approach are explained in section 5.3. The actual design that resulted from this approach follows in section 5.4, 5.5 and 5.6.

5.3. Aerodynamic models

For the aerodynamic design of the glider, two models were created. A lifting-line model was created to get an estimate of the aerodynamic properties of a finite wing. This is a rather simple approach and therefore has its limitations. To analyse the wing planform in more detail, a second model based on lifting-surface methodology, also referred to as vortex lattice method, was created. Both models are discussed below.

Lifting-line Model

The classical lifting-line theory is a powerful tool for preliminary calculations of finite wings and therefore was used as a first design tool [29]. This report will only highlight the most important steps of lifting-line theory in order to set up the model. The reader is referred to books on aerodynamics for an elaborate derivation [7] [29].

Assumptions

The lifting line model has some limitations due to the assumptions that are made. These assumptions together with their influence are listed below.

- *The flow is inviscid.*

Effect: This means that the wing will create no drag except lift induced drag. Hence no prediction of the overall drag coefficient can be made. Additionally, highly viscous phenomena such as stall cannot be modelled.

- *The flow is incompressible.*

Effect: Due to the low velocity of the glider, which will be flying much slower than Mach 0.3, the assumption of incompressible flow is justified. Therefore, it has almost no effect on the EcoGlide case.

- *The flow is steady.*

Effect: Steady flow has constant flow properties with time. Hence the freestream density or velocity are assumed constant. Although these will change during the flight, this assumption is considered appropriate to obtain first estimates.

- *The bound vortices are coincident along the lifting-line where the circulation distribution only varies along the wingspan and not along the chord.*

Effect: The model's use is limited to high-aspect-ratio unswept wings. Since the flying wing requires sweep for stability, a more elaborate model is required to find the required sweep angle.

Theoretical model

In essence, the theory replaces the wing by a finite number of horseshoe vortices running over a single line, called the lifting-line. These vortices are bound to the wing along that line and continue as free-trailing vortices from the wing tips to infinity. These free-trailing vortices are required by Helmholtz's theorem, stating that a vortex filament cannot simply end in a fluid.

The presence of vortices causes a circulation distribution along the wing, which can be used to calculate aerodynamic properties from the Kutta-Joukowski theorem: $L'(y_0) = \rho_\infty V_\infty \Gamma(y_0)$. In order to use this concept for preliminary calculations, the fundamental equation of lifting-line theory is exploited, given in this report as Equation 5.10 [29].

$$\alpha(y_0) = \frac{\Gamma(y_0)}{\pi V_\infty c(y_0)} + \alpha_{L=0}(y_0) + \frac{1}{4\pi V_\infty} \int_{-\frac{b}{2}}^{\frac{b}{2}} \frac{(\frac{d\Gamma}{dy})dy}{y_0 - y} \quad (5.10)$$

This equation states that the geometric angle of attack α is the sum of the effective angles of attack and induced angles of attack at each position y_0 along the lifting-line. For a certain wing geometry, $c(y_0)$ is the chord distribution, $\alpha_{L=0}$ the zero lift angle of attack, b the wingspan and V_∞ is the freestream velocity. The only unknown in Equation 5.10 is the circulation distribution $\Gamma(y_0)$. Once the circulation distribution $\Gamma(y_0)$ is known, the aerodynamic characteristics of a finite wing can be calculated. To solve Equation 5.10 numerically, a Fourier sine series was used.

$$\Gamma(y_0) = 2bV_\infty \sum_1^N A_n \sin(n\theta) \quad (5.11) \quad \alpha(\theta_0) = \frac{2b}{\pi c(\theta_0)} \sum_1^N A_n \sin(n\theta_0) + \alpha_{L=0}(\theta_0) + \sum_1^N n A_n \frac{\sin(n\theta_0)}{\sin(\theta_0)} \quad (5.12)$$

The series is shown in Equation 5.11, where N can be chosen based on the required accuracy. The coefficients A_n are calculated by inputting the circulation distribution, given in Equation 5.11, in Equation 5.10 and performing a transformation of the coordinate along the wingspan. The transformation $y_0 = \frac{-b}{2} \cos(\theta_0)$ is used to simplify the expressions that calculate the aerodynamic characteristics of the wing. This then gives Equation 5.12.

This equation is evaluated at each spanwise location θ_0 resulting in N unknown coefficients A_n . However, this equation is evaluated at N different spanwise locations θ_0 resulting in a system of N equations that can be solved algebraically. Once the values of the coefficients A_n and thereby the circulation distribution $\Gamma(y_0)$ are established, one can calculate the aerodynamic characteristics of the wing using Kutta-Joukowski. The lift distribution follows directly from Kutta-Joukowski and the induced angle of attack can be calculated using Equation 5.12. The lift coefficient and induced drag coefficient can be calculated using Equation 5.13 and 5.14, respectively. The span efficiency factor is calculated using Equation 5.15. Note that in these equations AR represents the aspect ratio of the wing.

$$C_L = A_1 \pi AR \quad (5.13) \quad C_{D,i} = \frac{(C_L)^2}{\pi e AR} \quad (5.14) \quad e = (1 + \sum_2^N n (\frac{A_n}{A_1})^2)^{-1} \quad (5.15)$$

As can be seen from the expressions above, this is a simple yet powerful tool to obtain first estimates of the aerodynamic characteristics of the wing.

Results

The lifting line model is implemented as a Python code. This code is able to calculate the aerodynamic characteristics of any arbitrary wing, given that it has zero sweep and dihedral. The code returns the lift distribution along the wing and uses Equation 5.13 to 5.15 to calculate aerodynamic parameters C_L , $C_{D,i}$ and e respectively. An example of the model output is shown in Figure 5.1, which uses the initial wing planform design from section 5.4 as input. The blue line given in the plot represents the spanwise lift distribution over the entire wing, where the negative coordinate represents the left half of the wing half and the positive coordinate the right half of the wing.

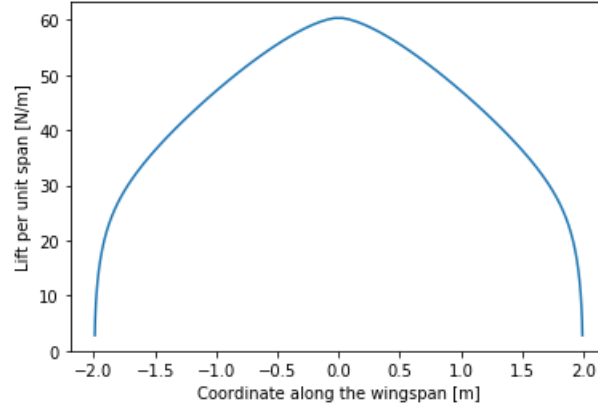


Figure 5.1: 2D lift distribution computed by lifting-line model

Lifting surface Model

In order to analyse the required sweep angle of the wing, a more elaborate lifting-surface or vortex lattice model was created. This is done by eliminating the last assumption stated for lifting-line model and allowing the circulation distribution to vary both in spanwise and chordwise direction. Once again, this report will only highlight the most important steps of lifting-surface theory to create the model. The reader is referred to aerodynamic textbooks for a more thorough derivation [7] [29].

Assumptions

The lifting surface model can be derived after making some simplifying assumptions. These assumptions are elaborated below. Note that the first three assumptions and corresponding influence are identical to the lifting-line model, therefore their effects are omitted for brevity.

- *The flow is inviscid.*
- *The flow is incompressible.*
- *The flow is steady.*
- *The free-trailing vortices extend to infinity in a straight line parallel to the body axis of the glider.*

Effect: The model's use is limited to wing geometries with small curvatures. If highly curved profiles are selected, the accuracy of the obtained results will decrease.

Theoretical model

In essence, the method discretises the wing into a number of panels which are used to model the effect of the wing on the incoming flow. On each panel, a horseshoe vortex is positioned together with a control point. The velocities induced by the horseshoe vortices are then assessed at each control point using the Biot-Savart law [7]. The contributions to all control points are summed to obtain a set of linear equations from which the vortex strengths can be calculated. Each of these linear equations must satisfy the tangency condition at the control point stating that no flow can penetrate the wing.

The bound vortex or lattice on each panel coincides with the quarter-chord line of that panel and is therefore aligned with the local sweep angle. The control point is placed on the three-quarter-chord line of the panel, halfway between both trailing vortices. The model exploits linearisation which means that the free-trailing vortices extend to infinity in a straight line parallel to the body axis of the glider rather than following the curvature of the airfoil. This simplifying assumption provides suitable accuracy for many engineering applications and is therefore deemed appropriate [7].

By applying the boundary condition at each control point for the induced velocity, a set of simultaneous equations is created. The unknowns in the equations are the vortex circulations strengths Γ_n , as was the case for the lifting-line model. Equation 5.16 is used to calculate the induced velocity at the control point of panel m caused by vortex n . In this equation (x_m, y_m) represents the coordinates of the control point whereas (x_{1n}, y_{1n}) and (x_{2n}, y_{2n}) represent the coordinates of the the left and right corner of the bound vortex respectively per panel.

$$w_{m,n} = \frac{\Gamma_n}{4\pi} \left[\left(\frac{1}{(x_m - x_{1n})(y_m - y_{2n}) - (x_m - x_{2n})(y_m - y_{1n})} \right) \left(\frac{(x_{2n} - x_{1n})(x_m - x_{1n}) + (y_{2n} - y_{1n})(y_m - y_{1n})}{\sqrt{(x_m - x_{1n})^2 + (y_m - y_{1n})^2}} - \frac{(x_{2n} - x_{1n})(x_m - x_{2n}) + (y_{2n} - y_{1n})(y_m - y_{2n})}{\sqrt{(x_m - x_{2n})^2 + (y_m - y_{2n})^2}} \right) + \frac{1}{y_{1n} - y_m} \left(1 + \frac{x_m - x_{1n}}{\sqrt{(x_m - x_{1n})^2 + (y_m - y_{1n})^2}} \right) - \frac{1}{y_{2n} - y_m} \left(1 + \frac{x_m - x_{2n}}{\sqrt{(x_m - x_{2n})^2 + (y_m - y_{2n})^2}} \right) \right] \quad (5.16)$$

After summing the contributions of all panels given in Equation 5.17, where $2N$ is the total number of panels, and applying the tangency condition given in Equation 5.18, one obtains a set of linear equations that can be solved to find Γ_n . This set of linear equations can be solved to get the circulations strength of every horseshoe vortex.

$$w_m = \sum_{n=1}^{2N} w_{m,n} \quad (5.17) \quad w_m + V_\infty \sin(\alpha) = 0 \quad (5.18)$$

Once the circulation distribution along the wing is known, one can calculate C_L and C_{Di} of the wing using Kutta-Joukowski. This is given in Equation 5.19 and 5.20 respectively, where Δy_n is the width of the bound vortex of panel n .

$$C_L = \frac{2}{V_\infty S} \sum_{n=1}^{2N} \Gamma_n \Delta y_n \quad (5.19) \quad C_{Di} = \frac{C_L^2}{\pi AR} \quad (5.20)$$

From the expressions above, it can be seen that this is a powerful tool to obtain aerodynamic properties of swept wings. The model is able to calculate the longitudinal position of the centre of pressure, by taking the average of each panel's distance to the leading edge, weighted by their contribution to the total lift. It will be used in combination with a centre of gravity estimation to determine the required sweep angle.

Results

The lifting surface model is implemented as a Python code. The code is able to generate a 3D lift distribution for a symmetric wing and calculate the associated $\frac{C_L}{C_{Di}}$ ratio. The total lift can also be an output of the model, calculated by summing the contribution of each panel, which is a useful sensibility check of the design. An example of the model output is shown in Figure 5.2, which uses the initial wing planform design from section 5.4 as input. The input is shown in Figure 5.3 and in the output as well. This output can also be used to compute the centre of pressure for preliminary longitudinal stability analyses.

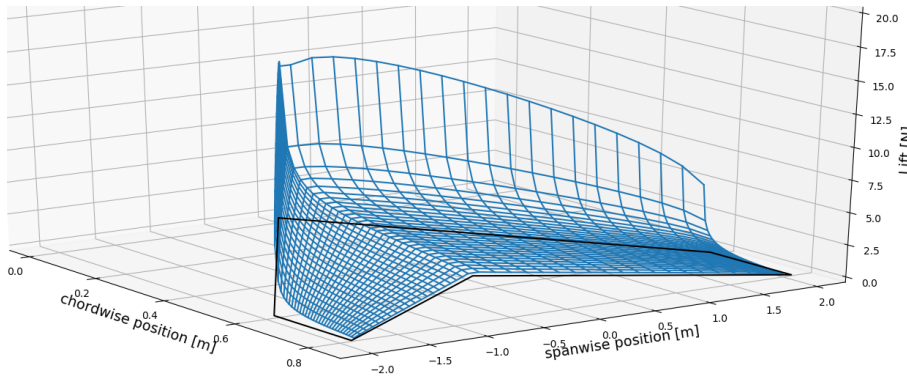


Figure 5.2: 3D lift distribution computed by lifting-surface model

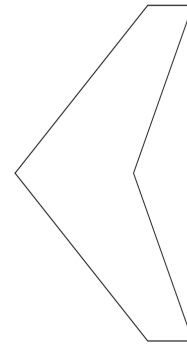


Figure 5.3: Input geometry

5.4. Wing Planform Design

The planform design started with sizing the surface area of the wing based on landing conditions. This was done by using Equation 5.3. For landing, the free stream velocity was set at $15 [m/s]$, as given in R_EG_AED_01, to limit the impact upon landing. The free stream density was assumed to be a standard sea-level value of $1.225 [kg/m^3]$. The weight of the glider was considered to be the maximum take-off weight of $245 [N]$. The maximum lift coefficient of the wing was derived based on several reflex airfoils for a Reynolds number of $5 \cdot 10^5$. This Reynolds number was based on landing conditions and an assumed average chord of $0.4 [m]$. The C_{Lmax} was estimated to be 1.3 using an online airfoil database.^{3 4 5 6 7} Rearranging Equation 5.3 and using the above values as input, a wing surface area of $1.5 [m^2]$ was obtained.

The next step was to calculate the aspect ratio of the wing planform. First, the required glide ratio that provides an 80% availability at both mission locations as required by R_EG_PERF_07 had to be determined. The performance analysis resulted in a minimum C_L/C_D ratio of 33.5, which is equivalent to the required glide ratio. An exact explanation on how this number was obtained can be found in section 5.9. Secondly, the zero lift drag coefficient C_{D0} was estimated using Equation 5.6. The friction coefficient and wing surface area were both known at this point, and the total wetted area was graphically estimated. The accuracy of this estimate increased with increasing number of design iterations. The Oswald efficiency factor was estimated to be 0.97 using a method proposed by literature [48]. Inputting these values into Equation 5.7, an aspect ratio of 10.4 was calculated. The wingspan and average chord could then be calculated

³URL <http://airfoiltools.com/airfoil/details?airfoil=pw75-pw> [cited 11 Jun 2020]

⁴URL <http://airfoiltools.com/airfoil/details?airfoil=naca25112-jf> [cited 11 Jun 2020]

⁵URL <http://airfoiltools.com/airfoil/details?airfoil=naca24112-jf> [cited 11 Jun 2020]

⁶URL <http://airfoiltools.com/airfoil/details?airfoil=e335-il> [cite 11 Jun 2020]

⁷URL <http://airfoiltools.com/airfoil/details?airfoil=mh60-il> [cited 11 Jun 2020]

straightforwardly, using Equation 5.8 and 5.9, which resulted in a wingspan of 3.96 [m] and an average chord of 0.38 [m].

The next step was to determine the required taper ratio λ . The lifting-line model as described in section 5.3 was used. The input to the model was the geometry as given above without twist, dihedral or sweep. The optimal taper ratio was defined as the value resulting in the maximum $\frac{C_L}{C_{Di}}$, as can be seen in Figure 5.4. This resulted in a taper ratio of 0.38. It should be noted that although the value of the maximum $\frac{C_L}{C_{Di}}$ is dependent on both freestream velocity and angle of attack, the taper ratio resulting in maximum $\frac{C_L}{C_{Di}}$ is independent of these conditions. Therefore a generic case of $\alpha = 2$ [deg] and $V_\infty = 30$ [m/s] was used to obtain Figure 5.4.

The final step of the wing planform design was to define the sweep angle Λ . Wing sweep is needed for longitudinal stability and also increases resistance to yaw disturbances, the so-called weather vane stability. To determine the sweep angle needed for longitudinal stability, a lifting-surface model was created. The aerodynamics and performance department also made a simple class I weight estimation tool to predict the total weight of the glider and the longitudinal position of the centre of gravity. These tools could then be combined to calculate the static stability margin for a range of sweep angles, which is shown in Figure 5.5. The initial minimum static stability margin was set at 10%, and the resulting optimum sweep angle was 15°. With this sweep angle the wing planform was deemed sufficiently stable. It should however be noted that this optimum sweep angle was likely to be altered when the complete design of body and wing would be integrated due to the large influence it has on stability.

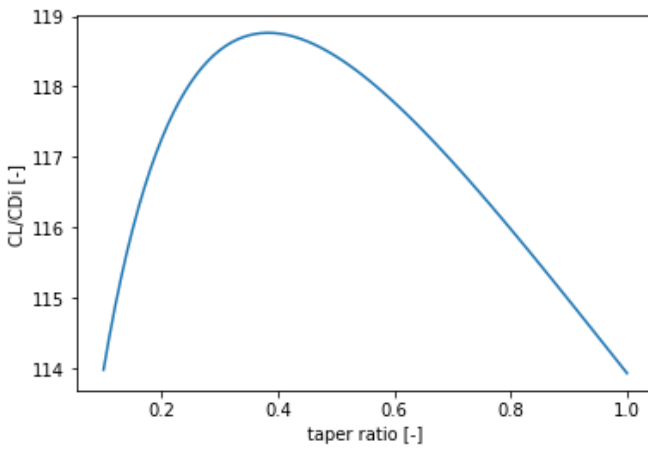


Figure 5.4: Glide ratio $\frac{C_L}{C_{Di}}$ as a function of taper ratio

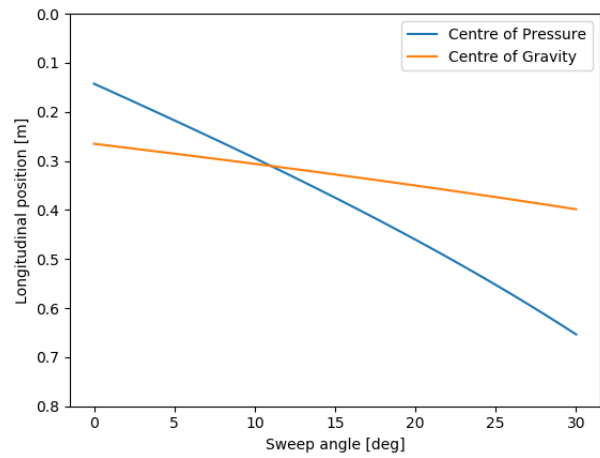


Figure 5.5: Static margin as function of sweep angle

The wing planform design is summarised in Table 5.2 to improve transparency and research reproducibility. The table shows the relation between the parameters in the design and gives the value of the wing planform parameters.

Table 5.2: Wing planform design summary

Parameter	Input	Model	Value
S	$W, n, V_{landing}, \rho_0, C_{Lmax}$	Equation 5.3	1.5 [m ²]
AR	$\frac{C_L}{C_D}, C_{d_0}, e$	Equation 5.7	10.4 [-]
b	S, AR	Equation 5.8	3.96 [m]
c_{avg}	S, b	Equation 5.9	0.38 [m]
λ	S, AR, $\frac{C_L}{C_D}$	Lifting line model	0.38 [-]
Λ	S, AR, λ , Class I weight estimation	Lifting surface model	15 [deg]

5.5. Airfoil Selection

Airfoil sections could now be added to the wing planform. For the wing and body design, two different airfoils were selected. First, an airfoil was chosen for the main wing of the glider, followed by the selection of an airfoil for the body.

Main Wing Airfoil

For the main wing, it was decided to only consider airfoils with reflex. These airfoils are characterised by an upward curvature of the chord line near the trailing edge, thereby creating downforce to obtain a favourable moment coefficient. This is especially relevant for tailless aircraft such as the EcoGlide glider. The different airfoils considered were already introduced before when estimating the maximum lift coefficient and were taken from an online airfoil database⁸. In order to find the most suitable airfoil, a trade-off was performed. The different trade-off criteria considered together with their corresponding weights are given below. It should be noted that each criterion was assigned

⁸URL: <http://www.airfoiltools.com> [cited 14 June 2020]

a weight ranging from 1 to 10 based on their importance. This was then normalised into a percentage such that all weights sum to 100%.

Trade-off Criteria

Maximum lift coefficient: determines the wing surface area required to satisfy the landing conditions. The larger the maximum lift coefficient, the smaller the required surface area which results in a lighter, less draggy design operating at higher wing loading. Since this parameter influences multiple design aspects, a weight of 9 was deemed appropriate.

Angle of attack at maximum lift coefficient: should be as high as possible such that during normal cruise conditions, a wind gust cannot increase the angle of attack above that for maximum lift, thereby avoiding stall. This is however only important when flying at high angles of attack whereas the intent is to limit the cruise angle of attack of the glider as much as possible. Hence this criterion was weighted with a 4.

Lift coefficient at zero angle of attack: should be as high as possible such that the design lift coefficient can be attained at a low angle of attack, creating less drag. The drag directly influence the range that can be attained by the glider and therefore this criterion was given a weight of 7.

Minimum drag coefficient: needs to be minimised to create an efficient aerodynamic design. Reducing the drag created by the glider means that an increased glide ratio can be achieved when providing the same lift. Following the same reasoning as for the previous criterion, a weight of 7 was chosen.

Lift coefficient at minimum drag: should be as close as possible to the design lift coefficient, estimated to be somewhere between 0.3 and 0.6, as it will result in a reduced drag at the design point itself. Once again following the reasoning from above, this was given a weight of 7.

Maximum glide ratio: needs to be maximised as it directly affects the range performance of the glider. Since range is the primary performance requirement for the glider, this criterion was given the highest score of 10.

Lift coefficient at maximum glide ratio: should be as close as possible to the design lift coefficient, which is estimated to be in the range of 0.3-0.6. Reaching the maximum glide ratio close to the design lift coefficient means that one can profit more from the glide ratio attained by the airfoil. Therefore a weight of 8 was chosen.

Width of drag bucket: is favourable to be as wide as possible. Having a wide drag bucket results in having a large operational range with efficient aerodynamic characteristics. Even though this criterion assesses the operational flexibility of the design, the glider's payload will be fixed for all missions. Therefore a medium weight of 5 was given as it still might allow for opportunities in different markets.

Static longitudinal stability: should be as small as possible. Having a negative C_{M_α} results in a longitudinally statically stable configuration. However, when the value is positive but small in magnitude, the wing planform can be adjusted to create stable glider although less efficiently. Since part of the challenge in designing a flying wing lies in efficiently creating a stable configuration, a weight of 8 was selected for this criterion.

Moment coefficient at zero lift: is wanted to have a small absolute value to allow for trimming of the aircraft. The airfoil itself however does not contribute largely to the moment of the aircraft when using the stabilising body design as explained before. Therefore a small weight of 3 was deemed appropriate.

Stall behaviour: it is required to obtain gradual stall behaviour for the glider. This is to allow sufficient time to the control system to recover from this stall and to make sure the landing behaviour can be predicted. Since the chosen landing method is a stalled landing, this criterion was given a weight of 8.

The resulting normalised criteria weights are summarised in Table 5.3.

Table 5.3: Airfoil selection criteria weights

$C_{l_{max}}$	$\alpha@C_{l_{max}}$	C_{l_0}	$C_{d_{min}}$	$C_{l}@C_{d_{min}}$	$\frac{C_l}{C_d}_{max}$	$C_l@\frac{C_l}{C_d}_{max}$	Drag bucket	C_{m_α}	$C_m@C_l = 0$	Stall
12%	5%	9%	9%	9%	13%	11%	6%	11%	4%	11%

Trade-off Results

The scoring of each airfoil per criterion was done based on the scoring scale given in Table 5.4. The score was provided based on the numerical value of the aerodynamic properties of the airfoils, where the average values were credited a 3, the excellent values a 5 and the unacceptable values a 1. It should be noted that the aerodynamic properties of the airfoils were obtained from an identical 2D analysis in XFLR5, using a Reynold number of $5 \cdot 10^6$ and an amplification factor of $N_{crit} = 9$, to ensure a fair comparison was performed. A summary of the trade-off can be found in Table 5.5.

Table 5.4: Airfoil selection trade-off scoring scale

Score	1	2	3	4	5
Level of performance	Unacceptable	Correctable	Acceptable	Good	Excellent

Table 5.5: Summary table of airfoil trade-off

Criterion	Airfoil					Trade-off Score				
	HS522	MH60	NACA25112	NACA22112	Eppler335	HS522	MH60	NACA25112	NACA22112	Eppler335
$C_{l_{max}}$	1.268	1.247	1.359	1.455	1.359	2	2	3	4	3
$\alpha@C_{l_{max}}$	11.75	12.0	13.5	15.25	12.25	3	3	4	5	3
C_{l_0}	0.189	0.112	0.112	0.073	0.145	5	3	3	2	4
$C_{d_{min}}$	0.00582	0.00594	0.00729	0.00664	0.00802	5	5	3	4	2
$C_{l}@C_{d_{min}}$	0.0754	0.0599	0.0531	-0.0028	-0.1769	5	3	3	2	2
$\frac{C_l}{C_{d_{max}}}$	83.315	82.83	89.93	67.66	81.33	3	3	4	2	3
$C_{l}@C_{d_{max}}$	0.8043	0.8159	1.0486	1.1326	1.1833	4	4	3	2	2
Drag bucket	1.7	1.73	2.03	1.95	1.76	3	3	4	4	3
C_{m_a}	-0.021	-0.14	-0.010	0.0042	-0.0014	4	5	4	2	3
$C_{m}@C_{l=0}$	-0.010	-0.016	-0.0015	0.0057	0.027	2	2	3	4	5
Stall	excellent	good	good	acceptable	correctable	5	4	4	3	2
<i>Final Trade-off Result</i>						3.82	3.45	3.46	2.89	2.78

From the table above it is clear that HS 522 is the most suitable airfoil for the wing of the glider having the highest overall score of 3.82. A graphical representation of this airfoil can be seen in Figure 5.6.

A sensitivity analysis of the airfoil trade-off was performed where both the scores and weights of the trade-off were altered. The conclusion is given, but the analysis' details are omitted for the sake of brevity.

In the vast majority of cases, the HS 522 airfoil remained the preferred outcome based on the trade-off results. Therefore it was concluded that the trade-off conclusion is robust and that the airfoil could be included in the wing design.

Body Airfoil

The design philosophy for the aerodynamic package of the EcoGlide glider was to have a stabilising body section. Where the wings would be responsible for generating almost all lift, the body section would be focused on minimising drag and producing a large pitch up moment, while fitting all the payload inside to comply with requirement R_EG_ENBD_03. Because no existing airfoil could be found that met all those requirements, the aerodynamics and performance department took it on themselves to design a 2-D airfoil section from scratch. This subsection describes the airfoil section that will be used for the body of the EcoGlide glider.

The design of the body section was an iterative process. The start of the design were the requirements: it should have a high pitch up moment and it should be able to fit the payload. Several iterations were then made to optimise the design for minimum drag. A simple Excel tool was made to generate DAT files from drawn airfoil geometry. These DAT files could then be used as input to the XFLR5 software for aerodynamic analysis.

The space needed for payload in the chordwise plane consisted of two rectangles with dimensions 0.12x0.16 [m], separated by a spar with an assumed thickness of 0.06 [m]. This made for an effective rectangle of 0.12x0.38 [m] that had to be fully enclosed by the body section. The aforementioned Excel tool was also used to check the fit.

The body section that is used for the final design is the third iteration. The profile features a strongly curved surface at $\frac{1}{4}$ chord at the upper side and a strongly curved surface at $\frac{3}{4}$ chord at the lower side to produce a pitch up couple moment. It also has a distinct reflexed trailing edge to further increase the moment coefficient. The shape of this airfoil can be seen in Figure 5.7.

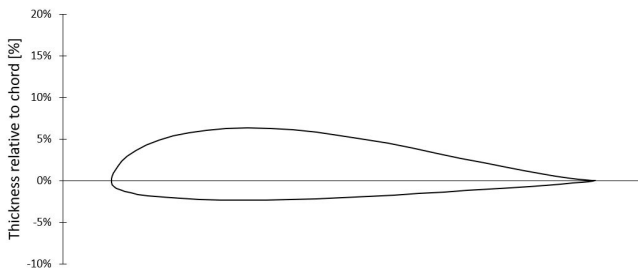


Figure 5.6: HS 522 airfoil section

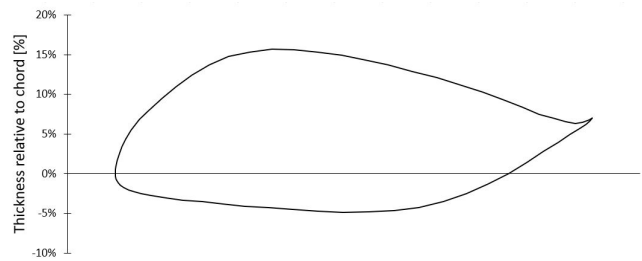


Figure 5.7: Body airfoil section

5.6. Integrated Wingbody Design

Once the design of the body section was established, an integration of the wing planform with the body was required. The basic wing design as given in section 5.4 was cut halfway through and both halves were attached to the body. This provided a baseline for the glider from which design iterations were performed. The analysis of the integrated wingbody design was performed in XFLR5 and provided the results as given in Figure 5.8 to 5.10, where a comparison is made between the initial and final configuration.

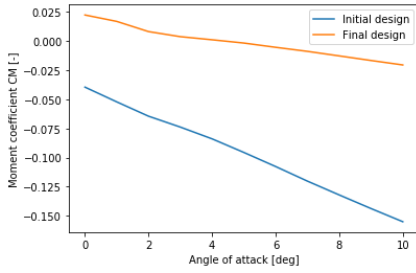


Figure 5.8: Comparison of moment coefficient C_m as a function of angle of attack α .

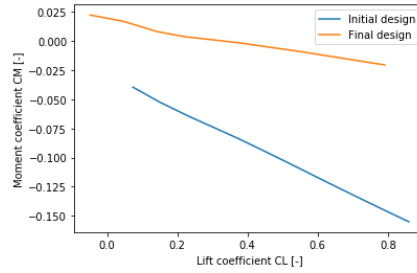


Figure 5.9: Comparison of moment coefficient C_m as a function of lift coefficient C_L .

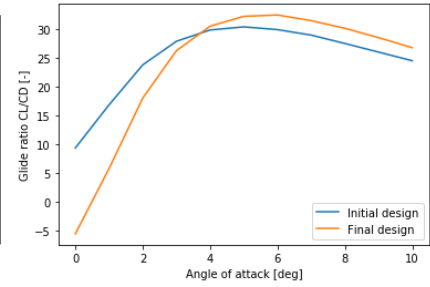


Figure 5.10: Comparison of glide ratio $\frac{C_L}{C_D}$ as a function of angle of attack α .

As explained before, it is required for longitudinal stability that C_{M_α} is negative and it is required for longitudinal controllability that C_{M_0} is positive, as given in Equation 5.1 and 5.2. It can be seen that for the initial design, C_{M_α} is indeed negative but C_{M_0} is also negative. The design is therefore stable but not controllable, hence the wing cannot be trimmed when creating positive lift. Additionally it can be seen that the required glide ratio of 33.5 cannot be attained. Design iterations were performed and analysed in XFLR5 to obtain a final design with better stability characteristics and increased performance.

To solve the issues provided above, three main design parameters were adjusted. Firstly, the wing incidence angle was altered. Based on the 2D analysis of the airfoil used for the body, the angle at which drag was minimal could be found. This provided the wing incidence as the body needs to remain at this angle when the main wing flies at its own optimal angle. It resulted in a wing incidence of 2 [deg] meaning that the body is always at an angle of attack that is lower when compared to the main wing. Secondly, washout was introduced for the main wing. The effect of washout is twofold: it provides favourable stall behaviour as the wing tip remains at a lower angle of attack with respect to the root, ensuring that the tip will stall after the root, and washout reduces lift generation at the wing tips which increases C_{M_0} . An optimal design value for washout was set at -4.2 [deg] meaning that the tips are always at angle that is lower by 4.2 [deg] with respect to the root. Finally, the sweep angle was reduced to increase the lift generated by the wing and thereby increasing $\frac{C_L}{C_D}$. Reducing sweep also causes the wing to generate its lift closer to the centre of gravity and thereby increasing C_{M_0} . It was found that a sweep angle of 10 [deg] was most favourable.

After implementing these changes to the wing design and inspecting Figure 5.8, C_{M_α} remains negative and therefore the design is longitudinally stable. Additionally it can be seen that the moment coefficient C_M is zero at a positive angle of attack $\alpha = 4.4$ [deg] resulting in a positive lift coefficient $C_L = 0.332$. Therefore the glider is trimmed at 4.4 [deg] with a corresponding lift of approximately 250 [N]. The glide ratio that can be obtained by the glider at this design point equals 31.13. This is lower than required by availability, imposing a glide ratio of 33.5. It is however not considered an issue as the aerodynamic design currently excludes winglets due to time constraints. It was found that properly designed winglets can increase the glide ratio by 2 to 3, even for high performance sailplanes⁹. Thus, implementing well-designed winglets in a subsequent design iteration will likely increase the glide ratio such that it satisfies the availability requirement.

5.7. Stability Analysis

The static and dynamic stability of the final design were assessed by considering the stability derivatives and eigenvalues of the aerodynamic design. For static stability, longitudinally it is required that C_{M_α} is negative, laterally that C_{L_β} is negative and directionally that C_{N_β} is positive. Additionally, it is required that the magnitude of these derivatives is as high as possible to increase stability. This, however, negatively affects controllability and therefore a balance must be found. The stability derivatives are calculated using XFLR5 after inputting the MTOW and centre of gravity position into the program. This resulted in $C_{M_\alpha} = -0.33217$, $C_{L_\beta} = -0.014487$ and $C_{N_\beta} = 0.001989$. Hence it can be concluded that the final design is statically stable in longitudinal and lateral direction. Since the magnitude of C_{N_β} is close to zero, the glider is assumed to be only marginally stable. Once again this is not considered an issue as the addition of winglets to the design will provide weathervane stability, thereby increasing C_{N_β} . Additionally, if in a future analysis it is found that the magnitude of C_{L_β} is too small, it can be easily increased by adding positive dihedral to the wing. This was however omitted at this design step.

For dynamic stability, the eigenvalues of the symmetric and asymmetric state matrices were calculated using XFLR5. For symmetric motion, two complex conjugate pairs of eigenvalues were obtained. Both conjugate pairs have negative real parts of the eigenvalues and are therefore dynamically stable. For the phugoid motion however, the magnitude of the real part of the eigenvalue is small resulting in low damping. The damping can however be increased by use of the control surfaces of the glider if deemed necessary. For asymmetric motion, one complex conjugate pair and two real eigenvalues were obtained. Both the dutch roll and aperiodic roll motion have negative real parts of the

⁹URL <http://www.soaridaho.com/Schreder/Technical/Winglets/Masak.htm> [cite 14 June 2020]

eigenvalue implying dynamic stability. This is in contrast with the unstable spiral motion containing a positive real part. Therefore spiral stability should be provided by the control system. The eigenvalues are summarised in Table 5.6.

Table 5.6: Eigenvalues of state matrices for symmetric and asymmetric motion

Symmetric Motion		Asymmetric Motion	
Short period motion	$-6.546 \pm 11.54i$	Dutch roll motion	$-0.1121 \pm 0.975i$
Phugoid motion	$-0.006487 \pm 0.5745i$	Aperiodic roll motion	-14.07
		Spiral motion	0.04358

The final step in the stability analysis is to analyse how far aft the neutral point is with respect to the center of gravity, characterising the stability margin. The center of gravity of the entire glider at MTOW is positioned $0.38 [m]$ aft the leading edge of the body whereas the neutral point, obtained from XFLR5, is located at $0.41 [m]$ aft the leading edge of the body. The stability margin was calculated using Equation 5.21.

$$SM = \frac{x_{n.p.} - x_{cg}}{MAC} \quad (5.21)$$

With a mean aerodynamic chord of $0.4 [m]$, this resulted in a stability margin of 7.5%.

5.8. Design Overview

This section summarises the aerodynamic design of the glider and lists recommendations for future development. The design process has been explained in section 5.2 to 5.7 and an overview of the outcomes is given below. Based on the limitations of the current design, recommendations will be made for the next design phase.

Final design

This overview includes the most important aerodynamic characteristics and overall dimensions of the design. The overall dimensions of the aerodynamic subsystem are graphically presented in Figure 5.11. The most important span-wise dimensions, chord lengths at several locations together with the quarter chord sweep angle are denoted.

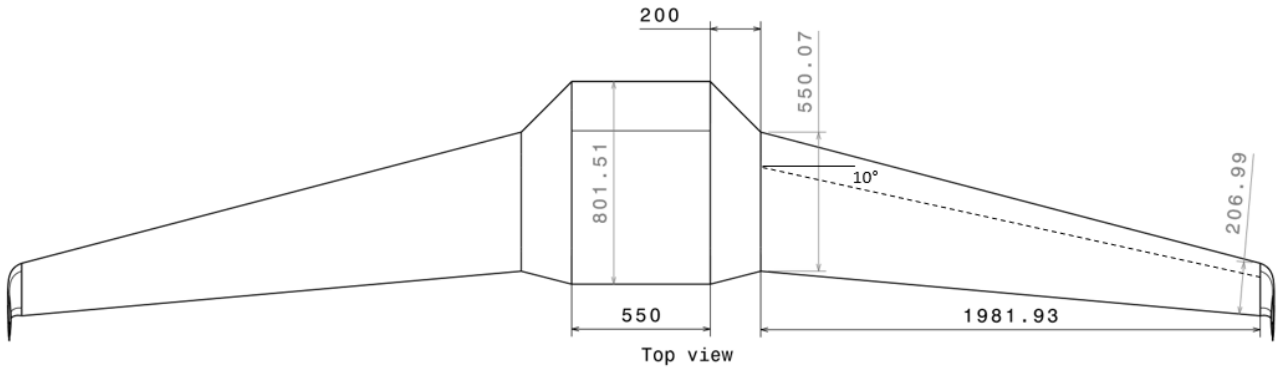


Figure 5.11: Topview of blended wingbody design

The important numbers of the aerodynamic subsystem are listed in two tables below. The dimensions of the subsystem are presented in Table 5.7. The aerodynamic properties of the subsystem are presented in Table 5.8.

Table 5.7: Aerodynamic subsystem dimensions

Parameter	Value
Surface area	$2.21 [m^2]$
Total wingspan	$4.91 [m]$
Wing incidence angle	-2°
Wing mean aerodynamic chord	$0.40 [m]$
Wing aspect ratio	$10.47 [-]$
Wing sweep angle	10°
Wing taper ratio	$0.376 [-]$
Wing washout	4.2°
Wing dihedral	0°

Table 5.8: Aerodynamic subsystem characteristics

Parameter	Value
C_{L_0}	$-0.048 [-]$
C_{L_α}	$4.97 [1/rad]$
α_{trim}	4.4°
$C_{L_{trim}}$	$0.33 [-]$
$\frac{C_L}{C_D}_{trim}$	$31.4 [-]$
C_{M_0}	$0.022 [-]$
C_{M_α}	$-0.33 [1/rad]$
C_{L_β}	$-0.014 [-]$
C_{N_β}	$0.002 [-]$

The aerodynamic properties for a range of angles of attack are shown in the figures below. The lift polar is shown in Figure 5.12 and the drag polar is shown in Figure 5.13. Finally, the moment polar is shown in Figure 5.14.

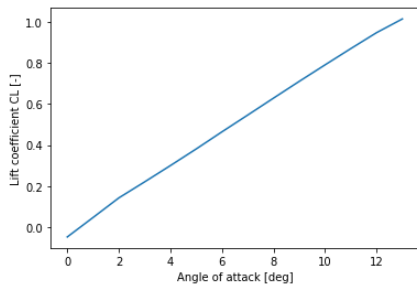


Figure 5.12: Aerodynamic design lift polar

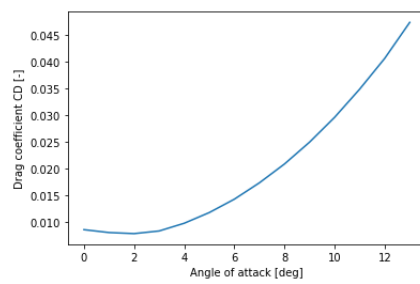


Figure 5.13: Aerodynamic design drag polar

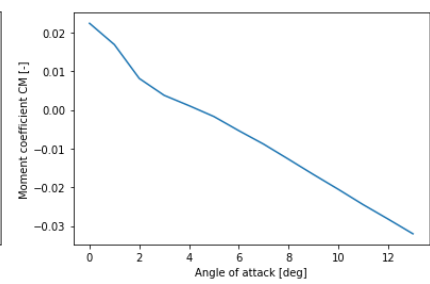


Figure 5.14: Aerodynamic design moment polar

Recommendations

Based on the preliminary aerodynamic design presented above, three main recommendations are made.

Firstly, the winglets included on the glider have to be designed. Efficient winglet design will increase the glide ratio by 2 to 3 units, which is required to satisfy the availability requirement R_EG_PERF_07. Additionally, winglets will increase directional stability of the glider by providing a small vertical surface with sufficient moment arm. Hence C_{N_β} is increased and thereby a statically stable glider is created. It is evident from this discussion that winglets will be part of the glider's design, but their exact shape is still to be determined in a future stage.

Secondly, if the lateral stability needs to be increased it can be done by adding some dihedral to the wing. The dihedral might however affect other aerodynamic properties than just C_{L_β} , which could not be analysed yet due to time constraints. Therefore, if dihedral becomes necessary in a following design phase, it is required to analyse its effect on the aerodynamic performance of the glider and to assess the impact of its implementation.

Finally, it is recommended to validate the results provided by the XFLR5 software with real flight data of the glider. In order to do this, a physical flight model has to be created and hence could not be performed at this design stage. It is however a crucial aspect of the design and is therefore one of the first steps that needs to be executed in the subsequent phase.

5.9. Performance Analysis

In this section the performance of the glider is analysed using two numerical models. The models aim to estimate the effect of the wind on the gliders' performance. The first model takes historic data on wind speed and direction from the two mission locations and determines the probability that the glider can reach the target range in those conditions. Based on the availability requirement R_EG_PERF_07 a minimum $\frac{C_L}{C_d}$ ratio will be proposed. The second model shows the effect of glider weight on the gliders' range in different wind conditions. It will be used to explain why a heavy glider is good for overall performance.

Modelling the effect of wind on availability

This model aims to predict the effect of wind speed and direction on range. The International Standard Atmosphere (ISA) was used as a starting point in the design. However, it was soon recognised that the velocity and direction of the wind have a non-negligible influence on the performance of the glider. Because wind is not included in the ISA model, a computer simulation programme was built to estimate the effects of the wind. The model and its limitations will be described in this subsection. The numerical models used for integration, interpolation and discretisation are build-in functions and will only be discussed very briefly.

Assumptions

When building the model, several assumptions were made as given below.

- *The glider always glides at its maximum $\frac{C_L}{C_D}$.* Without wind, the glider will glide the furthest when flying at its maximum C_L/C_D . However, when a strong headwind or tailwind is present, a C_L/C_D that deviates from the maximum will actually result in the largest range. Because the relation between wind speed and C_L/C_D deviation is non-linear and heavily dependent on the exact aerodynamic characteristics of the glider, this optimum C_L/C_D deviation was neglected.

Effect: The model will slightly underestimate the range of the glider when a strong headwind or tailwind is present. This means that the estimations of the model for the extreme cases are on the conservative side.

- *The glider glides from the launch site towards its destination in a straight line.* The maximum range that is calculated for a specific combination of wind direction and glider heading always assumes that the glider flies in a straight line. If the wind is coming from the side, the glider will alter its heading with a wind correction angle to keep flying straight.

Effect: If it is known that the glider has to take a detour, for example to fly around an air exclusion zone, the range predicted by the model will overshoot the actual value.

- *The balloon that launches the glider does not drift with the wind.* The tethered balloon that is used to launch the gliders will drift with the wind if a strong wind is present. This means that the glider might be launched at a position that is shifted with respect to where the balloon is tethered. However, the location where the balloon is tethered will always be used as the origin of the model.

Effect: Balloon drift will effectively decrease the range of the glider in headwind direction and increase its range in the direction of tailwind. The difference in range due to drift is small compared to the target range, but it will induce an error in the order magnitude of $1e-3$.

- *The wind speed and direction are constant throughout the entire flight.* The model is based on historic wind speed data measured at ground level. Each unique combination of wind speed and wind direction will be assumed as constant for the whole calculation.

Effect: In reality, the wind speed and direction change over time and distance during flight. These effects can only be predicted with more advanced weather models for a given flight trajectory and specific time of the day. Because the wind data is the average of 30 years of hourly weather model simulations, these discrepancies are likely to even out when so many scenarios are calculated for. However, the model can not be used to calculate the range-probability for a single flight.

- *Only the horizontal component of the wind is taken into account.* The available historical wind data was limited to wind velocities in the horizontal plane. This also means that the effect of heat sinks or thermals is not taken into account.

Effect: Because no accurate data was available, the wind effect will only be calculated in the horizontal plane. A vertical wind has much more effect on range than a horizontal wind with the same velocity, however, vertical winds are often smaller in magnitude. The accuracy of the model is limited due to the exclusion of the vertical wind.

- *The wind velocity is assumed to linearly increase in magnitude with increasing altitude.* It is well-known that wind velocity increases with increasing altitude. Based on literature, a wind velocity gradient of $1.5 [m/s/km]$ was determined [33]. This means that the wind velocity at $5 [km]$ altitude is $7.5 [m/s]$ higher than the measured wind velocity at ground level. The direction will remain constant.

Effect: The assumption of a linear wind velocity increase with altitude will introduce an error in the model, as this increase is not truly linear. The value of the gradient was found by a linear approximation of the figure in literature.

- *The temperature at ground level is equal to the minimum temperature of the yearly average.* The temperature has an effect on the range of the glider. If, for example, the ground temperature is high, the air will be less dense and thus the glider can fly faster. That in turn means that the glider is less affected by headwind. The lowest temperature of the monthly average from 30 years will be used.

Effect: Low temperatures decrease glider speed and increase the effect of headwind. Therefore, by taking the lowest temperature, the predicted range is always on the safe side. This assumption thus introduces an error which causes the model to underestimate the range for most of the year.

Theoretical model

The aim is to estimate the effect that wind has on glider performance. The main effect of the wind is that it changes the speed of the glider with respect to the ground, which changes the effective glide ratio. If the glide ratio becomes too low, user requirements on range can not be satisfied anymore and mitigation measures have to be taken.

Since it is assumed that the wind is purely horizontal, only the horizontal component of the gliding velocity will be affected. It can be derived from simple vector addition that the effective glide ratio scales by a factor of V_g/V_a , where V_g is the gliders' speed with respect to the ground and V_a is the true airspeed. Both are a function of altitude h , which results in Equation 5.22. This function can be integrated over altitude to get the total range as shown in Equation 5.23. The deployment altitude is h_0 , usually $5000 [m]$, and the altitude at which landing starts, h_1 , is taken at $50 [m]$ to have some margin for the stall landing.

$$GR = \frac{C_L}{C_D} \cdot \frac{V_g}{V_a} \quad (5.22) \quad \text{Range} = \int_{h_0}^{h_1} \frac{C_L}{C_D} \cdot \frac{V_g(h)}{V_a(h)} dh \quad (5.23)$$

If the ground speed is higher than the airspeed, which is the case for tailwind, the effective glide ratio increases. The expression for the true airspeed can be worked out further using the ISA relations to make it a function of altitude only, with all other parameters constant. Equation 5.24 for true airspeed is taken from literature, Equation 5.25 is taken from ISA relations and Equation 5.26 for the optimum lift coefficient is also taken from literature. [46]

$$V_a = \sqrt{\frac{W}{S} \cdot \frac{2}{\rho} \cdot \frac{1}{C_{L_{opt}}}} \quad (5.24) \quad \rho = \rho_0 \cdot \left(\frac{T_0 + a \cdot h}{T_0} \right)^{\left(\frac{-g}{a \cdot R} \right) - 1} \quad (5.25) \quad C_{L_{opt}} = \sqrt{\pi \cdot C_{d0} \cdot AR \cdot e} \quad (5.26)$$

Similarly, the equation for ground velocity can be worked out such that, for a given wind direction and ground wind speed, it is a function of altitude only. Equation 5.27 for the ground velocity is function of true airspeed, wind speed and wind direction. The wind direction angle ϵ is defined as being 0° when the wind directly opposes the flight direction, i.e. pure headwind [46]. The wind speed is a function of altitude too, as can be seen in Equation 5.28, and is assumed to scale linearly with altitude. The wind speed measured at ground level, V_{gw} , is assumed to be constant and taken from local wind data.

$$V_g = V_a \cdot \sqrt{1 - \left(\frac{V_w}{V_a} \cdot \sin \epsilon\right)^2} - V_w \cdot \cos \epsilon \quad (5.27)$$

$$V_w = V_{gw} + 0.0015 \cdot h \quad (5.28)$$

Numerical methods

The equations from the wind model were implemented in a Python programme to straightforwardly calculate the range for a given combination of ground-level wind speed, wind direction and glider heading. To integrate Equation 5.23, the quad function from the *scipy* integrate module was used. To calculate the range of the glider in all directions, this integration was performed for all possible glider headings, with increment steps of 1° . This results in a circle with an offset from the origin, that shows what range the glider can reach in any direction for a given wind condition.

To get the probability that the glider can reach the required target range, historical wind speed data was used. For the two mission locations, Kabul¹⁰ and Timbuktu¹¹, data on the yearly averages of wind speeds and direction was available. This data is based on a weather model that takes 30 years of data into account. The wind speeds vary between 0 and 50 [km/h]. The wind direction is split up into 16 different directions. The number of hours per year for every combination of wind speed and wind direction are given in the data. Additionally, the lowest average temperature was also provided in these sources.

For every combination of wind speed and wind direction, the range of the glider was calculated. The range was then multiplied by the number of hours per year that this wind condition occurred, and divided by the total number of hours in a year. The results of every wind condition were then added to get the complete range-direction probability. This probability was then evaluated along the circular line of the target range. The probability for every direction was averaged, giving the final result of this model: The average probability that the glider can reach the target range of 125 [km], as specified in requirement R_EG_PERF_03. This is called availability of the glider.

Results

According to R_EG_PERF_07, the average availability of the glider has to be at least 80%. For a given data set on wind speed, the main tool that can be used to alter the availability percentage is the C_L/C_D ratio. With an initial C_L/C_D estimate of 25, which is in theory sufficient to reach a range of 125 [km] from a deployment altitude of 5000 [m], the average availability was less than 50%. That means that the risk of a glider not reaching its destination is too high. To mitigate that risk, the C_L/C_D ratio has to be increased until the 80% barrier has been comfortably cleared. After several optimisation loops, the required C_L/C_D ratio was found to be 33.5.

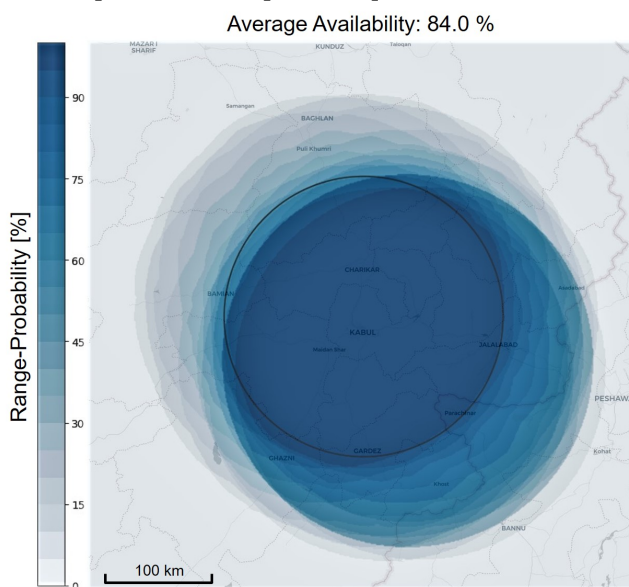


Figure 5.15: Availability heat map Kabul

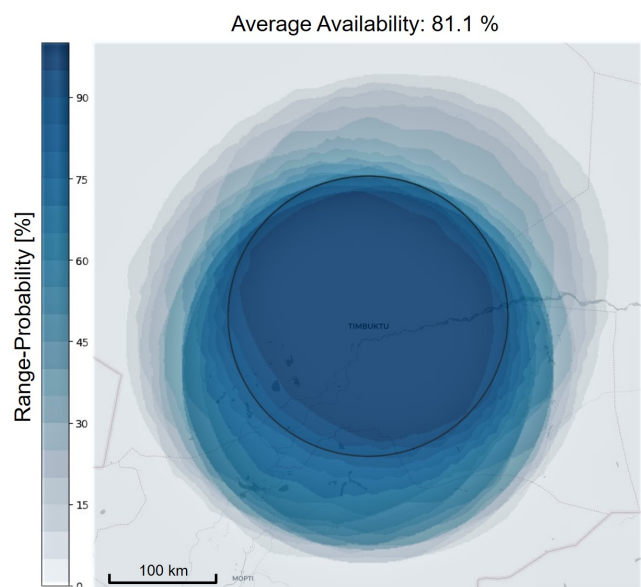


Figure 5.16: Availability heat map Timbuktu

¹⁰URL: https://www.meteoblue.com/en/weather/historyclimate/climatemodelled/kabul_afghanistan_1138958 [cite 12 June 2020]

¹¹URL: https://www.meteoblue.com/en/weather/historyclimate/climatemodelled/timbuktu_mali_2449067 [cite 12 June 2020]

With the C_L/C_D ratio known, the availability heat maps can be made for the two mission locations. The heat map for Kabul is presented in Figure 5.15 and the heat map for Timbuktu is presented in Figure 5.16. The black circle indicates the 125 [km] target range where the availability is calculated. The average availability now exceeds 80% for both mission locations. It should be noted that for the given wind speed data, the range is never less than 60 [km] and can increase up to 275 [km] with the right wind conditions.

Modelling the effect of glider weight on range

This model aims to predict the effect of glider weight on range. It was based on the performance model provided above. The weight of the glider, including payload, was limited to a maximum of 25 [kg] by the customer, as specified in requirement R_EG_ENBD_01. For the design of a conventional aircraft, a logical next step would be to try to save weight where ever that is possible, as it increases performance. However, for the specific application of the EcoGlide project, it is the other way around, as being at the maximum weight limit boosts performance.

Assumptions

The assumptions that were made when the model was built are largely the same as the ones made for the first model in section 5.9. The rationale and effect of these repeated assumptions will be omitted for brevity. The new assumption, however, will be described in more detail.

- *The glider always glides at its maximum $\frac{C_L}{C_D}$.*
 - *The glider glides from the launch site towards it's destination in a straight line.*
 - *The wind speed at ground level and the direction of the wind are constant throughout the entire flight.*
 - *Only the horizontal component of the wind is taken into account.*
 - *The wind velocity is assumed to linearly increase in magnitude with increasing altitude.*
 - *The ground-level temperature is assumed to be 288.15 [K]. A difference in temperature does not create a difference in analysis outcome, as the analysis is only used to compare different glider weights against each other. The choice of temperature is therefore set at ISA sea-level conditions.*
- Effect:** Since the temperature does not create a difference within the model itself, the chosen temperature has no effect on the outcome of the analysis. However, the model output cannot be used to compare with other models or real life data.
- *The surface area of the glider is assumed to be constant.* The final result of the model will predict range for a certain wing loading. This wing loading is basically the weight of the glider, normalised by the gliders' surface area of 1.5053 [m].

Effect: If the weight increases for the same surface area, the landing velocity of that configuration increases. This violates R_EG_AED_01, which prescribes a maximum landing velocity of 15 [m/s]. However, the model is not used for sizing but only to show what the effect of higher glider weight would be. This assumption therefore doesn't influence the final dimensions of the glider, as this is only a conceptual study.

Theoretical model

The theoretical model is very similar to the first performance model, but there were some slight tweaks to suit this performance analysis. The exact derivation as described in the previous section still holds. The leading equation is Equation 5.23, where Equation 5.24 to 5.28 are used to create an integral that can be solved as function of altitude. This gives the theoretical range for any combination of deployment altitude, wind speed, wind direction angle and glider characteristics.

The difference with the previous analysis was that now the range of the glider would be calculated for varying wind directions at different glider weights. For this analysis, the absolute value of the wind speed V_{gw} measured at ground level was set at 11 [m/s] and the wind direction angle ϵ was varied from 0° to 180°. The value for headwind shown in the analysis is equal to $V_{wg} \cdot \cos\epsilon$. It should therefore be noted that at the point of 0 [m/s] headwind, the glider still experiences a wind of 11 [m/s] coming from the side.

Results

The result of this performance analysis is the heat map given in Figure 5.17. The colour indicates range of the glider for a combination of wind velocity and direction, with positive velocities indicating headwind and negative velocities indicating tailwind. Glider weight is normalised by the wing surface area to get wing loading on the horizontal axis.

It is clear from the plot that a lower weight means the glider is more sensitive to wind. A lighter glider will have a range advantage with tailwind, but a much bigger range disadvantage with headwind. For increasing wing loading, the glider

will reach further in headwind conditions while sacrificing only a little range in the tailwind direction compared to a lighter variant. Therefore, a glider that performs well in headwind conditions will have a higher average availability. To conclude, the aerodynamics and performance department recommends to any operator of the glider to always make sure that the glider is at its maximum weight of 25 [kg], as the surface area of the wing is designed for this specific case. The use of ballast is suggested in case the take-off weight is lower than this 25 [kg] to increase the effective range of the glider, while also increasing the gliding speed and thereby shortening the delivery time.

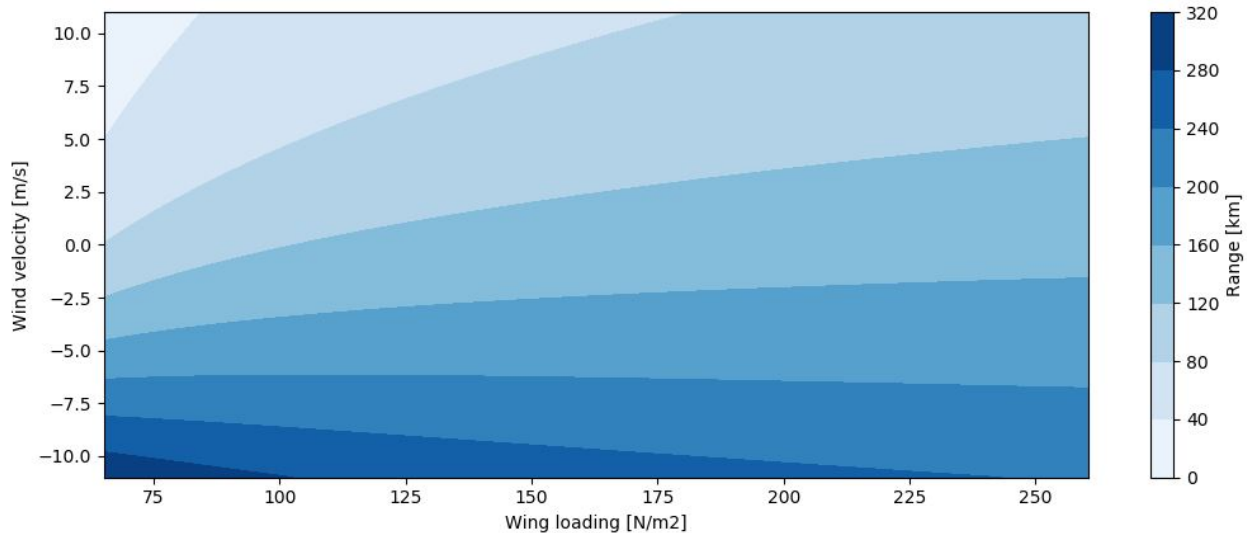


Figure 5.17: Glider range as function of wing loading and wind speed

5.10. Verification & Validation

In order to assure that the results obtained from the models are accurate, verification and validation of those models needs to be performed. This section will elaborate the steps taken to verify and validate the results of the aerodynamic models. Additionally, a brief discussion on the correctness of graphs obtained from performance analysis is given.

Lifting-line Model

For the verification of the lifting-line model, a comparison was made to the analytical solution provided by Anderson for an elliptical lift distribution [29]. In order to generate an elliptical lift distribution, an elliptical chord distribution is needed. This was the input in the lifting-line model and the obtained results are compared to the analytical solution.

In order to verify the program, it was assessed that the lift distribution indeed has an elliptical shape, constant induced angle of attack along the wingspan and a span efficiency factor equal to 1. This is in accordance with the analytical solution and therefore can be assumed to be verified. Additionally, the results of the program for non-elliptical wings are compared to an online lifting-line model. The online model was obtained from a web textbook¹² for university level undergraduate engineers and therefore deemed appropriate. The coefficients of the Fourier sine series given in Equation 5.11 are compared for the online tool and lifting-line model, based on the same input wing. A summary of the wing geometry used in both models is given in Table 5.9.

Table 5.9: Wing geometry used as input for lifting-line models

Parameter	Unit	Value	Parameter	Unit	Value
Wing span	[m]	4.69	Taper ratio	[-]	0.35
Root chord	[m]	0.545	AoA	[deg]	4
Aspect ratio	[-]	12.8	Zero lift AoA	[deg]	0

The results for the coefficients together with the percentage error are summarised in Table 5.10. For symmetric wings, which was the input for both models, all even coefficients A_n are equal to zero [29]. This is clear from the external lifting-line model but for the own model however, these values are non-zero. This occurs due to a rounding error when converting degrees to radians in python resulting in the really small non-zero values. This then also influences the value of the other coefficients resulting in a small error between the coefficients. As can be seen from the table above, the maximum error is only 3.36% and therefore the lifting-line model is assumed to be verified. It should be noted that the error between the even coefficients is so small that it is practically zero in Table 5.10.

¹²URL: <http://www.aerodynamics4students.com/> [cited 12 June 2020]

Table 5.10: Comparison of Fourier coefficients in lifting-line models

Coeff.	External LL model	Own LL model	error [%]	Coeff.	External LL model	Own LL model	error [%]
A1	9.415038e-03	9.38736415e-03	0.294	A9	1.336117e-04	1.33628608e-04	0.013
A2	0.0	-1.12732036e-19	0.0	A10	0.0	-6.51275208e-20	0.0
A3	-5.023560e-05	-5.19230405e-05	3.360	A11	1.597530e-06	1.62531471e-06	1.740
A4	0.0	9.45765669e-19	0.0	A12	0.0	2.43205707e-20	0.0
A5	5.933213e-04	5.92537361e-04	0.132	A13	4.374952e-05	4.37785933e-05	0.066
A6	0.0	6.44145497e-20	0.0	A14	0.0	3.77706281e-20	0.0
A7	7.302729e-05	7.29375582e-05	0.123	A15	-1.803806e-05	-1.80390918e-05	0.006
A8	0.0	-1.74791495e-19	0.0				

The lifting-line model was validated in two ways. First, a comparison with XFLR5 was made. This is another numerical analysis tool and hence not a direct comparison with reality. It was however agreed with the principal tutor to be appropriate for the validation of the lifting-line model. The same input variables as given in Table 5.9 are used together with sea-level atmospheric conditions and a freestream velocity of $V_\infty = 30 [m/s]$. A comparison is made between the lift polars, given in Figure 5.18, and the induced drag polars, given in Figure 5.19. It should be noted that for the XFLR5 wing analysis, first an airfoil has to be selected. Therefore a common symmetric airfoil, NACA 0012, was chosen.

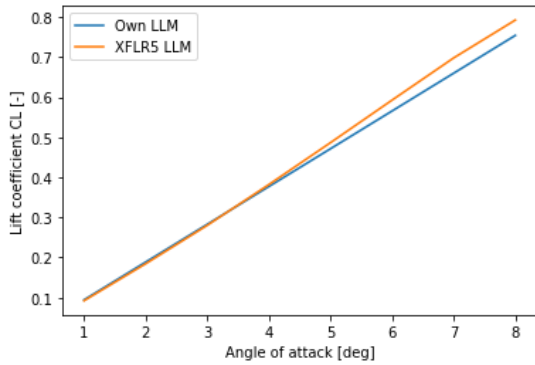


Figure 5.18: Lift polar comparison of lifting-line models

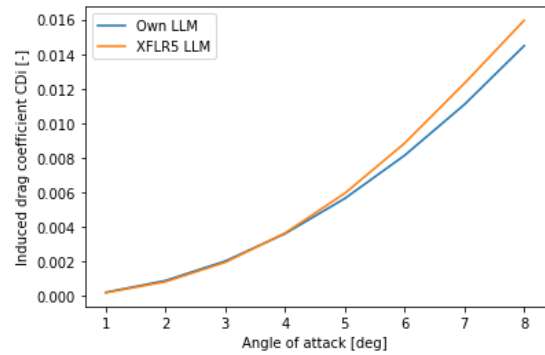


Figure 5.19: Induced drag polar comparison of lifting-line models

The average percentage error is calculated for both polars and resulted in a 3.1% error for the lift polar and a 7.0% error for the induced drag polar. From Equation 5.13 and 5.14 it is clear that the C_L calculation only considers the first Fourier coefficient whereas the C_{D_i} calculation uses all coefficients. As a consequence, a larger error remains for C_{D_i} with respect to C_L due to the rounding error when calculating the coefficients. The comparison is also affected by the fact that a flat plate wing planform was compared to a wing planform with a symmetrical airfoil.

The second validation was done by comparing the lifting-line model to wind tunnel data of finite wings. Since the lifting-line model takes no airfoil curvature into account, a comparison was made with wind tunnel data for a simple flat plate. Two inputs were used for the comparison. The first input was a simple rectangular wing planform with a wingspan of 0.267 [m], where the planform had no taper and a constant chord of 0.089 [m]. The second input was a tapered wing planform with a span of 0.343 [m], a taper ratio of 0.5 and an aspect ratio of 4. The wind tunnel data was obtained at a Reynolds number of 80,000 [24]. The lift curve was compared for moderate angles of attack. The resulting comparison plots for the first and second input are shown in Figure 5.20 and Figure 5.21 respectively.

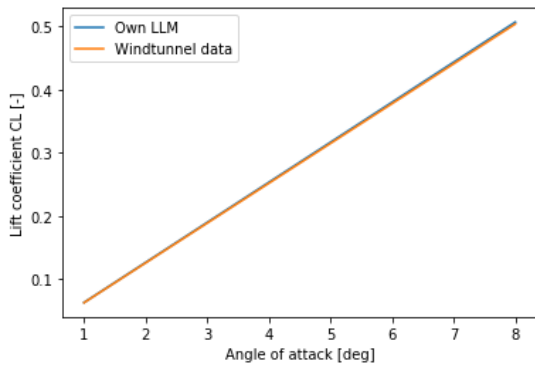


Figure 5.20: Rectangular wing planform lift polar comparison

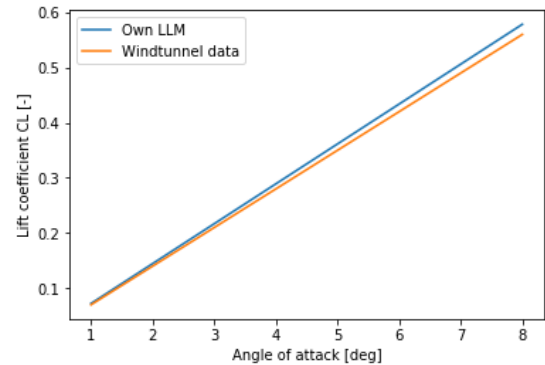


Figure 5.21: Tapered wing planform lift polar comparison

The average percentage error between the lifting-line model and the wind tunnel data is 0.60% for Figure 5.20 and 3.11% for Figure 5.21. Part of this error was caused by converting wind tunnel data graphs to a finite number of points

for the comparison plot. This makes that the accuracy of the lifting-line model is better than expected for a simulation that uses so many simplifying assumptions.

To conclude, the numerical errors are found to be small, as they are caused by rounding rather than an incorrect method. The comparison with another model and wind tunnel data shows that the model gives very realistic outcomes for un-swept wings with slender airfoils. The lifting-line model was therefore deemed sufficiently accurate for the preliminary aerodynamic design of the glider.

Lifting-surface Model

The first verification of the lifting-surface model was done by comparing the numerical model to an analytical solution. A comparison was made with Example 7.4 given in Aerodynamics for Engineers [7] where the circulation distribution of a swept wing geometry is calculated analytically using the vortex lattice method. The input geometry used for the model is summarised in Table 5.11.

Table 5.11: Wing geometry used as input for lifting-surface models

Parameter	Unit	Value	Parameter	Unit	Value
Wing span	[m]	1	Taper ratio	[-]	1
Root chord	[m]	0.2	Tip chord	[m]	0.2
Aspect ratio	[-]	5	Sweep angle	[deg]	45

Each wing half is discretised into 4 spanwise panels, where each panel extends from leading edge to trailing edge. The discretisation of the numerical model is verified by comparing the position of the bound vortices and control points with the coordinates given in Table 7.2 in [7]. All outcomes of the numerical model are exactly equivalent to the analytical solution and therefore the results are omitted in this report.

Since the considered wing is symmetrical, the circulation distributions on the left and right side of the symmetry plane are equal. Hence the circulation distribution of only one side needed to be found, but the influence of both sides needs to be considered when satisfying the tangency condition. The strengths of the circulations for the analytical solution and the numerical lifting-surface model are given in Table 5.12.

Table 5.12: Comparison of circulation distribution in lifting-surface models

Circulation	Analytical solution	Numerical solution	error [%]
Γ_1	0.0273	0.0273	0.0
Γ_2	0.0287	0.0287	0.0
Γ_3	0.0286	0.0286	0.0
Γ_4	0.0250	0.0250	0.0

From the table above, it can be seen that the error is zero and therefore the numerical lifting-surface model is verified.

For validation of the lifting-surface model, once again a comparison is made with XFLR5. The input variables are equal to the ones given in Table 5.9 with an added sweep angle of 30 [deg]. Sea-level atmospheric conditions are used along with a freestream velocity of 30 [m/s] for both models. The selected airfoil is once again NACA 0012. The lift polars are compared in Figure 5.22 and Figure 5.23 compares the induced drag polars.

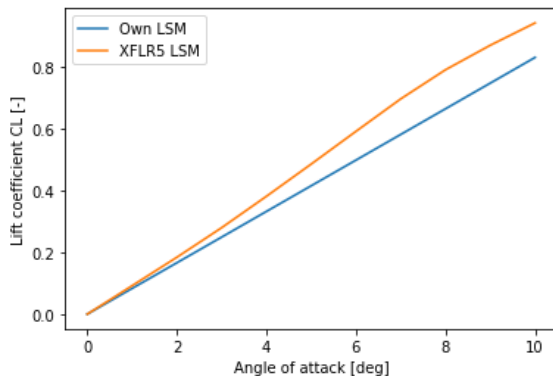


Figure 5.22: Lift polar comparison of lifting-surface models

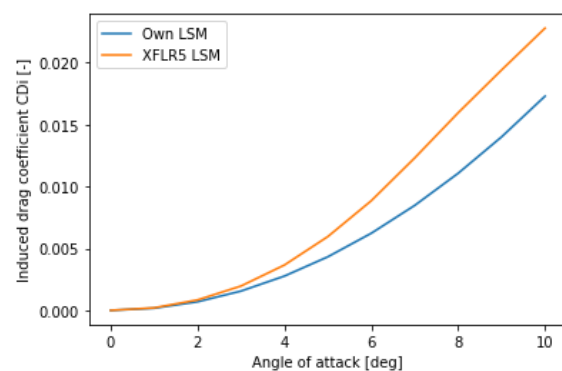


Figure 5.23: Induced drag polar comparison of lifting-surface models

The average percentage error for the lift polar equals 12% and for the induced drag polar 22%. The large discrepancy is caused by the final assumption stated for the lifting-surface model. As given in section 5.3, it was assumed that the free-trailing vortices extend to infinity in a straight line parallel to the body axis whereas for XFLR5, these vortices follow the curvature of the airfoil such that the calculated lift and induced drag coefficients are higher. These

errors are quite high, especially for the calculation of the induced drag. Considering the cause of the discrepancy, the lifting-surface model is assumed to be invalid when results for highly curved wings are required. Furthermore, it was decided to use the lifting-surface model only for a first approximation of the sweep angle of the wing planform. As a consequence, XFLR5 would be used when more accurate results were needed for the aerodynamic design of the glider.

XFLR5 model

Due to wide implementation of the XFLR5 software by professional engineers, it is assumed that no verification of the program is required. Although the software is considered to provide accurate results, it is recommended to validate those results with actual flight data. This is however only possible once a physical model has been created and hence could not be performed at this design stage. Therefore, it is recommended to execute this validation as one of the first steps in subsequent designing.

Performance models

The models for the performance analyses in section 5.9 use the same theoretical method and very similar numerical implementations. The verification of the two models was logically done in near identical fashion and will therefore only be described once. It should be noted that because the models have such an unique and specific application, no appropriate validation could be done.

The performance models rely on the solving of the integral in Equation 5.23. To verify the correct implementation of this equation in the python code, several unit tests were performed and an example case was solved by hand to cross check the outcome. Finally, the code output was compared to that of a similar model made in Excel. All these tests confirmed that the theoretical model had been correctly implemented. For the numerical integration, the module *linalg* from the python package *numpy* was used. This module is widely used and verification showed that its error was only in the order of $1e-9$. Hence the numerical error does not significantly influence the output.

5.11. Sensitivity Analysis

In order to assess the robustness of the aerodynamic design provided above, a sensitivity analysis was performed. In this analysis, the estimated weight, lift and drag were adjusted in a range of $\pm 10\%$ around the base estimate and, based on the current design, the influence of these changes on performance was assessed separately. The effect of these parameters on the gliders availability is graphically represented in Figure 5.24 to 5.26.

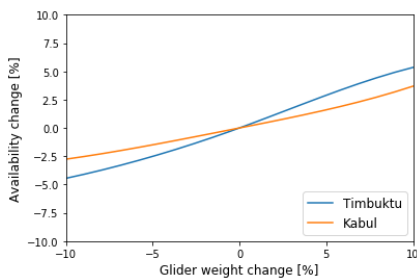


Figure 5.24: Availability sensitivity to weight

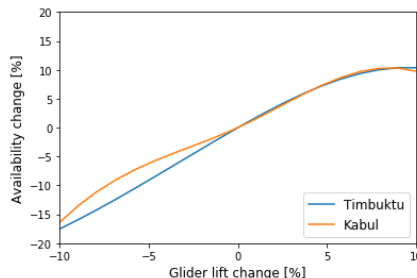


Figure 5.25: Availability sensitivity to lift

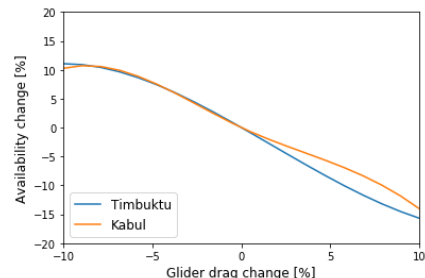


Figure 5.26: Availability sensitivity to drag

The changes in availability per mission location are similar for all graphs. A $\pm 10\%$ change in weight results in approximately a $\pm 5\%$ change in availability. For lift and drag, the design is even more sensitive. A 10% loss of lift or a 10% increase in drag will lead to a reduction in availability of more than 15%. On the other hand, less drag or more lift lead to a better glide ratio which increases the availability by approximately 10%. This means that the glider is more sensitive to a decrease in $\frac{C_L}{C_D}$ than it is to a $\frac{C_L}{C_D}$ increase. To conclude, it is important to accurately estimate lift and drag, as a small changes for these values might mean requirement R_EG_PERF_07 can not be satisfied anymore.

Since lift should equal weight throughout the entire flight, also an effect on landing velocity and payload mass was found as can be seen in Table 5.13.

Table 5.13: Sensitivity of landing velocity and payload mass to aircraft weight and lift

Weight [%]	Landing velocity [%]	Lift [%]	Payload mass [%]
+ 10	+ 4.88	+ 10	+ 23.41
- 10	- 5.13	- 10	- 23.41

When the weight increases and the rest of the design remains unchanged, the landing velocity of the glider will have to increase to avoid stall. In case the weight decreases however, the landing velocity can decrease which is beneficial for impact during landing.

For lift, an increase results in a larger weight that can be carried by the wing. Assuming that the rest of the design remains the same, the mass of the payload can then be increased, whereas a decrease in lift results in a decreased

payload mass that can be carried. It should however be noted that the overall MTOW cannot exceed 25 [kg] as per requirement R_EG_ENBD_01.

5.12. Risk Assessment

This section contains the risk assessment of the glider's aerodynamics and performance. In Table 5.14 the risks are listed along with their mitigation methods. Table 5.15 provides the corresponding risk map, where the global risk level is provided for this subsystem, from which the effectiveness of the risk mitigation method can be derived.

Most of the risks deal with the effect of adverse weather conditions on glider performance and range. These are mitigated by making an analysis of the conditions in section 5.9 and setting a new C_L/C_D ratio to account for them. Inaccuracy of the design tools that were used is mitigated by verification and validation. Local effects such as storms or heat sinks can not be fully accounted for in this stage of the design, and the mitigation of these risks relies on a good flight planning. Finally, the risk of upsets due to gust is mitigated by cruising at the lowest angle of attack possible and having predictable stall behaviour.

Table 5.14: Aerodynamics and performance risks

Index	Risk Factor	Severity	Probability	Risk	Mitigation Method	Severity	Probability	Risk
1	Missing landing area by more than 2km due to lack of range	c	p	mh	Ideal range has been increased from 125 km to 167 km	c	n	l
2	Losing aircraft (lands further than 2km from landing site) due to adverse weather conditions: wind	c	h	h	Higher glide ratio from performance analysis with local wind conditions resulted in availability of 80%	c	i	m
3	Losing aircraft (lands further than 2km from landing site) due to adverse weather conditions: precipitation	c	i	m	Do not fly in stormy conditions	c	n	l
4	Losing aircraft (lands further than 2km from landing site) due to adverse weather conditions: thunder storm	c	i	m	Do not fly in stormy conditions	c	n	l
5	Aircraft untrimmable due to cargo shift	c	i	m	Static margin equal to 7.5% MAC	m	i	l
6	Lifting-line model provides inaccurate results	m	p	m	Perform validation using XFRL5	m	i	l
7	Lifting-surface model provides inaccurate results	m	p	m	Perform validation using XFRL5	m	i	l
8	Reduced range due to local sinks	m	p	m	Consider local sinks during flight planning	m	i	l
9	Wind gust increases angle of attack causing stall	c	p	mh	Glider cruises at low angle of attack to have margin to the stall angle	c	i	m

Table 5.15: Aerodynamics and performance risk-map

(Unmitigated) / Mitigated	Highly Probable (h)	Probable (p)	Improbable (i)	Negligible (n)
Catastrophic (ca)				
Critical (c)	(AP2)	(AP1) (AP9)	(AP3) (AP4) (AP5) AP2 AP9	AP1 AP3 AP4
Marginal (m)		(AP6) (AP7) (AP8)	AP5 AP6 AP7 AP8	
Negligible (n)				

6

Structures & Materials

This chapter covers the structural design of the glider. The structure will carry all the loads and maintain the aerodynamic shape of the glider. First, the requirements for the structure are listed in section 6.1. Section 6.2 covers the design approach with a detailed layout of this chapter. In section 6.3 the structural elements are covered in more detail together with the material section and how they were sized. Section 6.4 gives a design overview with all elements. After that, the structural tool is verified and validated in section 6.5. The risk are assessed after that in section 6.7 and finally the sustainability of the structure is analysed in section 6.8

6.1. Functional Analysis

The requirements for the structure dictate how the structure should be designed. All the requirements related to the structure of the glider are covered in Table 6.1. These requirements will serve as a guide throughout the rest of this chapter. Note that many of these requirements are related to the materials being used in the glider. Requirement R_EG_STRUC_03 on the maximum load factors is derived from certification recommendations [13]. The requirement R_EG_REG_01 on the icing condition accounts for situations that the glider is flying in freezing temperatures with a significant icing threat. It is recommended that the extent and potential consequences of icing are evaluated in further design iterations.

Table 6.1: Aerodynamics & Performance requirements

Identifier	Requirement Statement	Compliance
R_EG_PL_01	The glider shall allow for accessing the cargo hold.	section 11.3
R_EG_REG_01	The UAS shall be able to cope with icing conditions.	unknown
R_EG_ENBD_01	The maximum total mass of the glider including cargo shall be 25kg.	section 3.6
R_EG_STRUC_01	The glider shall protect the payload during landing.	section 6.3
R_EG_STRUC_02	The glider shall protect the payload during flight.	section 6.3
R_EG_STRUC_03	The structure shall withstand load factors between -1.52 and $3.8 g$	section 6.3
R_EG_STRUC_04	The structure shall not deform more then $0.3 [m]$ measured from the wing tip at any point in time.	section 6.3
R_EG_SUST_01.1	The glider shall consist of components made of non biodegradable materials if and only if no biodegradable alternatives are feasible.	section 6.3
R_EG_TRA_07	The cargo compartment shall allow for thermal insulation to be added when temperature sensitive cargo is transported.	section 6.4
R_EG_TRA_08	The glider shall be made with widely available materials.	section 6.3
R_EG_FA_02	The glider shall be water resistant during its flight.	section 6.3
R_EG_SUST_03.2	A minimum of 70% of the mass of the glider shall degrade within 10 years after landing.	section 6.3
R_EG_SUST_01	Biodegradable materials shall constitute equal to or greater than 75% of the glider mass.	section 3.6

6.2. Design Approach

In this section the design approach and its different steps are explained. The goal of the approach is to ensure the resulting design fulfils the structural requirements, i.e. it can withstand and transfer the loads while also fulfilling manufacturing and sustainability requirements. It is therefore important to have a good understanding of the requirements and their impact on the design. Sustainability requirements mainly apply to the material selection. No non-biodegradable materials shall be considered, to comply with R_EG_SUST_01.1, as alternative, biodegradable materials exist with acceptable structural properties. A number of requirements are sizing requirements, e.g. R_EG_TRA_07, which means the glider can be designed exactly to those requirements. The mass requirement R_EG_ENBD_01 is unlikely to be a driving requirement as it is actually favourable for the performance of the glider to be as close as possible

to the 25 [kg] limit. Therefore, the mass of the structure will be given less priority than other aspects like sustainability and manufacturability.

In order to be able to take any decisions on materials and sizing of the the structural components, it is necessary to first determine which components will be carrying the main part of the loads. First, different spar, skin and rib configurations were chosen. While determining those configurations it is important to always consider manufacturability, as it can be greatly influenced by the choices made at this stage. The overall layout, function and rough shape of each component were then decided based on this design trade-off. This makes it possible to choose materials that are fitting for the different components, while also complying with manufacturing and sustainability requirements. The material selection concludes the first part of the structural design.

The goal of the next steps is to refine the initial design to obtain a more detailed design. This involves sizing the components to comply with the dimensions and loads found during the aerodynamic sizing, followed by a structural analysis. If the structure's performance is found to be unacceptable, the sizing and analysis steps have to be iterated until an acceptable design is reached. If it turns out that the structure cannot be made to withstand the aerodynamic loads by only varying dimensions, the aerodynamic sizing has to be iterated.

To streamline this iteration process, it was decided that a custom structural analysis tool should be developed. This tool should be able to compute the peak stresses throughout the load carrying structure by making use of a number of input parameters, such as the dimensions of structural elements, the properties of the materials used and the aerodynamic loads.

6.3. Design Subsystem

The requirements on biodegradability narrowed the available materials to mostly natural materials. In the early days of aviation natural materials were common aircraft building materials. This means that the structure of older aircraft could be used as a guide.

Structural Configuration

The first step was to determine what structural elements will be load carrying. For the aerodynamic performance a smooth skin is important for the design. Similarly, skin buckling does not favour the aerodynamics performance. This favours a skin that is not a structural element. The ease of manufacturing is also important. If the skin would be a structural element, compared to being just an aerodynamic shell, a stronger connection between the skin and the rest of the structure would be required. For these two reasons, it was opted to have the skin as just an aerodynamic covering. The skin should be able to width-stand the aerodynamic pressure and transfer it to the ribs, which in turn transfer these loads to the spar. The second function of the ribs is to maintain the aerodynamic shape of the airfoil.

This means that the spar will be the backbone of the wing structure. The different design options for the spar are a wing box, single or double beam. There was also the idea of completely filling the inside of the wing with a filler. This concept was however not carried forward, since it was deemed that it would unnecessarily complicate the production compared to the other alternatives. An important load case of the wing is the bending. The three considered design options are all feasible structural element to transfer the moments. There is however a larger difference in the torsion of the wing. The blended wing body needs a sweep angle to be stable during flight. This creates torsion which needs to be design for. A single spar is therefore inferior to the wing box and the double spar. The wing box is a good design option. It is a closed shapes, which makes it better at handling the torsion. The two individual spars are also good at handling torsion with differential bending. From a manufacturing perspective, it would easiest be to use two beams, since this would save the manufacturing of the wing box. Other wooden aircraft like the De Havilland Mosquito¹ and many WWI biplanes like the Albatros D.I² and the Sopwith Camel³ have two wing spars. These reasons lead to the selection of two main spars for the wing structure.

The fuselage structure is designed with the same philosophy in mind. The skin is once again just an aerodynamic shell with a number of ribs on the inside that transfer the loads to the spar.

Material selection

The spar material needs to be carefully selected so that is complies with the requirements. Some proposed materials already drop out when the requirements are considered. Delignified wood seemed very promising at first, especially in densified form. It even outperformed glass fibre, but the manufacturing was so far only done at small scales in the laboratory[34]. That does not comply with R_EG_TRA_08. Paper pulp also seems a very promising material, but it is not optimal to make solid structures like spars and flanges. The two other materials were solid wood and plywood. Solid wood has the benefit over plywood that it doesn't need the extra production steps of shaving and building up the plywood layers. A drawback of solid wood is that defects inside the wood can not be seen, which will require a safety

¹URL <https://ecrivelo.eu/the-stories/mosquito-in-the-forest/mkiv-de-havilland-mosquito/> [cite 10 June 2020]

²URL <https://web.ipmsusa3.org/content/albatros-di-dii> [cite 10 June 2020]

³URL <http://www.johnsshawaviation.co.uk/wordpress/sopwith-camel-f1-2/sopwith-camel-reconstruction/sopwith-camel-construction-lower-wings/> [cite 10 June 2020]

margin that increases thickness. Plywood does not have this problem since the individual layers can be inspected. The layers are bonded using adhesive. These adhesives include chemicals like formaldehyde, which is a volatile organic compound. It causes cancer in high concentration. However, the concentrations of volatile gasses become negligible after a few weeks⁴. That should thus not form a problem upon biodegrading and does not harm the environment. The environmental impact of plywood was researched and it showed that plywood did not harm the bacteria digesting the wood in any way. It also showed that plywood degrades the fastest compared to other types of wood[18]. This makes plywood the preferred material for the spar, since it is not more harmful compared to the solid wood alternative. It can also be inspected on defects, making its performance more predictable and therefore the preferred choice of material for the spar.

Compressed paper pulp was not an optimal material for the spar, but it is perfect to be used as a skin. The paper pulp is made from recycled materials, which allows the skin of the aircraft to be completely made out of recycled material. The process of pressing the pulp allows the material to be shaped into smooth and complex shapes, which is ideal for the aerodynamic shape of the skin. The manufacturing process is the about same as for egg cartons. The part is made on a mesh screen, meaning that the final part is always a flat surface. This would be ideal for the skin of the glider. The skin does require a surface finish. The cardboard skin is not smooth enough for aerodynamics and will start to fall apart when it gets wet. An extra watertight smooth layer over the skin is thus needed, so the glider complies with R_EG_FA_02. Two potential options were cellophane and PLA. Both are a thin, transparent sheets that are able to biodegrade with these high surface to volume ratio. This film should form a tight wrap around the wing, which is done by using the shrink wrap properties of the materials. Under the presence of heat, the material shrinks and forms the tight required layer. Both cellophane and PLA perform the same function with the same result, however, PLA is more widely used in the industry which made it the preferred choice as per R_EG_TRA_08. The material properties shown in Table 6.2 are taken from the CES *Edupack*2019 software. The Plywood values come from a 7 layer beech plywood with in plane isotropic properties. The paper pulp properties are taken from values of cardboard, with exception of the shear strength, which was not provided in that category. It was assumed that the paper pulp will have similar properties to a cellulose board. The PLA properties are taken from a general purpose PLA.

Table 6.2: Material Parameters

Material	Youngs Modulus[GPa]	G Modulus[GPa]	Comp. Strength[MPa]	Tens. Strength[MPa]	Shear Strength[MPa]	Density[kg/m ³]
Plywood	7.5	0.3	31	65	5	750
Cellulose Pulp	4.1	2	10	10	12	350
PLA	3.4	1.24	76.2	58.5	35.3	1260

Biodegradation timespan

The time for the glider to biodegrade needs to be checked in order to ensure compliance with R_EG_SUST_03.2, to make sure the glider biodegrades within a reasonable time. The plywood spar biodegrades within 1 to 3 years, depending on the weather conditions, which is faster than regular solid wood⁵. The paper pulp skin will biodegrade within 3 month when it is in contact with water. When it is dry, cardboard could last for multiple years⁶. The PLA skin biodegrades in a little less than 12 months when at 25 [°C] and some contact with water, with the first fragmentation after 6 months [56].

The overall decay speed is heavily influenced by the presence of water. The decay process of the plywood and the paper pulp skin can be postponed if the water tight PLA film is still intact, although that is unlikely after the landing. In optimal conditions, the glider is expected to fully degrade within 1 year. However, very dry conditions will limit the microorganisms, meaning it can take multiple years for the glider to decay. Although it can be dry in the mission area, it is quite certain that 70% of the glider structure will have degraded within 10 years, which ensures that the glider complies with R_EG_SUST_03.2.

Structural Sizing

In order to size the wing, a structural analysis is performed in 2 parts. First bending stresses and deflections are analysed, and secondly shear stresses and wing twist is analysed. Before the analysis can be done however, the internal loading of the wing needs to be determined.

Wing Loading

The internal loads are derived from a quarter chord distributed load that was scaled to a load factor of 3.8, to adhere to R_EG_STRUC_3. The structure is split and evaluated in discrete steps as shown in Figure 6.1 and 6.2. All parameters are assumed to be constant along the discrete elements.

⁴<https://www.famitchell.com.au/formaldehyde-plywood/> [cite 19 June 2020]

⁵<https://www.familyhandyman.com/list/how-long-until-this-waste-is-gone/#:~:text=The%20glue%20used%20to%20hold,with%20your%20left%20over%20plywood> [cite 18 June 2020]

⁶<https://www.planetpaper.com/long-cardboard-take-decompose/#:~:text=In%20more%20typical%20garden%20conditions,broken%20down%20within%20three%20months> [cite 18 June 2020]

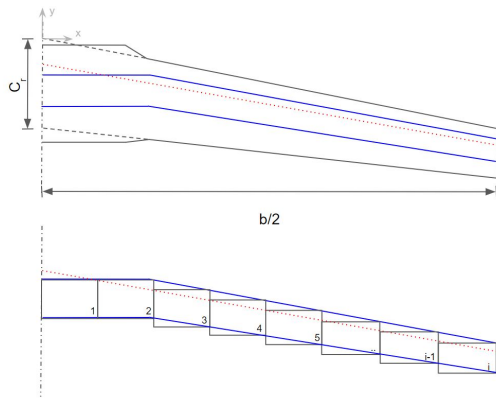


Figure 6.1: Discretized wing structure, top view

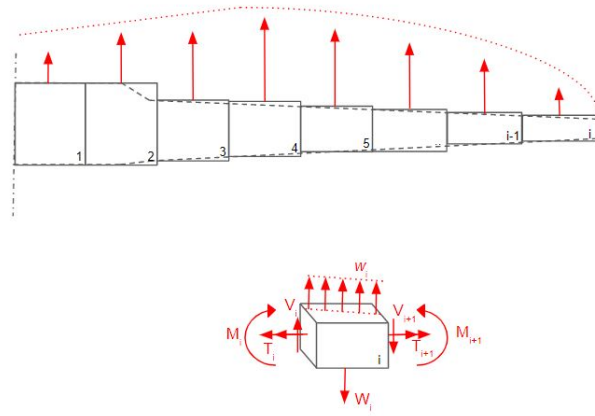


Figure 6.2: Discretized wing structure, front view and element free body diagram

The force acting in the centre of each element is determined with Equation 6.1. The distributed load at the outward boundary, w_m , is multiplied by the step size, resulting in a lift force acting on the element. The weight of the element, W_m , is then subtracted from the lift. The internal shear force is determined by summing all forces, F_m , outward of the boundary. This can be seen in Equation 6.2. The internal bending moment was determined at each element boundary using Equation 6.3. The moment at the m^{th} boundary is determined by summing up all forces multiplied by the moment arm along the x -axis for the following elements. The internal torque was determined in a similar fashion as the internal moment, the only difference being that the moment arm was determined by the displacement along the y -axis.

$$F_m = w_m \text{step} - W_m \quad (6.1) \quad V_m = \sum_{n=m}^i F_n \quad (6.2) \quad M_m = \sum_{n=m}^i F_n (x_n - x_m) \quad (6.3)$$

The result of the internal load analysis can be found in Figure 6.3. The top left figure depicts the distributed load, the left bottom figure the internal shear, the right top figure the internal moment and the right bottom figure the internal torque. These distributions were used in the subsequent sections to determine the maximal internal stresses and the deformations.

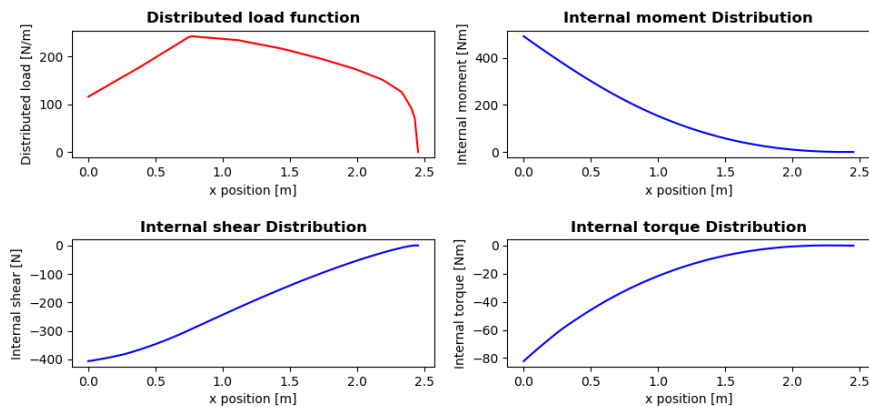


Figure 6.3: Distributed load and Internal load diagrams

Bending Stress

Due to the high stiffness of the spars with respect to the skin, it is assumed that the contribution of the skin to bending resistance is negligible. Therefore, only the spars are taken into account to determine the 2^{nd} moment of area. Equation 6.4 determines the moment of inertia using the height of the trailing and leading spar as well as their respective thicknesses. Due to the symmetry, I_{xy} is deemed to be zero, leading to Equation 6.5. As the stress is linearly dependent on the z position, z was chosen to be the highest point on either the leading or the trailing spar, dependent on which was higher. The resulting stresses are shown in Figure 6.4. The values can be seen as compressive and tensile stress, since the stresses are symmetric. Plywood has its lowest strength in compression. However the figure clearly shows, that the stress are well below the maximum stress. The sudden drop of the stress around 0.27 m in span direction is there due to the sudden rise of the spar height, when it enters the body section of the glider.

$$I_{xx} = \frac{t_{lspar} h_{lspar}^3 + t_{tspar} h_{tspar}^3}{12} \quad (6.4) \quad \sigma = \frac{Mz}{I_{xx}} \quad (6.5)$$

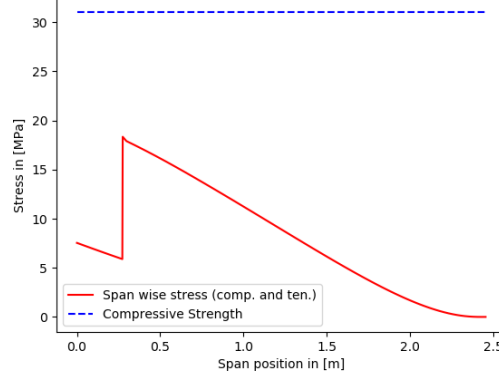


Figure 6.4: Bending stress distribution along Wing

Wing deformation

In order to estimate the deformation of the wing it is assumed that each beam section seen in Figure 6.1 and 6.2, is a cantilever beam fixed at on end with a moment acting on the other end. The slope of each section is determined by Equation 6.6, where the slope of the previous element, θ_{m-1} , is added in order to take into account that they are connected. The deflection is estimated with Equation 6.7. Both the angle of the element as well as the deflection of the previous element are taken into account to determine the total deflection in z. The small angle assumption is used to derive the deflection due to the element slope. The results can be seen in Figure 6.5. The maximum wing deflection expected during a manoeuvre with a load factor of 3.8 is 0.3 [m].

$$\theta_m = \theta_{m-1} + \frac{M_m \cdot step}{EI_{xx}} \quad (6.6)$$

$$\delta_m = \delta_{m-1} + \theta_m \cdot step + \frac{M \cdot step^2}{EI_{xx}} \quad (6.7)$$

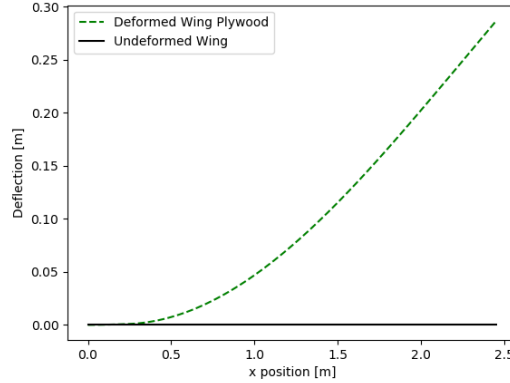


Figure 6.5: Wing deflection over span

Shear Stress

The shear stress was analysed with the assumption that the skin and the 2 spars create a cell that takes all the shear loading. The cross-section used for the calculations of moment of inertia and the paths taken for the shear flow can be seen in Figure 6.6. The new 2nd moment of inertia is determined by adding the skin contribution, Equation 6.8, to the I_{xx} as seen in Equation 6.9.

$$I_{sk} = \frac{t_{sk} l_{sk}^3 \sin^2(\beta)}{6} + l_{sk} \left(\frac{h_{lspar} + h_{tspar}}{4} \right)^2 \quad (6.8)$$

$$I_{xx+sk} = I_{xx} + I_{sk} \quad (6.9)$$

The shear force and torque are assumed to act on the origin of the coordinate system drawn in Figure 6.6. The basis shear flow is calculated with Equation 6.10, starting at the cut made at the beginning of S_1 . This line integral is performed around the cross-section. The moment of the internal shear flow is then determine using Equation 6.11. The moment is put in the rearranged moment equilibrium Equation 6.12 to determine the correcting shear flow, q_0 [11]. The corrected shear flow can be obtained by summing q_b and q_0 . Shear stresses can be determined by dividing the shear flow at a certain point by the local thickness. The result can be seen in Figure 6.7. All stresses are well beneath the respective shear strengths of the spar and the skin. It is again possible to observe a sudden drop in stresses where the spar joins the wing body.

$$q_b = \frac{-V}{I_{xx+sk}} \int t y dS \quad (6.10)$$

$$M = \oint q_b r dS \quad (6.11)$$

$$q_0 = \frac{M - T}{2A} \quad (6.12)$$

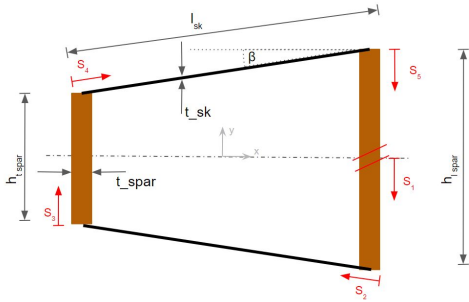


Figure 6.6: Cross-section used to determine shear stress

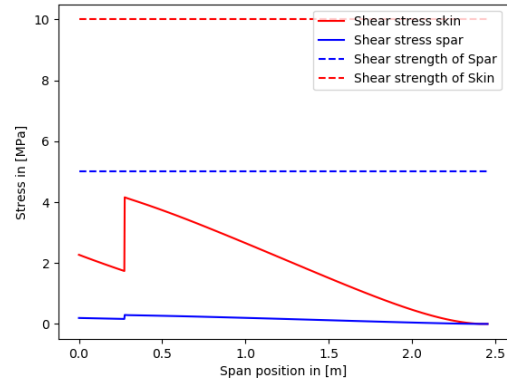


Figure 6.7: Shear stress Distribution

Wing Twist

The assumptions made in the previous section also apply to this section. The rate of twist was determined for each element using Equation 6.13, which takes the spar thickness t , the shear flow q , the cross-section area A and the shear modulus G into account. The resulting twist rate is multiplied by the step size, equal to the length of each element. The twists along the span are then added to determine the total wing deformation. This results in Equation 6.14, which leads to the twist distribution shown in Figure 6.8.

$$\frac{d\phi}{dx} = \frac{1}{2A} \oint \frac{q}{Gt} dS \quad (6.13)$$

$$\phi_m = \phi_{m-1} + \frac{d\phi}{dx} \text{ step} \quad (6.14)$$

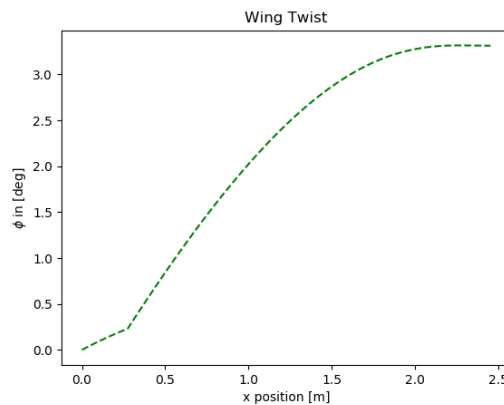


Figure 6.8: Wing twist along span

Rib spacing

For the Euler column buckling formula is to determine the rib spacing. The rib spacing will be optimised such that buckling can be prevented with a minimum number of ribs. To determine the rib spacing a few assumptions were made. The skin was designed to not be load carrying. Bending stresses are thus not directly taken up by the skin and it only deforms together with the spars. A graphical representation of this is shown in Figure 6.9. The wing tip deflection is $d = 50 \text{ [mm]}$ which is assumed to be at the neutral line of the deflection. To simplify the calculations for the compressive strain, the wing deflection is assumed to be circular. With the wingspan of the glider, this gives a radius of $R = 60.3 \text{ [m]}$. With an average airfoil thickness of $2t = 30 \text{ [mm]}$, the strain in the top skin is $\epsilon = 2.49e-4$ which results in a stress of $\sigma = 0.746 \text{ [MPa]}$.

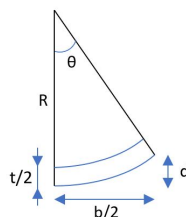


Figure 6.9: Graphical representation of strain top skin

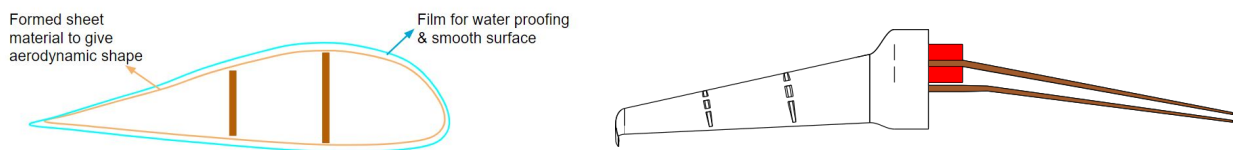
The top skin panel of the airfoil is taken from 30% to 80% of the skin. This is the straight part of the top skin which is deemed to be the most sensitive to buckling. It is assumed that this top skin experiences the same amount of stress. The taper of the wing makes it necessary to evaluate the buckling criteria at different locations along the span. The locations of $1/4 c$, $1/2 c$ and $3/4 c$ are chosen as the evaluation points. These fractions are taken over just the wing, and exclude the fuselage. These fractions translate to the airfoil sections at a distance of 1121 [mm], 1580 [mm] and 2051 [mm] from the centre of the fuselage section. With the cross-sectional area and the moment of inertia around the neutral axis at these positions, rib spacing of 2.86 [m], 1.97 [m] and 1.52 [m] is required for the three sections respectively. The root of the wing can thus handle a larger rib distance. These values mean that 1 rib per wing should be sufficient to prevent buckling in the top skin. However, a conservative value of 2 ribs per wing is selected to take any uncertainties due to the assumptions into account.

It is recommended to reevaluate the rib spacing in the next design iteration. The strain due to the wing deflection is here selected as the main load case. The aerodynamic loads could however also be the dominant load case dictating the rib spacing. This will have to be checked in further evaluation of the structure.

6.4. Design Overview

The final structure will have 2 main spars with a cardboard skin and a PLA film. The spars will be placed at 20% and 50% of the chord. The spars have a 5 [cm] thickness and taper down in height towards the wingtips. The spars will be made out of plywood. To have more space in between the spars in the fuselage, the spars are located parallel to each other in the fuselage. This introduces kinks in the spars. Sharp corners in the spars will be avoided to get a strong joint between the spars. The cardboard skin around the spars forms the aerodynamic shell, which is maintained by the two ribs in the wing. The wing is made out of paper pulp. The manufacturing process for this material is optimal to combine the ribs and the skin as one part. To prevent the cardboard skin from falling apart a water tight PLA film is shrink-wrapped around the wing for better aerodynamic performance.

The fuselage will be manufactured in the same way. The aerodynamic shape is made with the paper pulp shell. A few ribs on the inside transfer the aerodynamic loads to the underlying structure. PLA shrink wrap is applied around the fuselage section. A graphical representation of the design overview is shown in section 6.4 and in section 6.4. The aerodynamic shape is seen on the left side, which also shows the layout of the double skin together with the two spars. The top view with a cut out showing the two tapered down spars with the kink can be seen on the right hand side.



6.5. Verification & Validation

This section will elaborate how the structural analysis performed in section 6.3 is verified, and what steps have to be taken to validate the model.

Wing Loading

The internal forces and moments depicted in Figure 6.3 are derived from an Euler integration. In order to verify that this simple integration scheme is correctly integrated and is accurate, a simple distributed load is applied and the outcome is compared to the analytical solution. The wing is assumed to be a cantilever beam with a triangular distributed load applied to it, as can be seen in Figure 6.10. ω_0 is the highest value the distributed load reaches over the length of the beam L . With help of the free body diagram shown in Figure 6.11, Equation 6.15 for the internal shear force V and Equation 6.16 the internal moment M can be deduced. The resulting analytical solution can be compared with the solution of the model.

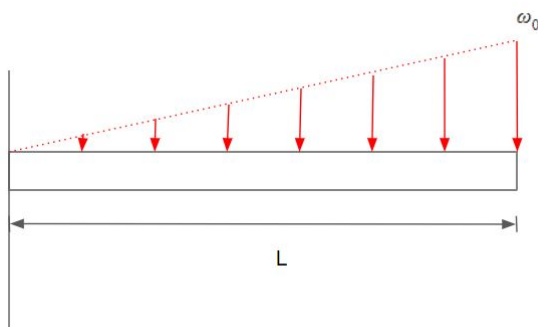


Figure 6.10: Distributed test Load

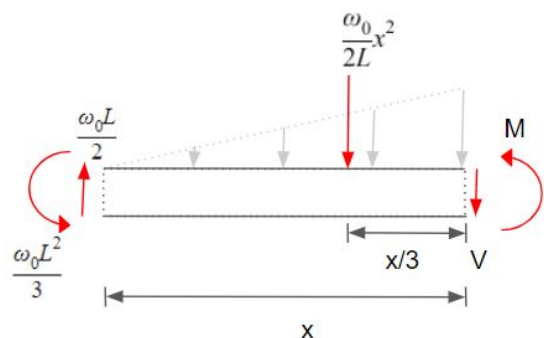


Figure 6.11: Free body diagram of beam

$$V = \frac{\omega_0}{2L}(L^2 - x^2) \quad (6.15)$$

$$M = \frac{\omega_0}{6L}(-2L^3 + 3L^2x - x^3) \quad (6.16)$$

In order to achieve comparable results out of this comparison the length of the beam is set to be equal to half the wing span and the numerical integration is performed with the same amount of steps as are used in the structural analysis performed in section 6.3. Figure 6.12 and 6.13 show the analytical and numerically determined internal shear forces and moments. The magnified area shows the area of the biggest error. The internal shear has an average percentage error of 0.69% with a maximum error of 0.126 [N]. The internal moment has an average percentage error of 0.6% with a maximum error of 0.157 [Nm].

The results of the comparison show that the analytical model is very close to the numerical model. The internal torque is deduced with the same integration scheme and hence it can be assumed that it is also very close to the analytical solution. Therefore, the internal forces and moments are assumed to be verified.

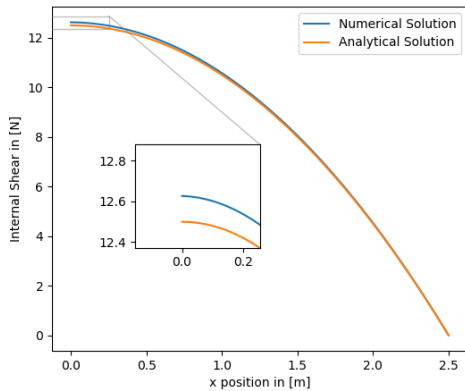


Figure 6.12: Comparison of internal shear derived from analytical and numerical model

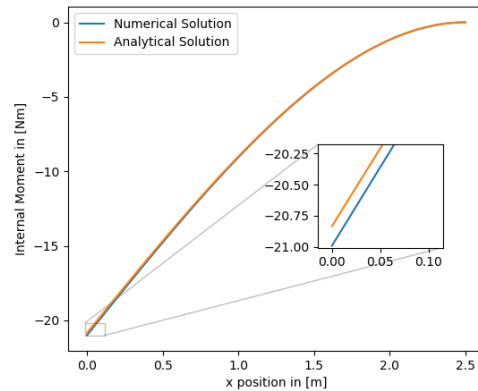


Figure 6.13: Comparison of internal moment derived from analytical and numerical model

Wing deformation

In order to verify the numerical model used in section 6.3, it is compared to a analytical model that is based on the same assumption. The assumption that makes both models possible is based on Equation 6.17 taken out of R.C Hibbeler's Mechanics and Materials[11]. This equation can be integrated twice with respect to x in order to obtain the deflection. The numerical model splits the beam into elements with constant moment along them leading to Equation 6.6 and 6.7 which describe how the total deflection of the beam can be determined by summing up the deflections of the individual elements. In order to compare the two models a simple case was chosen, as can be seen in Figure 6.17. Figure 6.15 shows the free body diagram leading to Equation 6.19.

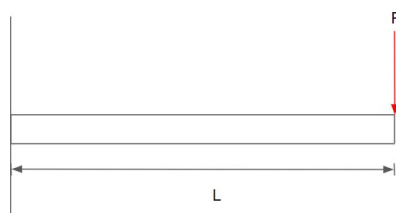


Figure 6.14: Deflection test applied load

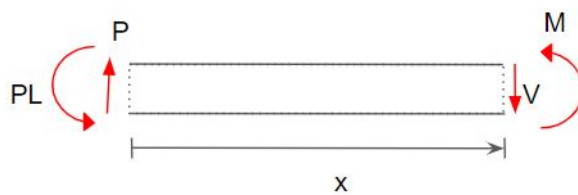


Figure 6.15: Free body diagram of deflection test

$$\frac{d^2\delta}{dx^2} = \frac{M}{EI} \quad (6.17) \quad M = P(x - L) \quad (6.18)$$

$$\delta = \frac{P}{6EI}(-L - x)^3 + 3L^2(L - x) - 2L^3 \quad (6.19)$$

L was chosen to be half the wing span and the numerical integration was performed with as many steps as used in the structural analysis performed in section 6.3. A moment of inertia taken from the root chord was applied along the whole span. Several different loads where applied but no significant change in the average percentage error was found. The numerical model was also used to determine the internal moment distribution. Figure 6.16 depicts the resulting internal moments and Figure 6.17 the deflections. The internal moment has a average percentage error of 3.3% with an maximum error of 0.25 [Nm]. The comparison of the deflection models in Figure 6.17 resulted in a average percentage error of 5.9% and a maximum error of 0.005 [m].

The error of the internal moment curve is higher due to the nature of the load case. The load is applied on the outer edge of the beam. Due to the way the numerical model works, however, the force is simulated to be applied on the middle of the last element, causing the moment curve to shift forward. When the graph is closely observed it can be seen that the two curves are parallel to each other with a constant distance of 0.25 [Nm]. The maximum error of the deformation occurs in the middle of the wing. The error at the tip is much lower with a difference of 0.00023 [m].

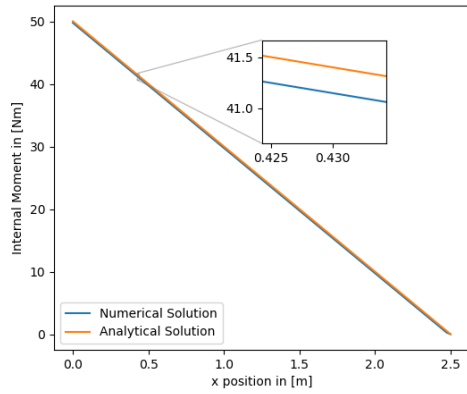


Figure 6.16: Comparison of internal moment derived from analytical and numerical model

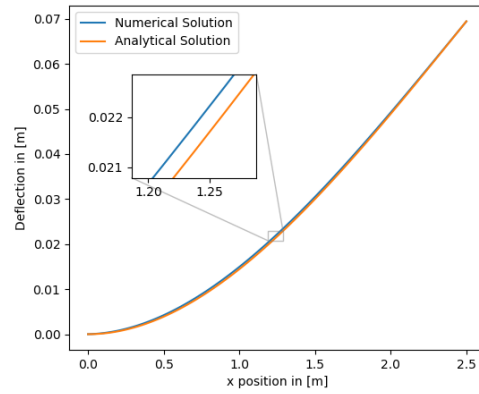


Figure 6.17: Comparison of deflection derived from analytical and numerical model

Moments of Inertia, Stresses and Wing Twist

Moments of inertia, stresses and wing twist have all been verified in the same way. The moment of inertia of the root chord was determined by hand and compared to the result of the model. The same was done with compressive and tensile stresses as well as the shear flow and the wing twist. Since all values were determined the same way, a 0% deviation could be found. This verifies that the numerical model works in the intended way. It can however not be verified that the results are close to reality.

Recommendations for Verification and Validation

The verification's performed in the previous subsections show that the program works as intended and that the numerical integrator in the model produces errors small enough to use the results. They however do not prove that the assumptions made in the model, such as that the spars take all the bending loads, are valid. In order to verify these assumptions, a model based on different principals has to be used. It is recommended to use a finite element program such as *abaqus* together with the *catia* model, to verify the assumptions.

In order to validate the structure, a physical prototype has to be build and tested. Strain gauges can be used to determine the stresses in the structure. The structure can also be tested in parts. For example, the spars can be tested for bending, without the skin being attached, which will simplify the process significantly.

6.6. Sensitivity Analysis

Parameters that might change in the real product will be changed in this section. The influence of these changes on the internal stresses and deformation of the wing are investigated. Firstly the load case will be increased and decreased by 25%. The same will be done with the young's modulus, shear strength and ultimate strength of the materials used. Figure 6.18 and 6.19 depict the effects of changing the load case on the bending stress and deflection of the wing. The bending stress increases by 27.65% when the load case is increased and decreases by the same amount when the load case is decreased. The deflection increases by 27.60% for the increased load and decreases by the same amount for the decreased load. This means that in case of an extreme manoeuvre that reaches 125% of the intended load factor, requirements R_EG_STRUC_04 will no longer be fulfilled. The stresses, however, are still below the compressive strength of the structure.

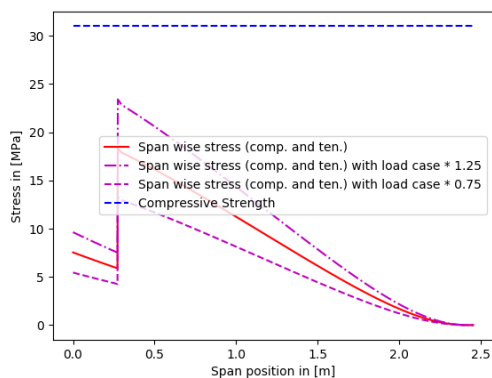


Figure 6.18: Internal bending stresses under different load cases

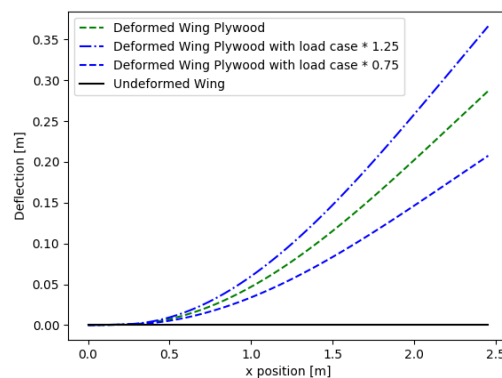


Figure 6.19: Wing deflections under different load cases

Figure 6.20 and 6.21 show the behaviour of the shear stress and the wing twist when the wing load is increased or decreased. The maximum shear stress in the skin increases and decreases 24% with the change in the load factor, the twist changes by 22%. Therefore, all shear stresses remain below the shear strength of the materials used, also the shear stress in the spar which is not shown in Figure 6.20.

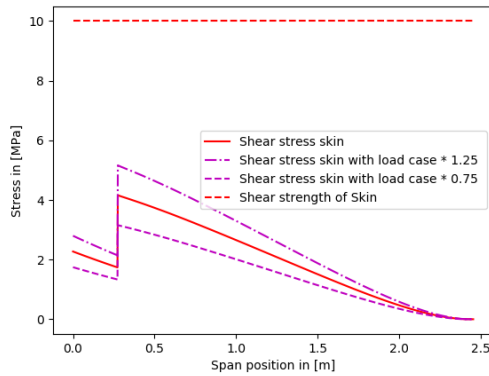


Figure 6.20: Comparison of internal moment derived from analytical and numerical model

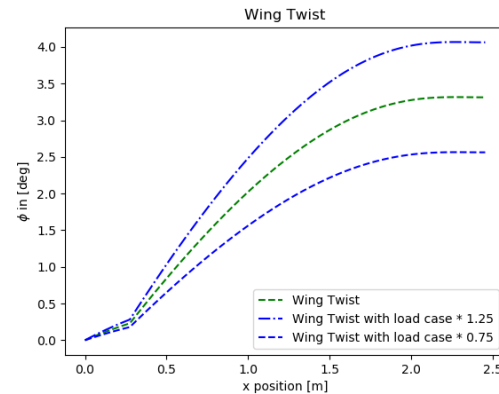


Figure 6.21: Comparison of deflection derived from analytical and numerical model

The material properties have also been changed. The shear and compressive strength of the spars have been reduced by 25%, shear moduli of the spars and the skin have been increased and decreased by 25% and the same is done with the shear strength of the spar and the skin. The change of parameters had no effect on the stresses predicted by the numerical model. Only the maximum stress that the materials could withstand was lowered. The stresses however still remained under the max strength. Figure 6.22 and 6.23 depict how the wing deflection and twist react to the change of properties. Decreasing the shear modulus and the young's modulus is effectively decreasing the stiffness of the materials, hence the deformation for the same load increases. The wing deflected 33% more with the decreased young's modulus and the wing twist increased by the same percentage for the lower shear modulus. This leads to a violation of requirement R_EG_STRUC_04. An increase of the moduli led to a decrease of the wing deflection and twist by 20%.

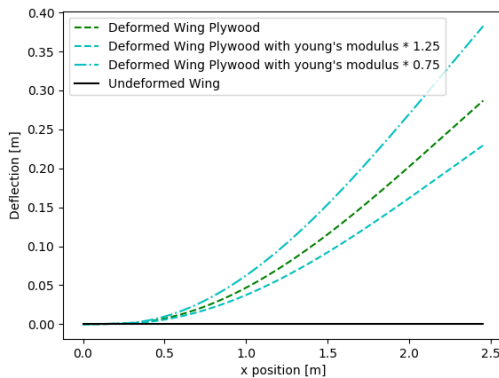


Figure 6.22: Comparison of internal moment derived from analytical and numerical model

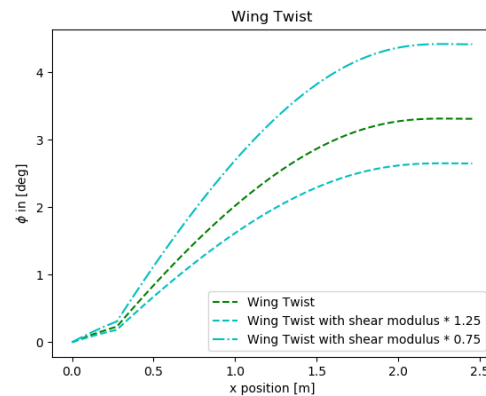


Figure 6.23: Comparison of deflection derived from analytical and numerical model

6.7. Risk Assessment

This sections covers the risks related to the structure of the glider. Different types of risks are covered based on their severity and their probability. The risks can be mitigated by taking action. All this is shown in Table 6.3. The mitigated risks are presented in an overview in Table 6.4.

As can be seen, a lot of risks originate from the structure failing due to different reasons, like loads being higher in reality or wrong assumptions. These risks are well mitigated by using a safety factor or verifying and validating the design. These are straightforward steps, but greatly reduce the risks involved for the structural aspect of the glider.

Table 6.3: Structures and materials risks

Index	Risk Factor	Severity	Probability	Risk	Mitigation Method	Severity	Probability	Risk
1	Structural failure during high load manoeuvre	c	i	m	Use safety factor to size structure	c	n	l
2	Structural strength is overestimated due to wrong assumptions	c	p	mh	Use verification in order to make sure estimations are valid & validate model by testing the prototype	c	n	l
3	Overestimation of structural properties of materials	c	p	mh	Perform experiments to measure material properties before final design iteration	c	i	m
4	Assumptions made in structural analysis code lead to under-designed structure	c	p	mh	Perform verification and validation of code.	c	i	m
5	Underestimating density of materials	c	p	mh	Measure density of materials before final design iteration	c	i	m
6	Premature buckling of structure	c	p	mh	Build and test prototype up to failure	c	n	l
7	Paper pulp parts failing due to contact with water	c	h	h	Wrap pulp parts in water resistant film	c	i	m
8	Spars failing due to delamination of plywood	c	i	m	Ensure plywood is provided by dependable supplier and perform quality control of the plywood sheets	c	n	l

Table 6.4: Structures and materials risk-map

(Unmitigated) / Mitigated	Highly Probable (h)	Probable (p)	Improbable (i)	Negligible (n)
Catastrophic (ca)				
Critical (c)	(SM7)	(SM2) (SM3) (SM4) (SM5) (SM6)	(SM1) (SM8) SM3 SM4 SM5 SM7	SM1 SM2 SM6 SM8
Marginal (m)				
Negligible (n)				

6.8. Sustainability Analysis

The sustainability analysis of the structure will be briefly discussed here. The analysis for the whole glider is presented in Chapter 14.

The structure is thus made out of plywood, paper pulp and PLA. All the materials are from the short carbon cycle. Plywood is made from sliced logs. These logs can be grown responsibly, further reducing the footprint. The paper pulp is made from recycled material. The exact colour of the pulp is not that important allowing for a large variety of paper or cardboard being used. It is a good way to use waste paper for a new life. However, the life of the paper does end after being used for the glider if left to biodegrade. PLA is made from biomass, which is also the short carbon cycle. The carbon footprint on the environment thus greatly reduces by not having parts that are produced from fossil fuel, but only from organic natural materials.

Guidance, Navigation & Control

The difference between guidance, navigation and control is a nuanced but important one. For the EcoGlide project guidance is defined as the determination of the glider's orientation, velocity and the path that the glider should follow for it to reach its desired ending location, while navigation is defined as the determination of the glider's actual orientation, path and position. Control is defined as the use of the glider's control surfaces to follow the commands given by the guidance system.

In this chapter, first the requirements of the GNC will be explained through a functional analysis that defines the mission profile in section 7.1. After this the method used to size the glider's control surfaces and actuators is detailed in section 7.2. After this the hardware and software used in the GNC subsystem is determined in section 7.3 and a summary of the design is given in section 7.4. The chapter closes with verification and validation and risk assessment in section 7.5 and section 7.6, respectively.

7.1. Functional Analysis

For the guidance, navigation and control system, it makes sense to split the mission up into 3 distinct phases, namely the deployment phase, the cruise phase and the landing phase. Each of these phases present unique obstacles that the glider will have to overcome from a GNC perspective.

The functions for the EcoGlide system as a whole can be found in section 4.4 and section 4.4. For these functions to be determined, the mission profile must first be completely established which is done in the following section for each phase of the mission. At the end of this section the requirements are listed and justified.

Deployment Phase

As soon as the glider is released from the balloon, it will dive down, gaining speed until the glider reaches the initial cruise airspeed, where it will pitch up. Once the cruise attitude has been reached, the glider will fly to a safe distance from the balloon and tether. From this point, it will start to turn towards the destination, while maintaining a safe distance from the deployment system.

The pull-up manoeuvre is the manoeuvre during which the glider will first dive down to gain speed and then pull-up to enter almost horizontal flight. At the point of deployment, the glider will be oriented with the wind, so that it will naturally drift away from the deployment system. Once the glider has reached its cruise speed it will pull up to fly more level. During this pull-up manoeuvre the glider will continue to accelerate and thus surpass the initial cruise speed. This means that once the glider is level that it will be generating excess lift which will result in it flying in a phugoid oscillation that the GNC will have to dampen through use of the control surfaces.

Once the glider has pulled up out of the dive, it will fly away from the deployment system. This safety distance mitigates the risks of the glider hitting the tether or the balloon, which could drift due to winds. This flight will also allow the glider to stabilise its velocity and attitude out of the aforementioned phugoid motion.

Once the balloon has been cleared and the glider's velocity and attitude has stabilised, it will make turn towards its final location. This procedure could either be programmed into the on-board flight controller in multiple ways. It could be done by means of a number of small waypoints on the arc of the turn or a circular zone around the deployment point with a clearance radius could be programmed into the glider which it must avoid. This last method would resemble some open source flight controllers' features such as altitude limits¹ and distance limits².

Cruise Phase

During cruise the GNC system will guide the glider from waypoint to waypoint till the glider makes it to where it can begin the landing procedure. The GNC system will also be able to detect certain environmental anomalies such as thermals and sinks and use these to gain altitude or bleed altitude as necessary. How the glider will do this will be explained in the following subsections.

¹URL <https://ardupilot.org/plane/docs/fly-by-wire-low-altitude-limit.html> [cite 22 June 2020]

²URL <https://ardupilot.org/copter/docs/parameters.html#avd-w-dist-xy-distance-warn-xy> [cite 22 June 2020]

Point to point navigation

Point to point navigation is a simple and commonly used guidance method in aerospace applications such as drones. The aircraft is given various waypoints that it must travel between in order. This is a proven method and various examples of waypoint-based guidance for similar gliders have already been explored [17]. Off-the-shelf flight controllers such as *ArduPilot* also have built in methods of planning a mission using waypoints³.

The glider does not actually choose the waypoints itself, but before hand a separate program does. How these waypoints are chosen will have a large impact on the accuracy of the guidance system. The waypoints should be chosen taking the weather conditions and obstacles such as mountains along the whole flight path into account. Since the EcoGlide system is being designed for the military it has been assumed that accurate weather and topography models will be available and that these can be used to allow for the generation of proper waypoints. If thermals or sinks can be detected prior to the glider's deployment, this can also be taken into account during the waypoint programming, allowing for the glider to, for example, avoid sinks all together or use thermals to extend its range.

Thermals and sinks

For most of the glider's flight it will be flying too high for thermals and sinks to have any real influence of its flight as it will be flying above the clouds. For the last portion of the flight, however, it may encounter various thermals and sinks that could have an impact on the glider's altitude. The flight controller will be able to use these thermals to gain or bleed altitude so that the glider is able to reach the field hospital without any issues.

Open source algorithms are already available for flight controllers that allow for autonomous soaring through thermals⁴. This algorithm takes the aircraft's orientation, GPS position and airspeed as well as the wind velocity and then allows for the aircraft to alter it's flight path through the thermal to gain altitude [49]. Since this algorithm requires the wind velocity and the glider will not have any method of measuring this itself, this data will have to be passed onto to the data before deployment using weather models.

Landing Method

In this subsection the various landing methods that were considered are presented. At the end of the section a trade-off is performed between the various landing methods and the deep stall method is chosen as the best landing method. The landing methods considered are shown in Figure 7.1 to 7.6. Each landing starts at 20 [m] above the ground, to allow for clearance of obstacles such as trees. From the figures it can already be seen that each of the landings have different advantages and disadvantages, such as required landing distance. To choose the best landing method for the EcoGlide system it was therefore necessary to perform a trade-off, which is detailed in the next subsection.

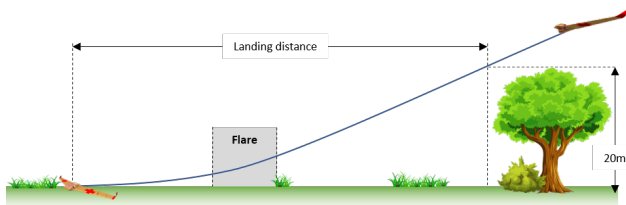


Figure 7.1: Sketch of the conventional landing concept (not to scale)

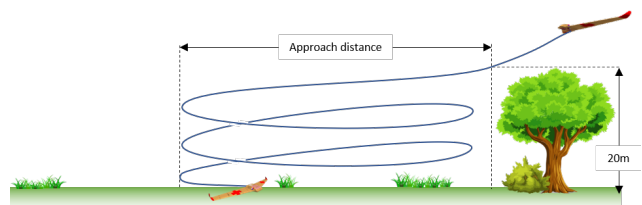


Figure 7.2: Sketch of the corkscrew landing concept (not to scale)

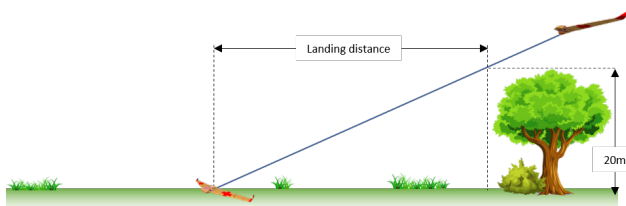


Figure 7.3: Sketch of the no-flare landing concept (not to scale)

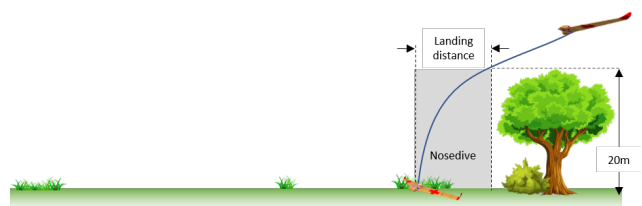


Figure 7.4: Sketch of the nosedive landing concept (not to scale)

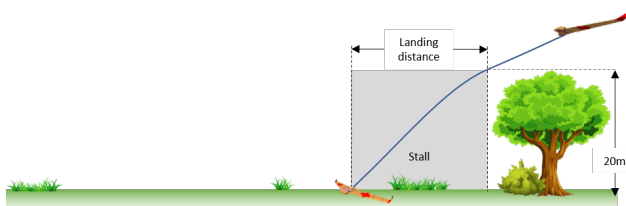


Figure 7.5: Sketch of the stall landing concept (not to scale)

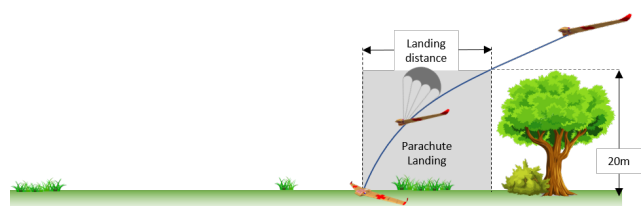


Figure 7.6: Sketch of the parachute landing concept (not to scale)

³URL <https://ardupilot.org/plane/docs/common-planning-a-mission-with-waypoints-and-events.html> [cite 19 June 2020]

⁴URL <https://ardupilot.org/plane/docs/soaring.html> [cite 18 June 2020]

Landing Method Trade-off

To choose the landing method best suited for Ecoglide's application, a trade-off was performed. The different landing methods shown above in Figure 7.1 to Figure 7.6. are compared to each other based on five different criteria: approach forces, touchdown forces, control complexity, clearance needed and accuracy. Different weights are assigned to each criteria, depending on the importance given to them.

The different criteria reflect the key aspects considered for the different landing methods. To assess each of these, appropriate values are estimated or calculated. These values are then scored according to the scale shown in Table 5.4. The first criteria, the approach force, relates to the forces the glider will experience during the approach to the landing spot for each landing method considered. Unpredictable small forces such as wind gusts are neglected. The structural properties of the gliders need to be high enough for this.

Computing these forces is done differently for each approach, as no common method was found. The no-flare landing does not experience an increase in loads during its approach. Therefore, a maximum load of 1.1 g was assumed to take small perturbations into account. In the case of the conventional approach, a maximum loading of 1.5 g was assumed as the glider needs to flare which will lead to additional forces depending on how aggressively the glider pulls up. For the stall and nose dive landing, it is assumed that the transition to the stall or nose dive is achieved in 1 second to improve precision, thus generating a 2 g load. This load was also given by the structural department as an initial 2 g upper limit load case. This is why, the same load is also used for the corkscrew landing. The last deployment method, the parachute, is assumed to have a 2 g deceleration due to the parachute. Later on in the design the upper load limit was increased to 3.8 g, but by this point the trade-off had already been completed.

The second criteria, the touchdown forces, relates to the forces the payload will experience at landing. These are key for the payload protection as well as for the safety of bystanders. Indeed, the payload's touchdown forces are comparable with the glider's touchdown forces, key parameters for the bystander's risk of injuries in case of collisions. These forces are computed using Equation 7.1 and Equation 7.2, which are derived from the kinematic formulas. In these two formulas, t_a , Δx , V_{vert} , a are the deceleration time, the deceleration distance, the vertical velocity and the deceleration in G-force, respectively. The deceleration distance is found from initial estimates of the distance between the payload and the point of impact. It is assumed to be 0.2 [m] for all "belly landings", that is all landings but the nosedive - the parachute landing is assumed to keep the glider horizontal and land on the belly. For the former, a distance of 0.5 [m] is assumed. This distance was derived from the initial estimates made by the team's structural department of the aircraft's dimensions. For the "belly landings", an initial estimate of the distance between the payload and the bottom, or belly, of the glider was taken. For the nose landing, the horizontal distance between the payload and the nose was chosen. For this trade-off, these distances are assumed to be fully "crushed" upon landing, comparable to the crumple zones of cars.

$$t_a = \frac{2 * \Delta x}{V_{vert}} \quad (7.1)$$

$$a = \frac{V_{vert}}{t_a * 9.81} + 1 \quad (7.2)$$

The result of these computations is that all but one landing method creates loads around 1.15 g. In fact, the no-flare and corkscrew landing, both are found to cause a load of 1.14 g. The conventional landing, where the flare is assumed to raise the glide ratio from 30 to 35, results in a G-force of approximately 1.09 g and the stall would lead to a force of 1.49 g. The nose dive, with its high vertical velocity, results in a deceleration load of 93.1 g.

The third criteria to be assessed is the control complexity. This encompasses the control program's complexity as well as the hardware related to the electronic sensors, type of aerodynamic surfaces and additional systems.

This criteria is the least objective, as the complexity cannot be given an accurate value without fully designing a GNC system for each of these landing methods. Therefore, the rating is done by means of reasoning, taking into account the number of control systems needed, the apparent controller software complexity and the novelty of the landing concept from a GNC point of view. The no-flare landing is given the highest score since it does not require much more control than the glider would need for the previous flight phases. The conventional landing gets a score of 4 because it would require more precision when flaring. The nose dive would also require additional attention for the diving manoeuvre, hence the score of 4. The stall landing is considered acceptable in terms of control complexity, since it requires a more complex control program for the unstable stall condition, but is still a feasible landing option used for UAVs [50]. The corkscrew landing also benefits from the fact that UAV researchers have demonstrated and use this method [42] [50], however it is not an easy method as it requires attention to the creation of the helix-like flight path. Finally, the parachute landing receives a score of 2 mainly due to the additional system it adds to the glider.

The fourth criteria is the clearance area needed for each landing method. This is an aspect which will influence the versatility of the glider, as the larger a required landing area, the more infrastructure that need to be put in place.

With some landing methods requiring separate calculations to quantify this criteria, multiple equations were used. The conventional, no-flare and stall require rectangular shaped clearances, since they approach the destination in a straight line. Note that an average glide ratio of 31 is assumed for the conventional approach, to take into account the extended flight length due to the flare. The same rectangular clearance area shape will be assumed for the nosedive,

which will be allowed to have a glide ratio of up to 0.25. Equation 7.3 is used for these three methods, with GR , h and w being respectively the glide ratio, the clearance height of 20 [m] and the width of the clearance, taken to be 10 [m], allowing the glider some margin during the approach.

With this equation, it can be found that the conventional, no-flare, stall and nosedive landing methods require a clearance area of 6,200, 6,000, 2,000 and 50 [m²] respectively. This shows why the first two methods got a very poor score, while the stall has got an acceptable one and the nose dive an excellent one.

$$A_{Str\ clear} = GR * h * w \quad (7.3)$$

The clearance area needed for the corkscrew landing is assumed to be a circle with the minimum turning radius allowed for the load factor of 2 g , plus an additional 3 [m] half wingspan of based on initial estimates. The radius is found using Equation 7.4, which can be found in literature [46].

The minimum radius for a 2 g load is found to be 30 [m]. When adding to this the half wingspan, it is easy to find that an area of 3,421 [m²] has to be cleared for this landing method. This relatively high value explains why a score of 2 is assigned to the clearance criteria of this landing method.

$$r_{corkscrew} = \frac{V^2}{g\sqrt{n^2 - 1}} \quad (7.4)$$

The area required for the parachute landing method is also assumed to be a rectangle: for this trade-off, it will be assumed that the glider reaches terminal velocity and starts to drift with the wind immediately after parachute deployment. For this, Equation 7.5, derived from the kinematic formulas and the drag equation is used, where V_w , h , r_{par} , m , g , ρ , $C_{D_{par}}$ are the wind velocity, the parachute deployment height, the parachute radius, the glider's mass, the gravitational acceleration, the air density and the parachute drag coefficient, respectively. The first variable, V_w is taken to be 6.7 [m/s], as this was the first estimate of the average wind to expect at ground level. The parachute deployment height is 20 [m], effectively the clearance height defined in the paragraphs above. The parachute's radius is taken to be 5 [m], based on existing airplane parachute systems, such as the *Cirrus Airframe Parachute System* (CAPS) [12]. The drag coefficient is assumed to be 1.75, following the typical drag coefficient given by NASA⁵.

With these values, it is possible to find a clearance area of 1530 [m²]. This gives the parachute landing method a score of 3 for the clearance needed, as it is quite a large area.

$$A_{Par\ clear} = V_w * h * \sqrt{\frac{\rho * \pi * r_{par}^2 * C_D}{2mg}} * 10 \quad (7.5)$$

The fifth and final criteria is the landing accuracy. This is a criteria which takes into account the effect of a GPS error during final approach and the landing approach's general accuracy and susceptibility to external factors. It is found by simply multiplying the glide slope specific to the landing method with a GPS altitude error of 1 meter. For the parachute deployment, the glide ratio right before the parachute deployment of 30 is used.

Each of these criteria are given a weight in percentage which reflects how important each of those is found to be for the military stakeholder. These percentages add up to 100%.

The clearance needed is ranked with its 34.5% importance, as the most important aspect for the landing method. It is important for the stakeholder to set up its field hospital, the glider's destination, in any location, irrespective of how big a nearby field is.

The criteria is followed by the accuracy of the landing method, which has a weight of 24.1%. This is important from a safety perspective, as no bystanders are to be hit by the landing glider, and also from the perspective of the urgency of the situation. A field medic does not have time to search a nearby forest for the blood he might need to save a life. The aircraft must thus land reliably within a small designated area such that the blood can be retrieved quickly.

The third most important criteria is that of the touchdown forces, which are important for the safety of bystanders, but also for some of the electronic components. It was found through a discussion with a military blood expert that the standard blood bags can sustain high forces as long as they are full encapsulated [27]. For various components from the GNC and EPS subsystems and the payload compartment, however, the landing must be relatively soft so that these parts are not damaged too much and can be reused for future missions. The touchdown forces were therefore given a weight of 20.69%

The approach forces and the control complexity each receive a weight of 10.34% as it is deemed that the control systems can always be engineered in a good way, given enough literature, regardless of the relative complexity. The approach force criteria also receives a low weight because they are will not be very high when compared to other phases of the mission, such as the pull up during deployment, and thus have only limited impact on the structural design of the glider.

⁵URL <https://www.grc.nasa.gov/www/k-12/VirtualAero/BottleRocket/airplane/rktvrecv.html#:~:text=The%20air%20density%20has%20a,produces%20a%20lower%20terminal%20velocity.> [cite 19 2020]

Table 7.1: Trade-off scores of the landing methods

	Approach Forces	Touchdown forces	Control complexity	Clearance needed	Accuracy
Conventional	4	5	4	1	3
Crash (No-flare)	5	5	5	1	3
Stall (abrupt)	3	4	3	3	4
Corkscrew Landing	3	5	2	2	3
Nose dive (abrupt)	3	1	4	5	5
Parachute	3	4	1	4	2

Table 7.2: Landing methods criteria weights

	Approach Forces	Touchdown forces	Control complexity	Clearance needed	Accuracy
Weights	10.34%	20.69%	10.34%	34.48%	24.14%

Table 7.3: Landing methods total scores

	Total score
Conventional	2.93
Crash (No-flare)	3.14
Stall (abrupt)	3.45
Corkscrew Landing	2.97
Nose dive (abrupt)	3.86
Parachute	3.10

From the trade-off table it can be seen that only the stall and corkscrew landings have no criteria with an unacceptable level of performance and that, of these two, the stall landing has the higher score. For this reason the stall landing was chosen as the landing method for the EcoGlide gliders. Since the glider will only enter a stall at 20 *m*, the glider will need to bleed altitude in the likely scenario that it reaches the final waypoint at too high an altitude. This will be done following a corkscrew flight path that will transition into stall at 20 *m* above the ground.

Requirements

After the mission has been defined and the various functions of the guidance, navigation and control subsystem had been established in section 4.4 and section 4.4, the requirements of the subsystem could be defined. These requirements are split up for the different phases of the mission: deployment, cruise and landing. These requirements can be seen in Table 7.4, Table 7.5 and Table 7.6, respectively. All the requirements are labelled 'TBD' under compliance. This is because it is impossible to determine if the EcoGlide system will be able to meet these requirements at this stage of the design. Simulations and flight tests will be necessary to determine this and the EcoGlide team recommends performing these tests as soon as the design has reached a stage where this is possible.

Table 7.4: Deployment requirements

Identifier	Requirement Statement	Compliance
R_EG_DEP_01	The glider shall detect its release from the balloon within 0.2 [s].	TBD
R_EG_DEP_02	The orientation of the glider shall be calculated with an accuracy of at least 0.5° on all axes.	TBD
R_EG_DEP_03	The glider shall keep a distance of no less than 50 [m] when performing the turn into the direction of the destination.	TBD
R_EG_DEP_04	The glider shall at no point be closer than 10 [m] to the tether.	TBD
R_EG_DEP_05	The glider shall dive till it reaches an airspeed of 30.5 [m/s].	TBD
R_EG_DEP_06	The glider no more than 2 <i>g</i> during the whole launch manoeuvre.	TBD

During the deployment of the glider, the glider must clear the deployment system while gaining the speed and orientation needed for the transition to the cruise phase. The first step in this is that the glider needs to detect that it has been released from the balloon. It was decided that the glider should be able to detect this within 0.2 [s] because at this point the glider will have fallen less than 20 *cm* and will have a speed of less than 2 [m/s]. This speed is well under the stall speed and there is no chance of the glider colliding with the tether if it only travels 20 *cm*. Since the glider is released with the wind, the wind should naturally push the glider away from the tether so the point of the release, where the glider is 5.8 [m] from the tether, should be the closest point that the glider is to the tether within a small margin of error.

After the glider has been released it will enter a dive to gain speed. This dive will continue until the aircraft has achieved the initial cruise speed of 30.5 [m/s]. To ensure that this manoeuvre is performed correctly it is important that the

glider's orientation can be accurately measured. The value of 0.5° was taken as this is a typical value for the small gyroscopes in mobile phones [55], but this value can most likely be improved upon.

After the dive the glider will have to pull up and perform a turn towards its final destination. This will likely result in the highest forces on the glider of the whole deployment procedure. To ensure that no damage is caused to the glider structure, it is required that the accelerations are kept under $2 g$. During the turn the glider should still keep its distance from the balloon. To account for any drifting of the balloon it was decided that the glider should keep a minimum distance of $50 [m]$ from the glider.

Table 7.5: Cruise requirements

Identifier	Requirement Statement	Compliance
R_EG_CRU_01	The glider shall follow a cruise and loiter flightpath up to an accuracy of $10 [m]$.	TBD
R_EG_CRU_02	The glider shall detect sinks and thermals of at least that displace the glider more than $1 [m]$ vertically.	TBD
R_EG_CRU_03	If at any point in the mission the glider is less than $20 [m]$ above the ground, the glider will initiate an early landing	TBD

During the cruise phase of the mission the glider will follow a straight path between waypoints. It was decided that the glider should follow this flight path with an accuracy of $10 [m]$. This was chosen as it allows for an GPS error as well as an additional error due to wind gusts [52].

During the glider's flight it may encounter thermals or sinks that could have an impact on the glider's altitude. The glider should be able to detect sinks that have displaced it more than $1 [m]$ vertically as anything less would have a negligible impact on the flight path. Once these thermals or sinks have been detected the glider should be able to use them to either gain or bleed altitude as necessary. The locations of these sinks and thermals could also be input into the glider before deployment through the use of a weather model.

If at any point the glider falls under an altitude of $20 [m]$ it should start the landing procedure. This height was chosen as it is the clearance height that the glider is expected to clear during landing and it is unlikely that the glider will be able to recover altitude at this close to the ground without colliding with obstacles.

Table 7.6: Landing requirements

Identifier	Requirement Statement	Compliance
R_EG_LA_01	The glider shall be able to limit its airspeed to $15 [m/s]$ for landing.	TBD
R_EG_LA_02	The glider shall start a stall landing approach within $200 [m]$, horizontally, of the destination.	TBD
R_EG_LA_03	The glider shall start to loiter above the landing spot until an altitude of $20 m$ is reached. TBD	
R_EG_LA_04	During loiter the glider shall experience an acceleration of no more than $2 g$.	TBD
R_EG_MA_03	The landing accuracy shall be no less than $50 m$.	TBD
R_EG_PERF_06	The glider shall be able to land autonomously at its designated landing area.	TBD
R_EG_LA_05	The glider shall be able to clear obstacles of $20 [m]$ height at a TBD distance of the landing spot.	TBD
R_EG_LA_06	The glider shall perform the approach at a slope of no less than 20% .	TBD
R_EG_LA_07	The payload shall be accessible after landing.	TBD

The first stage of the landing procedure will start with the glider entering a spiral flight path to bleed any excessive altitude. This is referred to as the loiter phase. Much like in the deployment phase, the glider should not experience any accelerations above $2 g$ so as to preserve its structural integrity. The loiter phase shall continue till the glider is at a height at which it can enter a stall for its final approach.

The height at which the glider will enter this stall was chosen to be $20 [m]$. This was chosen as it should allow for the glider to fly over most obstacles such as trees and most buildings. The glider will then have a horizontal distance of $200 [m]$ to make it to the ground. This was chosen from an assumed maximum glide ratio of 10 during stall. This also directly gives the approach flight path slope of 20% .

During the actual landing is when the payload will likely experience the highest forces. These forces can not be too great or the blood bags will burst. To ensure that this is the case, the airspeed should be limited to $15 [m/s]$ as this will result in forces that the glider structure and payload compartment will be able to absorb. During the actual landing the glider will break apart, but it is important that the payload is still accessible after this. Part of ensuring this falls under the responsibility of the GNC system, as the manner in which the glider first hits the ground will play a big part in the payload's accessibility.

The remaining two requirements, R_EG_MA_03 and R_EG_PERF_06, were set during an earlier design phase in a previous report [26]. R_EG_PERF_06 is vital for the mission that the EcoGlide was designed for. If the glider needs to be controlled for it to land then the EcoGlide system will be a significantly less attractive product for the military. The same applies for the landing accuracy in R_EG_MA_03, if the glider lands too far away from the desired location, the end user will have to spend time searching for the glider which would be unacceptable for the time sensitive case of blood delivery.

7.2. Design Approach

It was decided early on in the design process to use off-the-shelf hardware and software for the GNC subsystem. Using components that are widely used in other similar aircraft will improve the reliability of the system as these components have already seen extensive testing. It will also lower the initial costs of the system as hardware and code such as servos and a flight controller do not need to be separately designed and tested. To size these components however, first the control surfaces have to be sized. This is due to the fact that the forces acting on these control surfaces will directly affect the sizing of the actuators which will have a knock on effect as to which flight control boards are compatible with these servos. For this reason it was decided to consider the control surfaces as part of the GNC subsystem. This subsection will detail the design approached used to size the control surfaces and calculate the forces acting on these control surfaces.

Elevon Sizing

Due to the blended wing body design of the EcoGlide, the only control surfaces the EcoGlide gliders will be elevons located on each of the wings. Elevons are a combination of both ailerons and elevators and therefore have to be able to control all pitching and rolling motions of the glider.

Due to this being a less conventional design concept, there is not as much literature available for how to size elevons. For this reason, it was chosen to size the elevons using a combination of both analytical and statistical methods. First, the control surfaces were sized as if they were only ailerons, taking solely the roll performance into account. This was done using an aileron sizing method found in literature [47].

After initial values for the elevon size were obtained by treating them solely as ailerons, these values were compared to the elevons of similar pre-existing aircraft. This allowed for the sizing process to be iterated on until the elevons followed the trend of the other aircraft.

Analytical Sizing of Ailerons

The first step taken in the elevon sizing was to treat them solely as ailerons and size them analytically using the method from literature [47]. The first step in this method is to determine the aircraft class and from this the roll requirements. It was decided that the EcoGlide glider should fall under class I for small light aircraft. This means that the aircraft should be capable of rolling 60° in 1.3 [s] [47].

The second step is to set limits for the aileron size and determine the aileron effectiveness, τ . It was decided to have the aileron extend all the way to the wing spar as the spar would make a sturdy hinge point. This meant that the aileron would cover 45% of the chord. From Figure 7.7 it can be seen that this results in an aileron effectiveness of 0.65. Initial spanwise starting and ending positions for the ailerons were also chosen at 60% and 90% of the half span respectively. This lead to the aileron starting at $y_i = 1.473$ [m] and ending at $y_o = 2.33225$ [m].

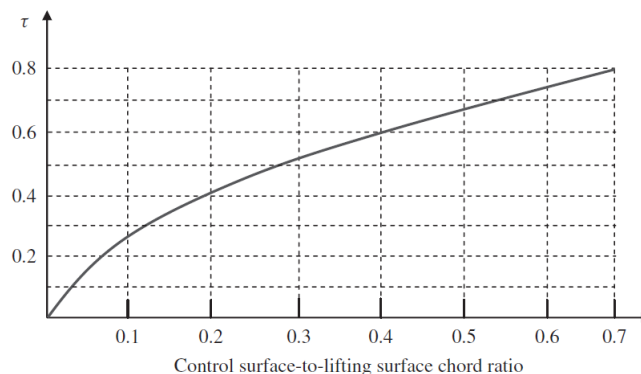


Figure 7.7: Aileron effectiveness vs aileron chord to wing chord ratio

Now that the initial aileron dimensions and requirements have been determined the $C_{l_{\delta A}}$, the aircraft rolling moment coefficient due to aileron deflection derivative, must be calculated. This represents how much the rolling moment coefficient of the aircraft changes with aileron deflection. This coefficient can be determined using the Equation 7.6. In this equation y is the spanwise location. The aircraft variables can be found in Table 7.7. Equation 7.6 returns a $C_{l_{\delta A}}$ of 0.3962.

$$C_{l_{\delta A}} = \frac{2C_{L_{aw}}\tau C_r}{Sb} \int_{y_i}^{y_o} y + 2y^2 \left(\frac{\lambda - 1}{b}\right) dy \quad (7.6)$$

Table 7.7: Aircraft variables used for the aileron sizing

Variable	Description	Value
S	Wing surface area [m ²]	1.5053
S _{tot}	Wing surface area + Fuselage surface area [m ²]	2.21
b	Wingspan [m]	4.91
λ	Taper ratio [-]	0.38
C _r	Root chord [m]	0.542
C _{L_{aw}}	Lift slope of the 3D wing [-]	4.9722
V _{stall}	Airseed at stall [m/s]	15
I _{xx}	Aircraft mass moment of inertia [kg*m ²]	10.934

With the aircraft rolling moment coefficient due to aileron deflection derivative now calculated the aircraft rolling moment coefficient C_l , not to be confused with the lift coefficient, at maximum aileron deflection can be determined. This is done by multiplying $C_{l_{\delta A}}$ with the maximum aileron deflection. The maximum aileron deflection was taken to be 25°, or about 0.436 [rad] to avoid aileron stall [47]. This gives the aircraft rolling moment coefficient to be 0.1729. From the roll moment coefficient the rolling moment, L_A , due to maximum aileron deflection can be computed. This is done using Equation 7.7. The moment was calculated at stall as this would be the critical case where the ailerons would not be as effective due to the lower speed. Since the aircraft will enter stall during landing, the air density, ρ , was taken to be equal to the air density at sea level, 1.225 [kg/m³]. L_A was calculated to be 176.1060 [Nm] for this configuration.

$$L_A = \frac{1}{2} \rho V_{stall}^2 C_l S b \quad (7.7)$$

The steady state roll rate, P_{ss} can be derived from the rolling moment through Equation 7.8. For this equation the rolling drag coefficient, C_{D_r} , and the distance between the rolling drag centre and the centre of gravity, y_D , are needed. The C_{D_r} was taken to be 0.9 in accordance to literature [47] and similarly the distance between the rolling drag centre and the centre of gravity was taken to be 0.4% of the half span leading to a y_D value of 0.982 [m]. This equation gives P_{ss} to be equal to 12.3552 [rad/s].

$$P_{ss} = \sqrt{\frac{2L_A}{\rho S_{tot} C_{D_r} y_D}} \quad (7.8)$$

After the steady state roll rate has been calculated, the bank angle at which the aircraft reaches this roll rate must be determined. This can be done with Equation 7.9. From this equation the bank angle at which the aircraft roll rate becomes steady is given to be 23.8277 [rad] or 1365.2267°. This means that the aircraft will reach the bank angle of 60° in the class I requirement before the roll rate has become constant.

$$\Phi_1 = \frac{I_{xx}}{\rho * S_{tot} * C_{D_r}} \ln P_{ss} \quad (7.9)$$

The angular acceleration of the aircraft in roll with ailerons fully deflected till the aircraft has reached the steady state bank angle, Φ_1 , can now be computed. This is done using Equation 7.10. Calculating the angular acceleration for this configuration gives 3.2032 [rad/s²].

$$\dot{p} = \frac{P_{ss}^2}{2\Phi_1} \quad (7.10)$$

Now finally the time required until the aircraft will reach a bank angle of 60° can be determined. The equation, Equation 7.11, for this is simplified because the glider will reach this bank angle before it reaches a steady state. The time is found to be 0.8086 [s] which is quite a bit quicker than the required maximum of 1.3 [s]. This means that the aileron size can be lowered significantly. This whole process was iterated upon several times until an aileron size was found that met the class I requirements while not being too over designed. The aileron size was also compared to other aircraft to get the final elevon sizing. This is explained in the following subsection.

$$t = \sqrt{\frac{2\Phi_{req}}{\dot{p}}} \quad (7.11)$$

Statistical Sizing of Elevons

In order to size the elevons, it was needed to perform statistical comparisons between similar aircraft, as the EcoGlide team was unable to find methods to numerically determine the required elevon size. Indeed, after calculating the necessary size of the elevons were they to cat solely as ailerons, the team had trouble finding a direct method of calculating the elevon size for elevator functions. More conventional aircraft, those with a tail, have well documented equations to compute the required size of the tail and its elevator. For these however, the tail volume coefficient is required [41], which is impossible to calculate for a blended wing body aircraft.

Therefore, data from ten different radio controlled blended wing body aircraft and flying wings and data from two existing human piloted flying wings were found in the hope of finding a relation between certain parameters. The radio controlled aircraft include off-the-shelf hobby aircraft as well as custom creations by individual hobbyists. The human-piloted aircraft include old flying wings which were designed as gliders. The main search criteria used is a relatively high aspect ratio wing and relatively docile flight characteristics. That is, the aircraft in the list are not specifically designed for agile flying, such as aerobatic flights, but rather more conventional flights.

Data was collected on their wingspan, sweep, chord, elevon root and tip position along the wingspan as well as the elevon's trailing edge with respect to the local chord. To find this information, the team often had to measure manually the different variables on top view pictures of the aircraft. It is summarised in Table 7.8. With this data it is possible to find information on, among other aspects, the wing and elevon surface area and aspect ratio using the equations described in the section above.

Scatter plots comparing different variables with each other were created, however none showed a reliable trendline. The most promising plot is that of Figure 7.8, which seems to show through its trendline a linear relation between the elevator area and the wing area. The R^2 value is close to 1, indicating a close fit.

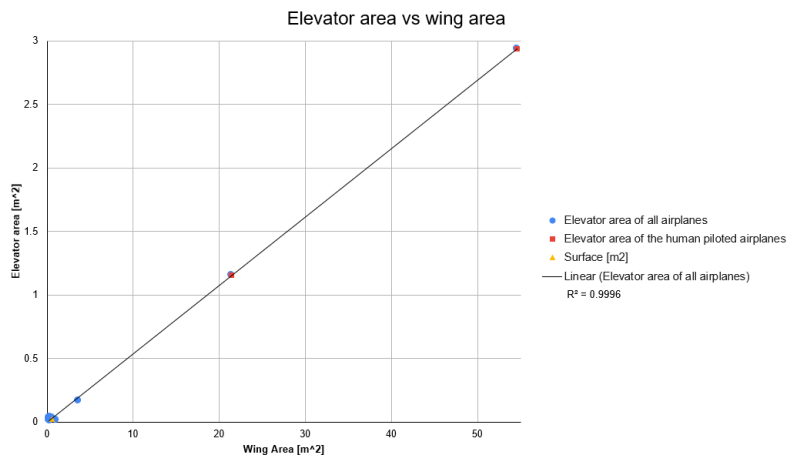


Figure 7.8: Statistical data of the model aircraft and human piloted aircraft's elevon versus their wing area

However, when one zooms in on the part of the graph in Figure 7.9 showing the data points belonging to the radio controlled and UAV blended wings, significant dispersion can be observed. It is probable that the two far off data points of the human piloted aircraft cause the trendline to be excessively skewed towards them.

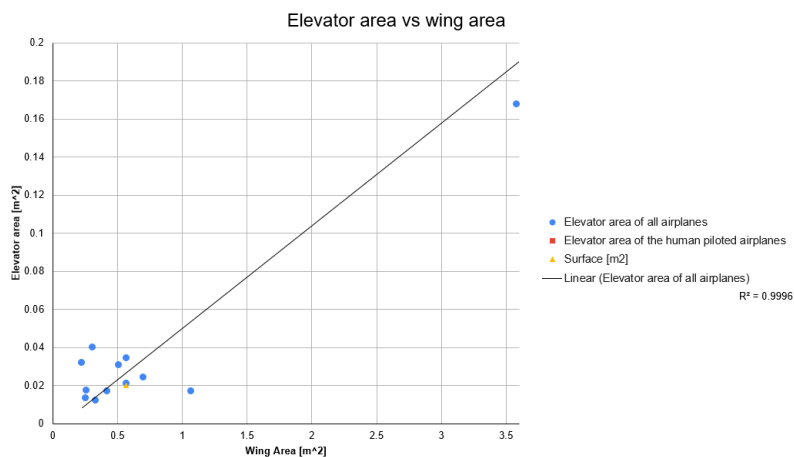


Figure 7.9: Zoomed in graph of Figure 7.8 showing the statistical data of the model aircraft and human piloted aircraft's elevon versus their wing area

Table 7.8: Data about the elevons and wings of existing UAV and real aircraft

Name	Wingspan[m]	Wing sweep	Root chord	Tip chord	Elevon span start [% of .5b]	Elevon span end [% of .5b]	Elevon chord start [% of c]	Elevon chord end [% of c]
5 Foot Flying Wing (Big Aspect Ratio) ⁶	1.524	15	0.17	0.127	12.50	100	33	33
HobbyKing®™ Go Discover FPV Plane ⁷	1.6	30	0.32	0.1	38.90	90	13	23
FT Versa Wing ⁸	0.96	29	0.4	0.15	23	100	24	16
FT Spear ⁹	1.04	32	0.42	0.17	11.60	100	28	40
Boeing Insitu ScanEagle ¹⁰	3.1	25	0.2	0.13	48	99	33	25
Opterra 2m Wing ¹¹	2	25	0.5	0.2	52	95	23	22
Skywalker X8 ¹²	2.12	19	0.38	0.16	54	98	18	27
3 metre wing soaring bopeep ¹³	3	15	0.19	0.19	50	98	25	25
Flying wing glider ¹⁴	2	25	0.24	0.18	48	97	25	15
Prandtl-D No.3 ¹⁵	7.62	28	0.67	0.27	42	88	25	25
Flying Wing UAV Evolution ¹⁶	3.4	15	0.49	0.14	65	99	12	20
Horten H.IX V2 ¹⁷	16.8	28	4.8	1.7	54	100	33	40
Horten H.I b ¹⁸	12.4	21	3.1	0.36	45	91	25	62
THE BLACKWING EBW-160 UAV ¹⁹	1.6	23	0.26	0.06	65	100	30	80

Nevertheless, in this plot as well as in the other plots made, one could still assess how much the current elevon size makes the team's Ecoglide glider design fit into the cloud of the data points for other similar aircraft. As such, iterations were performed to see to what extent the design would resemble that of the other similar aircraft. At the same time, the torque caused by such elevons was recalculated for each iteration (with the method described in the next section), to assess what kind of servo would be needed to actuate these elevons.

The final elevon is chosen to span from 70% to 95% of the halfspan and have a constant relative chord of 55%. This was chosen not only to maximise the resemblance with the statistics as much as possible, while also meeting the required roll rate and preventing excessively high torques on the servo.

Calculating Force on Elevons

Now that the elevons have been sized, the forces acting on each of these elevons can be determined. This will allow for the sizing of the actuators needed to rotate the elevons to be designed. The force on the elevons was calculated as the difference in lift and drag acting on the wing due to an elevon deflection. It was assumed that this difference in force acts directly through the centre of pressure of the elevon. This is an overestimation as the difference in the resultant force would likely not act entirely on the elevon but be distributed over the wing. This method however will provide a first estimation that will likely result in the slightly higher predicted force than the actual force which is acceptable.

The largest force difference would occur when both elevons are deflected downwards to the maximum deflection. Deflecting the elevons during cruise increases the effective angle of attack of the whole aircraft as shown in Figure 7.10. With a cruise angle of attack, α_{cruise} of 4.4° or 0.0768 [rad], a maximum elevon deflection of 25°, the elevons starting and ending at 70% and 95% of the half-span, respectively, and the elevons covering 45% of the chord, the "virtual" angle of attack, $\alpha_{virtual}$ was found to be 0.2882 [rad] at cruise.

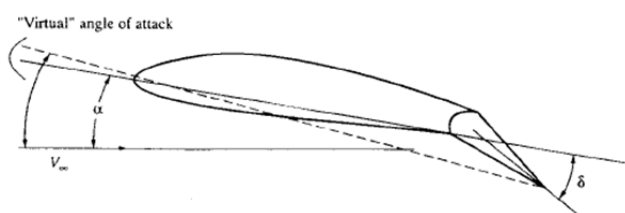


Figure 7.10: Virtual angle of attack due to elevon deflection [28]

The new lift coefficient for the wing with elevons fully deflected at cruise, $C_{L,\delta_{max}}$, was taken as the weighted average of the lift coefficient at the higher virtual angle of attack and the lift coefficient of the wing without the elevons deflected.

¹<https://www.youtube.com/watch?v=bdlxhvqbAe4>

²https://hobbyking.com/en_us/hobbykingr-tm-go-discover-fpv-plane-epo-1600mm-kit.html

³<https://s3.amazonaws.com/plans.flitetest.com/stonekap/FT-Versa-plans.pdf>

⁴https://s3.amazonaws.com/plans.flitetest.com/stonekap/FT_Spear_v1.0_Full-Size.pdf

⁵<https://www.boeing.com/defense/autonomous-systems/scaneagle/index.page> and https://en.wikipedia.org/wiki/Boeing-Insitu_ScanEagle

⁶<https://www.horizonhobby.com/product/airplanes/airplanes-14501--1/bind-n-fly/opterra-2m-wing-bnf-basic-p-efl111150>

⁷<https://www.readymaderc.com/products/details/skywalker-model-x8-black-wing>

⁸https://www.youtube.com/watch?v=oMtc3_0WYws

⁹<https://www.youtube.com/watch?v=ZA5148NrOZs>

¹⁰<http://www.nestofdragons.net/weird-airplanes/flying-wings/special-horten-flying-wings/nasa-prandtl-project/>

¹¹<https://www.youtube.com/watch?v=zAC1RvqefKc>

¹²https://en.wikipedia.org/wiki/Horten_Ho_229

¹³https://en.wikipedia.org/wiki/Horten_H.I

¹⁴<https://www.eclipson-airplanes.com/ebw-160-uav>

This can be seen in Equation 7.12 where the 0.25 comes from the fact that the ailerons extend over 25% of the wing span. The zero angle of attack lift coefficient, C_{L0} , is equal to -0.048 and the lift slope for the wing, $C_{L_{\alpha w}}$, is equal to 4.9722 . Equation 7.12 gives $C_{L,\delta_{max}}$ to be equal to 0.5966 .

$$C_{L,\delta_{max}} = C_{L0} + C_{L_{\alpha w}}(0.25 * \alpha_{virtual} + (1 - 0.25) * \alpha_{cruise}) \quad (7.12)$$

The total difference in lift and drag due to full elevon deflection can now be determined using Equation 7.13 and Equation 7.14 where $C_{D,\delta_{max}}$ can be obtained from $C_{L,\delta_{max}}$ and the equation for the drag polar, found in Equation 5.4. Again the cruise values were taken because this will result in the largest difference in forces due to the fact that the airspeed will be the highest during cruise. The air density was also taken to be the sea level value of $1.225 [kg/m^3]$. From these equations and the aircraft parameters, S equal to $1.5053 [m^2]$, $C_{L,cruise}$ equal to 0.3338 and $C_{D,cruise}$ equal to 0.0119 , the difference in lift and drag are equal to $131.01679 [N]$ and $3.8318 [N]$, respectively.

$$\Delta L = \frac{1}{2} \rho V_{cruise}^2 S (C_{L,\delta_{max}} - C_{L,cruise}) \quad (7.13)$$

$$\Delta D = \frac{1}{2} \rho V_{cruise}^2 S (C_{D,\delta_{max}} - C_{D,cruise}) \quad (7.14)$$

To calculate the moment caused by these forces on the hinge, the total force acting perpendicular to the elevon and the distance between the point at which this normal force acts and the hinge point of the elevon is needed. Since the lift always acts perpendicular to the airspeed vector while the drag always acts parallel to the airspeed vector the total normal force, N can be found with simple trigonometry as seen in Equation 7.15. From this equation the total force acting normal to the elevon chord is given to be $116.0247 [N]$. The normal force per elevon is obtained by taking half of this value, $58.01235 [N]$.

$$N = \Delta L \cos(\delta_{max} + \alpha_{cruise}) + \Delta D \sin(\delta_{max} + \alpha_{cruise}) \quad (7.15)$$

The elevon will be hinged at the rear spar and it was assumed that the force will act halfway through the mean aerodynamic chord of the elevon. In reality, it will act closer to the leading ledge of the elevon.²⁰ This will result in a higher calculated moment than the actual moment, but this was done intentionally as not to underestimate the torque that would be required to deflect the servo. The distance between the acting point of the normal force and the hinge is therefore set to be $0.0728 [m]$. The moment acting on the hinge for each elevon can now be calculated by multiplying this distance with the normal force per elevon. This moment is equal to $4.2239 [Nm]$.

7.3. GNC Software and Hardware

In this section the various components of the GNC system will be described. This section has been split up into three subsections, one explaining the actuator mechanism sizing, one on the sensors and the final on the flight controller software and hardware.

Actuation mechanism

Once the moment acting on the elevon hinge has been determined, in section 7.2, the actuator that will deliver this moment can be chosen. It was decided to use off-the-shelf shelf servos. Servos were chose due to their rapid and accurate responses to control inputs. Off-the-shelf servos are also widely used in the RC and UAV communities which leads to them being low cost and because they are well known it is easy to find information such as their accuracy and compatibility with different flight controllers.

After looking at multiple different servos, it was chosen to use the *ANNIMOS 25kg RC Digital Servo*²¹ for the control surface actuation. This servo is capable of delivering up to $2.4517 [Nm]$ of torque, but at the $5.5 [V]$ that it will be run at in the EcoGlide system it will deliver closer to $2.2065 [Nm]$. This is less than the moment that will be acting on the hinge of the control surfaces but this difference will be made up for with the actuation mechanism. The small size, $40 \times 20 \times 40.5 [mm]$, and low weight, $75 [g]$, of this servo also means that it will easily be compatible with the EcoGlide gliders.

With the control surfaces sized and the servo chosen the mechanism can now be designed that will transfer the actuation torque to the control surfaces. Different options were considered and are shown in Figure 7.11. The two main options are to place the servos in the wings or in the fuselage. The latter is the most preferred option as it would allow the military a quick and easy retrieval of the electronics after the glider has landed.

²⁰URL <https://www.grc.nasa.gov/WWW/K-12/airplane/cp.html> [cite 10 Jun 2020]

²¹https://www.amazon.com/ANNIMOS-Digital-Torque-Waterproof-Control/dp/B07GJ6ZCVY/ref=psdc_2234131011_t3_B073F92G2S

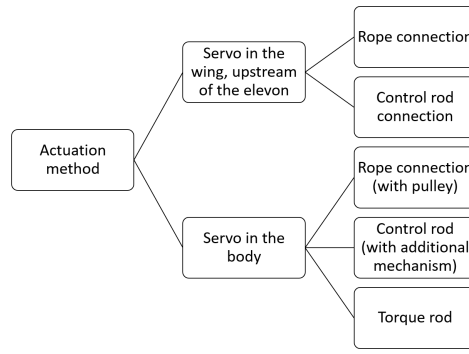


Figure 7.11: Design options for the actuation mechanism

After choosing to place these servo in the body, a mechanical connection can be made through rope, control rods or a torque rod. The first presents the difficulty during manufacturing, as the ropes must pass through pulleys and will complicate the assembly. The ropes must be attached correctly to the servos, such that they are in tension. The control rods also present challenges, as an additional mechanism which rotates the load transfer from being parallel with the trailing edge to being perpendicular to it. This adds weight. The last option, the torque rod, is the most simple as the rod would be directly connected to the elevon and only a small control rod needs to be connected to the servo with the torque rod. For this reason it was chosen to use a torque rod.

The torque rod was chosen to be biodegradable Hachiku bamboo so it can be disposed of in the same way as the rest of the glider. This wood provides high strength at a low weight. According to a 2010 study, the shear modulus, G of Hachiku bamboo is $1.6 [GPA]$ and the density of this bamboo is $0.824 [kg/m^3]$ [30]. This means that a solid bamboo rod with a radius, r , of $2 [cm]$ and a length, L , of $1.7185 [m]$ results in only 1.0284° of twist, θ for the $4.2239 [Nm]$ maximum torque, T_{max} calculated to act on the elevon. This can be verified using Equation 7.16.

$$\theta = \frac{2T_{max}L}{G\pi r^4} \quad (7.16)$$

With the torque rod sized, the connection between the servo and the torque rod can now be designed. This connection will be made of a control rod between the servo's arm and an arm extended from the torque rod. Since this control rod will be easily retrievable together with the servos and the rest of the electronics, it can be assumed that it is made out of some strong metal, and to be relatively short and therefore lightweight. The control rod's sizing is for now assumed to be done in later stages, possibly through testing.

The remaining part of the actuation system which needs to be sized is the arm ratio, that is the ratio of the torque rod arm, d_{torque} , over the servo arm, d_{servo} . To do so, one can simplify the problem by assuming that the control rod keeps the same orientation, and that both arms are perpendicular to the control rod at a zero deflection angle. The second assumption is quite justifiable, as this can be realised in practice. The first one, however, might not be fully correct, as the short control rod would rotate slightly, but not enough to make the approximation invalid for the preliminary design.

With the above assumptions, one can derive Equation 7.17, which computes the arm ratio using the angles of deflection of the servo arm, α_{servo} , and of the torque rod, α_{torque} . Using this, one can plot Figure 7.12, which shows that the arm ratio required increases, as the servo's maximum deflection increases. The *ANNIMOS 25kg RC Digital Servo* has a 90° deflection range (for a total rotation capabilities of 180°). This would imply an arm ratio of almost 2.4, which is quite significant. In order to reduce this, it is chosen, for this preliminary design, that the servo would only use its deflection range until 50° . As such, an arm ratio of only 1.9 is required to make the elevon rotate by 25° . This has the added benefit that if the control surfaces are found to be too ineffective, one can always make the servo rotate a bit more, in the hope of increasing the effect of the surfaces.

$$\frac{d_{torque}}{d_{servo}} = \frac{\sin(\alpha_{servo})}{\sin(\alpha_{torque})} \quad (7.17)$$

This actuation mechanism led to the design shown in Figure 7.13 and Figure 7.14, where the dark grey square represents the servo, the blue rectangle the elevon, the black rectangle the torque rod arm and the dark brown elongated rectangle the torque rod. The black rod serves as the initial connection between the servo and the remaining torque rod. The actual connection between the black and dark brown rod will have to be designed in a further stage. It should not pose significantly big difficulties, as the required rotational range of the torsion rod is only 50° , 25° in each direction.

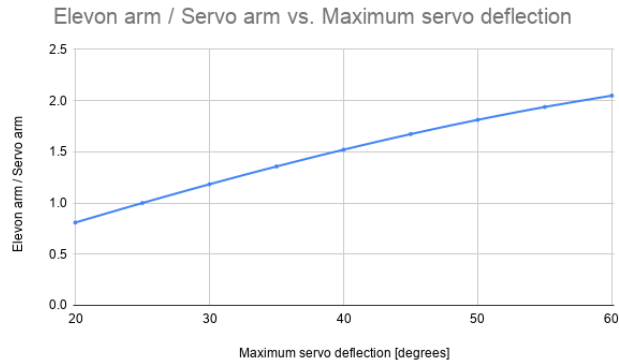


Figure 7.12: Arm ratio required for a given maximum servo deflection

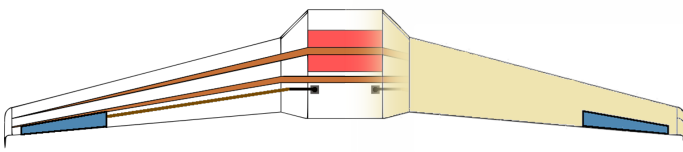


Figure 7.13: Top view of the elevon actuation mechanism

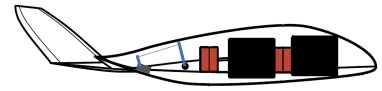


Figure 7.14: Side view of the elevon actuation mechanism

Key Sensors

In order to perform Guidance, Navigation and Control, adequately, the glider needs to be able to determine its current state through sensors. This can be done by means of a large combination of different sensors. However, because the glider is single use product, the electronics must be kept as simple and low cost as possible. This is why it was chosen to try and stick to the bare necessities: a GPS, accelerometers and gyroscopes. All the different sensor data could then be combined through a special algorithm, such as a Kalman filter [19], which would have the ability to increase the accuracy of the state estimation. Each of the key sensors will first be described and then the flight controller hardware, including sensors, and software that will be used in the gliders will be determined in this subsection.

The GPS receiver is a key sensor, as it is the simplest and most common means of determining a UAV's location and ground speed. Common, off-the-shelf UAV GPS receivers such as *Radiolink Electronic's* SE100 GPS module have positional accuracy's around 2 meter [54]. This error is small enough that the glider could use this GPS and meet all requirements but the error can also be reduced by means of a Kalman filter for an even higher accuracy.

The accelerometer is an important sensor since it gives information about the glider's movement, deployment and can even be used to measure if the glider is passing through sinks or a thermals. This sensor measures the acceleration in the three body axes of the glider. It therefore can sense if the aircraft accelerates in some particular direction. This is useful to confirm the breaking of the break-wire as a consequence of the glider's release from the balloon. An accelerometer would also be key in detecting major sinks and thermals, as they let the glider know if it is accelerating vertically. Finally, the in-flight accelerometer data can also be integrated to add to the GPS velocity and positional measurements. A Kalman Filter can greatly help with this [19].

Gyroscopes are the third essential type of sensors needed for the EcoGlide glider. They provide the airplane with key information on its attitude during all flight phases. Knowing the angular orientation is needed in particular during the deployment, where the glider starts vertically and has to level out horizontally, and the landing, during which the glider has to maintain a high angle of attack. During the waypoint navigation of the cruise phase, it is of course also crucial to make sure that the wing remains level.

Flight Controller

There are many different commercially available flight controllers and flight control boards. It was decided to first choose an open source flight controller and then pick a flight control board that was compatible with this software. Open source flight controllers have the benefit of being easily modifiable, which will allow for a more versatile system. This will also help future-proof the EcoGlide system as the system can be easily updated. Since not all flight control boards are directly compatible with all flight control software, the control board could only be chosen after the control software had been determined.

Flight Controller Software

The EcoGlide team considered several different possible open source flight controllers: *ArduPilot*²², *LibrePilot*²³, *Cleanflight*²⁴, *Betaflight*²⁵, *MultiWii*²⁶, *AutoQuad*²⁷ and *PX4*²⁸.

Many flight controllers are designed for more traditional remote control drones. Since the EcoGlide will be a fixed wing autonomous glider it was decided to immediately eliminate the controllers more solely focused on multicopters and the controllers with limited autonomy capability. This left *ArduPilot*, *LibrePilot*, *PX4*.

ArduPilot has been around longer than the other flight controllers and due to this has the most additional features. It has been adapted to be able to control all kinds of autonomous vehicles from submarines to helicopters and the large use base adds to the trustworthiness of the controller. *ArduPilot* even already has a soaring mode that takes advantages of thermals²⁹.

For all the reasons listed above, *ArduPilot* would have probably been the controller that was chosen for the EcoGlide project were it not for how it is licensed. *ArduPilot*, and also *LibrePilot*, are both available under general public licenses or GPL. Due to this any modifications made to the code must also be made open source. This is part of the reason that so many features are so easily available for *ArduPilot*. This, however, may pose an issue for the EcoGlide, as for main users, the military, it would be unacceptable that all the source code of one of their logistics drones is so openly accessible. Due to this it was chosen to avoid any control software that is available under GPL.

This leaves *PX4* as the only viable flight controller. Like *ArduPilot*, *PX4* also has a large user base and can be used for a large range of different vehicles. It is easy to find support online and the documentation is easily accessible. *PX4* is available under a Berkeley Software Distribution, or BSD, license. This is similar to the license that *ArduPilot* is available under, but it allows for modifications of the code without having to make these changes public. This is a positive for the military, but it does mean that there are less features openly available for the *PX4* controller. However, since the code and algorithm for features such as autonomous soaring for the *ArduPilot* system are so openly available, porting this functionality to a *PX4* controller would not be too difficult [49].

The Px4 software also uses such a Extended Kalman Filter (EKF) algorithm³⁰. This will combine the data from all sensors to allow for a better estimate the glider's state [20].

The Px4 software architecture is shown below in Figure 7.15 It is adapted from the Px4 architectural overview.³¹ The diagram shows the different software blocks and their order. First, the computer estimates the gliders position and orientation based on sensor input. Then, it calculates the required direction to stay on track and the movement needed to achieve this. Finally, a mixer converts these signals to motor commands, which are sent to the servos.

Flight Controller Hardware

After the flight controller software had been determined, a flight control board that supports this software could be chosen. All of the different flight controllers listed on the *PX4* website³² were looked at and considered. In the end it was chosen to go for the *PixHawk 4 Mini*³³.

The *PixHawk 4 Mini* is listed as one of the *Pixhawk* standards, meaning that it has been designed and tested to be completely compatible with the *PX4* software. Along with the *PixHawk 4* it is the newest version of the *Pixhawk* flight control boards and therefore will ensure for certain future-proofing of the EcoGlide glider. The lower price and smaller size of the *Mini* is why it was chosen over the standard version.

Various sensors are either built into or come with the *PixHawk 4 Mini*. Built in are two accelerometers/gyroscopes, a magnetometer and a barometer. These sensors are more than the bare necessities listed in Figure 7.3 but since they are all built into the flight control board they will not take up any extra space.

Included with the *PixHawk 4 Mini*, but not built inside the actual control board, is a GPS sensor that has an accuracy of 2.0 [m] [54]. Through the use of the other sensors and the *PX4* Kalman filter the accuracy can be improved³⁴. With these filters the sensor will be able to determine the location of the glider with more than enough accuracy to meet the GNC requirements.

The main downside to using the *PixHawk 4 Mini* is the price. Other gliders are available that are cheaper than this flight controller, but they do not all have the same compatibility guarantees. An example of a cheaper flight control board that could be used with *PX4* is the *Kakute F7*³⁵. This flight control board is, however, missing several features

²²<https://ardupilot.org/>

²³<https://www.librepilot.org/site/index.html>

²⁴<http://cleanflight.com/>

²⁵<https://betaflight.com/>

²⁶<http://www.mutiwii.com/>

²⁷<http://autoquad.org/>

²⁸<https://px4.io/>

²⁹URL <https://ardupilot.org/plane/docs/soaring.html> [cite 18 June 2020]

³⁰https://docs.px4.io/v1.9.0/en/advanced_config/tuning_the_ecl_ekf.html

³¹<https://dev.px4.io/v1.9.0/en/concept/architecture.html>

³²<https://px4.io/autopilots/>

³³https://docs.px4.io/v1.9.0/en/flight_controller/pixhawk4_mini.html

³⁴https://dev.px4.io/v1.8.2/en/tutorials/tuning_the_ecl_ekf.html

³⁵https://docs.px4.io/master/en/flight_controller/kakutef7.html

such as a GPS and a protective casing, but if needed these could be added later. This would however complicate things which is why the team decide not to go for this option.

The hardware present in the glider is summarised in Figure 7.16. As can be seen, the Pixhawk computer is central in the configuration. Furthermore, various types of interactions are shown by the colored arrows.

Flight Controller Data Flow and Block Diagrams

With the flight controller hardware and software now chosen, the data flow can be analysed. This is visualised in Figure 7.17. Relevant pieces of hardware are shown with the data they provide. This is then processed using the Extended Kalman Filtering (EKF) algorithm previously mentioned. This data is then combined with the destination in the Guidance and Control software. The destination is set using a different computer before deployment. The hardware and software block diagrams for the GNC are also shown below in Figure 7.15 and Figure 7.16, respectively.

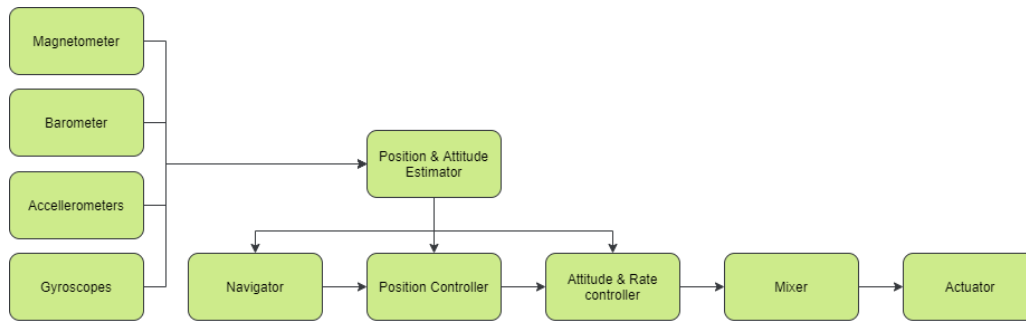


Figure 7.15: Software Block Diagram

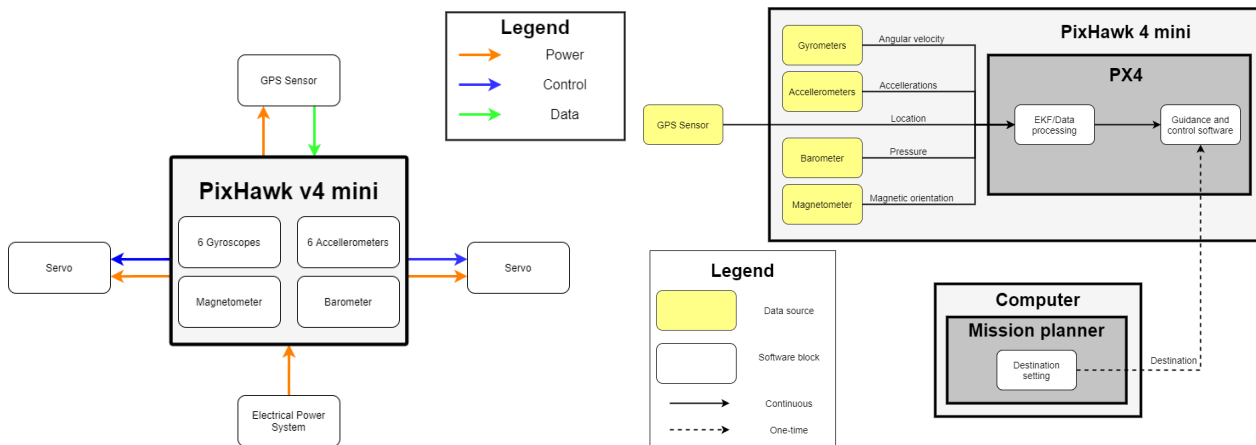


Figure 7.16: Hardware Block Diagram

Figure 7.17: Data Block Diagram

7.4. Design Overview

The role of the guidance, navigation and control subsystem can be split over the three mission phases, deployment, cruise and landing. The GNC subsystem can be seen as the brains of the glider as it gives the glider commands regarding what it should do, be that travelling between waypoints during cruise or entering a deep stall for landing. The glider then executes these commands through actuation of the control surfaces. Through deflecting the elevons located near the wing tips of each wing, the glider is able to perform all the actions needed to complete its mission.

In terms of hardware, the Guidance Navigation and Control design requires a flight controller, sensors and actuators. It was chosen to take off-the-shelf components, as this would simplify the design significantly. The final components chosen are listed in Table 7.9 together with their dimension, mass and relevant specific information. The final dimensions of the control surfaces that will allow for the glider to perform any of the manoeuvres necessary during flight are given in Table 7.10.

Table 7.9: Final components used for the GNC design

Item	Quantity	Dimension [mm]	Mass [kg]	Specific info
Holybro Pixhawk 4 Mini with GPS receiver	1	38x55x15.5	0.037	NA
ANNIMOS 25kg RC Digital Servo	2	40x20x40.5	0.075	[22 kg * cm] at 5.5 [V]
Hachiku Bamboo Torque Rod[30]	2	20(radius)x1719	0.002	NA

Table 7.10: Final elevon dimensions

	Spanwise starting position [m]	Spanwise ending position [m]	Elevon area [m ²]	Maximum moment on hinge [Nm]
Elevon	1.7185	2.3323	0.0731	4.2239

The communications diagram of the whole system can be seen below in Figure 7.18. Here a complete overview of how all the different components of the system interact with each other can be seen. All the sensors output data to the on-board computer, or the flight controller. The flight controller also takes GPS coordinates from GPS satellites, whether the glider has been deployed or not from the break wire and the locations of the waypoints which are manually inputted by Tom Kazansky. The flight controller then uses all this data to output commands to the servos which actuate the control surfaces.

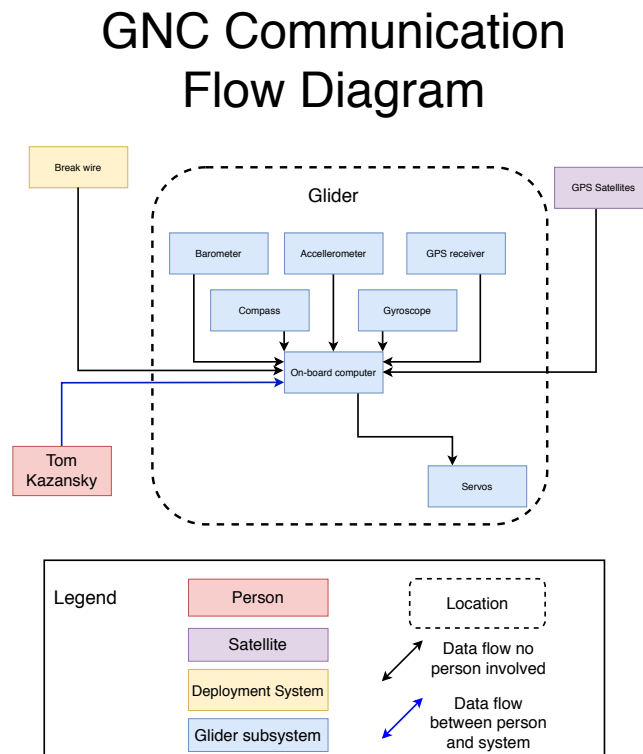


Figure 7.18: GNC communications diagram

7.5. Verification & Validation

The control surfaces were sized partially analytically and partially statistically. The analytical sizing method has to be verified and validated to confirm that it was implemented correctly. The statistical method used was, in a way, also a form of validation since it compared the elevon size to elevons that are being used in real aircraft. Since all the data for this statistical sizing method was obtained from real aircraft and not from calculations that the EcoGlide team made themselves, this can not really be verified or validated separately and it would be unnecessary to do so.

The analytical sizing method used for the elevon sizing followed the aileron sizing method found in literature [47]. This method consists of many separate intermediate calculations. To make sure no errors were made in any of these steps, it was decided to perform each calculation twice, separately. Doing this would quickly point out any inconsistencies between the two sets of calculations. This allowed for the quick detection of any errors in the implementation of the calculations and once both sets of calculations could be made consistent with each other it could be verified that each individual calculation had been correctly applied.

To verify that all the different components were working together correctly a system test was performed. It was decided to plot the aileron surface area against the time it would take the glider to rotate 60° with ailerons of that size. This was done because a size for the ailerons is the initial input for the calculations and the rotation time is the final output. The graph plotting these variables can be seen in Figure 7.19.

Figure 7.19 shows that with an increasing aileron size the time required reduces. This is logical as a greater surface area will be able to generate more force and thus a higher roll rate. The graph shows that there are diminishing returns for larger aileron sizes, which can be explained by the fact that the angular acceleration scales with the natural logarithm of the roll rate squared, i.e. $\frac{\ln(3)}{\ln(2)} > \frac{\ln(1001)}{\ln(1000)}$. The shape of the graph is therefore as expected and the calculations can be verified to be working correctly as a whole.

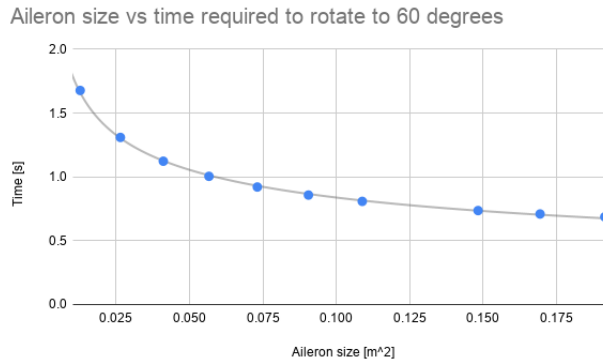


Figure 7.19: Aileron surface area vs. time required to rotate 60°

To validate the GNC system flight tests and wind tunnel will be needed. The exact effect of deflecting the elevons should be tested using a prototype of one of the EcoGlide gliders in a low speed wind tunnel, such as that available on the TU Delft campus. This would give a much better idea of how the glider will perform during an actual mission.

Validating that the GNC software is operating as intended will also have to be done through flight tests. This will give much more accurate results than any simulation. Ideally, the flight tests would be performed in the exact environment where the actual missions will be performed, but even testing in the Netherlands will provide an abundance of useful data that would help improve the design.

7.6. Risk Assessment

The GNC system defined above presents a number of potential risks which ought to be mitigated. These risks can be found in Table 7.11 together with their mitigation method. Some of the more important risks are those numbered 2 and 8, which deal with the glider hitting an obstacle or the sensor data being too noisy or wrong. Both would have critical or catastrophic consequences. Nevertheless, even these can be mitigated in such a way that their risk level is much lower (moderate instead of moderately high and high, respectively).

Table 7.11: Guidance navigation and control risks

Index	Risk Factor	Severity	Probability	Risk	Mitigation Method	Severity	Probability	Risk
1	The elevon sizing is insufficient	ca	i	m	Small scale and/or full scale test to assess the glider's controllability	ca	n	l
2	Glider hits an obstacle during the approach	c	p	mh	Implement stall landing to reduce the landing area size and analyze visually the landing area before launch	c	i	m
3	Electronics get wet due to rain	c	i	m	The PLA coating of the wings should make the airframe withstand water for a period of time	c	n	l
4	Servos do not produce enough torque	ca	i	m	Perform tests to assess the servo torque	ca	n	l
5	Torque rod fails due to the high torques applied	ca	i	m	Test the rods before the first test flight and increase if necessary the thickness	ca	n	l
6	The Flight controller is unable to keep the glider stable during the stall approach	c	i	m	Perform small scale test flights and if needed, perform further research into software for stalled approaches	c	n	l
7	The glider does not follow the pre-programmed flight path correctly, resulting in a loss of the glider	c	i	m	Review the navigation code if this is a re-occurring problem, or send a new glider if it only happens once.	c	n	l
8	The flight controller receives erroneous or too noisy data from its gyroscope and accelerometers	ca	p	h	Attach the Flight Controller firmly to the aircraft to prevent vibrations of the FC and calibrate the sensor data before the flight.	ca	i	m

Table 7.12: Guidance navigation and control risk-map

(Unmitigated) / Mitigated	Highly Probable (h)	Probable (p)	Improbable (i)	Negligible (n)
Catastrophic (ca)		(GN8)	(GN1) (GN4) (GN5) GN8	GN1 GN4 GN5
Critical (c)		(GN2)	(GN3) (GN6) (GN7) GN2	GN3 GN6 GN7
Marginal (m)				
Negligible (n)				

7.7. Sustainability Analysis

All of the electronic components of the GNC components can be easily removed from the glider and reused for future flights, given that they are not too damaged during flight. The components that are not removed are either made from the same materials as the rest of the glider structure, elevons, or made from bamboo, torque rods, which can be disposed of in the same sustainable manner as the rest of the glider. This means that in most cases the GNC subsystem will have no discernible effect on the sustainability or life-cycle costing of the EcoGlide system.

The only scenario where this may not be the case would be if the electronics were damaged during a mission to the point where they could not be reused for a subsequent mission. In this case the electronics would either have to be repaired or disposed of along with the other non-biodegradable waste in accordance to the military's guidelines.

8

Payload Box

As explained in chapter 1 Pete needs near daily deliveries of blood, and he needs 6 litres per delivery. While it is very important for the glider to reach Pete, this doesn't matter if the blood doesn't survive the trip. The payload compartment, which serves to protect the blood is thus a crucial subsystem. The blood is stored inside bags that hold 0.5 [l] of blood each. The team received two bags from the military stakeholder for testing. The bags were filled with water to find the dimensions of a full bag, which are 115x170x32 [mm³]. In total, twelve of these bags must be transported. This chapter elaborates the design of this compartment. The first section serves to clearly define the functions the payload container must fulfil, and the design requirements that come with it. The design approach explains the physics behind the design, gives reasoning for the design choices and explains the calculations that are used. In section 8.3 the final payload box concept is presented. The following sections serve to substantiate the final concept. Starting with the material choices, which are elaborated in section 8.4. The thermal and structural analysis models used for calculations are explained in section 8.5 and section 8.6 respectively. These models are then verified and validated in section 8.7. section 8.8 shows the sensitivity to small changes in input parameters. A risk assessment is given in section 8.9. Finally, in section 8.10 the sustainability of the payload compartment is analysed.

8.1. Functions and requirements

By exploring the functions the blood storage must fulfil in order to succeed in the mission, proper requirements can be set. These requirements then help to guide the design and ensure the final concept is suitable. The functions shown in the functional flow diagram are elaborated below, after which the payload requirements are presented.

Functions

The primary function of the payload container is protecting the blood it contains during the mission. The optimal storage temperature for blood is 4 [°C]. However, it may deviate from this temperature by ± 2 [°C]. The upper limit serves to limit bacterial growth, the lower limit ensures the blood cells don't get ruptured¹. Additionally, the blood bags in which the blood is stored can break, causing the blood to spill out. The payload box must protect the blood bags, to ensure they don't get damaged. The box as a whole should also be sturdy, such that it does not break during handling. Furthermore, in the scope of the mission the box has to be easily loaded and unloaded after landing. The box also needs to actually fit inside the glider. Finally, after the blood has been extracted at the field hospital, it doesn't cease to exist. As mentioned in chapter 1 small subsystems may be retrieved occasionally. To cover all bases the box and cooling elements should both be reusable and biodegradable. This ensures even the worst case end of life scenario is a sustainable one.

Requirements

As explained in chapter 4, user requirements were given to the team by Prof. C.A. Dransfeld. The ones relevant to the payload storage are listed in Table 8.1. Additional requirements are distilled from the functions discussed before, they are shown in the same table. This table also contains a column indicating whether the final concept complies with the requirement. In an earlier phase of the project, requirements were already discovered meaning some functions already had a suitable requirement [26]. However, as the design has progressed some of these older requirements are no longer relevant and are omitted. Additionally, new requirements have come to light.

As explained in the functional analysis, the boxes and cooling elements should be both biodegradable and reusable. This inspires the addition of two requirements stating the subsystem as a whole should be biodegradable and reusable. With the mission parameters now more clearly defined, two requirements based on the operational envelope are added. The first states the payload boxes will be effective in the expected ambient temperature range. The second states the payload boxes will be effective for at least the expected transit duration.

The blood bags are prone to breaking when subjected to impact forces, this is covered by the requirement stating the payload shall be protected during landing. The blood itself, does not get damaged by these impact forces. [14] [27]

¹URL <https://rmlh.nic.in/index1.aspx?lid=552&lsid=558&pid=47&lev=4&langid=1> [Cited 29 June 2020]

Table 8.1: Payload subsystem requirements

Identifier	Requirement Statement	Compliance
R_EG_ENBD_02	The glider shall be able to transport a payload of at least 6 [L] of blood.	section 8.2
R_EG_ENBD_01	The maximum total mass of the glider including cargo shall be 25 [kg].	section 8.2
R_EG_STRUC_1	The glider shall protect the payload during landing.	section 8.2
R_EG_STRUC_2	The glider shall protect the payload during flight.	section 8.2
R_EG_PL_04	The blood will be in a temperature range between 2 and 6 [°C]	section 8.5
R_EG_PL_06	The payload subsystem will be effective in an ambient temperature range between -4 and 44 [°C].	section 8.5
R_EG_PL_07	The payload subsystem will be effective for at least three hours.	section 8.5
R_EG_PL_08	The payload subsystem will be able to support its own weight while loaded.	section 8.6
R_EG_PL_09	The payload subsystem will fit inside the glider.	section 8.2
R_EG_PL_10	The payload subsystem will be simple to load and unload.	section 8.2
R_EG_PL_11	The payload subsystem will be biodegradable.	section 8.4
R_EG_PL_12	The payload subsystem will be reusable.	section 8.4

8.2. Design Approach

This section serves to describe the design approach which lies at the basis of the payload box design. The payload box design was done in close contact with the A&P and structures departments as the subsystems impact each others dimensions and weight budgets. It should be noted that this section presents only the methodology used for the thermal and structural analyses while the final results of the analyses are presented in section 8.3. Finally, the reasoning behind specific material choices is presented in section 8.4.

Configuration

In section 8.1 a requirement is identified that states the payload box has to fit inside the glider. As mentioned in chapter 6 two spars run through the body of the glider. Additionally, it is aerodynamically favourable to have a thin body design as explained in chapter 5. This does not leave enough space for all the blood bags to be placed in a single container. The team therefore chose to split the payload up into two containers. This is unfavourable for temperature control due to an increased surface area, as will become clear in the section on insulation. However, this downside is relatively minor compared to the performance loss of a thicker airfoil and added weight and of a disturbed spar. A disturbed spar would also complicate production and assembly. Additionally, splitting the payload over two containers places the cg of the glider more forward, which is favourable for stability.

The payload containers are shaped as cuboids. While a more complex shape could be used to limit surface area and mass, this would greatly complicate production and assembly of the boxes. For this same reason, the boxes are designed to be identical, each holding six bags of blood. Figure 8.1 shows the maximum cuboid volumes that could fit inside the glider. While the rear compartment is larger, the boxes are identical in size, meaning the front compartment decides the maximum outer dimensions of the box.

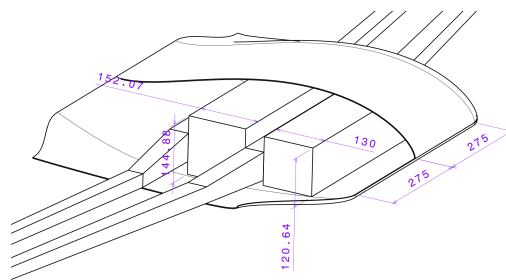


Figure 8.1: Maximum cuboid volumes that fit in the glider

Impact resistance

As mentioned in section 8.1 the blood bags are vulnerable to rupture. During manoeuvring and especially during landing, the glider may experience shocks that could cause damage to the blood bags if they are not properly protected. Blood bags are often centrifuged to separate the blood components, this happens at high RMP². The blood bags do not break in this process because they are supported on all sides. In this way the blood bag material is only loaded in compression, while avoiding tensile forces that damage the bags.

In order to support the blood bags on all side a filler material will be used inside the payload boxes. This ensures the blood bags can not move inside the container and will not be loaded in tension. Filler materials are often used when

²URL <https://www.hettichlab.com/en/product/rotixa-500-rs/> [Cited 29 June 2020]

shipping fragile goods and allow for easy assembly³.

Thermodynamics and temperature control

A proper understanding of the thermodynamic principles that affect the payload box design is necessary to control the blood temperature during the mission. Therefore this section will briefly explain thermal energy, heat transfer, temperature and phase change.

Thermal energy and heat transfer

Thermal energy is a form of kinetic energy and is measured in Joules. It explains the vibrations of atoms inside a system. Similarly to thermal energy, heat is measured in Joules. This addition of heat can take place in three ways: Conduction explains heat transfer through the collision of molecules or atoms. This is the main mode of heat transfer in solids, because here the particles are close together. Convection only takes place in fluids, as it requires the movement of particles from one location to another. This mass movement relocates thermal energy. Heat transfer can also occur in a vacuum, through radiation. Radiation is a type of electromagnetic radiation, meaning it does not need a medium to travel. To aid in understanding, Figure 8.2 shows the principles discussed.

Heat flow (q) is the amount of heat added to a system per second, its unit is $[J/s]$ or $[W]$. This heat flow takes all modes of heat transfer into account. Heat flows from warmer to colder regions on its own accord, as stated by the second law of thermodynamics⁴.

Temperature and phase change

Thermal energy is a total value like mass, Temperature on the other hand indicates the intensity of the manifestation of thermal energy⁵. Every material changes temperature with more or less ease, this is reflected in the specific heat of a material, given in $[J/kgK]$. When heat is added while maintaining constant pressure c_p is used, when a constant volume is maintained c_v is used.

Phase changes involve high amounts of thermal energy as a reorganisation of the particles takes place. The latent heat of fusion of a material describes the amount of energy required to melt. The same amount of energy is released when a material solidifies. While this change in phase takes place, the temperature does not change.⁶

Figure 8.3 graphically shows the temperature of a fixed mass of material with increasing thermal energy. The effect of this latent heat must not be underestimated, the latent heat of fusion for water is $335 [kJ/kg]$, this is more than 80 times the c_p of liquid water.

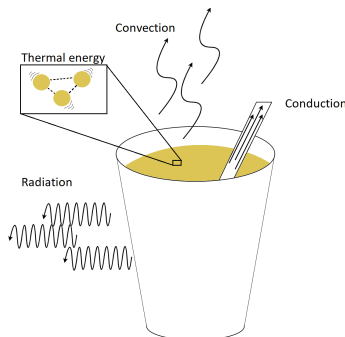


Figure 8.2: Thermal energy and heat transfer of a cup of tea

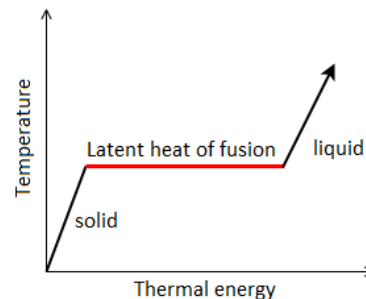


Figure 8.3: Latent heat of fusion

Temperature control

From the previous discussion, two main ways of temperature control follow to keep the contents of the payload box within the safe temperature range. Heat flow should be obstructed to limit the decrease or increase of thermal energy. At the same time, using the effect of phase changes a thermal buffer can be created such that a larger change in thermal energy is acceptable. Limiting the heat flow can be done through insulating the box, building the thermal buffer is done using phase change material elements. Both subjects will be elaborated in the following subsections.

Insulation

To limit the heat flow from a hot location to a cold location, a barrier wall can be placed between them. This barrier stops radiation and, if not permeable, convection. Energy still flows through the wall, through conduction. Naturally the properties and dimensions of the wall determine how well the heat flow is hindered. The difficulty with which the

³URL <https://www.dhlexpress.be/en/shipping-and-receiving/choosing-the-right-filler-material-to-protect-your-shipment/> [Cited 29 June 2020]

⁴URL <https://www.livescience.com/50941-second-law-thermodynamics.html> [Cited 29 June 2020]

⁵URL <https://sciencing.com/thermal-energy-definition-equation-types-w-diagram-examples-13720809.html> [Cited 29 June 2020]

⁶URL <https://courses.lumenlearning.com/boundless-physics/chapter/phase-change-and-latent-heat/> [Cited 29 June 2020]

heat is transferred between the air and the surface of the barrier is quantified with surface resistances. The heat flow through a one dimensional wall is considered first, then the heat flow calculation is expanded to including the edges and corners of a structure.

1D heat flow

A materials thermal conductivity (λ) quantifies the ease with which the conductive heat transfer through the wall happens. Thermal conductivity is measured in watts per meter Kelvin, denoted as $[W/mK]$. The thermal resistance (R) of a one dimensional barrier plate takes the thickness of said barrier into account as well. It is calculated by dividing the thickness of the plate by the thermal conductivity of the material. This resistance is given as $[m^2K/W]$. It quantifies the plates resistance to heat flow. When multiple barriers are placed in series, the resistances of both layers can be added together. Figure 8.4 graphically shows the thermal flow through a multiple layer wall.

This figure is incomplete, as mentioned before both sides of the barrier bring about a surface resistance. The heat has to be transferred between the wall and the surrounding air, before it can move through the wall. That is why, in order to find the full resistance of the wall, two surface resistances are added. Like the wall resistances, they are measured in $[m^2K/W]$. A more in depth explanation for surface resistances is given in a later subsection. Figure 8.5 shows the same layered wall as before, now including the surface resistances.

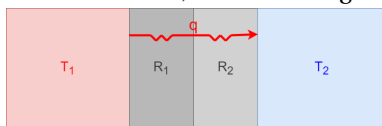


Figure 8.4: Thermal flow through a wall



Figure 8.5: Thermal flow through a wall, including surface resistance

Both surface resistances and the wall resistances can be summed up to find the total resistance of the wall. As discussed earlier, the resistances of the wall are determined by dividing the thickness of each layer by the thermal conductivity of the material. The reciprocal of the total thermal resistance is the U-value. It's units are $[W/m^2K]$, meaning this U-value indicates how many Watts of heat pass through one square meter of wall, per degree of temperature gradient over the wall. Equation 8.1 shows the equation for calculating the U value of a wall. Using this U value, the heat flow over the one dimensional wall with n layers can be calculated using Equation 8.2.⁷

$$U = \frac{1}{\sum_{i=0}^n \frac{t_i}{\lambda_i} + R_{s1} + R_{s2}} \quad (8.1)$$

$$q_{1D} = U * A * \Delta T \quad (8.2)$$

Before the surface resistances are further explored, Equation 8.2 is expanded from a 1D wall, to an actual box.

Thermal bridging, 2D and 3D heat flow

Thermal energy doesn't only escape perpendicularly through the walls. When two walls are joined together, heat also travels through the edges between two walls. This can be seen in Figure 8.6, the orange arrows represent the thermal flow not considered in the 1D case. This additional thermal flow is called linear thermal transmittance, the edges of the cube are so called linear thermal bridges. Similarly, point thermal bridges are located at the corners, where three walls meet. Figure 8.7 shows a cube with its thermal bridges highlighted, light blue showing the linear bridges, and dark blue showing the point bridges. [10]

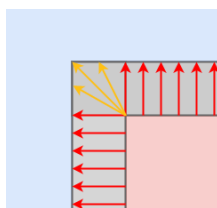


Figure 8.6: Heat flow in a linear thermal bridge

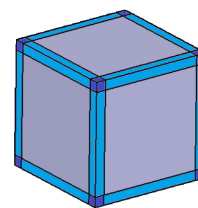


Figure 8.7: Linear and point thermal bridges on a box

Equation 8.2 can now be expanded with thermal bridging terms to form the heat flow equation in 3D, this yields Equation 8.3 [10]. This equation considers the heat flow over the borders of a cuboid with 6 walls, 12 linear thermal bridges and 8 point thermal bridges. The length of the j^{th} thermal bridge is denoted by l_j , ψ_j is the linear thermal transmittance of this bridge in $[W/m * K]$ and χ_k the point thermal transmittance of the k^{th} point thermal bridge, also in $[W/m * K]$. This expanded equation for heat flow also considers the possibility for the different walls around the volume to have different U values.

⁷http://fac.ksu.edu.sa/sites/default/files/uvalues_definition_and_calculation.pdf [Cited 29 June 2020]

$$q_{3D} = \Delta T * (\sum_{i=0}^6 U_i * A_i + \sum_{j=0}^{12} l_j * \psi_j + \sum_{k=0}^8 \chi_k) \quad (8.3)$$

Surface resistance

The heat transfer onto or from the wall happens through all three modes of heat transfer. The convective and radiation modes are highly dependent on the surface properties and air conditions such as wind velocity. This makes it unfeasible to accurately calculate exact surface resistances without testing, the surface resistance are therefore estimated using equations detailed in ISO 6946 [38]. These calculations do not consider conductivity, as air is a poor conductor. Surface resistances are calculated using Equation 8.4 [38].

$$R_s = \frac{1}{h_c + h_r} \quad (8.4)$$

h_c is the convective coefficient and h_r is the radiative coefficient, both are in [$m^2 K/W$]. The radiative coefficient again is highly dependent on surface and environmental conditions making accurate calculations unfeasible, it can be estimated using Equation 8.5 [38], where σ is the Boltzmann constant [J/K], T_{mn} is the mean temperature of the surface and its surroundings, in Kelvin, and ε is the unitless emissivity of the surface. The emissivity is a material property that explains how well it reflects radiation⁸

$$h_r = 4 * \varepsilon * \sigma * T_{mn}^3 \quad (8.5)$$

For the convective coefficient, a distinction is made between internal and external surfaces. This is because wind velocity inside a closed space is considered close to zero, while this is generally untrue for external conditions. For internal surfaces, this leads the convective coefficient to be dominated by the natural convection currents where warm air flows upwards and colder air flows downwards. Due to this natural convection, the internal surface resistance is different for walls with different orientations as the flow interacts with these surfaces differently. Table 8.2 gives the internal convective coefficients (h_{c_i}) that are used in calculations per ISO 6946 [38].

Table 8.2: Internal convective coefficients [38]

Direction of heat flow	Upwards	Horizontal	Downwards
$h_{c_i} [m^2 K/W]$	5	2.5	0.7

On the outside surface, convection is dominated by the wind velocity. The external convective coefficient (h_{c_e}) and can be estimated using Equation 8.6 [38], where V is the ambient wind velocity.

$$h_{c_e} = 4 + 4 * V \quad (8.6)$$

It is important to reiterate that surface resistances are dynamic, as they are highly dependent on the continuously changing conditions of the air around the wall. They are also dependent on the surface properties such as texture and colour. Therefore, the calculations yield estimations, the real surface resistances may be different.

PCM elements

As mentioned earlier, changes in phase take up a lot of thermal energy. The effect can be harnessed to control the temperature inside the payload boxes. This is done through the use of elements consisting of specialised phase change materials, or PCM for short.

When the Ambient temperature is higher than that of the blood in the payload box, adding a PCM element that changes phase at a temperature larger than the starting blood temperature of 4 °C helps to keep the blood cool. At this starting temperature, the PCM is in a solid state. As heat transfers into the payload box this material will start melting, absorbing the thermal energy such that a temperature increase does not occur. Similarly, adding a PCM with a phase change temperature lower than the starting temperature keeps the blood warm when ambient temperatures are low. It is important to note, that these PCM elements may also change density when their phase changes. This causes volume changes inside the box. Because of this, the filler material chosen for the design must be compressible. This way, when the PCM element expands, the filler material can accommodate this extra volume. When the PCM element is expected to shrink, the filler material can be compressed during assembly by firmly pressing down on the lid of the cargo boxes. this then allows the void to be filled by the expanded filler material.

As explained in chapter 1 retrieval of small component of the glider is possible. The team suggests retrieving the PCM elements alongside the electronics, since this enhances sustainability and minimises cost. Nevertheless, PCM elements that are biodegradable are chosen to ensure sustainability even when the elements are not reused.

⁸URL <https://www.npl.co.uk/resources/q-a/why-is-emissivity-important> [Cited 29 June 2020]

Thermal inertia

When the temperature on the outside of the box is increased, this does not lead to an immediate equal change in the heat addition/removal on the inside volume. The insulating walls around the box also absorb some of this heat. When the heat source outside the box is removed, the walls release this energy again. This effect helps stabilise the temperature inside the box. Effectively, a phase shift between the ambient and inside temperature is realised, this can be seen in Figure 8.8, which shows the difference between housing wall insulation with low and high thermal mass.

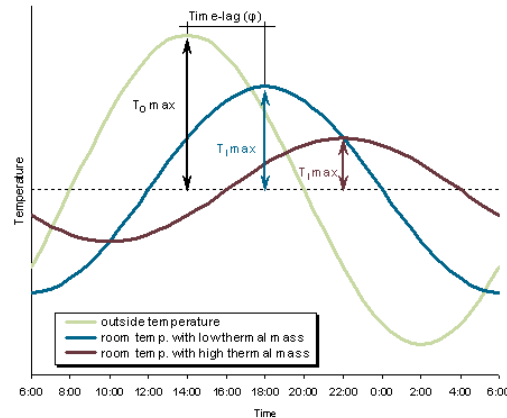


Figure 8.8: Thermal delay visualised⁹

Clearly, the higher thermal mass stabilises the inside temperature more. Thermal mass describes the ability of a material to store heat. To quantify this effect, the volumetric specific heat capacity of a material is used. It is simply calculated by multiplying the specific heat and density.^{10 11 12}

By combining the volumetric heat capacity, thickness of the walls and the U-value, the time lag seen in Figure 8.8 can be calculated. While the exact calculations are beyond the scope of this design phase, an excel tool provided by *the Concrete centre*¹³ can be used.

Thermal homogeneity

With methods discussed earlier in this section, the heat entering or leaving the payload boxes can be calculated. However, it is crucial that the temperature distribution inside the payload boxes is homogeneous. If this is not the case hot or cold spots may form, which means some of the blood may spoil after all.

In order to combat this, the blood bags and PCM elements will be evenly distributed inside the payload box.

Additionally, a uniform insulation thickness aims to distribute the heat flow over the different walls evenly. The reinforcement layer which is discussed in the next subsection does however introduce uneven thickness to the different walls. The surface resistances also vary per wall.

Heat transfer inside the payload box is much easier than through the insulating walls. The thermal conductivity of blood and PCM elements is much greater than that of insulating materials. The filler material does increase the difficulty of this heat flow. However, the blood bags and PCM elements will still form a continuous thermal bridge through direct contact.

Structural integrity of the payload box

While the thermal insulation of the box ensures that the integrity of the blood itself remained un-compromised, it is also necessary to make sure that the box would not collapse on itself or buckle while carrying the blood and PCM. In addition to this, for the outer layer of the box, i.e. the primary structural support layer, the decision to use a strong but low environmental impact material is made. This is because materials with good insulation properties generally tend to be weaker resulting in wall thicknesses that are too high. Hence, in order to limit the thickness, it is necessary to use a material with good strength properties. The outer layer is also of course considered in the thermal analysis in order to ensure a complete thermal analysis of the payload box. The box is structurally sized using plate buckling theory and the approach is elaborated on further in the following paragraphs.

In order to employ plate buckling theory, each side of the box is analysed individually based on the forces it will be facing.

¹⁰URL https://www.new-learn.info/packages/clear/thermal/buildings/building_fabric/properties/time_lag.html [Cited 29 June 2020]

¹¹URL <https://www.new-learn.info/packages/euleb/en/glossary/index6.html> [Cited 29 June 2020]

¹²URL <https://www.amorimcorkinsulation.com/en/advantages/thermal-inertia/> [Cited 29 June 2020]

¹³URL [https://www.concretecentre.com/Publications-Software/Design-tools-and-software/Dynamic-Thermal-Properties-Calculator-\(1\).aspx](https://www.concretecentre.com/Publications-Software/Design-tools-and-software/Dynamic-Thermal-Properties-Calculator-(1).aspx) [Cited 29 June 2020]

Bottom panel

The bottom plate carries the weight of the contents of the box, a uniform transverse load case is considered and shown more clearly in Figure 8.9. The formula used to size the bottom plate and it's re-arranged form in order to obtain the thickness is shown in Equation 8.7 [21].

$$\sigma_{cr} = \frac{K_b \pi^2 E}{12(1-\mu^2)} \left(\frac{t}{b}\right)^2 \implies t = b \sqrt{\frac{12(1-\mu^2)\sigma_{cr}}{K_b \pi^2 E}} \quad (8.7)$$

where K_b represents the buckling stress parameter which has a value of 24.1 due to the simply supported boundary conditions [21]. E represents the Young's Modulus of the material while μ represents the poisson's ratio of the material and σ_{cr} represents the yield stress of the material. Finally, b represents the length of the shorter side of the plate, while t is the thickness that needs to be calculated.

Side plates

The load case considered in the case of the side plates is tensile forces and is represented in Figure 8.10.

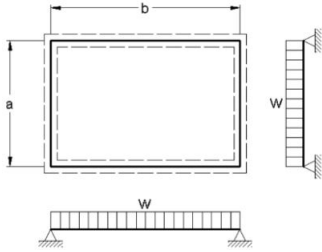


Figure 8.9: Bottom plate loading

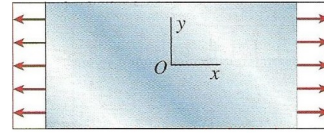


Figure 8.10: Bottom plate loading

The equation used in order to determine the required thickness of the side panels and its re-arranged form is given in Equation 8.8, obtained from [21].

$$\sigma_{cr} = \frac{C \pi^2 E}{12(1-\nu^2)} \left(\frac{t}{b}\right)^2 \implies t = b \sqrt{\frac{12(1-\nu^2)\sigma_{cr}}{C \pi^2 E}} \quad (8.8)$$

where C is a parameter that is derived based on the boundary conditions of the plate being analysed, including ν which is identical to μ , have the same meaning as the ones in Equation 8.7.

Mission parameters

The length of the mission is a crucial piece of knowledge for the payload box design, while it is impossible to know for sure how long all mission phases will take, the preliminary estimates are that loading will take 15 [min], deployment will take 30 [min], the flight phase will last for 105 [min] and unloading is done in 30 [min]. This brings the total mission duration to three hours. As will be explained in the following subsection, a safety margin is added to further increase the likelihood that the boxes will protect the blood successfully.

During the mission ambient conditions that are relevant for the thermal design of the payload boxes change continuously.

The wind velocity around the payload boxes influence the surface resistance. These wind velocities differ every day. On this same note, when the boxes are placed inside the glider for deployment and flight they are protected from the outside wind velocity.

During the deployment and flight phase, the ambient temperature and pressure change as the altitude changes. This change in temperature is relevant for the temperature gradient over the insulation and surface resistances. The pressure is relevant for the box integrity and will cause convection between the air inside the box and the ambient air. The altitude during the mission is shown in Figure 8.11.

Figure 8.12 shows a plot of the ambient temperature progression for the coldest and hottest ground temperature in the operational envelope. The temperature change as a result of altitude is calculated using the ISA convention that the ambient temperature drops with 6.5 [°C/km] in the troposphere. [9] Since the ambient temperature lines for any temperature in between those are thus only translations on the y axis, the area between the upper and lower limit is shaded.

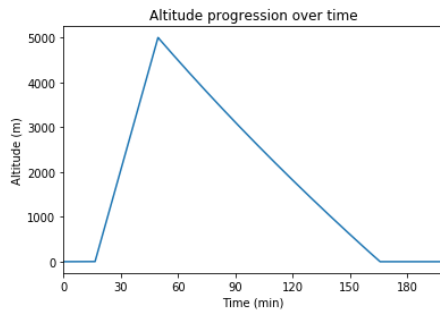


Figure 8.11: Altitude during mission

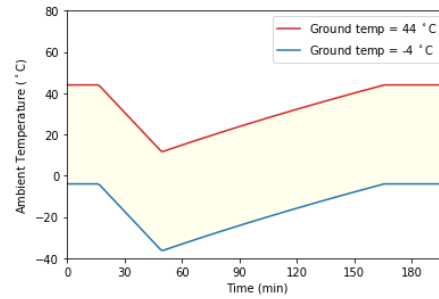


Figure 8.12: Ambient temperature during mission.

Assumptions and safety margins

In order to simplify the payload box analysis and design, a number of assumptions is made. These assumptions are listed below, each assumption also states the effect on the calculated performance of the payload boxes.

A few safety margins are used during sizing, they are listed below the assumption. These safety margins are necessary since assumptions introduce some error in the design. Additional reasons for the specific safety margins are also given.

Assumptions

- The payload box is considered to not be in contact with the glider structure. This structure effectively adds insulation, meaning this assumption decreases the calculated performance.
- The temperature inside the glider is assumed to be equal to the ambient temperature. In reality, this may be different depending on solar intensity, effective wind velocities and other factors. This assumption may therefore lower or increase the calculated performance.
- The exact values for the linear and point thermal transmittance are often unknown, default are used as an approximation. For the payload box design, ISO standards are followed. These neglect the point thermal bridges. The payload box most closely resembles linear bridges C2, C3 and C4. Therefore, a linear thermal transmittance of 0.075 is used in calculations. This assumption may lower or increase the calculated performance. [10]
- The thermal energy stored in the air inside the box is not considered as the mass of the air is negligible. This assumption lowers the calculated performance.
- The contents are considered to be in direct contact with the inner surface. This means there is no air between the wall and the contents, inner surface resistance is thus considered negligible. This assumption lowers the calculated performance.
- Phase changes occur in a narrow temperature range, in calculations the phase change is assumed to happen exactly at the center of this range. This assumption increases the calculated performance.
- Volume change as a result of transferring heat with constant pressure is negligible. This assumption may lower or increase the calculated performance.
- The boxes are not airtight, this leads to four assumptions:
 - The pressure inside the box will equalise with the ambient pressure continuously and without lag.
 - Volume changes in the contents due to the lower pressure at altitude are considered negligible.
 - Specific heats are defined at a specific pressure. The specific heats that will be used are those defined at 1 [atm]. This assumption may lower or increase the calculated performance.
 - Convection due to pressure gradient as a result of altitude is negligible. The change in air volume inside is in the order of grams of air. This assumption increases the expected performance.
 - Natural convection due to the box being not airtight is negligible. This assumption increases the calculated performance.
- The temperature distribution inside the payload box is considered to be homogeneous. This assumption increases the calculated performance.
- Volume changes due to different densities for the cooling element states are in the order of 10^{-1} leading to two assumptions:
 - Volume changes are fully accommodated with (de)compression of the filler material. This assumption increases the calculated performance.
 - The pressure forces exerted on the box walls are considered negligible. This assumption increases the calculated performance of the box.
- Thermal delay is not considered in the analysis as this is in the order of 10^1 minutes and the most challenging mission profiles do not have a change in sign for the temperature gradient. This assumption lowers the expected performance of the box.
- The box will preferably be pre-cooled, but this is not taken into account. This assumption lowers the expected performance of the box.

- The total loaded mass of the box varies depending on the PCM element used as can be seen in Table 8.4. The shift in cg this causes is considered negligible.
- The hoisting velocity in deployment is considered linear. In reality the glider moves horizontally near the balloon as explained in chapter 10. This assumption may increase or decrease the calculated performance.
- With respect to the bottom reinforcement plate, it is firstly assumed that plate is loaded under uniform transverse loading. While this assumption is not exact in terms of reality, it is nevertheless valid since the PCM elements and blood bags have similar densities in addition to being uniformly distributed over the bottom panel.
- The bottom reinforcement plate is assumed to be simply supported on all sides. This results in a buckling stress parameter (K_b) of 24.1 based on literature.¹⁴
- In the case of the side reinforcement plates, the loading assumed is uniform tensile forces. It is also assumed that the side plates are also simply supported on all sides, resulting in a value of 4 for C, used in Equation 8.8, obtained from literature.¹⁵

Safety margins

- The duration of all mission phases are extended by 10%. In this design phase, there is still uncertainty in the duration of the phases. Additionally, as explained in chapter 7, thermals may increase the duration of the flight phase.
- A constricted safe temperature range of 2.5[°C] to 5.5 [°C] is used. This safety margin is used to limit the risk of hot and cold spots.
- The inner insulation layer is not considered load bearing. While the reinforcement layer is considered in the thermal analysis, the insulation layer is not used in the payload boxes structural analysis. This allows for some margin in the structural integrity of the payload box to accommodate for handling.

Sizing and Optimisation

This subsection explains the sizing and optimisation utilised in the payload boxes design. Optimisation is performed such that the payload boxes are not over designed.

While it is possible that the payload boxes as a whole can be retrieved, the design is optimised for the case when only the PCM elements are retrieved. In order to keep the blood in it's safe temperature range, many combinations of PCM element mass and insulation thickness can be considered. With sustainability in mind, using a larger PCM mass with lower wall thicknesses is favourable, as this decreases the amount of non-reusable materials. Therefore, the payload boxes are optimised for empty weight.

There are however constraints to this optimisation. As seen in Figure 8.1 the maximum outer dimensions of the box are 130x550x120.64 [mm^3]. There should be no space between the walls and the blood bags, meaning the inner dimensions for length and depth are fixed to be 115 [mm] and 96 [mm] respectively. Additionally, to keep the MTOW of the glider below 25 [kg] the boxes may not weigh more than 6 [kg] each.

With these constraints in mind, increasing the PCM mass means the PCM elements are thicker, which increases the width of the payload boxes. The PCM elements may increase in volume during the mission, as the different phases have different densities. The maximum thickness the elements can obtain is designed for such that the elements still fit the box when expanded. Through iteration the ratio of different materials in each element is optimised to limit this maximum thickness. When a thinner PCM element is used in a mission, extra filler material is required.

The optimisation is performed using guided trial and error, where results are analysed to quickly converge to the optimal thickness to PCM mass and PCM material ratios. This is done using the thermal analysis tool presented in section 8.5.

Finishing Touches

As an added safety measure, thermal indicator stickers such as *Thermax strips*¹⁶ can be added in the payload boxes. These stickers can be used by Pete to help him asses whether or not the blood survived the trip. Thermal logging devices such as *Tinytag*¹⁷ are much larger than the stickers and therefore not advisable.

To keep the box closed, a biodegradable tape like *Shurtape CT-109*¹⁸, should be used. This taping should be done in such a way that the box is not airtight, the goal is only to keep the box closed.

¹⁴<https://www.abbottaerospace.com/downloads/naca-tn-3781-handbook-of-structural-stability-part-i-buckling-of-flat-plates-2/> [cite 10 June 2020]

¹⁵<http://www.steel-insdag.org/TeachingMaterial/Chapter7.pdf> [cite 10 June 2020]

¹⁶URL www.hallcrest.com/irreversible/thermax-standard-portfolio [Cited 29 June 2020]

¹⁷URL <https://www.gemindataloggers.com/data-loggers/tinytag-transit-2/tg-4080> [Cited 29 June 2020]

¹⁸URL <https://www.findtape.com/Shurtape-CT-109-Biodegradable-Cellulose-Carton-Sealing-Tape/p603/?idx=0&tid=0> [Cited 29 June 2020]

8.3. Design Overview

The final payload compartment concept consists of two identical payload boxes. Each of the boxes holds six blood bags and four PCM elements. The boxes feature an inner layer of expanded cork and an outer layer of plywood, together with the PCM elements this ensures the blood does not spoil for at least three hours when ground temperatures are between -4 and 44 [$^{\circ}\text{C}$]. The outer plywood layer ensures the box's structural integrity. To protect the blood bags from damage during manoeuvres and the landing impact, cork granules are used as filler material. This filler is compressible, accommodating for the volume change in the PCM elements. To keep the lid shut, a biodegradable cellulose tape is used. The boxes have an empty mass of 382 [g] each and the PCM elements add up to a mass of 1750 [g] per box. A visualisation of one of the boxes is shown in Figure 8.13, a lengthwise section cut is shown in Figure 8.14, various box dimensions are given in Table 8.3.

There are two types of PCM elements, consisting of PCM A and B (detailed in section 8.4) respectively in different ratios. Element 1 is used when ground temperatures are low, element 2 is used for higher ground temperatures. For a wide overlapping temperature range of 16 [$^{\circ}\text{C}$] to 33 [$^{\circ}\text{C}$], either element can be used. The different PCM elements dictate certain parameters, which are shown in Table 8.4.

As an extra safety measure, the team advises using thermal indicator stickers such that if the blood does leave its safe temperature range, this will be known by the medical personnel receiving the blood.

The boxes, filler and PCM elements are fully biodegradable but are also suitable for reuse. An elaboration on the material choices is given in section 8.4.

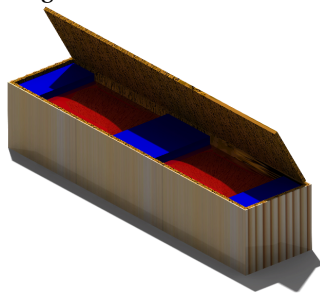


Figure 8.13: One of the two payload boxes when loaded. The filler material is not shown.

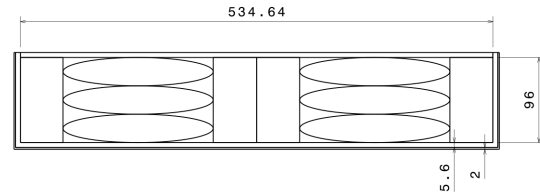


Figure 8.14: A lengthwise section cut of one of the payload boxes.

Table 8.3: Box dimensions

Dimension	Value [mm]	Dimension	Value [mm]	Dimension	Value [l]
Inner length	115	Outer length	129.6	Inner volume	5.9
Inner width	534.4	Outer width	549.2	Outer volume	7.8
inner depth	96	Outer depth	109.2		
Expanded cork layer	5.6	Plywood walls	1.7		
Plywood bottom	2	Plywood top	0		

Table 8.4: PCM element type dependent parameters

Parameter	Element 1	Element 2
Temperature range [$^{\circ}\text{C}$]	-4 to 33	16 to 44
PCM ratio A/B []	61/39	100/0
Starting thickness [mm]	46.47	42.27
Max ΔV [l]	0.101	0.166
Filler mass [g]	58.19	69.97
Max filler compression [%]	11.3	15.4
Total loaded weight [kg]	5.37	5.38

8.4. Materials

Many materials were considered during the design, this section serves to reason the materials presented in section 8.3.

Insulation and filler

While there are many options for sustainable insulation materials, none beat cork¹⁹²⁰. By using cork granules, a waste product of cork stopper production, the material becomes even more sustainable. The cork granules are

¹⁹URL <https://www.buildinggreen.com/blog/expanded-cork-greenest-insulation-material> [Cited 29 June 2020]

²⁰URL https://www.researchgate.net/publication/272110436_Cork_Sustainability_and_New_Applications [Cited 29 June 2020]

used directly as filler material, since cork has a high compressibility²¹. This filler has a ρ of 65 [kg/m^3] and λ of 0.04 [W/mK]²². Using this same filler, expanded cork is produced. The λ of expanded cork is 0.04 [W/mK] and its ρ is only 115 [kg/m^3]²³. Since thermal delay is negligible either way, a weight reduction is favourable. As this allows a stronger structure or the addition of ballast to shift the cg. This was the primary reason for choosing expanded cork over regular cork. Finally, the ϵ of expanded cork is 0.7²⁴.

PCM

The selected phase change materials are *Puretemp 4*²⁵ and *Plusice*²⁶, referred to as PCM A and B respectively. The materials boast very narrow phase change temperature ranges centred around 5 [$^{\circ}C$] and 3 [$^{\circ}C$] respectively. The latent heats of the materials are 187 [kJ/kg] and 230 [kJ/kg] respectively. Both materials are biodegradable which is quite remarkable. They may also be reused, with PCM A being stable through 10000 thermal cycles. The c_p of liquid PCM A, solid PCM A and PCM B are 2260, 1780 and 2200 [J/kgK] respectively. Finally, the ρ of liquid PCM A, solid PCM A and PCM B respectively are 880, 960 and 765 [kg/m^3] respectively. For both c_p and ρ , the specifications of PCM B don't differentiate between phases.

Reinforcement

The material choice in terms of structural integrity was largely based on the environmental impact of the material, due to the fact that the required structural properties were not very demanding. Plywood was chosen as the reinforcement material used. Plywood has a very low environmental impact and in addition to this, has a low λ of 0.1154 [W/mK]²⁷ [Cited 29 June 2020] compared to its structural properties. The Young's modulus of plywood (E) and the yield strength (σ_{cr}) is 7 [GPa] and 35 [MPa] respectively. Finally, the ϵ is 0.82²⁸.

8.5. Thermal analysis model

The calculations explained in section 8.2 are performed using a thermal analysis model made in Python. This model is based on a single box, since the boxes are identical. The model sizes the box based on the mass of PCM and wall thicknesses provided, when other input parameters are kept fixed. It then simulates the heat flow over box in order to find the internal temperature over time. The thermal analysis diagram explains the tools unit blocks with inputs (blue), intermediate results (yellow) and outputs (green). This data is given a code containing a number and a letter such that they are easily found in Table 8.5 which follows the same coding and colour scheme. Three units in the model may not be immediately clear, they are briefly elaborated below.

Thermal range points detail the amount of thermal energy stored in the payload box contents for the temperature points of interest. These can later be used to calculate the temperature inside the box. An example of such a point is the stored thermal energy at the upper internal temperature limit. If the stored thermal energy found in the Heat flow simulation exceeds this value, the mission fails.

At the start of the mission, the internal temperature is known. While the heat simulation loops through the mission, a new internal temperature is calculated and used for the next step. As mentioned in the assumptions, the internal temperature at the start of the time step is used to calculate the temperature gradient over said time step.

During loading and unloading, the surface resistances and U values do not vary over time. However, during deployment and flight, the surface resistances vary with the ambient temperature. Additionally, during these two mission phases, the boxes are inside the glider meaning a different h_c is used.

²¹URL https://www.apcor.pt/wp-content/uploads/2015/07/Caderno_Tecnico_F_EN.pdf [Cited 29 June 2020]

²²URL <https://www.mikewye.co.uk/product/granulated-cork/> [Cited 29 June 2020]

²³URL <https://www.corkstore24.co.uk/shop/32-expanded-insulation-cork-boards/> [Cited 29 June 2020]

²⁴URL <https://static-int.testo.com/media/e3/42/3656a3520cb9/Emissivity-table-EN.pdf> [Cited 29 June 2020]

²⁵URL <https://www.puretemp.com/stories/puretemp-4-tds> [Cited 29 June 2020]

²⁶URL <http://www.pcmproducts.net/files/A%20range-2018.pdf> [Cited 29 June 2020]

²⁷URL <http://www.australply.com.au/technical/thermal-properties>

²⁸URL <https://www.thermoworks.com/emissivity-table> [Cited 29 June 2020]

Thermal analysis diagram

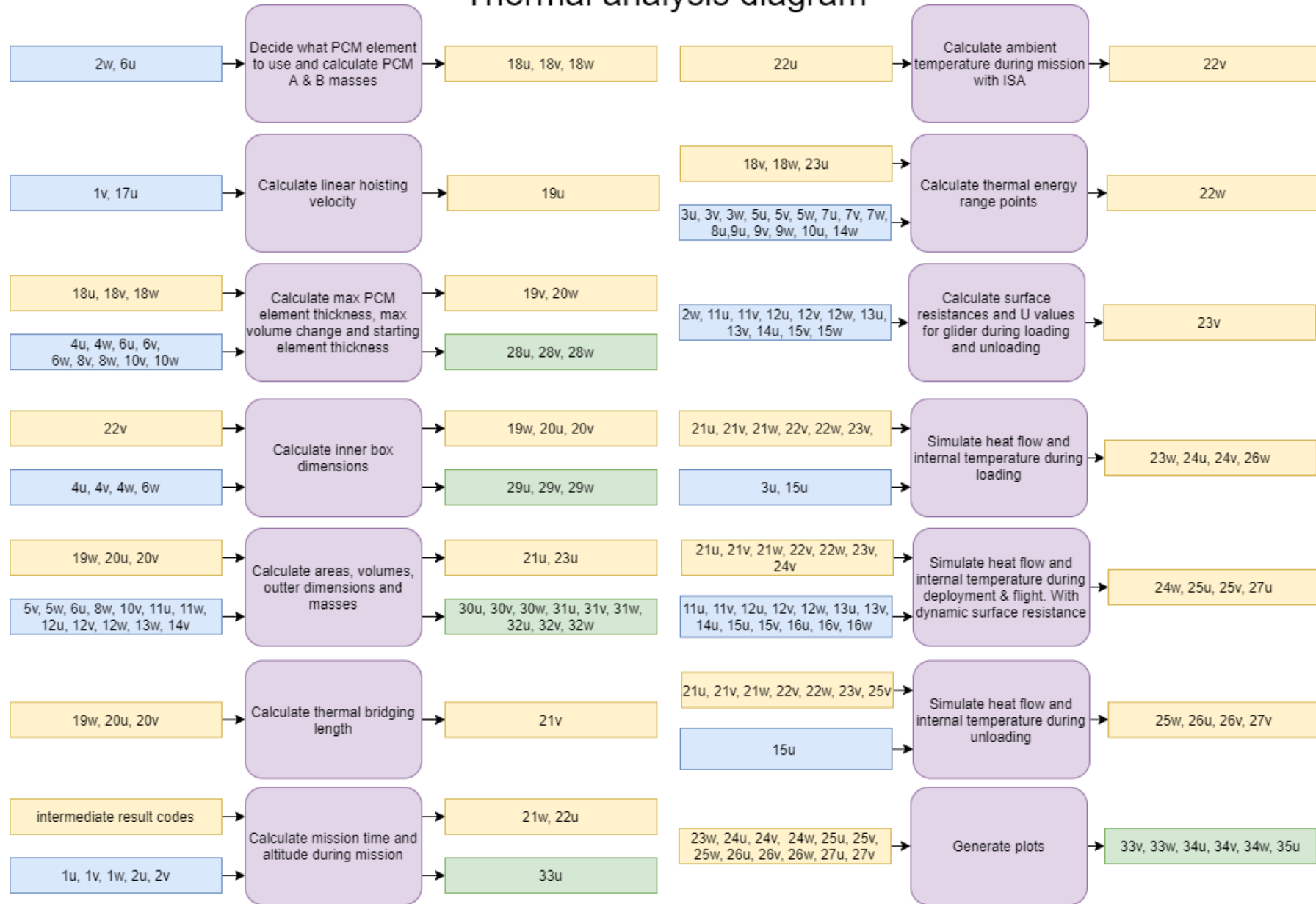


Table 8.5: Thermal analysis tool inputs, intermediate results and outputs

	u	v	w
Inputs			
1	Loading duration [s]	Deployment duration [s]	Unloading duration [s]
2	Flight velocity [m/s]	Glide ratio []	Ground temperature [°C]
3	Inside starting temperature [°C]	Inside upper temperature limit [°C]	Inside lower temperature limit [°C]
4	Blood bag width [m]	Blood bag length [m]	Blood bag thickness [m]
5	c_p of blood [J/kgK]	Density of blood [kg/m ³]	Volume of blood [l]
6	PCM mass [kg]	PCM A/B ratios []	Number of PCM elements []
7	Phase change temperature A [°C]	Latent heat A [J/kg]	c_p PCM A liquid [J/kgK]
8	c_p PCM A solid [J/kgK]	ρ PCM A liquid [kg/m ³]	ρ PCM A solid [kg/m ³]
9	Phase change temperature B [°C]	Latent heat B [J/kg]	c_p PCM B liquid [J/kgK]
10	c_p PCM B solid [J/kgK]	ρ PCM B liquid [kg/m ³]	ρ PCM B solid [kg/m ³]
11	thickness inner layer [m]	λ inner layer [W/mK]	ρ inner layer [kg/m ³]
12	thickness outer layer sides [m]	thickness outer layer top [m]	thickness outer layer bottom [m]
13	ϵ outer layer []	λ outer layer [W/mK]	ρ outer layer
14	ϵ inner layer []	ρ filler [kg/m ³]	c_p filler [J/kgK]
15	ψ [W/m ² K]	Boltzmann constant [J/K]	Ground wind velocity [m/s]
16	h_{ci} upwards [m ² K/W]	h_{ci} downwards [m ² K/W]	h_{ci} horizontal [m ² K/W]
17	Deployment altitude [m]		
Intermediate results			
18	PCM A/B ratio used []	PCM A mass [kg]	PCM B mass [kg]
19	Hoisting velocity [m/s]	Max PCM element thickness [m]	Inner box length [m]
20	Inner box width [m]	Inner box depth [m]	Starting PCM element thickness [m]
21	Inner wall areas [m ²]	thermal bridging length [m]	Mission time [s]
22	Altitude during mission [m]	Ambient temperature during mission [°C]	Thermal energy range points [J]
23	Filler mass [g]	U values (loading & unloading) [W/m ² K]	Temperature gradient (loading) [°C]
24	Heat flow (loading) [J/s]	Internal temperature (loading) [°C]	Heat flow (deployment & flight) [J/s]
25	Temperature gradient (deployment & flight) [°C]	Internal temperature (deployment & flight) [°C]	Temperature gradient (unloading) [°C]
26	Heat flow (unloading) [J/s]	Internal temperature (unloading) [kJ]	Stored energy (loading) [kJ]
27	Stored energy (deployment & flight) [kJ]	Stored energy (unloading) [kJ]	
Outputs			
28	Maximum PCM element thickness [mm]	Max volume increase [l]	Starting PCM element thickness [mm]
29	Inner box length [mm]	Inner box width [mm]	Inner box depth [mm]
30	Inner volume [l]	Outer volume [l]	Filler volume [l]
31	Empty box mass [g]	Total loaded box mass [kg]	Filler mass [g]
32	Outer box length [mm]	Outer box width [mm]	Outer box depth [mm]
33	Total mission duration [s]	Altitude graph	Ambient temperature graph
34	Temperature gradient graph	Heat flow graph	Stored thermal energy graph
35	Internal temperature graph		

Results

As explained in section 8.2 the box is optimised for empty weight. A lower wall thickness is found to reduce the empty weight more than a lower PCM mass. However, a higher PCM mass widens the box, that must still fit inside the glider. Additionally, a higher PCM mass increases the required reinforcement thickness as the total box weight increases. For every iteration step, the output graphs are inspected in order to guide the process to convergence. Since PCM B has a larger latent heat than PCM A, while having a lower density, the mixture in element 1 was iterated to contain as much PCM A as possible. This allowed the maximum PCM thickness to be lowered, which gives more space width wise. The optimal values for the boxes are given in section 8.3. Figure 8.15 shows the stored thermal energy progression over time in this box for three ground temperatures. This graph includes the safety margins used in sizing. For the upper and lower ground temperature limits, the stored thermal energy almost touches the ceiling/floor of the graphs, which reflect the upper and lower limits respectively. Interestingly, when ground temperatures are mild, the box can last much longer than the mission duration it's been designed for. As can be seen in the graph, for a ground temperature of 16 °C the stored thermal energy is far removed from its limits when the mission ends. Another interesting detail is the starting thermal energy in the box, which is caused by the different PCM elements being used.

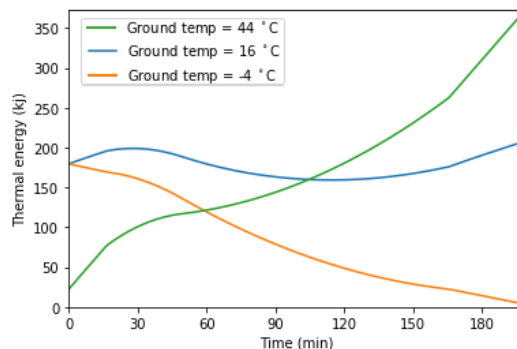


Figure 8.15: Stored thermal energy progression over time for three ground temperatures

For the same three ground temperatures, the heat flow progression is shown in Figure 8.16. The graphs clearly show the surface resistance increasing instantaneously when the payload boxes are loaded in the glider. Similarly, they decrease when the gliders are unloaded. For the ground temperature of $-4\text{ }^{\circ}\text{C}$ it seems this does not hold at first sight, however this is due to the heat flow being negative here. The graphs also clearly show the major effect the temperature gradient has on the heat flow.

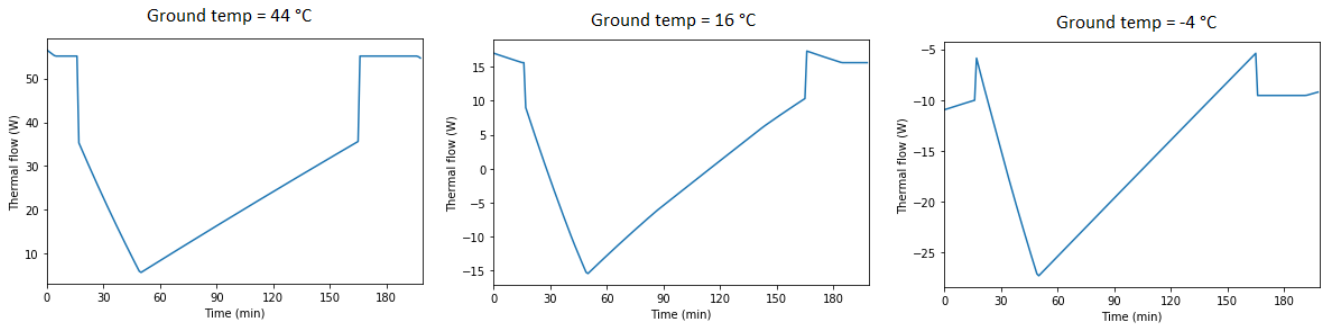


Figure 8.16: Heat flow progression over time for three ground temperatures

Figure 8.17 shows the internal temperature progression of the box for the three ground temperatures. The effect of the PCM element is extremely prevalent. During the phase changes, the internal temperature stays constant. In all three cases, large parts of the charts are dominated by these constant temperatures. Interestingly, with a moderate ground temperature the internal temperature never drops below or rises above the phase change temperatures. This is to be expected however, as the stored thermal energy shown before in Figure 8.15 does not vary much.

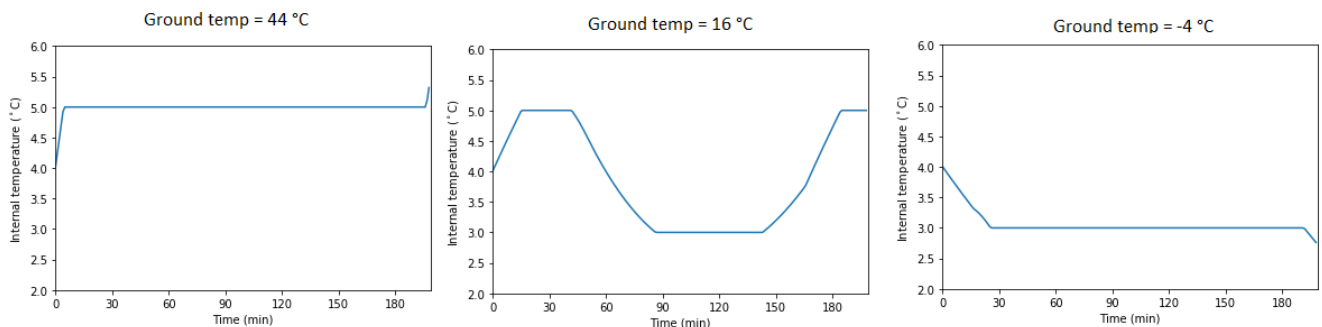


Figure 8.17: Internal temperature progression over time for three ground temperatures

8.6. Structural Analysis Model

While an analytical approach is considered sufficient in order to determine the required thicknesses of the box, a simple python code was developed based on Equation 8.7 and Equation 8.8 such that it was easier to carry out iterations pertaining to changing materials or dimensions of the box, both of which are provided by the user.

8.7. Verification & Validation

In order to assess the accuracy of the numerical tools used in the payload box design, an attempt is made to verify and validate the models.

Thermal analysis tool verification

The thermal analysis tool relies mainly on simple calculations that can be checked analytically. Some of the code units shown in the thermal analysis diagram are omitted for brevity, as their verification is straightforward. When errors are in the order $10^{-1}\%$ or less, 'no error' is stated as this is caused by rounding errors due to the discrete nature of computers. For brevity the wording a 'case' is used to substitute a 'run of the model using a set of input parameters'.

For all lists, the values at critical points are inspected. For example the first non zero altitude entry should be after the first second of deployment. The maximum PCM element thickness, volume change and starting element thickness were calculated analytically for two cases, both yielded no error. The box dimensions, including thermal bridging length, areas and volumes were verified using a CATIA model of the payload box. The masses are calculated analytically using these volumes. This yielded no error. The surface resistances and U values are calculated analytically for two cases, both for those during loading/unloading and for a random time step in the deployment & flight phase. This yielded no errors. The first ten and last ten steps of the heat simulation for loading were analytically performed for two

cases. This yielded no errors. To check the robustness of the code, input parameters are changed to extreme values to see if the code can handle these inputs. Two examples of such a bizarre cases results are shown in Figure 8.18. The code is proven to be robust to changes, while the mission may fail, the model yields it's results properly.

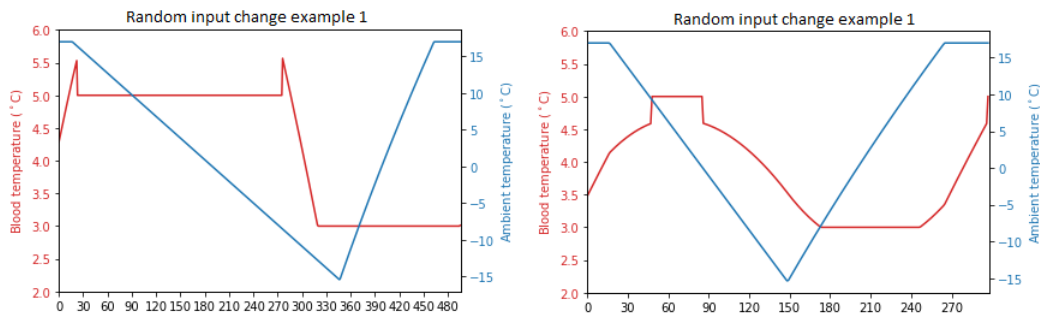


Figure 8.18: Ambient and blood temperature graph of a robustness test

Finally, during sizing, the plots generated by the tool are visually analysed for inconsistencies. This aims to verify the system as a whole. While the results seem to be correct, this is an inaccurate method that does not yield exact errors. The team recommends verifying the code with an off the shelf verified heat simulation tool such as *SimScale*²⁹ or *HTflux*³⁰. While these programs may use a different method for calculations, they provide similar results that can be compared with.

Over all, the model can not be assumed to be fully verified. However, the separate units may be considered verified and the model is robust.

Thermal analysis tool validation

The thermal analysis tool is validated using experiments conducted by the team. In total, five experiments were conducted, where two were used to validate an earlier iteration of the thermal analysis tool. When the tool finds the mission succeeds, the error is calculated by extending the final ambient temperature phase until the mission fails and comparing this to the experiment duration.

The experiments use a 2.4 [l] Styrofoam cooler box with a uniform wall thickness of 15 [mm]. The λ is 0.03 [W/mK]³¹. The payload of the box consists of water, in either liquid or solid form. The ρ of water is 998 [kg/m³] at 20 [°C]³², for ice the mass is directly used. The c_p of liquid water is 4187 [J/kgK] and 2108 [J/kgK] for ice [37].

Early experiments

Two early validation tests yielded a high error, where the model predicted failure much sooner than was found through experiment. Based on these results the thermal bridging calculations were altered. After the thermal bridging calculations were altered, a large error still persisted. The reason for this is most likely that in these experiments the box was placed on the ground whereas the tool assumes the glider is free floating. Inside the glider, the payload box will be in contact with the glider structure, meaning this error may hold true. This means the payload boxes could perhaps be reduced in weight even more. While these experiments indicate the payload box may be over-designed, this does not endanger the blood.

Later experiments

Three experiments were conducted to validate the final iteration of the thermal model. For the first two experiments, internal surface resistances were not considered 0 as the water was not in full contact with the walls.

- 1.4l of 6.3 [°C] water inside bags was placed inside the styrofoam box for 4 hours until it measured 10.3 [°C]. The ambient temperature was 18.5 [°C] The tool overestimated the performance of the box by 2.3 [%].
- 350 grams of ice measuring [°C] was placed in the box, inside a bag. The ambient temperature was 18 [°C], after 2 hours it had risen to 18.5 [°C] where it stayed constant for 8 hours before dropping to 17 [°C] at the end of the experiment. There was 60 grams of ice left inside the box, the water measured 2.3 [°C]. This experiment yielded an error of around 10.4 [%]. This is a rather large error, but the tool calculated the box would perform worse than it did.
- 1l of water at 5.9 [°C] without bags was placed inside the styrofoam box for 9.5 hours, such that the assumption of no inner surface resistance could be partly tested. The internal surface resistance was scaled with a factor 1/2.4. The ambient temperature started at 16.5 [°C], decreased to 15.5 [°C] after 3 hours and was 18 [°C] at the end of the experiment when the water measured 14 [°C]. The error was found to be 3.1 [%].

²⁹URL <https://www.simscale.com/product/thermal-analysis/> [Cited: 28-06-2020]

³⁰URL <https://www.htflux.com/en/> [Cited: 28-06-2020]

³¹URL https://www.engineeringtoolbox.com/thermal-conductivity-d_429.html [Cited 29 June 2020]

³²URL <http://www2.ucdsb.on.ca/tiss/stretton/Database/DofWater.htm> [Cited 29 June 2020]

Figure 8.19 shows a graph of the ambient and calculated water temperature over time for all three validation experiments. As can be seen, the tool overestimates the performance of the box in the first experiment and underestimates the performance for the last two experiments.

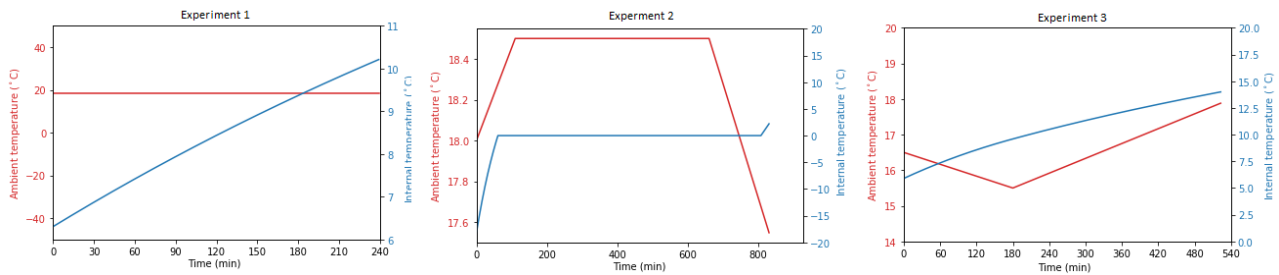


Figure 8.19: Ambient and internal temperature for the three validation tests

To conclude, preliminary validation experiments are promising. The errors found are acceptable, especially because they indicate an over-designed box, which does not endanger the blood. Errors are likely caused by small variations in material properties and due to the estimation of surface resistance and thermal bridging. The experiments do not fully cover the model and while carefully conducted, may include large inaccuracies in measurements. The latter being due to the experiments being conducted with household appliances.

Structural Analysis Tool Verification

As stated section 8.6, the model developed is rather simple and primarily used for iterations, and therefore in order to ensure that the tool is accurately built, calculations are carried out by hand in order to ensure there were no errors in the code. The verification did not reveal any errors in the code and hence it is considered verified.

Structural Analysis Tool Validation

The ideal method of validating the acquired thicknesses of the outer walls would be to carry out a simple finite element analysis to ensure that the box does not buckle under the applied forces. While this could not be performed due to time constraints, it is added as a recommendation for the future stages of the project.

8.8. Sensitivity Analysis

The input parameters used in sizing may turn out different in practise. This section analyses the effect of small changes in the parameters that are most likely to vary. Instead of varying the separate parameters used to calculate the surface resistances, the resistances as a whole are varied.

For a ground temperature of 44 [°C], the thermal analysis model is ran with the parameters being varied by 10% one by one. Table 8.6 shows the resulting errors. A positive error denotes an error where the tool finds the box lasts longer than the mission duration, when the mission fails this is denoted by a negative error. In order to quantify the positive errors, the unloading mission phase is extended until the mission fails, the time to failure is then compared with the nominal mission duration. Errors are rounded to 1 decimal.

Table 8.6: Model errors as a result of a change in input parameters

Parameter	Error when increased [%]	Error when decreased [%]
λ of both layers	- 3.2	+ 4.2
Latent heats of both PCMs	+ 5.0	- 4.9
c_p of all contents	+ 0.4	- 0.3
R_s in all phases	+ 1.7	- 1.6
ψ	0	0
ρ blood	+ 0.3	- 0.2
PCM mass	+ 3.3	-3.3
Inner layer thickness	+ 3.5	- 3.3
outer layer thickness	+ 0.3	- 0.2
Blood starting temperature	- 0.8	+ 0.9

The resulting errors are fairly small. The sensitivity analysis was performed with the safety margins in place. In all tests, the mission succeeds when these safety margins are removed. This means the Payload box design is robust and will likely still survive its mission if some input parameters vary.

To clarify, the positive errors are larger than or equal to the negative errors in all cases, this is a result of the error calculation method.

8.9. Risk Assessment

The risks related to the payload are listed in Table 8.7 and the resulting risk map is shown in Table 8.8.

The key risks related to the payload all have the consequence that the payload is not usable upon delivery, be it because of burst blood bags or unacceptable (local) temperatures within the box. To mitigate these risk safety factors are applied to ensure that small unexpected variations in conditions do not affect the payload. Additionally, the design features careful design choices to mitigate the risk of bags bursting and hot or cold spots forming.

Table 8.7: Payload risks

Index	Risk Factor	Severity	Probability	Risk	Mitigation Method	Severity	Probability	Risk
1	Blood bags burst due to landing impact	c	h	h	Using filler to fully encapsulate the blood bags in the coolboxes	ca	i	m
2	The blood bags will become too warm or cold	c	h	h	Use insulation, PCM elements and a safety margin on the bloods allowed temperature range	ca	i	m
3	The mission takes longer than is planned for	c	p	mh	Implement safety margin of 10% for each mission phase duration	n	p	l
4	The true material properties vary from the ones considered in the design	m	p	m	Constrict safe temperature range as safety margin.	n	h	l
5	The assumptions made lead to an under-designed payload box	c	p	mh	Validation of the numerical models	c	i	m
6	The assumptions made lead to an over-designed payload box	n	h	l	Validation of the numerical models	n	i	l
7	The ambient conditions are not consistent with the design assumptions	c	h	h	A wide operational envelope is designed for	c	i	m
8	Hot/cold spots form in the payload box	c	p	mh	The contents are spread well throughout the box and form a continuous thermal bridge	c	i	m
9	The box collapses on itself	c	p	mh	A reinforcement layer is added	c	n	l
10	The receiver doesn't realise the box has failed to keep the blood safe	ca	p	h	Thermal indicator stickers are used	ca	n	l

Table 8.8: Payload risk-map

(Unmitigated) / Mitigated	Highly probable (h)	Probable (p)	Improbable (i)	Negligible (n)
Catastrophic (ca)		(PL10)	PL1 PL2	PL10
Critical (c)	(PL1) (PL2) (PL7)	(PL3) (PL5) (PL8) (PL9)	PL5 PL7 PL8	PL9
Marginal (m)		(PL4)		
Negligible (n)	(PL6) PL4	PL3	PL6	

8.10. Sustainability Analysis

This section includes a brief but comprehensive analysis of the environmental impact of the payload box.

One of the most widely used materials in the manufacturing of the box is cork. In the case of the inner walls of the box, expanded cork is used. While cork in itself is a biodegradable material, the manufacturing process involved in the production of expanded cork is also quite sustainable. This is because expanded cork is generally made from cork stopper manufacturing waste. This same waste material is used as filler. Additionally, during the manufacturing process of expanded cork, there is a release of natural resin from the cork granules which holds the granules together and results in the expanded cork. This eliminates the need for artificial resin to be produced and used, therefore not only avoiding energy use and emission but also reducing the degradation time since synthetically produced resins generally prolong the degradation time of materials they're used on.

The outer walls of the box are made from plywood, which is also quite a sustainable material. Although plywood generally consists of artificial adhesives in order to combine multiple layers of wood, in the case of the box, natural adhesives will be used thus reducing the degradation time of the plywood, compared to commercially manufactured plywood.

Finally, the PCM elements and the blood bags are looked into. The PCM elements are quite sustainable overall since both the types of PCM elements are biodegradable and reusable, meaning a substantial amount of energy is saved through reuse of the elements. Additionally, at their end-of-life, the elements can be discarded and left to biodegrade naturally in a landfill with no harmful impact. The blood bags are the only element of the payload box that could be considered unsustainable, since they're normally made out of plastic that takes multiple years to degrade. While an alternative material has not been identified for this purpose, the ideal way of reducing the environmental impact of the blood bags would be to ensure that the blood bags are thoroughly cleaned after they are emptied and then recycled such that they may be repurposed for other uses and therefore limit the overall production of plastic.

9

Electrical Power Subsystem

This chapter discusses the Electric Power Subsystem (EPS), the subsystem which is responsible for storing and distributing electrical power to the glider throughout the full mission. This chapter discusses first the subsystem's requirements which flow from the functions in section 9.1. The approach used for the design is given in section 9.2. After this, the sizing of the power source is explained in section 9.3. The electric system together with the electric diagram is given in section 9.4. An overview of the EPS subsystem design is given in section 9.5. The chapter is concluded with a section on verification and validation in section 9.6, a risk assessment in section 9.7 and a sustainability analysis in section 9.8.

9.1. Functional Analysis

The EPS has as main objective to provide power during the full mission of the glider, be it in flight or when not flying but powered on. It must also be able to meet any spike in demand for power which could occur during flight. This is all reflected in the Functional Breeakdown Diagram in section 4.4.

Based on these functions, the requirements shown in Table 9.1 are derived. These requirements relate to the power output of the power source. The numbers which can be read in the requirements are derived in the following sections.

Table 9.1: Deployment requirements

Identifier	Requirement Statement	Compliance
R_EG_EPS_01	The power source shall provide no less than 8.2 [W] to the on-board electronics over a flight.time of 1.75 [h]	section 9.3
R_EG_EPS_02	The power source shall provide no less than 1.5 [W] when not in flight, during 1.75 [h].	section 9.3
R_EG_EPS_03	The power source shall be able to provide a spike power of 61.4 [W] during at least 2 [s] .	section 9.3
R_EG_EPS_04	The voltage input to the flight controller, GPS receiver and servos shall be equal to 5.5 [v].	section 9.4

9.2. Design Approach

The design of the EPS is mainly driven by the power requirements of the chosen electronics for the flight control system. In chapter 7, off-the-shelve flight controller, GPS sensor and servos are chosen. Data about their electric power needs are used to design and size the EPS

Firstly, a decision on the power source is made, based on commonly available batteries suitable for Ecoglide's application. Secondly, it is sized using the required power consumption of the chosen electronics. Thirdly, the full electronic system is drawn out.

9.3. Power source sizing

The main aim for the battery is to contain sufficient energy to provide power during the full mission span, that is for the time in flight as well as the time it is powered on, but not flying. The latter is defined for the EPS as the time between turning on the glider, the hoisting and the launch, plus the time the glider should remain operational after landing. The flight time is defined as the time between launch and touchdown.

The time spans during which the glider has to be powered are summarised in the requirements in Table 9.1. The flight time is based on the flight time used in chapter 8, that is 1.75 [h]. The same 0.5 [h] for the hoisting, used in that chapter is taken for the hoisting time. A total of 0.5 [h] are taken for the loading of the payload. That is 15 [min] more than the time used for the payload cooling in chapter 8, as it takes into account the fact that the operators might first have to switch on the glider, before inserting the payload and doing some extra pre-flight checks. Finally, a time of 0.75 [h] is taken to be the time that the electronics have to remain operational after landing.

This results in an in-flight time of 1.75 [h] and a non-flight time of 1.75 [h], as well. Therefore, the power source must be designed to provide sufficient energy for the electronics to operate properly during 3.5 [h]. However, these two different time spans have different electrical requirements, as can be seen in Table 9.2. This table shows the electric current requirements of the different components at 5.5 [V]. These values were obtained from common RC hobbyists websites ¹. In particular, it can be seen that the two servos would require more current than the other components combined when in flight. When not in flight, however, these servos need only barely any electric current to stay operational.

In this table, one can also see the maximum current required by the servo. This the stall current, a.k.a the current required by the servo when its arm does not rotate but does withstand the maximum torque. The manufacturer did not provide information about the stall current, hence common RC forums and websites were looked at for a first estimate ². A common rule of thumb was found, stating that for every 3 to 4 [kg * cm] increase in stall servo torque, the stall current will increase by 1 [A]. This would mean that the team's chosen servo would require approximately 5 [A] of electric current. This rule is confirmed when looking at servos with similar torque ³, where the current draw is indeed around 5 [A].

This high current draw will probably not be experienced often. In fact, the servo will probably only have to provide that much electricity during the transition to the stall before landing and perhaps during the pull-up manoeuvre at the deployment. During regular cruise flight, the attitude corrections will be much smaller. That is why the requirement R_EG_EPS_03 states that the power source should only be able to provide the maximum spike power for a short period of time.

Table 9.2: Values for the electric current required by the different electronic components, at 5.5 [V]

		In-flight Current [mA]	Non-flight Current [mA]
Servo	Max	5000	5000
	Avg.	500	10
Pixhawk 4 Mini		175	175
GPS receiver		55	55

The specific electric voltage of 5.5 [V] mentioned above is chosen to meet the input voltage operational ranges of the flight controller, the GPS receiver and the servos. In fact, the *Pixhawk 4 Mini* cannot handle a voltage of more than 6 [V] and requires an input voltage between 4.75 [V] to 5.5 [V] ⁴. The GPS receiver has the same limitations as the flight controller. The servo has an input range between 4.8 and 6.8 [V] ⁵. At 5 [V], it already provides enough torque to counteract the maximum forces generated by the elevons.

An input voltage of 5.5 [v] has been chosen to meet the electronics' voltage input requirements. This choice is mainly substantiated by the fact that the servo provides enough torque at that input tension. On top of that, it is know through experience that many Radio Controlled (RC) ad UAV voltage regulators which output 5 to 5.5 [V] exists on the market. That is in fact the voltage required for most RC electronics such as receivers and servos.

Computing the battery capacity is done in two steps. First, the power it needs to output is found through Equation 9.1, where $U_{electronics}$ is the input voltage of 5.5 [v] of the electronics, $\sum I_{electronics}$ is defined in Equation 9.2 and 1.2 is the safety factor. The latter is added to account for the uncertainty of the electric current values. Then, to find the energy required for the battery, Equation 9.3 is used, which is derived from equations found in literature [8]. In this equation, $t_{discharge}$, is the total mission time over which the battery will discharge, U_{BAT} is the voltage of the battery, DOD is the Depth of discharge of the battery and η_{BAT} is the efficiency of the battery.

$$P_{BAT} = U_{electronics} * \sum I_{electronics} * 1.2 \quad (9.1)$$

$$\sum I_{electronics} = I_{FC} + I_{GPS} + 2 * I_{SERVO} \quad (9.2)$$

$$C_{BAT} = \frac{P_{BAT} * t_{discharge}}{U_{BAT} * DOD * \eta_{BAT}} \quad (9.3)$$

The Equation 9.3 requires a choice of battery in order to input the voltage, Depth of Discharge and efficiency. Since off-the-shelf batteries for UAVs are highly preferred for the Ecoglide project, the choice lied between the commonly used Lithium-Polymer (LiPo), Lithium-Ion (Li-ion) batteries. For the purposes of this initial design, LiPo batteries were used, as these are the most frequently used batteries for RC hobbyists and UAV researcher. They are easily purchasable

¹<https://diydrone.com/profiles/blogs/pixhawk-and-apm-power-consumption>

²<https://forum.arduino.cc/index.php?topic=498713.0>

³<https://www.servocity.com/d956wp-servo>

⁴https://docs.px4.io/v1.9.0/en/flight_controller/pixhawk4_mini.html

⁵https://www.amazon.com/ANNIMOS-Digital-Torque-Waterproof-Control/dp/B07GJ6ZCVY/ref=psdc_2234131011_t3_B073F92G2S

from a wide variety of producers and have become more and more safe over the years. The LiPo batteries are assumed to have an efficiency of 90%, as this is "usually" the case for batteries according to literature [8].

The specific battery type chosen is a 2 cells LiPo battery, thus with a nominal battery voltage of 7.6 [V]. This choice for a battery with a higher voltage than the electronics require was made based on the finding that there exist more off-the-shelf voltage regulators, for RC and UAV airplanes, reducing the input voltage than those which increase it. Indeed, no regulators which increase the voltage were found during the team's search.

The Depth of Discharge is taken to be 100%, as the purpose of the Ecoglide is to be single use. Therefore, the number of life cycles is not important, thus it was deemed best to take full advantage of the energy stored in the battery. If the battery would be retrieved, it could possibly be reused a number of times again, however further analysis needs to be performed to confirm this.

By using Equation 9.3, a battery capacity of 2 [Ah] is found to be necessary. Such a battery would need to have a C-rating⁶ by the C-rating to obtain the maximum current (in [A] the battery is designed to output, at nominal voltage.) of approximately 1 to cover all flight phases.

Therefore, the *ZIPPY Compact 2700mAh 2S 25C Lipo Pack*⁷ was chosen as the battery for the electric power system. It is the battery which comes the closest to the requirements, while being low cost and easily purchasable. Indeed, despite this battery's slightly higher capacity than required, it has the lowest C-rating which could be found on RC stores: 10C. Furthermore, with its small size of 136x43x15 [mm], and light weight of 151 [g], it is ideal for Ecoglide's application.

9.4. Electric system

In order to complete the electric system, a voltage regulator must be found. The key criteria it must follow is that it must output 5.5 [V] while accepting an input of a 2 cell LiPo battery, such as the one found above. Different manufacturers were looked into and eventually the team settled on the *Jeti Voltage Regulator SBEC 5-8V/12A*⁸. This is a Smart Battery Elimination Circuit (SBEC), which is often used for radio controlled model airplanes and is more efficient than the more common Battery Elimination Circuits (BEC) according to retailers⁹. This particular SBEC is capable of delivering 12 [A], which is well over the minimum required for the Ecoglide. Despite this overdesigning, it was mainly chosen because the team found it difficult to buy a single SBEC or BEC which is not integrated on a motor speed controller. Nevertheless, *Jeti's* SBEC could serve as an initial choice, which could be revisited later, as this has no real consequence on the rest of the EPS.

In Figure 9.1, one can see the electric diagram of the full EPS. The battery's voltage gets reduced through the SBEC before entering the flight controller. The latter then uses part of this energy to perform the required processing and sensing. The remainder is distributed to the GPS receiver and the two servos. The yellow wire is the signal wire through which the flight controller can signal what position the servos should be at. It must be noted that the single signal wire for the GPS receiver is a simplification, as often multiple wires are present.

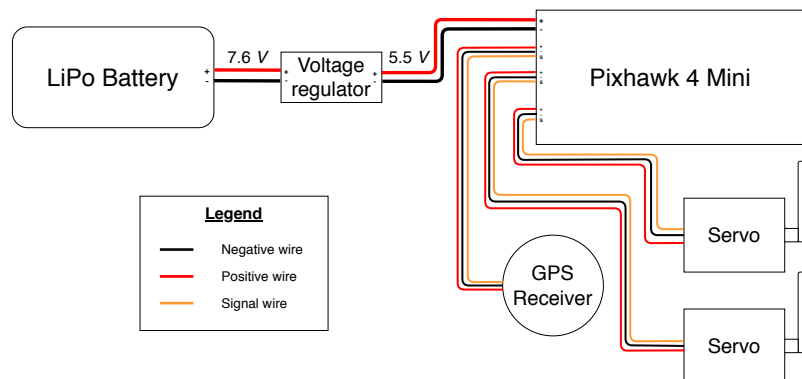


Figure 9.1: Electric Block Diagram

9.5. Design Overview

The EPS uses an off-the-shelf battery and voltage regulator (SBEC) which were chosen to meet the sizing requirements throughout this report. These can be found in Table 9.3

⁶The C-rating refers to a value given to a battery, which allows the customer to quickly identify how much current it can output. Indeed, as a first approximation, one can multiply the battery's capacity (in [Ah])

⁷https://hobbyking.com/en_us/zippy-compact-2700mah-2s-25c-lipo-pack.html?queryID=82b3e8e91d1efb86b813321f850d3ec5&objectID=24703&indexName=hbk_live_magento_en_us_products

⁸<https://www.amazon.com/Jeti-Voltage-Regulator-SBEC-2-10S/dp/B00L5QHxEE>

⁹<https://hobbyking.com/media/file/57396352X1338440X50.pdf>

Table 9.3: Final components used for the EPS design

Item	Quantity	Dimension [mm]	Mass [kg]	Specific info
<i>ZIPPY Compact 2700mAh 2S 25C Lipo Pack</i>	1	136x43x15	151	2700 [mAh], 7.4 [V]
<i>Jeti Voltage Regulator SBEC 5-8V/12A</i>	1	60x28x10	0.029	12 [A] max output

9.6. Verification & Validation

Verification of the calculations is done firstly by checking the source of the different equations used in this chapter and secondly by changing the input values to assess the outcome. All the equations used are found in trusted literature [8] or are commonly used in different engineering fields. These equations are therefore trustworthy and verified. Furthermore, changes were made in the input values of the equations in this chapter to assess how the calculation results change. The changes were found to scale in the way which is to be expected for each equation. That is, Equation 9.1 and Equation 9.2 scales linearly with single changes of one of their input variables, while Equation 9.3 scales linearly with the variables in the numerator and inversely with those in the denominator.

To validate the results of this chapter, it is advised to perform physical tests of the whole EPS system in action. Indeed, to size the EPS, data from RC hobbyists were mainly used. They might be inaccurate or altogether wrong. Therefore, it is necessary to validate the findings through full size testing.

9.7. Risk Assessment

The EPS related risks are shown in Table 9.4 and Table 9.5.

Table 9.4: Electrical power subsystem risks

Index	Risk Factor	Severity	Probability	Risk	Mitigation Method	Severity	Probability	Risk
1	The battery does not have enough energy capacity for the full mission	ca	p	h	Perform on-ground tests of the EPS system and/or in-flight tests of the full mission to assess the battery's lifespan	ca	i	m
2	The servos require more power than available	ca	p	h	Apply safety factor to SBEC and battery sizing	c	i	m
3	The wires create a short-circuit	c	i	m	Install all the electronics, including the wires, firmly to the aircraft	c	n	l

Table 9.5: Electrical power subsystem risk-map

(Unmitigated) / Mitigated	Highly Probable (h)	Probable (p)	Improbable (i)	Negligible (n)
Catastrophic (ca)		(EP1) (EP2)	EP1	
Critical (c)			(EP3) EP2	EP3
Marginal (m)				
Negligible (n)				

9.8. Sustainability Analysis

The sustainability is not assessed in the Life Cycle assessment chapter (chapter 14) because the electronics are to be retrieved from the airplane and reused if possible. Therefore, in terms of sustainability, the EPS does quite well. However, one might note that the decision of using a depth of discharge of 100% means that the battery will have a limited number of life cycles. Moreover, LiPo batteries need special disposal facilities to be disposed in an environmentally friendly way. Recycling of the entire battery is still difficult, as it requires very specific methods. Nevertheless, it is possible to reuse the batteries for other purposes than powering the glider. After its limited number of cycles, it could be used to power various electric devices, which could help when access to electric power is limited. This would increase the EPS' sustainability overall.

10

Deployment

This chapter focuses on the conceptual design and preliminary sizing of the tethered balloon system, chosen for the deployment of the EcoGlide glider. Section 10.1 explains the deployment system specific functions and requirements, that were driving the design. Table 10.5 describes the main elements that make up the tethered balloon system, highlighting their importance, and explaining their functioning. Section 10.3 does the same to the glider hoisting and launch mechanism, that makes up the payload of the tethered balloon, then the sizing of this payload follows, in section 10.4. Section 10.5 and section 10.6 explain the method used for the preliminary sizing, and presents their results. Section 10.7 and section 10.8 touches on the impact of the balloon size on sustainability and balloon performance, respectively. Recommendations for potentially improving the accuracy of the sizing tool, and the performance of the system are made in section 10.9. The validation of models used in the sizing process is attempted in section 10.10. Finally, the risks related to the deployment system, as well as the proposed mitigation are listed in section 10.11.

10.1. Functional Analysis and Requirements

The deployment system serves as a solution to provide enough initial energy to the EcoGlide glider, such that it can fly to its desired landing location. By choosing the tethered balloon concept (see section 4.2), the form of energy was set to be potential, thus the deployment system shall lift the glider to the desired altitude, and release it from there. In order to meet the desired frequency of blood resupply (see section 1.1), the length of a deployment cycle must be kept under a day. As mentioned in section 1.1, due to the dynamic nature of modern battlefield, the deployment system must be semi-agile, as occasionally it may be assigned to a different main hospital. If possible, the deployment system should not be the bottleneck in the availability of the EcoGlide system, and thus the maximum wind speed must match (or exceed) the maximum wind speed of the EcoGlide glider (see section 3.3). From these, and the user requirements, the requirements for the deployment system that were derived are listed in Table 10.1.

Identifier	Requirement statement	Compliance
R_OP_SUST_02	The chosen launch method shall have no detrimental effects on surrounding flora or fauna.	No compliance
R_OP_MA_02	The deployment system shall have an initial set-up time of TBD hours	TBD
R_OP_MA_04	The deployment system shall have a disassembly time of TBD hours	TBD
R_EG_LV_1	The glider shall be compatible with currently available launch vehicles.	No compliance
R_EG_IV_2	The glider shall be integratable with the launch vehicle.	Section 10.3
R_EG_LV_3	The glider shall maintain communication with the launch vehicle or ground station upon deployment.	Section 10.3
R_OP_SFRL_02	Preparation time between two successive launches shall be no more than 24 hours	Table 10.5
R_OP_MA_04	The launch system and the glider shall be able to fit in a volume of 5.89 x 2.35 x 2.36m	TBD
R_OP_IV_1	The launch system shall provide safe clearance for glider deployment.	Section 10.3
R_EG_IV_4	The launch system shall be able to operate in a maximum wind speed of 21.39 [m/s].	Section 10.5

Table 10.1: Deployment system requirements

In line with the focus on sustainability, and minimalized environmental impact, R_OP_SUST_02 was created. The compliance to this requirement, however, cannot be guaranteed, as the bedding down area must be clear (as explained in section 13.4). In case a large enough open field is not available, the obstructing trees (or other land features) must be removed.

In order to reduce the cost and logistical strain on the user of the EcoGlide system, R_EG_LV_1 was created. However as tethered balloons capable for a flight altitude of 5000[m] are currently not commercially available. This created the need for the conceptual design and preliminary sizing of the EcoGlide tethered balloon, explained in this chapter.

Finally, in order to decrease the logistical strain on the EcoGlide system operator, R_OP_MA_04 was made, so that the deployment system would fit in a standard 20ft shipping container. The tethered balloon system was designed with this constraint in consideration (see section 10.4), however the smallest and lightest commercially available winch, with the drum capacity that meets EcoGlide specifications, and the air compressor that can drive that winch, are much larger and heavier than expected. As established in section 12.3, the compliance to this requirement cannot be confirmed at this point.

10.2. Balloon System Description and Design Approach

The design altitude (or "pressure height") is the altitude at which the the balloon envelope is completely full of the lifting gas. The pressure height was assumed to coincide with the maximum altitude of 5000[m]. It is assumed that the balloon internal and ambient pressure are equal. The largest feasible angle of attack experienced by the balloon was assumed to be 20°. For all atmospheric calculations the International Standard Atmosphere was assumed, and helium was assumed to follow the Ideal Gas Law, with gas constant of $R_{He} = 2077.1 [J/kgK]$.¹

Figure 10.1 shows the communication lines between the different sections of the deployment system and with external elements. Further elaboration on the communication of the EcoGlide system is presented in chapter 13.

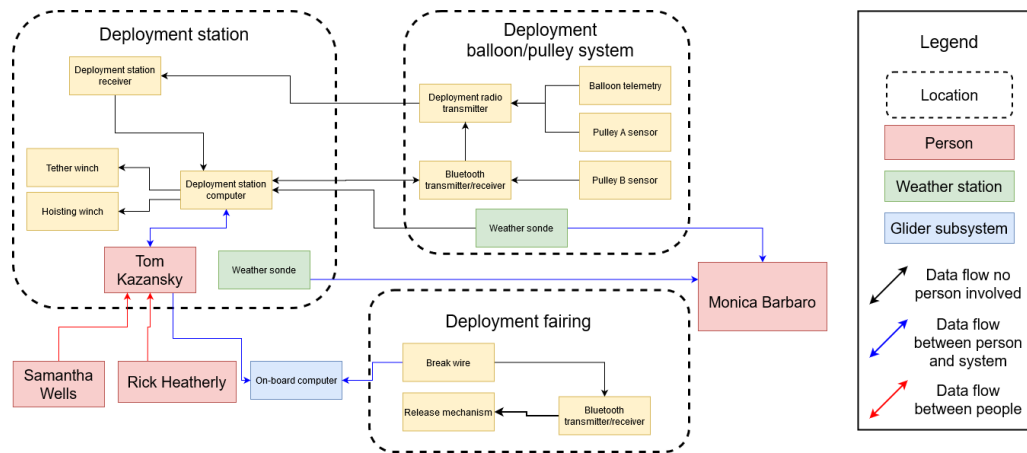


Figure 10.1: Deployment system communications diagram

Balloon

For glider deployment two aerodynamically shaped balloons were investigated, namely the US Navy Class C (Figure 10.2), and the Vee Balloon from Goodyear Aerospace (Figure 10.3).

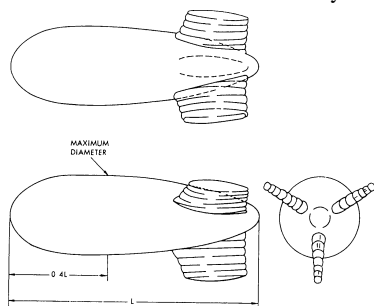


Figure 10.2: C-type balloon[35]

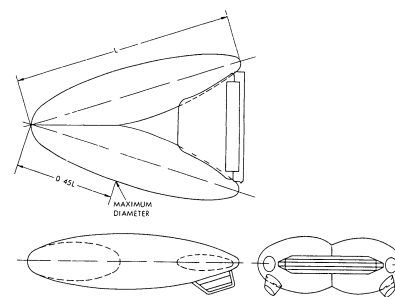


Figure 10.3: Vee balloon[35]

A preliminary sizing, based on "Tethered Balloon Handbook" by Philip F. Myers, was completed for both shapes.[36] The balloon sizing process is following the subsequent steps:

1. Calculate volume of lifting gas, that is required for lifting the pre-defined payload weight.
2. It is then multiplied by the factor K , which represents the additional gas required to lift the weight of the balloon envelope and rigging.
3. From the balloon volume, the balloon mass (including the rigging) is estimated.
4. From the maximum allowed wind speed, the required tether strength is estimated.

During this process it was found that the Vee balloon is associated with heavier balloon mass (balloon envelope and rigging), larger balloon volume, as well as higher lift and drag coefficients for almost all angles of attack. Since the balloon is sized such that it can lift its maximum payload even in zero wind, lift and drag forces must be carried by the

¹URL https://www.engineeringtoolbox.com/individual-universal-gas-constant-d_588.html [cite 5 Jun 2020]

tether line, potentially requiring stronger and heavier line. For these reasons the C-type was found to be superior to the Vee balloon, and only the former was considered in further design steps.

Tether

It is assumed that the tether is not affected by sag (it is straight), and the balloon is exactly above the deployment station (tether has 90° with ground). The aerodynamic drag of the tether is also neglected. These mean that it is assumed to be in pure tension. Only tether lines with constant diameter were considered. The force which the tether strength must meet is the sum of the resultant aerodynamic forces at maximum wind speed and angle of attack, the weight of the EcoGlide glider with MTOW, and the weight of the tether line itself. Once the cable is selected, its mass is added to the total mass of the balloon system. This necessitates an iteration on the balloon volume sizing. Note that the increased balloon size leads to increased aerodynamic forces, against which the selected tether cable would need to be checked, and iterated on if needed.

The list of cable types that were considered for use as tether line, are listed in Table 10.2. Manila natural fibre ropes were briefly investigated, as they are biodegradable, and have good resistance to UV light. It is however sensitive to age, and susceptible to rot and mildew.² Due to their poor strength-to-weight performance, they were found to not be feasible for the required altitude of 5000 meters. In fact, the breaking strengths of 1 and 1.5 inch diameter 3-strand manila ropes³ are only 1678[m] and 1457[m] respectively (with 20% of their break strength, as per advised for safe operation).⁴ *Saturn-12*⁵ is a 12-strand rope made with Dyneema SK78 high modulus polyethylene core, with abrasion and UV resistant coating. Dyneema SK78 was designed for marine application, with "improved service life in applications that are subjected to long-term static loads".⁶ Saturn-12 also has excellent tension fatigue characteristics, as it is estimated to withstand 2113 load cycles at 80% of its average break strength.⁷ Note that in Table 10.2, not the average, but the slightly lower minimum break strength of the Saturn-12 cables are listed. For Dyneema HMPE based ropes (Saturn-12), a factor of safety of 5 was taken, in order to avoid creep due to long-term static loads, while for other wires and cables, a factor of safety of 2 was taken.⁸ The Saturn-12 cable outperform the alternate options with regards to strength to weight ratio, even with the higher factor of safety taken into account.

Tether	Strength [lb]	Density [lb/ft]	FS
3-strand Manila Rope 1 inch	6720	0.244	5
3-strand Manila Rope 1.5 inch	13800	0.542	5
Carbon Rocket Wire[36]	3275	0.031	2
NS-355 Stainless Steel[36]	2370	0.0298	2
Music Wire[36]	3250	0.036	2
Saturn-12 1/4 inch	7700	0.016	5
Saturn-12 5/16 inch	12300	0.027	5
Saturn-12 3/8 inch	17600	0.034	5

Table 10.2: Cable types considered for tether line

Winch

Winches designed for tethered balloon applications are not commonly available, so it must be custom made for the EcoGlide balloon. The requirement that is driving the selection of the winch is the 5000[m] launch altitude (R_EG_PERF_02). The winch of the EcoGlide balloon must have a drum with large enough capacity to store 5000[m] long cable. Note that the drum capacity depends on the dimensions of the drum, as well as the diameter of the cable used. The pull force is required to match the maximum aerodynamic force on the balloon (20 °AoA, and 21.39[m/s] wind speed), plus excess static lift when the balloon is fully inflated.

While designed for a different application, some winches could be used in the the EcoGlide system, with slight modifications. They are proof for the feasibility of large drum capacity winches with sufficient pull force. Two such systems are Ingersoll Rand Infinity Guideline and Podline winches.⁹ Table 10.3 shows some specifications of these winches. Note that their drum capacities are given for 13[mm] and 20[mm] diameter winch cables, and is significantly higher when used with thinner cable.

Note that other than a low tether weight, an additional effect of high strength-to-weight ratio is smaller diameter, meaning a smaller winch drum.

²URL <http://phoenixrope.com/fiber-properties/>[cite 10 Jun 2020]

³URL <http://phoenixrope.com/rope-products/natural-rope/manila-rope/>[cite 10 Jun 2020]

⁴URL <http://phoenixrope.com/rope-products/natural-rope/manila-rope/>[cite 10 Jun 2020]

⁵URL <https://www.samsonrope.com/defense/saturn-12>[cite 8 Jun 2020]

⁶URL https://www.pelicanrope.com/pdfs/DyneemaSK75_Tech_Sheet.pdf[cite 7 Jun 2020]

⁷URL <https://www.samsonrope.com/resources/mooring/tension-fatigue-testing>[cite 7 Jun 2020]

⁸URL <https://www.samsonrope.com/resources/general/understanding-creep>[cite 7 Jun 2020]

⁹URL <https://www.ingersollrand.com/en-us/lifting-equipment-material-handling/products/winches/force-5i-infinity-winch-series.html>[cite 10 Jun 2020]

The winch speed is important for complying with requirement R_OP_SFRL_02: the balloon must be able to be winched down, serviced (maintenance and helium top-up), and released back up to 5000 meter altitude, within 24 hours. Assuming a constant maximum winch speed, the Podline and the Guideline winches would allow for 12.7 and 18.5 hours respectively for service and maintenance.

	Podline (FA7Ti-PL42XK1)	Guideline (FA7Ti-GL42XK1)
Minimum pull	4630 kg	1540 kg
Drum capacity	4825 m with 13 mm diameter	2042 m with 20 mm diameter
Winch speed	18 m/s	48 m/s

Table 10.3: Specifications of the Ingersoll Rand Infinity Guideline and Podline winches

Flight time

Due to permeation, there is a constant exchange of matter through the balloon envelope: the lifting gas diffuses, while air and water vapour infuses through the barrier, which result in a gradual loss of lift. This phenomena necessitates occasional top-offs, the frequency of which will set the upper limit on the balloon flight time. The rate of diffusion or infusion depends on the type and thickness of the barrier, and thus will increase with barrier degradation.[36] The process can be described with Fick's First Law. In order to approximate the permeability of the EcoGlide deployment balloon, the AeroBalloon AB-20¹⁰ was used for reference.

It was assumed that the envelop material and thickness (including the coating films), and the pressure difference between the balloon interior and exterior are the same for the AB-20 and EcoGlide balloons. By calculating the surface area of the EcoGlide balloon, the rate of loss of lifting gas, and thus the maximum flight duration can be estimated. The infusion of air and water vapour also degrades the lifting gas, however this was neglected in the sizing calculations. Nevertheless, re-purification will be required if the balloon is inflated over a lengthy period of time.[36]

10.3. Description of Balloon Payload

The payload of the balloon system consists of the EcoGlide glider, the pulley system, a radiosonde, and a radio communication system.

The pulley system is used to lift the EcoGlide glider to the balloon. Since the glider relies on the wind to move away from the tether line, it must be released from the aft of the balloon, as far down-wind from the tether line and hoisting ropes as possible. Providing this clearance is achieved via the same pulley system, by guiding the glider along a spacer beam, towards the aft of the balloon.

The radiosonde measures a number of atmospheric parameters, such as pressure, temperature, humidity, wind speed and direction, as well as geopotential altitude via its GPS device. These data are included in the atmospheric model, used for planning the trajectory of the EcoGlide glider for a given mission. It must have a power source that allows for measurements over the duration of the entire flight of the balloon. The example radiosonde that was selected is the RS41-SG from Vaisala¹¹. This variant measures temperature, humidity, pressure, wind speed and direction, and geopotential height via its GPS receiver. Its operating time is only 240 minutes. While this can be increased by decreasing the sample rate, an extended battery might be required in order to meet the flight duration of the tethered balloon.

A radio communication system is used to transmit telemetry, and the status of the glider during hoisting operations to the ground station.

Description of the pulley system

The system consists of a set of pulleys (marked with A, B, and C on Figure 10.4) attached to the spacer beam, a rope going through the pulleys (light blue on Figure 10.4), and a box. The box serves as fairing for the glider while it is being hoisted up in a vertical position, as it is not designed to withstand the loads exerted by wind perpendicular to the wings. The fairing hangs from two lines (green on Figure 10.4) which are clamped to the hoisting rope. It has a trap door on the opposite side, an actuator that can open it, a Bluetooth device, a break-wire, and room for the EcoGlide glider. "Pulley A" and "Pulley B" are equipped with magnetic field sensors. The spacer beam is hanging from the balloon such that it is positioned aft of the tether line. It houses another Bluetooth device that transmits information about the status of the deployment fairing through the balloon radio communication system (described below). The box with the glider inside, is oriented such that the fuselage is parallel with the hoisting rope, and the nose is pointing upwards. The clamp, fixing the top line from which the box is hanging, to the hoist rope is magnetised. The ground segment of the pulley system is made up of a pair of reels and a motor driving them, as can be seen on Figure 10.5. "Pulley A" is special in a sense that it is made up of two separate wheels with a gap in-between, as can be seen on Figure 10.6. For the hoisting rope it functions as a regular pulley, as the wheels are free to rotate, and the gap is too

¹⁰URL <http://aeroballoon.com/assets/aeroballoon-ab-20-brochure-2018.pdf>[cite 3 Jun 2020]

¹¹URL <https://www.vaisala.com/sites/default/files/documents/RS41-SG-Datasheet-B211321EN.pdf>[cite 15 Jun 2020]

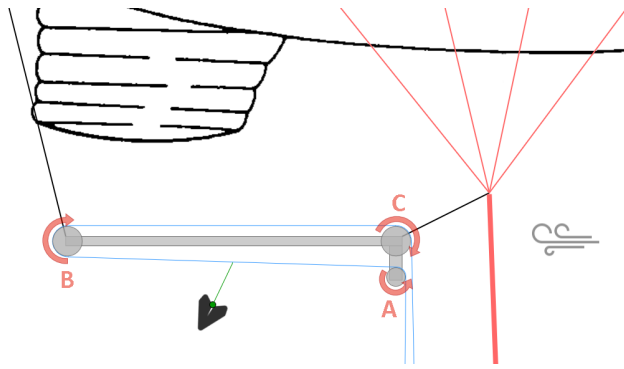


Figure 10.4: Schematic drawing of the "flying" segment of the pulley system.

narrow. It is however wide enough for the green line, meaning it can move through the pulley with the glider hanging on it.

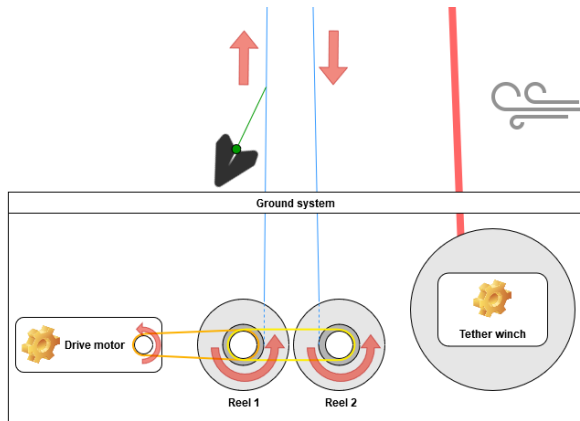


Figure 10.5: Schematic drawing of the ground segment of the pulley system.

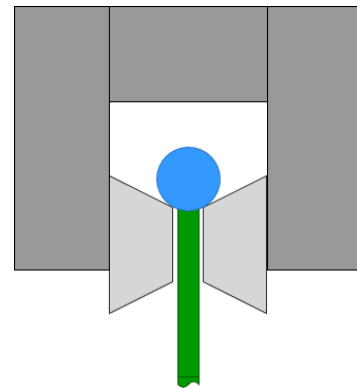


Figure 10.6: Schematic drawing of "Pulley A".

When the system is ready to deploy "Reel 1" has 5000 meters of hoisting rope, "Reel 2" is empty, and the clamp is at the level of the ground segment. The EcoGlide glider is put in the box, connected to the break-wire, and the trap door is closed. When the drive motor is turned on, "Reel 2" starts spooling up the hoisting rope, while "Reel 1" un-spools hoisting rope at the same pace. The equal pace is achieved by connecting shafts of the same diameter with a belt, which drives the reels. Once the magnetised clamp of the deployment fairing reaches "Pulley A", the balloon sends a signal to the ground segment, and the drive motor is stopped. The balloon operator must turn the drive motor back on, so the box moves through the pulley, and slides along the spacer beam. When the box reaches "Pulley B" another signal is sent to the ground segment, and the drive motor is stopped. The balloon must signal the deployment fairing that it shall release the glider, and for this purpose the two must have capability of short range communication. Bluetooth transmitters and receivers were selected for this application. They are widely available, inexpensive, and have a range of up to 100[m].¹² When the signal is received, the trap door opens, and the glider falls out, breaking the break-wire. This is communicated back to the balloon via the same short range device, and the balloon sends a third signal to the ground station, confirming the release of the glider. At this point, "Reel 1" should be empty, and "Reel 2" should have 5000[m] of hoisting rope spooled up. Then the drive motor is turned on again, but in reverse, pulling the now empty box back down, so it is ready for the next cycle of operation. "Reel 1", "Reel 2", and the drive motor shall chosen such that the glider can be hoisted to the maximum altitude of 5000[m] in 30 minutes or less.

10.4. Sizing of the hoisting system

The balloon must be designed for a payload mass that includes the EcoGlide glider of, the pulley and launch system, and additional instrumentation and avionics. The payload mass budget was set to 180[kg]. The glider has a maximum mass of 25[kg] (R_EG_ENBD_01).

The components of pulley and launch system that are expected to contribute to the total payload mass the most are the hoist rope, and the spacer beam. The hoist rope must be chosen, such that it can carry the fully loaded glider, the aerodynamic forces on the glider deployment fairing, and its own weight. Note that the aerodynamic forces on the rope are neglected. The maximum dynamic pressure with wind speed of 21.69[m/s] is 168.4[Pa]. The glider deployment fairing has the profile dimensions of 5.02[m]x1.04[m] (derived from the glider dimensions), and an assumed drag coefficient of 2.1.¹³ The mass of the box is assumed to be 10[kg]. The cable types considered for the pulley sys-

¹²URL <http://www.blunair.pl/bluetooth-range>[cite 15 Jun 2020]

¹³URL https://www.engineeringtoolbox.com/drag-coefficient-d_627.html[cite 20 Jun 2020]

tem are listed in Table 10.4. All of these meet the above strength requirement with a factor of safety of 2, except for the stainless steel options. While the $5/16[in]$ thick AmSteel-Blue¹⁴ rope is the lightest option, the $1/8[in]$ thick Tech-12¹⁵ rope was selected instead, because it was designed to be used around sheaves and winches. Thus the total mass of the rope is $196.85[lb]$ or $89.29[kg]$.

Hoisting cable	Strength [lb]	Density [lb/ft]
Carbon Rocket Wire[36]	3275	0.031
NS-355 Stainless Steel[36]	2370	0.0298
Music Wire[36]	3250	0.036
AmSteel-Blue 5/16 inch	1400	0.003
Tech-12 1/8 inch	2500	0.006

Table 10.4: Cable types considered for hoisting

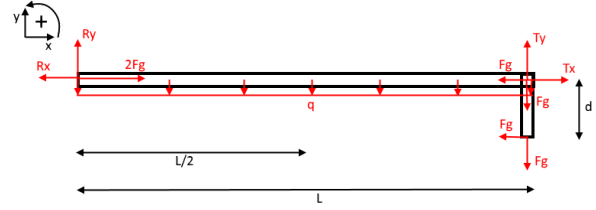


Figure 10.7: Free body diagram of the simplified spacer beam

The mass of the spacer beam is dependant on its length, the profile of its cross-section, and the material used. The length is limited by requirement R_OP_MA_04, so it was chosen to be $5.8[m]$, leaving some extra room for packaging and securing it in the 20 foot container. The free body diagram of the spacer beam with simplified loading is shown on Figure 10.7. Solving the static force and moment equations leads to the following:

$$R_x = T_x \quad (10.1)$$

$$R_y + T_y = L * A * \rho * g + 2 * F_g \quad (10.2)$$

$$F_r = \frac{L}{2} A * \rho * g - F_g * \frac{d}{L} \quad (10.3)$$

A is the cross sectional area, ρ is the density of the material used, g is the gravitational acceleration, and F_g is the force on the hoisting rope. A hollow square tube was chosen for shape, as its cross section has high moment of inertia in both directions. This plays a key role in resistance for column buckling, which was found to be the driving aspect of the spacer beam design.

$$P_{cr} = \frac{\pi^2 EI}{L^2} \quad (10.4)$$

From Figure 10.7, it can be seen that the compression on the beam is $2 * F_g$, where $F_g = 4281.17[N]$, the force pulling on the cable. For the critical buckling load, a safety factor of 2 was used. Choosing 7075 aluminium alloy¹⁶, widely used in the aerospace industry, results in a required moment of inertia of $4.1692 * 10^{-7}[m^3]$. Thus the profile of the beam can be chosen such that it is $5[cm]$ wide, and has a web thickness of $1[cm]$. Distance d equals $5[cm]$. The mass of the spacer beam is then $27.84[kg]$ or 61.377 .

The glider, the glider deployment fairing, the hoist rope, and the spacer beam add up to a mass of $152.13[kg]$. Defining the maximum payload mass of the balloon to be $180[kg]$, the mass budget for the power system, avionics, and instrumentation is $27.87[kg]$.

10.5. Balloon sizing for payload

This section details the balloon system preliminary sizing process. In order to stay consistent with the guide of "Tethered Balloon Handbook" by Philip F. Myers, imperial units are used for the most parts. It also uses mass for all force calculations, so all the results below that describe a force but given in pounds (lb) should be interpreted as a force that is the product of the given mass and $9.81[m/s^2]$ (or $32.17[ft/s^2]$).

With the maximum payload mass of $396.83[lb]$ ($180[kg]$), maximum wind speed of $42[knots]$ ($21.6[m/s]$), and design altitude of $16404[ft]$ ($5000[m]$) established, the first step of the preliminary sizing can be performed for each balloon shape design (C-type and Vee balloon). The first iteration only accounts for the payload mass, and the mass of the balloon itself, but not for the mass of the tether line. The reference volume of the balloon is computed by solving $V_{ref} = \frac{w_{pl}}{(\rho_{air} - \rho_{He})}$, which will be the same for both balloons. ρ_{air} and ρ_{He} are the density of air and Helium at $5000[m]$ ISA. This is then multiplied by the sum of K_0 and K_1 , leading to the balloon volume V . Altitude factor $K_0 = 0.0239 * (alt)^{0.6}$ for the C-type, and $K_0 = 0.07 * \left(\frac{alt}{1000}\right)^2 + 3.28$ for the Vee balloon, while K_1 is chosen via iteration, such that the balloon is as small as possible. The balloon weight, with rigging included, is estimated via $m_B = 0.0237 * V + 25$ for the C-type, and $m_B = 0.307 * V^{0.77} - 30$ for the Vee balloon. The balloon and payload weight is then checked against the static lift $L_{static} = V(\rho_{air} - \rho_{He})$.

¹⁴URL <https://www.samsonrope.com/defense/amsteel--blue>[cite 10 Jun 2020]

¹⁵URL <https://www.samsonrope.com/defense/tech-12>[cite 10 Jun 2020]

¹⁶URL <https://www.makeitfrom.com/material-properties/7075-AlZn5.5MgCu-3.4365-2L95-A97075-Aluminum>[cite 15 Jun 2020]

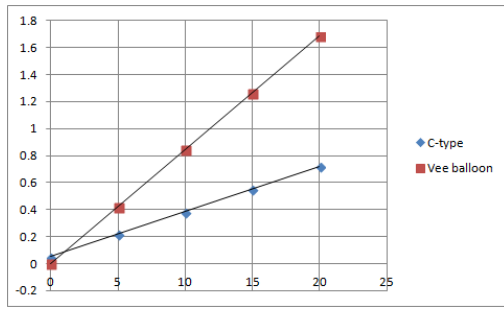


Figure 10.8: Lift coefficients of the two balloon types[35]

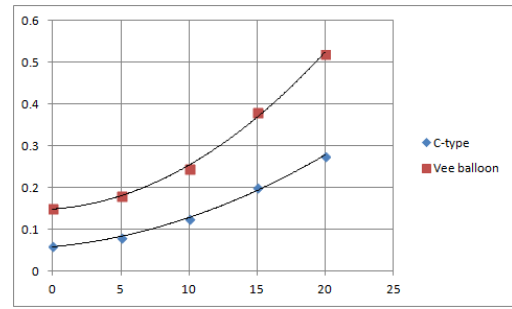


Figure 10.9: Drag coefficients of the two balloon types[35]

The aerodynamic forces are calculated with 21.6[m/s] airspeed, ISA atmosphere at 5000[m] altitude, lift and drag coefficients as seen on Figure 10.8 and Figure 10.9, and a reference area of $V^{2/3}$ (note that forces are calculated in Newtons, thus the balloon volume must be converted to cubic meters).

The performance of the two balloon designs, C-type and Vee balloon, are then compared. As it can be seen from Table 10.5, the Vee balloon is larger and heavier than the C-type. It also produces larger aerodynamic forces, which will increase the strength requirement on the tether rope, leading to a heavier tether. The C-type balloon is superior to the C-type in all measured aspects, and thus is chosen for the shape of the EcoGlide balloon. The following steps of balloon sizing will only consider the C-type.

		C-type balloon	Vee balloon
Altitude Coefficient	K_0 =	8.079247905	22.11684443
	K_1 =	1.65	-18.53
Balloon volume	V [m3] =	853.91	1017.82
Balloon mass	W_B [kg] =	335.52	434.76
Resultant aero. force	alpha [deg] =	20	20
	F [N] =	8723.041178	8610.376208

Table 10.5: Comparison of the two balloon shapes

The equation used for estimating the tether cable strength requirement in the "Tethered Balloon Handbook" by Philip F. Myers was unreadable. Instead the tether type is selected such that its strength exceeds $W_{box} + W_{glider} + W_{tether} + F_{aero}$ by a factor of safety (5 for the Saturn-12, and 2 for the rest, as explained in). Out of the considered options seen on Table 10.2, the 5/16 inch thick Saturn-12 rope was found to be the lightest one that meets this requirement.

10.6. Balloon sizing for flight time

This section explains the steps and results of increasing the size of the balloon, for longer flight duration.

Fick's First Law: $J = -D \frac{\partial \phi}{\partial x}$, where J is the diffusion flux, D is the mass diffusivity, ϕ is the concentration of the permeate, and x is the lengthwise position. This can be rewritten as $V'_{gas} = P \times A \times \frac{\Delta p}{\delta}$, where V'_{gas} is the rate of diffusion across the membrane, P is the permeability of the membrane for a given gas, Δp is the pressure difference across the membrane, A is the surface area and δ is the thickness of the membrane.¹⁷

It was assumed that the envelop material and thickness (including the coating films), and the pressure difference between the balloon interior and exterior are the same for the AB-20¹⁸ and EcoGlide balloons. The rate of loss of helium in the AB-20 balloon is 55[m³] per month, leading to $V'_{He_{AB-20}} = 0.07639 [m^3/hr]$. The surface area of this balloon is $S_{AB-20} = 1157.53[m^2]$. Thus its characteristic permeability is $6.599 \times 10^{-5} \left[\frac{m^3}{hr \times m^2} \right]$. This value for permeability will be assumed for the EcoGlide balloon. Note that this includes leaking through seams and valves. This assumption is valid, as modern gas storage balloons have nearly identical permeability characteristics.¹⁹

The volume of fins are assumed to be negligible. The volume of the balloon is approximated by the volumes of two half-spheroids. Volume of a spheroid is $V = \frac{4\pi}{3} a^2 c$. Looking at Figure 10.2, it can be established that $a = 0.4L$ for one, $a = 0.6L$ for the other spheroid. Based on the sketch, the maximum diameter is estimated to be $0.315L$, and thus $c = \frac{1}{2} \cdot 0.315L$ for both spheroids. This leads to the volume equation of $V_{total} = 0.051954 \times L^3$.

The surface area of a prolate spheroid can be expressed as $S_{prolate} = 2\pi a^2 \left(1 + \frac{c}{ae} \arcsin e \right)$, with eccentricity $e^2 = 1 - \frac{a^2}{c^2}$. By plugging in the previously defined values for a and c , the two eccentricities are $e_{0.4} = 0.91922$ and $e_{0.6} = 0.96494$, leading to $\frac{1}{2} S_{0.4} = 14.46347L^2$ and $\frac{1}{2} S_{0.6} = 23.08610L^2$. Summing up the surface area of the two half-spheroids leads to $S_{total} = 37.54957L^2$.

¹⁷URL <http://www.pathwaymedicine.org/Ficks-Laz>[cite 18 Jun 2020]

¹⁸URL <http://aeroballoon.com/assets/aeroballoon-ab-20-brochure-2018.pdf>[cite 10 Jun 2020]

¹⁹URL <https://www.ballonbau.de/en/gas-storage-balloons/>[cite 20 Jun 2020]

Altitude coefficient		
	K_0 =	8.08
	K_1 =	1.65
Balloon volume		
	V [m3] =	2760.81
Tether mass		
		m_T [kg] =
	Saturn-12 5/16 [in]	200.90
Total mass		
	m_total [kg] =	1440.34
Balloon dimension		
	L [m] =	37.60
	Dia [m] =	11.84
	S [m2] =	53092.01
Balloon flight time		
	Diffusion [m3/hr] =	3.50
	Flight time [hr] =	139.89
Resultant aero. force		
	alpha [deg] =	20
	F [N] =	8723.04
	F [lbs] =	1961.027

Table 10.6: 37.6 meter long balloon

Altitude coefficient		
	K_0 =	8.08
	K_1 =	8.98
Balloon volume		
	V [m3] =	4840.79
Tether mass		
		m_T [kg] =
	Saturn-12 3/8 [in]	252.99
Total mass		
	m_total [kg] =	2282.07
Balloon dimension		
	L [m] =	45.34
	Dia [m] =	14.28
	S [m2] =	77199.81
Balloon flight time		
	Diffusion [m3/hr] =	5.09
	Flight time [hr] =	244.02
Resultant aero. force		
	alpha [deg] =	20
	F [N] =	12929.96
	F [lbs] =	2906.78

Table 10.7: 45.34 meter long balloon

By iteration, the largest balloon that can be supported by a 5/16 inch diameter Saturn-12 tether was found for the given payload mass (180[kg]) and wind speed (21.6[m/s]). Its specifications can be seen on Table 10.6. The minimum volume that is required to stay afloat (lift the weight of the balloon envelope, tether, and payload), is 2270[m³]. With a permeability of $6.599 \times 10^{-5} [\frac{m^3}{hr \times m^2}]$, this volume is reached in a bit under 140 hours, which is the maximum flight time, before it must be winched down for helium top-up. A longer flight duration can only be achieved by employing a stronger tether cable. If the 3/8 inch diameter Saturn-12 is used as tether, a larger balloon can be designed, that is able to stay in the air for a longer time, as can be seen on Table 10.7.

10.7. Sustainability Analysis

Life-Cycle Assessment was not performed on the deployment system, however sustainability considerations were made during the sizing of the tethered balloon system. Their main concern was the regarding the balance between rate of loss of helium, and the power used by the winch.

A smaller balloon would need to be topped up more frequently, as it has less room for excess helium. Thus, the power consumption of the winch is higher. At the same time however, a smaller balloon also means a lower helium leakage rate, due to the smaller surface area. Assuming Ingersoll Rand Guideline²⁰ air winch is used, a compressor that can power it (Sierra SL132 Oil-Free Rotary Screw Air Compressors²¹) would have a power of 132[kW]. The yearly energy consumption of the winch can be calculated with the following equation: $E_{year} = 2 \times t_{winch} \times P_{compressor} \times \frac{365.25}{t_{flight}}$, where t_{winch} is the time it takes to bring the balloon up or down, $P_{compressor}$ is the power of the air compressor, and t_{flight} is the duration of flight in days. A comparison of power and helium consumption between two balloon sizes (specified in Table 10.6 and Table 10.7) can be seen on Table 10.8. If electric power generation is assumed to be completely sustainable, due to the proliferation of renewable power production, the smaller, 37.6[m] long balloon is more favourable due to its lower rate of helium loss.

Balloon length [m]	37.6	45.3
Balloon volume [m3]	2760.8	4840.8
Helium consumption per year [m3]	16374.4	23809.6
Energy consumption per year [MWh]	28.720	16.465

Table 10.8: Sustainability of two balloons of different sizes

Most of the tethered balloon system is made of non-biodegradable, synthetic materials. It was however designed to last, and it was predicted that natural materials would lead to a larger and heavier balloon design, resulting in increased helium loss rate.

²⁰URL <https://www.ingersollrand.com/en-us/lifting-equipment-material-handling/products/winches/force-5i-infinity-winch-series.html>[cite 10 Jun 2020]

²¹URL <https://www.ingersollrand.com/en-us/air-compressor/products/oil-free-rotary-screw-air-compressor/sierra-90-160-kw-125-200-hp-compressor.html>[cite 20 Jun 2020]

10.8. Sensitivity Analysis

For the sensitivity analysis of the tethered balloon system, the effects of changing maximum wind speed and payload mass on the balloon size and maximum flight time are investigated. For both the payload mass, and the wind speed a plus and minus 10% deviation from the nominal (180[kg] and 21.6[m/s]) was considered. A number of balloon sizes were calculated with the above inputs, based on which trend lines were interpolated and plotted on Figure 10.10, Figure 10.11, Figure 10.12, and Figure 10.13.

The step-down discontinuity on the plots are due to increased tether weight. In the case of Figure 10.10 and Figure 10.11, higher wind speeds mean larger aerodynamic forces, so a stronger tether must be employed. In order to accommodate the heavier tether, the balloon size must be increased. The horizontal gap between the plot of 19.4[m/s] wind speed (green dotted line) and 21.6[m/s] wind speed (blue continuous line) is considerably wider under 32.85 meters (1841[m³]) than over 37.6 meters (2761[m³]). This can be explained with the difference in strength-to-weight ratios of the three different tether cables used (1/4, 5/16, and 3/8 inch diameter Saturn-12). In the case of Figure 10.12 and Figure 10.13, the balloon with heavier payload must be bigger in order to provide sufficient static lift. The volume of the extra helium for this increase in static lift is the same for all balloon sizes, explaining the constant vertical offset between the plots of different payload masses. Note that balloons of the same payload and tether mass follow the same curve.

In conclusion, by comparing Figure 10.10 with Figure 10.12, it can be established that the balloon size for a given flight time, is more sensitive to changes in wind speed than changes in payload. Also, from Figure 10.11 and Figure 10.13, it can be clearly seen that increasing the volume of helium in the balloon leads to diminishing returns regarding the maximum flight time.

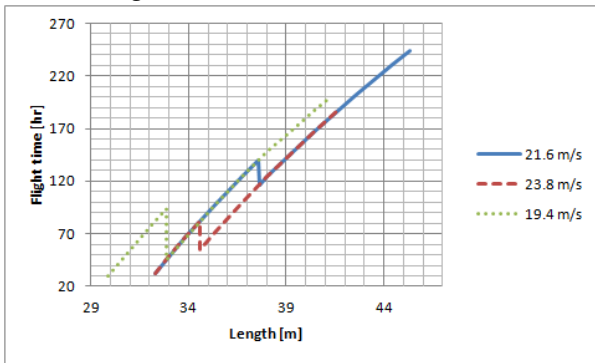


Figure 10.10: Changing length-flight time relation with changing maximum wind speed.

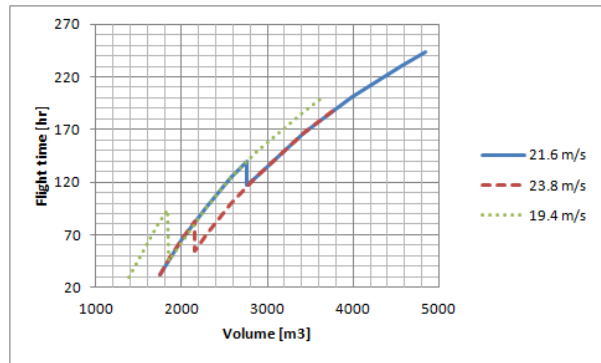


Figure 10.11: Changing volume-flight time relation with changing maximum wind speed.

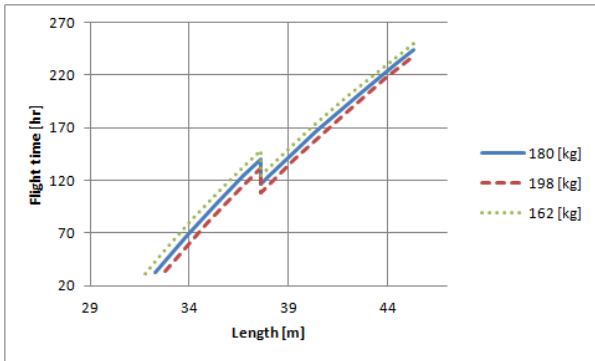


Figure 10.12: Changing length-flight time relation with changing maximum payload mass.

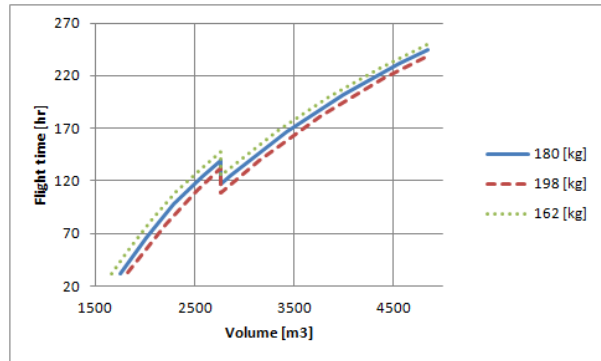


Figure 10.13: Changing volume-flight time relation with changing maximum payload mass.

10.9. Recommendations

Estimated cost of a balloon (almost half-million euros, see Table 16.1), and the mass and cost of the equipment required for its operation (Ingersoll Rand Infinity Guidline air winch is 1352[kg], and Ingersoll Rand Sierra SM132 air compressor is 3350[kg]) greatly exceed what were expected during the deployment system trade-off.[26] It is thus recommended, to repeat the trade with with the improved insight of this chapter. Note however, that the pull capacity of Infinity Guidline is larger than required for the EcoGlide tethered balloon, so a custom made winch would probably be smaller, also requiring a smaller air compressor (or in case of an electric winch, no compressor at all).

Additional tasks that are recommended in order to improve the accuracy of the tethered balloon system sizing are as follows:

- Calculate the increased length of tether and hoist cable due sagging from aerodynamic drag.
- Calculate the contribution of the fins to the balloon volume.

		TIF-6500 Estimated			TIF-3750 Estimated			TIF-1600 Estimated		
Inputs	Alt [m]	2438	2438	Ratio	914	914	Ratio	609	609	Ratio
	PL [kg]	126	126		49	49		16	16	
Outputs	L [m]	15.2	20.5	1.349	12.5	18.1	1.448	9.6	17.3	1.802
	V [m ³]	184.1	446.5	2.426	106.2	307.3	2.894	45.3	268.7	5.932

Table 10.9: Validation of the tethered balloon sizing tool

- Calculate the volume of US Navy C-type balloon, as a function of its length.
- Calculate the rate at which ambient air infuses into the balloon, and its effect on maximum flight time.
- Estimate the set-up and disassembly time of the balloon system as per R_OP_MA_02 and R_OP_MA_04.
- Estimate the duration of maintenance of the balloon system, each time it is winched down for helium top-up, as per R_OP_SFRL_02.
- Compare the environmental footprint of winching the balloon back and out, and the footprint of the production and transportation of helium, to optimise balloon size and balloon system operation for improved sustainability.

Additional tasks that are recommended in order to improve the performance of the tethered balloon system are as follows:

- Consider alternative balloon shapes, not covered in this chapter.
- Consider the use of tapered or stepped tethers, in order to decrease its weight and drag.[36]
- Look into novel materials for balloon envelope, in order to decrease its weight or permeability.
- Consider the use of sustainable materials for tether and balloon envelop.

10.10. Validation

It was attempted to validate the tethered balloon sizing guide using reference data. Payload and altitude data of existing tethered balloons (namely TIF-6500, TIF-3750, and TIF-1600 from Raven Aerostar²²) were passed through the sizing tool, and the results compared with the listed specifications. This can be seen on Table 10.9. Note that since there were very limited number of tethered balloon with payload, altitude, and dimension data available, using a tethered balloon with similar specifications as the EcoGlide balloon was not possible. It clearly shows that the sizing tool used in this chapter considerably overestimates the lifting gas volume required. The error however decreases with increasing altitude and payload requirements, which suggests that the sizing tool of the "Tethered Balloon Handbook" by Philip F. Myers was made for balloons larger than the ones shown on Table 10.9.[36] It must also be kept in mind, that the above mentioned sizing tool was published in 1967, and considerable advancements have been made in material science, thus it is expected that modern built tethered balloons would perform better than their counterparts from the 60s. Extrapolating the error as a function of balloon size may be used to increase the accuracy of the sizing tool.

The other model that must be validated is the approximation of the balloon volume via two half-spheroids. This was done with the help of the balloon CATIA model. Since no exact dimensions of the C-type balloon were available, the CATIA model was created by tracing the outline of the balloon (see Figure 10.2), and revolving it around its central axis. After scaling it up to the correct size, the volume of the solid was measured to be 2913.846[m³]. Thus, the approximation used in section 10.6 is found to be 94.7% accurate.

10.11. Risk Assessment

Table 10.11 shows the deployment risks, which are also represented in a risk map, see Table 10.10. The key risks are all related to failing components causing parts of the deployment to either fall down or get stuck. General mitigation methods are to perform preventive maintenance and inspections and to formulate clear operating instructions, which need to be followed.

Table 10.10: Deployment risk-map

(Unmitigated) / Mitigated	Highly Probable (h)	Probable (p)	Improbable (i)	Negligible (n)
Catastrophic (ca)		(DP1) (DP2) (DP3) (DP4) (DP14)	(DP12) DP3 DP14	DP4
Critical (c)	(DP8) (DP10)	(DP5) (DP6) (DP13)	(DP11) DP2 DP13	DP1 DP10 DP11 DP12
Marginal (m)	(DP9)	(DP7) DP8	DP5 DP6	
Negligible (n)		DP9	DP7	

²²URL <https://ravenaerostar.com/products/tethered-aerostats/tactical-aerostat-systems>[cite 25 Jun 2020]

Table 10.11: Deployment risks

Index	Risk Factor	Severity	Probability	Risk	Mitigation Method	Severity	Probability	Risk
1	Tether cable fails, and balloon floats away.	ca	p	h	Balloon must be equipped with emergency release valve that can vent helium from the balloon ensuring a timely descent. Tether cable must be inspected for deterioration each time balloon is pulled down.	c	n	l
2	Balloon envelope ruptures.	ca	p	h	If balloon interior is divided into multiple separate ballonets, the intact ones ensure a slower descend speed if one of them ruptures. Balloon envelope must be inspected for deterioration on a regular basis.	c	i	m
3	Spacer beam suspension fails, and spacer beam comes crashing down.	ca	p	h	Spacer beam and suspension must be inspected for fatigue and deterioration on a regular basis.	ca	i	m
4	Glider deployment fairing line/clamp/rope fails, and glider deployment fairing comes crashing down.	ca	p	h	Glider deployment fairing line and clamp must be inspected for deterioration prior to each deployment. Hoisting rope must be inspected for deterioration on a regular basis.	ca	n	l
5	Tether winch breaks, and balloon cannot be pulled back.	c	p	mh	Balloon must be equipped with emergency release valve that can vent helium from the balloon ensuring a safe descent. Tether winch maintenance must be completed on schedule as recommended by the manufacturer. Tether winch replacement parts must be available on site.	m	i	l
6	Hoist winch breaks, and glider cannot be deployed.	c	p	mh	Hoist winch maintenance must be completed on schedule as recommended by the manufacturer. Hoist winch replacement parts must be available on site.	m	i	l
7	Hoist winch breaks, and glider deployment fairing cannot be recovered.	m	p	m	Hoist winch maintenance must be completed on schedule as recommended by the manufacturer. Hoist winch replacement parts must be available on site.	n	i	l
8	Hoisting rope gets entangled, and glider cannot be deployed.	c	h	h	Balloon system operator must make sure at all times, but especially in windy weather that the hoisting cable is sufficiently tight. Balloon must be lowered to untangle the rope.	m	p	m
9	Hoisting rope gets entangled, and glider deployment fairing cannot be recovered.	m	h	m	Balloon system operator must make sure at all times, but especially in windy weather that the hoisting cable is sufficiently tight. Balloon must be lowered to untangle the rope.	n	p	l
10	Once "Pulley B" is reached, glider deployment fairing trap door doesn't open, or glider gets stuck in the box.	c	h	h	Design the deployment fairing with trap door that is normally-open. Equip the deployment fairing with a mechanism that forces the glider out.	c	n	l
11	The proximity of deployment fairing to "Pulley A" is not detected, the clamp hits the pulley with high speed, potentially damaging it.	c	i	m	Balloon system operator must keep track of the length of the hoisting rope reeled in, giving an estimate of the position and status of the deployment fairing, alerting him/her of the malfunction.	c	n	l
12	The proximity of deployment fairing to "Pulley B" is not detected, the deployment fairing is reeled up on "Pulley B", potentially damaging the pulley, and breaking the clamp or line which the deployment fairing is hanging on.	ca	i	m	Balloon system operator must keep track of the length of the hoisting rope reeled in, giving an estimate of the position and status of the deployment fairing, alerting him/her of the malfunction. Hoist winch must be equipped an emergency shut-down, that stops the winch if the force on the hoisting rope exceeds the break strength of the clamp or line the deployment fairing is hanging from.	c	n	l
13	Radio communication from the balloon signaling the status of the deployment fairing is not received by the ground segment, and so the hoisting winch is not stopped when deployment fairing reaches "Pulley A", potentially damaging the pulley.	c	p	mh	Balloon system operator must keep track of the length of the hoisting rope reeled in, giving an estimate of the position and status of the deployment fairing, alerting him/her of the malfunction.	c	i	m
14	Radio communication from the balloon signaling the status of the deployment fairing is not received by the ground segment, and so the hoisting winch is not stopped when deployment fairing reaches "Pulley B", potentially damaging the pulley, and breaking the clamp or line which the deployment fairing is hanging on.	ca	p	h	Balloon system operator must keep track of the length of the hoisting rope reeled in, giving an estimate of the position and status of the deployment fairing, alerting him/her of the malfunction. Hoist winch must be equipped an emergency shut-down, that stops the winch if the force on the hoisting rope exceeds the break strength of the clamp or line the deployment fairing is hanging from.	ca	i	m

Production and Assembly

This chapter discusses the production and assembly of the glider and its components. Some of the decisions related to the approach to production are strongly influenced by the logistics, treated in chapter 12. The requirements and needs are presented in section 11.1 and the design approach is briefly discussed in section 11.2. The production plan and some of the main production methods are described in section 11.3. A small section on a proof of concept experiment and future steps is also included, see section 11.4. Finally, the chapter is concluded by a risk assessment in section 11.5 and a sustainability analysis in section 11.6.

11.1. Functional Analysis

In this section the requirements, shown in Table 11.1, and constraints on manufacturing will be explored.

Table 11.1: Production requirements [26]

Identifier	Requirement. statement	Compliance
R_EG_COST_01	The Life Cycle Cost (financial, environmental and social) of the glider shall be minimal for a yearly production of 1000 gliders.	TBD
R_EG_SUST_04.1	The environmental impact and the energy use during the production of the glider shall be evaluated using a life cycle assessment and optimised, if necessary.	Chapter 14
R_OP_REG_08	The UAS manufacturer shall establish a procedure on the handling and storage of the UAS.	No compliance
R_EG_TRA_09	The glider shall be made by widely available production methods.	Section 11.3
R_OP_MA_04.1	The glider shall be able to fit in a volume of 5.89 x 2.35 x 2.36m	Section 11.3
R_EG_FA_01	The glider shall not require dedicated tooling for assembly	Section 11.3

A distinction between different production requirements can be made. The first type of requirements that apply to manufacturing are the sustainability requirements. Indeed, the glider should not only be non-polluting and sustainable during the operational and end-of-life phases, but also during production. This aspect is captured in requirements R_EG_COST_01 and R_EG_SUST_04.1. A further requirement that is very important for production is the transportability requirement R_OP_MA_04. The military customer has indeed expressed its willingness to perform the main part of the final assembly on location if this can improve the shipping of the gliders. It is thus necessary to design it such that the final assembly can be performed at the field hospital. This allows for more efficient storage of the gliders, but also adds a level of complexity to the production planning, as on site production should be simple and involve as few specialised tools as possible, as dictated by R_EG_FA_01. Additionally, to ensure availability of the gliders and keep the production costs low, requirement R_EG_TRA_09 shall be followed. Finally, requirement R_OP_REG_08 should be fulfilled to ensure that the gliders are up to specification and flight-worthy after final assembly. However at this stage of the design, too many details still need to be sorted out to establish a sufficiently detailed procedure.

11.2. Design Approach

Production can not be designed independently from the glider subsystems. Structural design and material choices in particular dictate in a large way how the glider will be produced. For this reason, a design for manufacturing approach was applied during the material selection and structural design. This has allowed to design a glider that is overall quite simple to manufacture and for which the main processes are already determined by these earlier choices. The steps that are left at this stage are the ones necessary to ensure the glider fulfils the transportability and on-site assembly requirements. In the upcoming sections, the final assembly of the glider will be discussed, as well as the manufacturing of certain components and subassemblies.

11.3. Production Plan and Methods

This section describes the production methods used to manufacture the different components and the assembly process. Additionally, it also contains explanations about which parts will be manufactured in-house, which ones will be produced by external suppliers and which parts of the assembly will be done by the customer.

Final Assembly

As described in chapter 6 the structure of the glider is made out of two spars and a skin shell. Additionally, there are also some non-structural components, the cool boxes, the electronics compartment and the control surfaces. The most voluminous and thus hardest to transport, of these components is the skin shell. It was therefore decided, that the skin shall be split into multiple sections. First, for manufacturing purposes that will be discussed in the next section, the shell will be split into a top and a bottom half. Additionally, the fuselage will also be a separate section from the wings. Finally the wings themselves will also be split in half, making all sections more or less 1 m wide. This leads to a total of 10 fuselage panels. The spars, while quite long, still fit inside a standard container and their limited width and height means that they can be stacked rather easily. For this reason the spars can be shipped preassembled, which also means that they can be built in a controlled factory environment with appropriate tooling to guarantee the quality of these main structural elements. The reusable electronics compartment meanwhile, will be of limited size and can thus be shipped in a preassembled format. It should however not be preinstalled, as most gliders will not fly with a new set of electronics, but rather with electronics salvaged from an used glider. The payload boxes, while they might take up a significant amount of volume, can most likely be used to store consumables required for assembly, like glue or the PLA film. They can thus be shipped in an assembled state. If it however turns out that shipping assembled payload boxes has an effect on the number of gliders that fit in a container, the boxes can also be shipped in kit format. Due to their simplicity it would not be a problem to assemble them on site. Finally, the control surfaces will not be attached to the wing prior to shipping, as the torque rod that connects them to the actuators also serves as the main attachment and can only be installed during final assembly.

A complete glider kit will contain the following items:

- Wing panels 8x
- Fuselage panels 2x
- Spars 2x
- Electronics compartment
- Payload boxes 2x
- Control surfaces 2x
- Torque rods 2x
- PLA shrink wrap
- Glue
- Tape

The final assembly process, as it will be carried out at the field hospital is shown schematically in Figure 11.1.

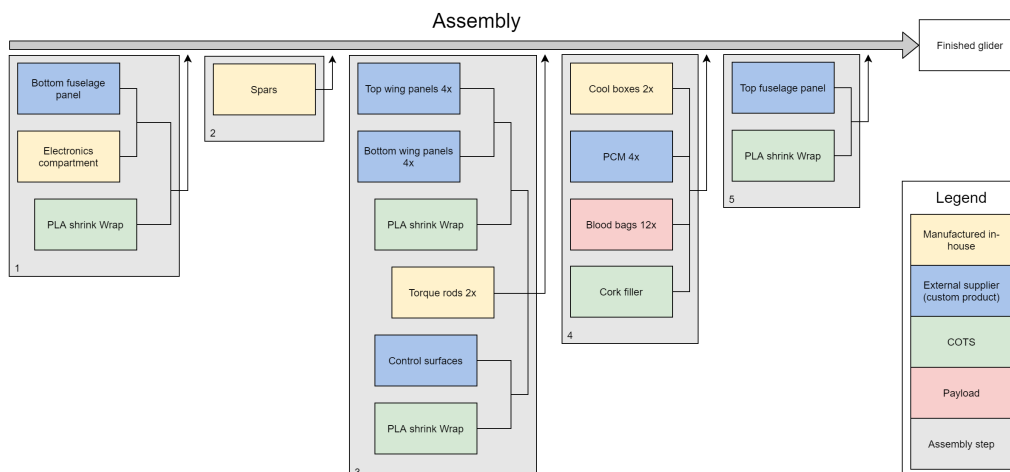


Figure 11.1: Diagram showing the final assembly process

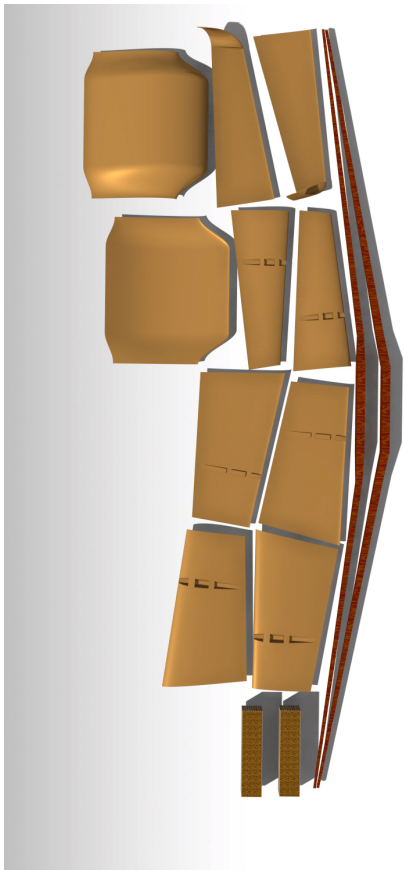


Figure 11.2: Main components of glider kit (electronics, PLA and control surfaces not included)

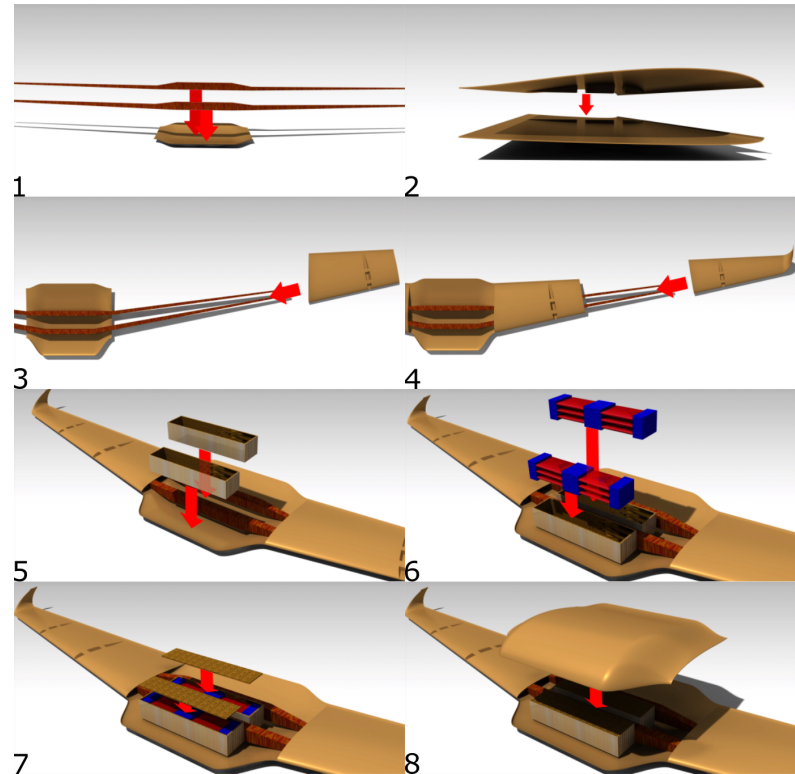


Figure 11.3: Detail views of main assembly steps

The assembly process can be split up into five main steps.

- Step 1: The electronics compartment is installed in the lower fuselage panel, which is then wrapped in PLA shrink film. The process of shrink wrapping the skin panels will be discussed in the next section. The lower fuselage section with the now installed electronics serves as the base for the assembly.
- Step 2: Both spars are placed in the designated slots of the fuselage section and glued in place (Figure 11.3 picture 1).
- Step 3: The corresponding top and bottom wing panels are glued (Figure 11.3 picture 2) together and shrink wrapped. Similarly, the control surfaces are also wrapped in PLA. They can then be positioned in the cut-out of the outer wing panel and the torque rod can be inserted to secure them in place. Finally, the inner wing panels are added to the spar-fuselage assembly, by sliding them along the spars (Figure 11.3 picture 3), followed by the outer sections (Figure 11.3 picture 4). When the wing sections meet the fuselage, the torque rod should be connected to the actuators located in the electronics compartment.
- Step 4: The payload boxes are placed in the intended slots in the fuselage (Figure 11.3 picture 5). They can then be filled with the blood bags, PCM elements and the cork filler (Figure 11.3 picture 6). Last, the lids of the boxes are closed and taped shut (Figure 11.3 picture 7).
- Step 5: The top fuselage panel is shrink wrapped and fastened to the lower half (Figure 11.3 picture 8), serving as a lid and fully enclosing the electronics and the payload.

Although a fixed series of steps is shown in Figure 11.1, the subassemblies within a certain step can be performed ahead of time and do not require the previous main step to be finished. This means that for example the shrink wrapping in step 5 can be performed before the payload boxes have been installed in the fuselage. In fact this is even recommended, as after the installation of the payload boxes, any time that is wasted on assembly reduces the amount of time that is available to perform the mission and retrieve the glider, because the PCM elements start heating up. During assembly no fasteners like screws, rivets or nails will be used. Instead water soluble and biodegradable¹ PVA glue shall be used to join the skin panels together and attach them to the spars. To cover any gaps between the panels and ensure good aerodynamic performance, biodegradable cellophane tape² can be used. This tape is also the perfect

¹<http://sustainable-graphic-design.blogspot.com/2011/08/glue-sustainable-designers-quick-guide.html>

²<https://www.findtape.com/packing-tape/biodegradable-cellophane-tape/c79/>

joining method to attach the fuselage top panel as it needs to be installed after the payload and using tape is a simple process that does not require any additional curing time.

Finally, although it is up to the customer to decide when they will assemble the gliders, it is recommended to pre-assemble a number of gliders up until step 3 included and do the subassembly of step 5 to have the gliders ready for a very quick deployment. The preassembly is also to some extent necessary as PVA glue has a curing time of 18 to 24 hours³.

Production of Components and Subassemblies

Having discussed the final assembly in the previous section, this section gives further details about a number of sub-assemblies and the production of some components.

Paper Pulp Fuselage and Wing Panels

As already mention in chapter 6 the fuselage and wing panels are made out of moulded paper pulp. This type of material is a very common sight in the packaging industry, with egg cartons being the most well known example. However paper pulp moulding is not limited to small items, in fact some large pallets are also manufactured that way⁴. There are different moulding methods that can be used with paper pulp. However, due to the need for low thicknesses of 2 to 3 mm only transfer moulding and thermoforming could be applied for the skin panels. Thermoforming results in a cleaner and smoother finish [16], which would be favourable for the glider, however, further research is needed to determine the advantages and disadvantages of either method and choose one specific method. As already mentioned, the skin sections will be split into a top and bottom half. This is to ensure that the pulp parts can be released from there moulds. Additionally, the wing panels are also split in a tip- and a root-section. This is to reduce the size of the required moulds.

Paper pulp moulding involves blending used paper with water to form the pulp slurry, which is then shaped in moulds under pressure to then be dried either by heating the mould (thermoforming) or in an oven (transfer moulding) [16]. This process requires heavy machinery, like presses and a large oven, as well as the equipment to blend the paper into a slurry. The production rate can however be very high, with production lines often having an output in the hundreds of pieces per hour. As the investment to set up such a line would be considerable and the required production rate is much lower for EcoGlide, it was deemed best if the paper pulp parts are produced by an external supplier who is already producing other parts with the same techniques. Additionally, the supplier's expertise could be extremely valuable during the design of the skin panels and associated moulds.

Having the paper pulp parts produced externally means that the initial investment only needs to comprise the moulds. To further reduce the costs during the prototyping and early production phases Fused Deposition Modeling (FDM) moulds could be used instead of metal ones, allowing to iterate the design at minimal cost⁵.

PLA Film Wrapping

The PLA shrink film is a product that is also being used in the packaging industry and is thus readily available from manufacturers. Typically, shrink wrapping is used to add a protective layer to items or to bundle a number of items together for transport and retailing purposes. These films tend to be very thin, with thicknesses of 50 microns⁶ or less. To wrap the paper pulp sections in PLA, a PLA sleeve is put around the pulp part and if necessary, the edges are welded and cut to the right size. Then, the whole film is heated to the required temperature in an oven and shrinks, to tightly wrap around the pulp part. This should result in a very smooth finish and cover the gaps left by the integrated ribs. The film should shrink to the point where it remains under tension even when the heat source is removed. This way, the residual tension should prevent it from buckling, even when the other wing components are under compression. Alternatively to an oven, which would need to be of quite a substantial size to fit the panels, a heat gun can also be used to shrink the PLA film. The choice between an oven and the heat gun still needs to be made. This will depend on customer preference and if satisfactory results are achievable with a heat gun at this scale.

Spars

Due to their complex shape, the spars will need to be manufactured out of multiple parts, which then need to be assembled into one single spar. The joints between the different parts will be located at the kinks, as this allows to orient the wood such that the grain direction is used most efficiently. To achieve the desired spar thickness, multiple sheets of plywood need to be stacked and glued. Once the correct initial thickness has been achieved, the plywood parts can be cut to size using common woodworking tooling like for example a band saw, set up with guides to help with getting the correct angles. Finally, the different spar parts can be joined at the kink locations, by once again gluing them. During each gluing step care should be taken to respect the clamping and curing times.

³<https://home.howstuffworks.com/multipurpose-glues.htm>

⁴<https://www.tart.eu/molded-pulp/>

⁵<https://www.stratasysdirect.com/technologies/fused-deposition-modeling/fdm-tools-paper-pulp-molding>

⁶<https://www.shrinkfilmroll.com/sale-9522391-heat-shrink-packaging-pla-plastic-film-50-mic-thickness-eco-friendly.html>

Payload Boxes

The payload boxes consist of three main components: the plywood shell, the cork inner layer and the cork filler. The plywood should be available commercially in a thickness close to that required and should therefore only require being sawn to the right dimensions. The cork filler is a byproduct of the wine bottle cork industry. Once the bottle corks have been punched out of cork sheets, the left-overs are shredded into small cork granules, which can directly be used as filler. The inner cork layer is made from these same granules, which are heated and pressformed into sheets of the desired thickness. The action of heating the cork granules releases natural resins, which act as a binder⁷. Such sheets are commercially available and also only require being cut to the correct dimensions. The flat plywood and cork sheets can then either be preassembled at the factory by gluing them, or shipped in sheet form and assembled on-site, at the field hospital. Finally, for a quick and smooth loading of the payload, the lid of the box should be taped on with biodegradable tape, once the payload has been installed.

Electronics Compartment

The electronics compartment mainly consists of off the shelf components, which only need to be connected and mounted in the compartment. Therefore, the production of the electronics compartment will only consist of the manufacturing of the compartment itself, which will be designed in a later design iteration, the mounting of the components using the supplied or additional hardware and the manufacturing of a custom wiring harness. All of these steps will be performed in-house and the electronics compartment will be shipped preassembled.

11.4. Proof of Concept and Future Steps

In order to validate the concept of using moulded paper pulp for the skin panels and to investigate the production of such parts, the team conducted a couple of small experiments. A small wing section including a rib was modelled as well as the corresponding moulds. Those were then produced using an FDM 3d printer. The mould consists of three parts, a top and a bottom surface and a frame to enclose the edges of the panel. The paper pulp was produced using shredded corrugated cardboard for the first experiment and egg cartons for the second one. Additionally, as suggested by XYZAidan⁸, a small quantity of adhesive was also added to the slurry. For the first experiment, this was wallpaper glue and for the second one, home made rice paste. Apart from the different pulp mixtures, the curing times and mould designs were slightly altered between experiments. As can be seen in Figure 11.4, the second experiment (right) yielded far better results, with a smoother, more homogeneous finish and far less warping. However, in both cases, the rib design proved to be problematic, as both samples broke at this location during release from the mould. The team is however confident, that an improved mould design with better draft angles should solve this issue. Finally, further experiments should be carried out to investigate the effect of using pulp without adhesives, as is the case for industrial production and experts or producers should be contacted to get their opinion on the design and its feasibility.



Figure 11.4: Paper pulp wing section samples, first experiment on the left, second one on the right.

11.5. Risk Assessment

This section contains the risk assessment of the glider production. In Table 11.2 the risks are listed along with their mitigation methods. Table 11.3 is the risk-map of the production risks, its purpose is to help assess the global risk level

⁷<https://www.corklink.com/index.php/expanded-cork-how-it-is-made/>

⁸<https://www.youtube.com/watch?v=0ItPfhx3ulw>

and evaluate the effectiveness of the risk mitigation.

Table 11.2: Production risks

Index	Risk Factor	Severity	Probability	Risk	Mitigation Method	Severity	Probability	Risk
1	Injury to worker during final assembly.	ca	p	h	Avoid dangerous operations during final assembly, such as sawing, or using high temperature tools.	ca	n	l
2	Injury to worker during component/subassembly production	ca	p	h	Use well trained workers and provide clear safety guidelines in factory.	ca	i	m
3	Delays in delivery from external suppliers.	c	p	mh	Have sufficient inventory to compensate for delays.	m	p	m
4	Delays in production line due to failure of machine	c	p	mh	Have spare parts at hand to limit downtime.	m	p	m
5	Poor glued joints due to poor clamping or shortened curing times.	c	p	mh	Provide clear guidelines on gluing procedures and implement regular quality controls.	m	i	l
6	Holes poked in PLA film at ribs due to careless handling of sharp objects near glider.	c	h	h	Fix holes with tape provided for assembly before they grow into full tears.	n	h	l
7	PLA overheating leads to melt holes during shrink wrapping.	c	h	h	Provide clear instructions on temperature range that needs to be respected during the shrink wrapping. Provide spare PLA film to rewrap failed parts.	m	i	l
8	Wings assembled the wrong way around (left wing on right side and upside down).	c	p	mh	Add 'right' and 'left' markings and colour code components (e.g. red right, blue left).	c	n	l
9	Steps being skipped during final assembly (e.g. forgetting to apply glue or to cover panel gaps with tape).	c	h	h	Provide assembly manual and checklists. Perform preflight checks.	m	i	l

Table 11.3: Production risk-map

(Unmitigated) / Mitigated	Highly Probable (h)	Probable (p)	Improbable (i)	Negligible (n)
Catastrophic (ca)		(PR1) (PR2)	PR2	PR1
Critical (c)	(PR6) (PR7) (PR9)	(PR3) (PR4) (PR5) (PR8)		PR8
Marginal (m)		PR3 PR4	PR5 PR7 PR9	
Negligible (n)	PR6			

As can be seen in Table 11.3, the risks are successfully mitigated, as no risks have a level higher than marginal after mitigation. From the two tables in this chapter it is also possible to identify the three main risk types related to production. Those three types are: injury to workers during production, poor production quality and delays in the production. Injury to workers can generally be mitigated through safety guidelines and good instructions. Similarly, poor quality can be improved through good instructions, but also quality control. Finally delays in production can be avoided by good planning and by thinking ahead.

11.6. Sustainability Analysis

While the LCA in chapter 14 also considers the manufacturing of the gliders, it is still worth discussing some sustainability aspects in this chapter.

While most of the production processes are by themselves rather sustainable, it is still important to consider the production as more than just processes and also take the sourcing of raw materials and transport of components into account. For this reason, it was decided, that the plant doing all the in-house processing, to get the kits ready to be shipped to the customer, shall be located in the same country as the customer. In this case this would mean that the plant will be based in the Netherlands, as the main customer is the Dutch Army.

The raw materials that will be needed in the largest quantities are plywood and paper pulp. To ensure a sustainable production, the wood used for the plywood shall be sourced locally and the plywood supplier shall also be located within a 100 km radius of the production plant. Similarly, for the paper pulp a local producer shall be chosen. The raw materials for paper pulp are old paper and water, which can both easily be sourced locally.

12

Logistics

The purpose of this chapter is to present the logistical aspects of EcoGlide and to explain the reasoning that led to the resulting logistics chain. It is also worth pointing out that the logistical aspect of EcoGlide has a strong impact on production and assembly, as it dictates in what state the glider should be shipped and thus where what part of the assembly can take place. However, production also has an influence on logistics, as the exact size of the glider kits determines how many gliders can be shipped in a single container. The logistics are thus presented in two sections section 12.2, giving a general overview and section 12.3 giving a more detailed description, which also takes into account the production and assembly processes. Section 12.1 contains the requirements and functional analysis that lead to the decisions taken in section 12.2 and finally in section 12.4 and section 12.5 the risks are assessed and the sustainability analysed.

12.1. Functions and Requirements

This section contains the most important functions and requirements relevant for the logistics of the glider. These are mainly generated from customer needs. They are presented in Table 12.1.

Identifier	Requirement statement	Compliance
R_OP_MA_04	The launch system and the glider shall be able to fit in a volume of 5.89 x 2.35 x 2.36 m	Section 12.3
R_OP_MA_05	The launch system and the glider shall be transported to the deployment location by truck and by ship	Section 12.2

Table 12.1: Logistics requirements

In addition to these requirements, there is also room for optimisation. As stated in Section 11.1, the military has requested to optimise the glider not just to fit inside of a standard 20ft. shipping container, but also to fit as many as possible inside such a container. The fact that this results in more assembly work on-site was of minor importance.

12.2. Logistics Overview

This section contains a general overview of the logistics chain. In this overview, the main links of the chain are identified and the effect they have on other subsystems is explained.

Transport

The first step to determine the logistics chain is to identify the locations to and from which items will have to be shipped. For EcoGlide, these locations are: the off-site production facilities, the main hospital and the field hospital. The offsite production facilities include both the main EcoGlide plant, as well as the external suppliers. These will be considered as a single unit in this report and the transport between suppliers and the EcoGlide factory will not be treated. The main hospital is the location from which the gliders are launched. The field hospital is the destination of the gliders and where the blood supply is needed.

After identifying the locations involved in the logistics chain, one can start discussing the connections between them. As all the equipment that will arrive at the field hospital does first pass through the main hospital, one can ignore the direct connection between off-site and the field hospital locations and vice-versa, from now on. This leaves only two two-way connections: from off-site to the main hospital and from the main to the field hospital, these are shown in Figure 12.1.

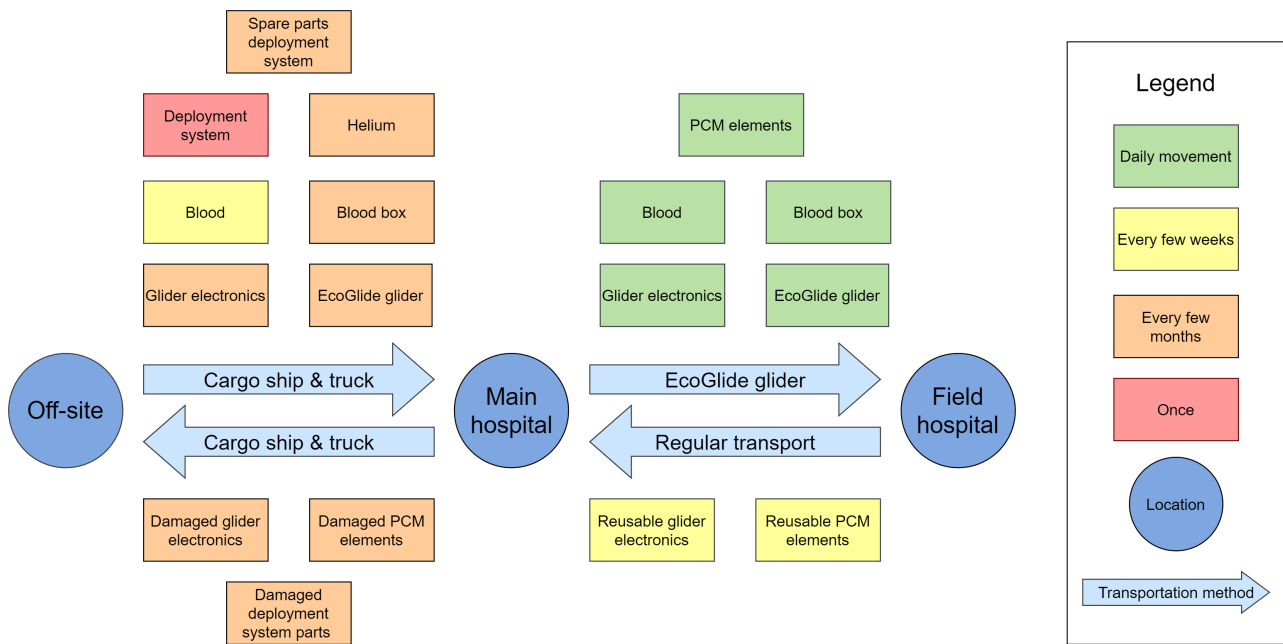


Figure 12.1: The logistics chain of the EcoGlide system

The link from the main to the field hospital is assured by the glider and as it is the purpose of this whole report to mainly present the glider and its operation, this will not be treated in any further detail in this section. This leaves only three connections that need to be analysed in more detail.

From the main hospital to off-site only small items, like electronics, PCM elements or broken deployment system parts occasionally need to be transported. For this reason, this part of the logistics chain is fairly straight forward and existing parcel shipping routes shall be used.

The link from off-site to the main hospital is one of the two more crucial links. Indeed, as can be seen in Figure 12.1, all of the equipment required to perform the mission has to transit to the main hospital. To comply with customer requirements, all of the items should fit in standard 20ft containers. Furthermore, to increase the efficiency of the transport, the items that can be optimised should be optimised for transport. This is mainly applicable to the glider itself, as it is the only voluminous item that needs to be shipped frequently. So for production and assembly this leads to the need to optimise the process such that a maximum number of gliders can be shipped simultaneously in a single 20ft container. As prescribed by requirement R_OP_MA_05 the main leg of the transport will be done by sea freight. The transport to- and from the sea meanwhile will be done by lorries. As during transport the containers are likely to be exposed to a variety of weather conditions, it is important to ensure that the inside of the containers the conditions remain within the acceptable boundaries. This is particularly important when it comes to moisture and condensation, as the paper pulp parts can quickly degrade when in contact with water. Temperature can also become an issue if it rises above acceptable levels, as it might cause the PLA film to prematurely shrink. Temperature controlled or insulated containers might thus be necessary. These are however not uncommon, as such containers are regularly used to transport temperature sensitive goods such as fruits or vegetables¹.

The last remaining part of the chain is the link from the field hospital back to the main hospital. Due to the nature of the EcoGlide mission, the land connection between the two hospitals is likely to be only sporadically available, as the conflict in the area dies down. Furthermore, even when available, this connection is likely to be poor and relying on it to frequently transport large quantities of equipment is not realistic. For this reason it is not feasible to bring gliders back to the main hospital and reuse them for multiple missions. The gliders will thus need to be disposed of at the field hospital, giving rise to the need for mostly biodegradable gliders. As some smaller components like the electronics compartment and the PCM elements are not biodegradable these still need to be recovered and shipped back to the main hospital for reuse. Due to the size of these components, they can however easily be stockpiled until there is a window of opportunity to organise the transport back to the launch site. This transport can take advantage of the return leg of other resupply missions, that for example bring food or equipment to the field hospital.

Inventory

Aside from the actual transport, another aspect that should also be considered are the inventories at each location. Indeed, to allow for contingencies such as delays in transport or faulty parts, the off-site production plant and the main hospital should always have a number of spare gliders and parts ready. This includes both parts for the gliders and the deployment system. The exact numbers of units necessary in each inventory strongly depend on the rate at

¹<https://www.budgetshippingcontainers.co.uk/info/the-ultimate-guide-to-shipping-container-condensation-treatments/>

which the gliders are used and shipped and can thus not be determined at this stage.

The production plant should always have at least one shipment worth of full glider kits and one complete deployment system available. This is to account for the fact that a shipment might not reach its destination or that there might be delays in the production.

Similarly, the main hospital should also have one shipment worth of full glider kits and one complete deployment system available. This is again to take into account lost or delayed shipments as well as possible failures of the deployment system. Furthermore, to avoid excessive in blood deliveries in case of a failed mission, a number of already assembled glider should also always be available.

12.3. Detailed Logistical Aspects

A logistical consideration for both the glider system as well as the deployment systems are given below.

Logistical considerations for the glider system

The glider must be stored as compact as possible while still being easy to assemble. The glider was therefore divided into several pieces, which could already be seen in Section 11.3. In summary, the gliders skin is divided into 10 pieces, the 2 spars remain uncut, and the payload boxes can also be shipped without further division. The skin and payload box were rearranged in a CAD model to get an impression of the shipping size. The spars were not considered during this considering their long and slender shape. They will be stacked together separately in the shipping container. Once the size of the boxes was determined, they could be stacked in a CAD model of a shipping container. The spars could also be placed. Using this method, it was concluded that a shipping container can hold a total of 64 gliders. The results can be found in the pictures below. The boxes follow a 2x4x8 arrangement, however for visibility only the back rows are fully shown. The leading edge and trailing edge spars make stacks of 32 and are placed next to each other.

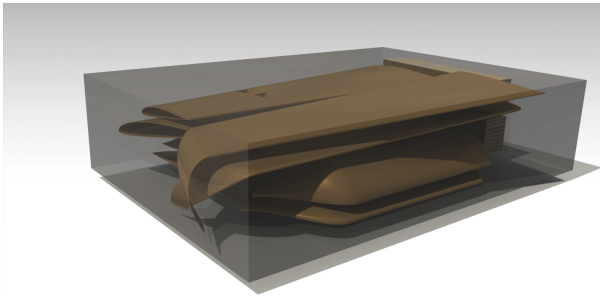


Figure 12.2: Disassembled glider kit fitting in shipping box

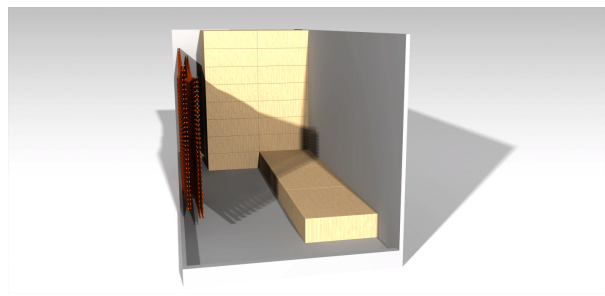


Figure 12.3: 64 gliders packages arranged in a standard 20ft. container

Logistical considerations for the balloon system

For the deployment system them parts that need to be transported can be found in Table 12.2. As can be seen from the table, most parts only need to be shipped in the initial container and unlike the gliders very few parts need to be transported regularly. This means, that the transportability of the deployment system is far less critical than that of the glider. Requirement R_OP_MA_04 shall however still be fulfilled, which is why it should be checked if all the components fit in a 20ft container. This is unfortunately not possible at this stage, as the dimensions of some components are unknown. The exact dimensions of the winches are not given by the manufacturer and the size of the envelope, when folded, is also impossible to estimate, as the extent to which it can be folded is unknown. A future step in the design of the deployment system would thus be to validate its transportability by contacting manufacturers.

Table 12.2: Deployment system equipment

Initial container:	Balloon envelope	
	Tether line	
	Balloon payload	
	Ground station:	Tether winch Mooring platform Hoist winch Ground control workstation
Regular resupply:	Helium	
Occasional resupply:	Spare parts	

12.4. Risk Assessment

This section contains the risk assessment of the logistics chain. The list of risks is shown in Table 12.3 and the corresponding risk map in Table 12.4.

Table 12.3: Logistics risks

Index	Risk Factor	Severity	Probability	Risk	Mitigation Method	Severity	Probability	Risk
1	Paper pulp parts soak up moisture and degrade during transport	c	h	h	Use climate controlled containers	c	n	l
2	PLA film starts shrinking during transport due to heat	c	p	mh	Use climate controlled containers	c	n	l
3	Delays in logistics chain	c	p	mh	Account for possible delays when determining the required inventory size at each location	c	n	l
4	Long period with no possibility to return electronics and PCm to main hospital	c	h	h	Allow for storage of used electronics at field hospital and ensure sufficient number of electronics is available at the main hospital	n	h	l
5	Glider parts damaged during transport	c	h	h	Perform inspection of parts before using them during assembly and use parts of other glider if damaged parts are found	m	h	m
6	Gliders stuck at customs due to military aspect	c	p	mh	Clearly indicate medical aspect of drones	c	i	m

Table 12.4: Logistics risk-map

(Unmitigated) / Mitigated	Highly probable (h)	Probable (p)	Improbable (i)	Negligible (n)
Catastrophic (ca)				
Critical (c)	(LO1) (LO4) (LO5)	(LO2) (LO3) (LO6)	LO6	LO1 LO2 LO3
Marginal (m)	LO5			
Negligible (n)	LO4			

The key risks for the logistics chain are that the material can be damaged during transport and possible delays or missing shipments. To mitigate those risks quality control checks should be implemented and sufficient inventories should be available to allow for faulty parts and delivery delays.

12.5. Sustainability Analysis

As logistics could have an important contribution to the overall pollution and energy consumption of EcoGlide, sustainability should also be kept in mind while working out the logistics. This is part of the reason why the glider production was partly optimised for transport efficiency, as this not only reduces cost, but also the ecological footprint of EcoGlide. Additionally, most items that need to be shipped from one location to another will be transported along with other regular supplies. Indeed, the initial shipment including gliders and the deployment system for example, can be shipped along with the equipment required to set up the hospitals at the mission location. Similarly, the electronics compartments and PCM elements that need to be shipped back to the main hospital will be transported on the way back from other supply missions. All of these measures help to improve the sustainability of the logistics chain.

13

Operations

In an earlier phase of the design a communication flow diagram was created. The team has decided to split this diagram up into smaller pieces, and these will be placed in the relevant subsystem chapters (Figure 7.18 and Figure 10.1). The interaction of personas with subsystems, are shown in the mission operations diagram. The reasoning behind these diagrams is to present the complicated mission in different levels of depth.

The functions and the requirements derived from them are presented in section 13.1. Section 13.2 and section 13.3 explain the importance and contents of the mission operations diagram. Section 13.4 detail some of the procedures regarding the handling of the EcoGlide system, namely proper storage, setting up of the tethered balloon system, loading of the payload box, and the retrieval of the reusable parts of the glider.

13.1. Functions and Requirements

Due to the life saving nature of the EcoGlide mission explained in section 1.1, and the sensitivity of the payload to exposure to elevated temperature, most requirements specific to operations are concerned with the time limitations set by the design of the payload box. As described in section 8.1, the payload box maintain the correct temperature for 3 hours, in the worst case scenario (R_EG_PL_07). In order to accommodate this schedule, handling times must be defined. These are listed in Table 13.1.

Table 13.1: Operations requirements

Identifier	Requirement statement	Compliance
R_OP_PL_01	Loading of the payload boxes shall not take longer than 15 minutes.	Section 13.3
R_OP_PL_02	The glider shall be deployed at most 30 minutes after it was assembled and loaded.	Section 13.3
R_OP_PL_03	The locating of the glider, and retrieval of its payload shall not take longer than 30 minutes.	Section 13.3
R_OP_MA_06	Storage at the main hospital shall be accommodated for a maximum of 4 months.	Section 13.4

Since the EcoGlide glider is designed to decrease its environmental footprint by bio-degradation after use, it is extremely important to create proper conditions for storage, so the vehicle maintains its reliability. While a requirements for long term storage has already been set by user (R_EG_SFRL_02), one must be also set for short term storage at the main hospital. A single 20ft shipping container contains 64 gliders, as explained in section 12.3. Assuming an average use of one glider per day (R_OP_SFRL_02), and taking the glider stockpile at the hospital into account, the maximum time a glider spends at the main hospital before deployment is about 4 months.

13.2. Design Approach

This section will detail the design approach used to find the final operations concept. This design approach was followed to ensure a streamlined operations concept with a robust mission. To allow for a streamlined mission, the steps that are to be taken by the personas are designed to be as easy and straightforward as possible. A sequence of all steps that have to be taken throughout the mission operation are given in the mission operations diagram. To uncover which of these steps might be too difficult, an analysis through the use of personas will be performed. In this analysis, the interactions of the personas throughout the mission operation is visualised in a product life journey map.

13.3. Design Overview

In order to implement the design approach proposed above, two diagrams were made. First a mission operations diagram is made to present all the steps that have to be taken in order to accomplish the mission. The different steps are summarised in a mission operations diagram. After this, an analysis with personas was performed to pinpoint difficult operational steps that might hinder a smooth mission. This analysis is presented in the form of a product life

journey map. It should be noted however that this is an iterative process between both diagrams and only the final versions are provided below.

Mission Operations Diagram

The mission operations diagram displays all the steps taken during the mission, including the end of life scenario. The table at the end of the chapter shows the interactions between personas and EcoGlide subsystems, by listing the input communications that are required to accomplish each actions, and the output communications resulting from the accomplishment of each actions. The actions are organised in a chronological order. An initial estimate for time allocated for each action is also included, where it is applicable and known.

13.4. Procedures

The different procedures regarding the handling of the EcoGlide system are elaborated below. Those procedures contain storage of the EcoGlide system, set-up of the Tethered balloon, loading of the payload box and finally unloading of the payload box and retrieval of electronics upon landing.

Storage

Throughout its lifetime an EcoGlide glider is in storage on two occasions, at two different places: the storage building for long term storage after production (10 years of shelf-life is set by R_EG_SFRL_01), and for short term at the main hospital until it is deployed. Since the material of structural components of the EcoGlide glider were selected and designed such that they would bio-degrade within 1-3 years (as explained in section 6.3), it is important to define the storage conditions, in a way that the structural performance of these materials are not impacted negatively.

In paper sheets, high temperature and humidity can cause mould, and moisture-loss leading to curling. Thus, the temperature must be kept under 25 °C, and the relative humidity must be kept under 45% in order to protect the paper pulp skin from permanent damage.¹[53]

While all wood will react to changing moisture content in its environment, leading to buckling and warping, plywood, the material selected for spars, is less susceptible. This is due to the veneers or strands supporting each other, restricting their ability to warp.² Additionally, with proper ventilation and spacing of panel edges, warping due to moisture can be eliminated.³ [6] Other than warping, fungi and insect activity can also contribute to wood degradation. When the moisture content of untreated wood is kept below 20%, and the ambient temperature is kept under 10 °C, both of these issues can be eliminated. Insect activity approximately doubles with every additional 10 °C increase in temperature.[44] Applying the Hailwood-Horrobin equation (see Equation 13.1, with h being the fractional relative humidity, T being the temperature in Fahrenheit, and M_{eq} being the equilibrium moisture content in percentage), we can determine that at 10 °C, the equilibrium moisture content is under 20%, as long as the relative humidity is kept under 88%.⁴

$$M_{eq} = \left(\frac{1800}{W} \right) \times \left(\frac{kh}{1-kh} + \frac{k_1 kh + 2k_1 k_2 k_2 h^2}{1 + k_1 kh + k_1 k_2 k_2 h^2} \right) \quad (13.1)$$

$$W = 330 + 0.452T + 0.00415T^2$$

$$k = 0.791 + 0.000463T - 0.00000844T^2$$

$$k_1 = 6.34 + 0.000775T - 0.0000935T^2$$

$$k_2 = 1.09 + 0.0284T - 0.0000904T^2$$

It can be concluded that the plywood used for spars, and the paper pulp used for skin have similar, but different optimal long term storage conditions. As explained in section 12.3, the spars are not included in the same box as the rest of the glider components, which also opens up the possibility of storing them separately: temperature below 20 °C, and relative humidity below 45% for the skin, and temperature around or below 10 °C and relative humidity below 88%. If all of the glider components are stored together, the intersection of the two must be applied: temperature below 10 °C, and relative humidity below 45%.

Glidgers are stockpiled at the main hospital for at most 4 months before they are deployed (R_OP_MA_06). During this time all the components must be stored under roof, protected from weather, as cold as possible. The spars must be stacked on each other, on top of legs to keep them off of ground, and weighted down.⁵ Moreover, the boxes containing the glider kits should include some moisture absorbents, such as moisture sensitive silica gel, in order to stabilise the relative humidity during those 4 months.

¹URL https://www.ehow.com/list_7459756_temperature-humidity-requirements-paper-storage.html [cite 25 Jun 2020]

²URL <https://www.norbord.com/na/blog/on-site-wood-panel-storage-guidelines/> [cite 25 Jun 2020]

³URL <https://www.norbord.com/na/blog/plywood-or-osb-panels-which-is-better-2/> [cite 25 Jun 2020]

⁴URL <https://www.wagnermeters.com/moisture-meters/wood-info/what-is-equilibrium-moisture-content/> [cite 25 Jun 2020]

⁵URL <https://www.norbord.com/na/blog/on-site-wood-panel-storage-guidelines/> [cite 25 Jun 2020]

Tethered Balloon System Set-up

After the deployment system equipment have been unloaded from the shipping container, the system can be set up. The area from which the balloon is launched must be clear and smooth area in the open, that is large enough to accommodate the the winch area and the bedding-down area. The bedding-down area must be large enough for the balloon itself, ground anchors, handling lines, and is recommended to be covered with a ground cloth, to protect the balloon envelope. When practical, the are should allow the balloon to turn into wind, and should be behind land features (large hill or buildings) for weather protection. [36]

Once the area of launch is established, the tether and hoist winches as well as other ground equipment is arranged, and the balloon inflation started. In the meanwhile, the tether cable is installed on its winch. Once the balloon is fully inflated, the pulley system and on-board instruments are installed. Before the balloon is launched, the balloon itself, its instrumentation, the tether winch, and the pulley system are prepared and tested. The flight altitude for the balloon is selected, such that the nominal wind does not exceed its limitation ($21.6[m/s]$). Performance of the balloon (such as altitude and internal pressure), and weather conditions are monitored throughout the launch and flight operations, and corrective action must be taken if any of them exceed operating limits.

Loading the Payload Box

The loading of the payload box is done as follows: First, four blocks of PCM is placed in the box, two in the middle, and one on each sides. In order to preserve the blood, the blood bags must be held in a cooler box until this point. A layer of filler material is laid on it, on top of which two blood bags are placed. This last step is repeated twice, such that there are three layers of blood bags. The final layer of blood bags is also covered with a layer of filler material, and a temperature indicator stickers are attached to the inside of the box. The box lid is then closed, and taped down.

Unloading of Payload Box and Retrieval of Electronics

Once the glider has landed and has been located, its payload, and the reusable electronics can be removed. In order to gain access to the payload box, the top fuselage panel must be removed by cutting the tapes securing it. Then the payload boxes can be lifted out from their slots. Once they are removed, the electronics compartment on the aft fuselage can be removed. The battery must be disconnected first. The control horn detached from the torque rod. It must however stay attached to the servo. Then the electronics compartment can be removed. Note that type and placement of fasteners, securing the electronics compartment to the lower fuselage panel are unknown, and will be designed in the detailed design stage.

ID	Operation phase	Action	Executor	Time allocated	Input		Output		
					Sender	Message	Receiver	Message	
01	PRE: Mission plan	Request blood resupply	Pete Michel - Medic				Rick Heatherly - Flight monitoring	Type and quantity of blood; urgency of resupply	
02	PRE: Mission plan	Designate landing location	Pete Michel - Medic				Rick Heatherly - Flight monitoring	Coordinates and dimensions of landing zone	
03	PRE: Mission plan	Forecast weather condition during flight operation	Monica Barbaro - Meteorologist				Rick Heatherly - Flight monitoring	Weather forecast for the next 24 hours	
04	PRE: Mission plan	Plan flight trajectory, and set glider waypoints	Rick Heatherly - Flight monitoring		Pete Michel - Medic	Quantity of blood; urgency of resupply; location of landing zone	Tom Kazinsky - Deployment	Deployment time and altitude	
05					Monica Barbaro - Meteorologist	Weather forecast	Perry Siedenthal - Assembly	Glider waypoint data	
06							Samantha Wells - Doctor	Type and quantity of blood; forecasted ambient temperature	
07	PRE: Deployment	Set balloon altitude to release altitude	Tom Kazinsky - Deployment		Rick Heatherly - Flight monitoring	Deployment altitude	Deployment station	Actuate the tether winch	
08	PRE: Loading	Assemble glider	Perry Siedenthal - Assembly						
09	PRE: Loading	Enter waypoints into glider on-board computer	Perry Siedenthal - Assembly		Rick Heatherly - Flight monitoring	Glider waypoint data	Glider	Glider waypoint data	
10	PRE: Loading	Prepare blood bags	Samantha Wells - Doctor		Rick Heatherly - Flight monitoring	Type and quantity of blood			
11	PRE: Loading	Determine PCM to be used in the payload box	Samantha Wells - Doctor	15 mins	Rick Heatherly - Flight monitoring	Forecasted ambient temperature			
12	PRE: Loading	Load payload box with PCM and blood bags	Samantha Wells - Doctor						
13	PRE: Loading	Load payload box in glider	Perry Siedenthal - Assembly						
14	PRE: Deployment	Load glider in deployment fairing	Tom Kazinsky - Deployment						
15	PRE: Deployment	Elevate the glider to the balloon	Tom Kazinsky - Deployment	30 mins			Deployment station	Actuate hoisting winch	
16	PRE: Deployment	Final HOLD before release	Tom Kazinsky - Deployment		Deployment balloon	Glider fairing has reached balloon	Rick Heatherly - Flight monitoring	Ask permission to release	
17	PRE: Deployment	Confirm mission conditions	Rick Heatherly - Flight monitoring		Tom Kazinsky - Deployment	Ask permission to release			
18	PRE: Deployment	Reactivate hoisting winch to release glider	Tom Kazinsky - Deployment		Deployment balloon	Weather sonde measurements	Tom Kazinsky - Deployment	Permission to release	
19	PRE: Deployment	Reactivate hoisting winch to release glider	Tom Kazinsky - Deployment		Rick Heatherly - Flight monitoring	Permission to release	Deployment station	Actuate hoisting winch	
20	PRE: Deployment	Confirm glider release	Deployment balloon				Tom Kazinsky - Deployment	Confirmation of the breaking of the break-wire	
21	FLT: Post-release	Glider pull-up manoeuvre	Glider		GPS satellite	Glider latitude, longitude, altitude			
22	FLT: Post-release	Glider leaves the proximity of the balloon system	Glider		GPS satellite	Glider latitude, longitude, altitude			
23	PRE: Deployment	Hoist the fairing back down	Tom Kazinsky - Deployment		Deployment balloon	Confirmation of the breaking of the break-wire	Deployment station	Reverse the hoisting winch	
24	FLT: Cruise	Glider turns to next waypoint	Glider	105 mins	GPS satellite	Glider latitude, longitude, altitude			
25	FLT: Cruise	Soaring through thermals	Glider		GPS satellite	Glider latitude, longitude, altitude			
26	FLT: Cruise	Glider reaches the final waypoint	Glider		GPS satellite	Glider latitude, longitude, altitude			
27	FLT: Landing	Corkscrew manoeuvre to bleed altitude	Glider		GPS satellite	Glider latitude, longitude, altitude			
28	FLT: Landing	Stall manoeuvre to land	Glider		GPS satellite	Glider latitude, longitude, altitude			
29	PST: Unload	Glider signals its location	Glider	30 mins	GPS satellite	Glider latitude, longitude, altitude	Pete Michel - Medic	Glider landing location	
30	PST: Unload	Check indicator stickers in payload box	Pete Michel - Medic		Glider	Indicator sticker shows if temperature inside the payload box has reached critical level			
31	PST: Unload	Blood bags are unloaded	Pete Michel - Medic						
32	PST: Unload	Payload box and reusable electronics are removed	Pete Michel - Medic						
33	PST: End-of-Life	Glider is discarded	Pete Michel - Medic						
34	PST: Unload	Blood bags are removed from the payload box	Pete Michel - Medic						
35	NM: Transport	Salvaged payload boxes and reusable electronics transported back to main hospital when possible							
36.A	PST: End-of-Life	Glider is incinerated. Mutually exclusive with 36.B	Glider						
36.B	PST: End-of-Life	Glider decomposes through bio-degradation. Mutually exclusive with 36.A	Glider	10 yrs					

Life-Cycle Assessment

14.1. End-of-Life Analysis

Concerning the fact that sustainability is a driving factor for this project, analysing potential end-of-life scenarios for the glider is vital. This is because the end-of-life phase, if mishandled, can adversely affect the sustainability levels of the EcoGlide mission through an increase in the environmental impact (EI) of the mission resulting from improper disposal of the aircraft. This chapter will start with an exploration of the potential end-of-life scenarios including the existing end-of-life disposal methods of the Dutch military following which an LCA of relevant methods will be done to estimate the cumulative energy demand (CED) and global warming potential (GWP) associated with each method. Based on the analysis, the recommended method of disposal will be suggested.

Potential Scenarios

In order to make an informed decision about the end-of-life scenario, as stated, first potential scenarios will be briefly discussed. The following methods are the current options for the disposal of the glider at its end-of-life:

- Scenario 1- The first method that is looked at is the incineration of the glider. It should be noted that this scenario is the most likely method to be employed in a real life use case as the associated logistics infrastructure is already in place. Although incineration does lead to energy retrieval, the energy use associated with this method is also expected to be higher than other disposal methods. This will be accounted in the comparison of the end-of-life methods, done in the following section.
- Scenario 2- The second method consists of natural degradation of the glider. In this scenario, at the end of the mission, the gliders would either be dumped into a landfill after every individual delivery or at the end of multiple deliveries, for example, at the end of the working week (7 days \implies 7 gliders). The associated environmental impact is the same in both cases and therefore they are not analysed individually.
- Scenario 3- The third and final scenario explored is recycling. In this scenario, the glider would have to be transported to a recycling facility. Analogous to the other cases, the energy use associated with recycling, and the energy saved by not designing an entirely new product will be used for the comparison between the different disposal methods.

Following the comparison of the aforementioned scenarios, recommendations will be made such that disposal methods in the future remain in line with the sustainability goals of the mission.

Comparison of Scenarios

This section consists of the quantification of the energy use and the global warming impact of the disposal methods such that they may then be compared. The quantification is done in terms of mass since incineration and recycling facilities generally carry out their activities according to the total mass of the waste being disposed rather than individual items. The method used to carry out the LCA will be clearly explained prior to the comparison such that the results of the assessment are easy to comprehend.

Assumptions

In order to carry out the assessment for the incineration and recycling scenarios, the OpenLCA application was used. Similar to other LCA applications, OpenLCA consists of databases which contain information about certain processes which is combined with user input pertaining to the energy use and environmental impact to present an overview of the major pollutants associated with the process being assessed. In the end-of-life analyses, certain assumptions had to be made when carrying out the LCA. These are stated below:

- The scenarios were analysed for disposal in a European setting. This is due to lack of information pertaining to waste disposal methods in the mission location. Nevertheless, the results may be considered viable as the primary purpose of the LCAs is to compare two disposal methods, and not to compare the disposal methods in multiple countries.

- It should be noted that in the case of the end-of-life scenarios, only the final products are considered, i.e. energy use and the EI of manufacturing processes are quantified in a separate LCA.
- At the time of conducting the LCAs, the payload mass estimated was equal to 12 [kg] Hence, taking into account the maximum take of mass of the glider (25 [kg]), a mass of 13 [kg] was used for the LCAs in both scenarios.
- The mass of 13 [kg] was further split into masses for individual parts and is presented below with the material used for each part:

Table 14.1: Part masses and associated materials used in LCA

Part	Mass [kg]	Material
Skin	3	Paper pulp
Spars	9	Plywood
Ribs	1	Paper pulp

- For both LCAs, a distance of 20 [km] to the incineration and recycling facilities was assumed. While the impact associated with transport had the same effect on both LCAs and hence did not contribute towards the determination of the ideal scenario, including it did give an overall idea of the EI associated with both scenarios.

With the assumptions stated, the results of the LCA may now be presented and are shown in the following sections.

Life-Cycle Assessment: End-of-Life

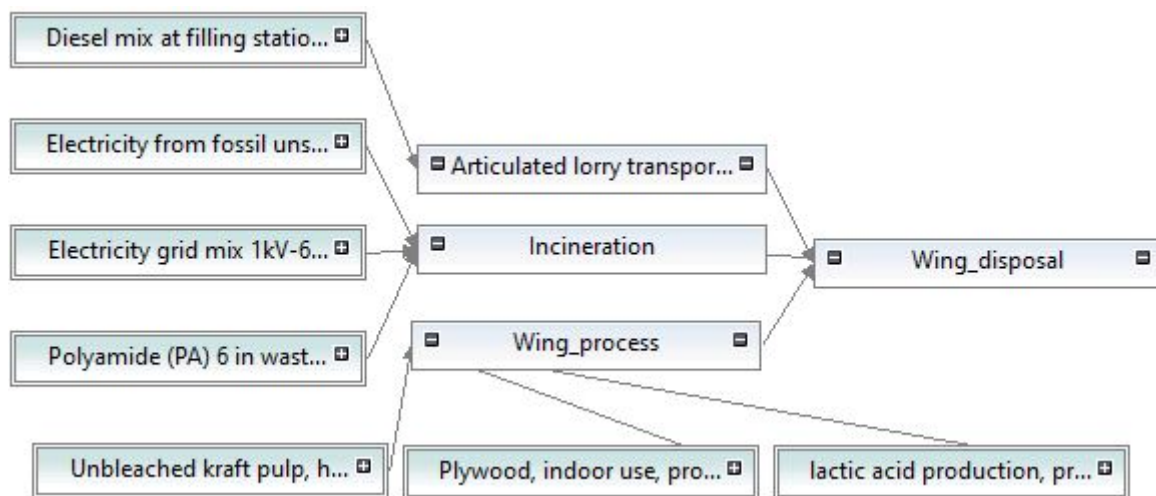
Incineration- Scenario 1

As stated, in addition to the materials that were accounted for in the incineration process, transport was also accounted for. Along with this, data pertaining to waste incineration had to be collected and inputted into the application. The data used for the incineration LCA is as follows:

- Total amount of waste incinerated: 1.4 million tonnes [23].
- Carbon dioxide (CO₂) emissions: 1 [kg] of waste incineration produces approximately 1.2 [kg] of CO₂ [57].
- Energy production from the incineration of the aforementioned amount of waste: 1 million [MWh] of electricity and 0.6 million [GJ] of heat → redirected to EcoGlide operations¹.
- Waste-to-energy plant efficiency and energy usage: Efficiency of 30% ⇒ Energy usage of 3.3 million [MWh] approximately [23].
- CO₂ avoided as a result of incineration and energy recovery: 0.1725 million tonnes.²

It should be noted that the aforementioned data was scaled down with mass. Additionally, the incineration process is modelled as a closed loop system, i.e. the energy recovered as a result of the incineration is assumed to be redirected to EcoGlide operations such that the benefit from the recovered energy is accounted for accurately. The overall process flow is shown in Figure 14.1.

Figure 14.1: Incineration process flow



¹URL <https://www.aebamsterdam.com/#:~:text=Energy%20and%20heat,central%20heating%20of%20Amsterdam%20households> [cite 18 June 2020]

²URL <https://www.aebamsterdam.nl/media/1552/aeb-corporatebrochure-en-screen.pdf> [cite 20 June 2020]

The results of the LCA after compilation of the aforementioned data are shown in Table 14.2. While there are a many number of other outputs, including but not limited to ecotoxicity, acidification and eutrophication, as previously mentioned, only the global warming potential (GWP) and cumulative energy demand (CED) are considered in the comparison of the scenarios. Finally, it should be noted that the results represent the impact of disposing 1000 gliders, pertaining to the number of deliveries the military expects annually.

Table 14.2: GWP and CED for incineration

Global warming potential (GWP) [kgCO ₂ eq]	Cumulative energy demand (CED) [MJ]
3.839E+4	4.133E+5

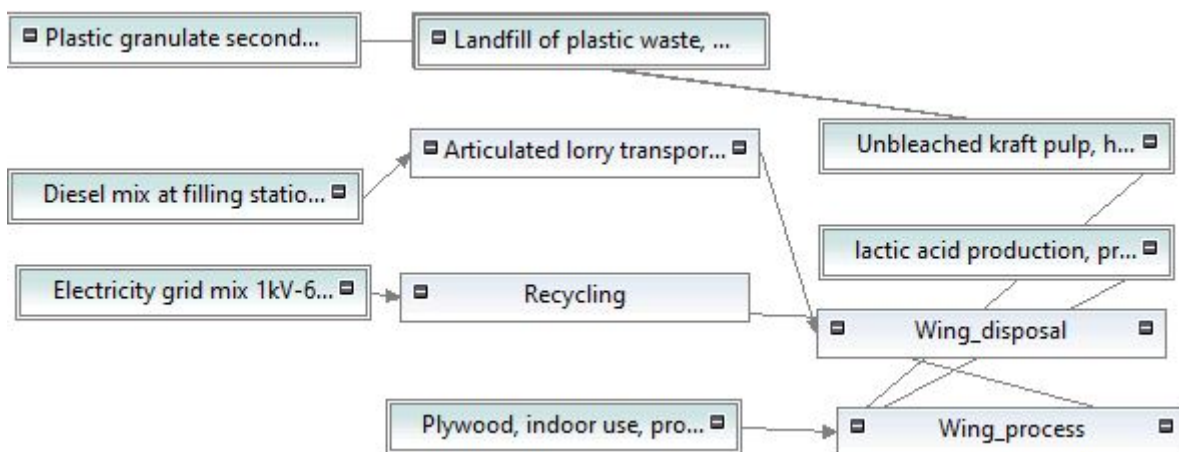
Natural degradation- Scenario 2

This scenario consist of very few steps compared to the previous scenarios and only involves moving the glider from it's landing location to an existing nearby landfill, manually. Although the energy balance associated with this scenario can largely be ignored as there is no energy being inputted or outputted in the disposal process, the environmental impact can become quite significant if the number of landfills consistently increase meaning eventually other disposal methods may have to be used. This will be accounted for in the comparison of disposal methods.

Recycling- Scenario 3

The LCA procedure pertaining to the recycling scenario is largely analogous to the incineration LCA. The differences in the two scenarios is the data used to estimate the GWP and CED, and also the energy recovery method, which in the case for recycling is accounted for by redirecting the recycled material to the EcoGlide manufacturing facilities, emulating a closed loop similar to the incineration process. The process flow in the case of recycling is shown in Figure 14.2.

Figure 14.2: Recycling process flow



The data used to estimate the impact is presented below:

- In order to account for the benefit from recycling, it was necessary to assume a certain percentage of recycled material use for the production of the glider. Therefore, it was assumed that the paper pulp used in the production would be recycled paper pulp, representing approximately 30% of recycled material of the empty mass of the glider.
- Energy requirement to produce cellulose based materials from non-recycled resources: 35.2 [MJ/kg].³
- Energy requirement to produce cellulose based materials from recycled material: 18.8 [MJ/kg].⁴
- Energy production avoided by using 30% recycled material for the empty mass of the aircraft, corresponding to a mass of approximately 4 [kg]: 65.6 [MJ].
- CO₂ emissions associated with producing cellulose based materials: 0.0017 [kg] of CO₂ for 1 [kg] of paper.⁵
- CO₂ emissions associated with producing cellulose based materials: 0.0017 [kg] of CO₂ for 1 [kg] of paper.⁶

³URL mgg-recycling.com/wp-content/uploads/2013/06/BIR_CO2_report.pdf [cite 15 June 2020]

⁴URL mgg-recycling.com/wp-content/uploads/2013/06/BIR_CO2_report.pdf [cite 15 June 2020]

⁵URL mgg-recycling.com/wp-content/uploads/2013/06/BIR_CO2_report.pdf [cite 15 June 2020]

⁶URL mgg-recycling.com/wp-content/uploads/2013/06/BIR_CO2_report.pdf [cite 15 June 2020]

- CO₂ emissions avoided by using 30% recycled material for the empty mass of the aircraft, corresponding to a mass of approximately 4 [kg]: 0.0012 [kg].

The results of the recycling end-of-life LCA are shown in Table 14.3. As in the case of incineration, only the GWP and CED are used for the comparison of the scenarios.

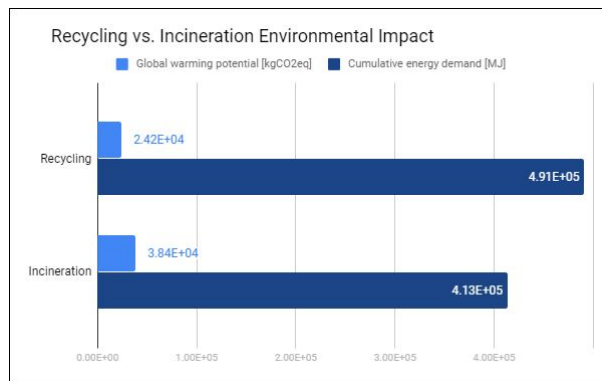
Table 14.3: GWP and CED for recycling

Global warming potential (GWP) [kgCO ₂ eq]	Cumulative energy demand (CED) [MJ]
2.415E+4	4.907E+5

Recommended End-of-Life Scenario

The different scenarios can now be compared to get a general idea of the most sustainable method of disposal based on the aforementioned energy uses and retrieval. The comparison of the results is shown more clearly in Figure 14.3.

Figure 14.3: End-of-life scenario impact comparison



Based on the fact that natural degradation has the lowest environmental impact since there is no energy use, and minimal GHG emissions, it would be the ideal method of disposal but considering that the amount of space for landfills is limited, the most realistic method of disposal would be to recycle. While this may not seem obvious as recycling does consume larger amounts of power compared to incineration, it must be kept in mind that the recycled amount of material was set at 30% meaning with a higher percentage of recycled material, the energy requirements for production would drop below the requirements for incineration. With respect to the GWP, as visible from the results of the two LCAs, recycling is a much better option. Recycling is also a very viable solution since it allows for up to 90% of the waste material to be reused, therefore drastically reducing the energy requirements and the associated CO₂ emissions.⁷ An additional reason as to why recycling is a much more sustainable option is because currently the efficiency of incineration plants is at 30% [23]. While this number may increase in the future, based on current standards, it is concluded that recycling is the recommended end-of-life scenario.

As a final note, it should be mentioned that although recycling is indeed the ideal disposal method, this is highly unlikely to be implemented by the Dutch military, pertaining to a multitude of reasons. The primary reason is that the infrastructure for waste incineration is already in place and is the current method used by the military. Additionally, in the case where the military is engaged in combat, waste disposal will not be a priority and hence in a combat scenario, the most likely method of disposal will be landfills. The two end-of-life LCAs were done so that, under normal circumstances wherein waste disposal may be attended to properly, the military can make an informed choice such that the disposal is carried out in the most sustainable and feasible manner.

14.2. Life-Cycle Assessment: Manufacturing

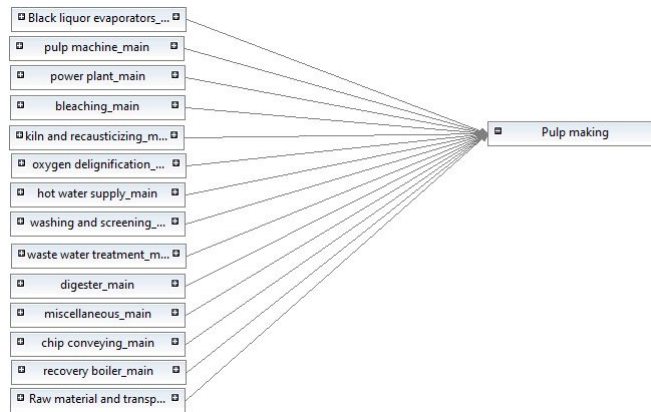
Paper Pulp Production

As stated in the Midterm Report [26], in addition to quantifying the environmental impact of the end-of-life scenarios, manufacturing is the other phase which is quantified pertaining to the large number of processes involved resulting in a significant environmental impact.

The first process that is looked at is the production of wood pulp. The process flow diagram is shown in Figure 14.4.

⁷URL mgg-recycling.com/wp-content/uploads/2013/06/BIR_CO2_report.pdf [cite 15 June 2020]

Figure 14.4: Pulp production process flow



The data used to create the process and estimate the associated energy use and some emissions is presented below. It should be noted that data for carbon dioxide emissions pertaining to individual steps in the pulp making process could not be found and hence, the carbon dioxide for only some of the steps have been presented.

- To obtain the raw material, i.e. wood, and transporting it, it is assumed that the used fuel source is diesel since deforestation and transportation are generally carried out using vehicles that use oil as fuel. This results in an associated energy use of 1.15 million Btu per per ton of wood obtained.⁸ This energy use is then converted to an approximate amount of diesel burned using the calorific value of diesel and results in an amount of 27 [kg] of diesel with an associated emission of 140 [kg] of CO₂.^{9,10}
- For the other steps involved in the pulp production process, the energy use data was obtained from [39] and is shown in Figure 14.5.

Figure 14.5: Energy use in paper pulp production

	Steam GJ/ADt	Electricity kWh/ADt
Chip conveying	0.0	20
Digester	1.7	40
Washing and screening	0.0	30
Oxygen delignification	0.5	75
Bleaching	2.3	100
Pulp machine	2.3	141
Black liquor evaporators	3.1	30
Power plant	2.3	60
Kiln and recausticizing	0.0	50
Hot water supply	0.0	32
Waste-water treatment	0.0	30
Miscellaneous	0.0	30

- As stated earlier, the CO₂ emissions for each of the steps could not be quantified due to a lack of data. Therefore, the emissions for the entire process was quantified using data from [4], revealing a total emission of 9 [kg] of CO₂ per ton of paper pulp produced.
- The previous quantification only took into account the CO₂ emissions and thus to account for other gaseous emissions, data from [3] was used. The data is also presented in Figure 14.6.

⁸URL <https://www.nap.edu/catalog/5734/wood-in-our-future-the-role-of-life-cycle-analysis> [cite 10 June 2020]

⁹URL <https://www.world-nuclear.org/information-library/facts-and-figures/heat-values-of-various-fuels.aspx>[cite 10 June 2020]

¹⁰URL <http://www.patagoniaalliance.org/wp-content/uploads/2014/08/How-much-carbon-dioxide-is-produced-by-burning-gasoline-and-oil.pdf> S.-Energy-Information-Administration-EIA.pdf [cite 10 June 2020]

Figure 14.6: Emissions from paper pulp production

Pollutant	Value	Unit
NO _x	1	kg/Mg air dried pulp
CO	5.5	kg/Mg air dried pulp
NMVOG	2	kg/Mg air dried pulp
SO ₂	2	kg/Mg air dried pulp
TSP	1	kg/Mg air dried pulp
PM ₁₀	0.8	kg/Mg air dried pulp
PM _{2.5}	0.6	kg/Mg air dried pulp
BC	2.6	% of PM _{2.5}

For the LCA results, the energy use and emissions of producing 1000 gliders was looked at. This corresponds to a total requirement of approximately 4000 [kg] of paper pulp, as shown in Table 14.1. The results are shown in Table 14.4.

Table 14.4: GWP and CED for paper pulp production

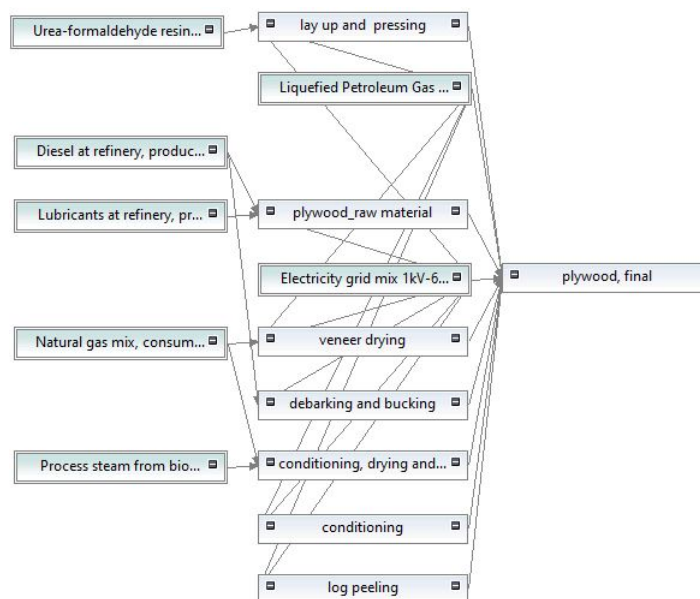
Global warming potential (GWP) [kgCO ₂ eq]	Cumulative energy demand (CED) [MJ]
5.690E+4	7.799E+5

These results will be further aggregated with the LCA of producing and manufacturing the spars for which plywood is used. Once this is done, the overall LCA results will be compared to an LCA of a reusable commercial drone so as to assess the sustainability pros and cons of choosing the EcoGlide glider over a conventional method of delivery, such as a commercial drone.

Plywood production

Following the life-cycle inventory and assessment of paper pulp production, the life-cycle impact of plywood production is looked at. The majority of the data used for the life-cycle impact assessment (LCIA) was obtained from [43]. Although the data is based on sources in the United States of America, for this impact assessment, the sources were assumed to be in Europe. The production process flow is shown in Figure 14.7.

Figure 14.7: Plywood production process flow



The above process represents inputs and outputs in order to produce 1 [m³] of plywood. This corresponds to 633.60 [kg] of ready to use of plywood [43]. As in the case of producing paper pulp, the impact associated with producing plywood for a 1000 gliders is modelled. This corresponds to a total plywood requirement of approximately 9000 [kg] Table 14.1. Shown in Table 14.5 is the associated cumulative energy demand (CED) and the global warming potential in order to produce plywood for 1000 gliders.

Table 14.5: GWP and CED for plywood production

Global warming potential (GWP) [kgCO ₂ eq]	Cumulative energy demand (CED) [MJ]
1637.967	3.465E+4

While the impact associated with producing plywood is much lower than that of paper pulp, the impact can be further lowered. The difference in impact is due to the fact that waste produced from paper pulp mainly consists of chemicals used in the treatment of the raw materials required to produce the pulp [39], while in the case of plywood, the majority of waste produced is biomass in the form of wood that can be reused for energy. The impact associated with using the waste wood as a form of energy is shown in Table 14.6.

Table 14.6: GWP and CED for plywood production with wood biomass as energy

Global warming potential (GWP) [kgCO ₂ eq]	Cumulative energy demand (CED) [MJ]
1317.481	3.048E+4

Impact Assessment Comparison

In order to determine the competitiveness of the EcoGlider with existing drone delivery systems, in terms of sustainability, the life-cycle impact of the EcoGlider was compared with that of the MD4-3000 UAV, for which the data was obtained from [22]. For the UAV, the energy consumption per unit distance-load was estimated to be 4.32 [Wh/kmkg] while the CO₂ emissions per unit distance-load was estimated to be 2.42 [kgCO₂/kmkg]. In order to compare the EcoGlide glider to the MD4-3000 UAV, an average distance of 100 [km] was assumed for a single mission, with a payload of 12 [kg]. The aggregated energy consumption and emissions calculated from the manufacturing LCAs is shown in Table 14.7. For the aggregate, the energy consumption and emissions from Table 14.6 and Table 14.4 were added together.

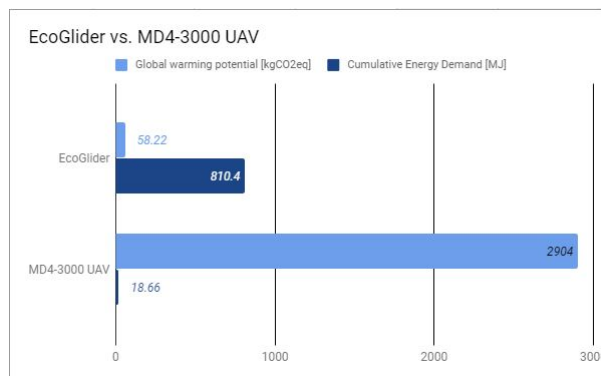
Table 14.7: Aggregate GWP and CED: EcoGlide

Global warming potential (GWP) [kgCO ₂ eq]	Cumulative energy demand (CED) [MJ]
5.822E+4	8.104E+5

As stated, the data in Table 14.7 pertains to the production of a 1000 gliders with an average distance of 100 [km] per mission and 12 [kg] of payload per mission. This means that for a single glider, the CED is 810.4 [MJ] while the GWP is 58.22 [kgCO₂eq]. In order to compare this to the data for the UAV, the data for the UAV was scaled up in the following way:

- CED for a single UAV → 4.32 Wh/kmkg
 ⇒ for 100 [km] and 12 [kg], the associated CED = 5184 [Wh] = 18.6624 [MJ].
- GWP for a single UAV → 2.42 kgCO₂/kmkg
 ⇒ for 100 [km] and 12 [kg], the associated GWP = 2904 [kgCO₂].

Figure 14.8: Comparison of the impact of the MD4-3000 drone against the EcoGlide glider



From the above results and Figure 14.8, it can be seen that the CED of the EcoGlide glider is 45 times higher than that of the UAV. While this is a rather large difference, it must be kept in mind that the CED for the glider can be reduced drastically with the proper end-of-life scenario, i.e. recycling. Recycling is much more promising in the case of the EcoGlide glider since the end products consist of biomass which can effectively be recycled such that raw materials

do not have to be used for every glider. Nevertheless, based on the current CED comparison, it is important that in the future, ways of reducing the energy use further should be prioritised.

In terms of the GWP, the glider performs much better and has a impact that is practically 50 times lower than that of the UAV. This of course stems from the fact that the glider is made almost exclusively out of biodegradable materials. Additionally the UAV runs on Li-ion batteries [22], which further increases the environmental impact compared to that of the glider, which does not need a propulsion mechanism.

Two potential methods of reducing the CED are mentioned below while further recommendations in order to reduce the overall environmental impact and improve the LCA quality are discussed in chapter 17.2.

- As already stated, increasing the amount of recycled content. especially in the case where paper pulp is used, would drastically reduce the CED.
- In addition to the aforementioned point, identifying individual process steps in the paper pulp manufacturing process could also aid in reducing the CED. The two most energy intensive processes involved in paper pulp production are the steps pulping and bleaching. Pulping of course is an essential step and hence cannot be eliminated but bleaching on the other hand, could potentially be eliminated. This is because paper pulp production from virgin materials, i.e. non-recycled materials involves the bleaching process in order to primarily ensure that the paper retains its color over a longer period of time.¹¹ While the discoloration of paper may not be an issue, bleaching has been shown to increase the paper strength by up to 29.5% in terms of the tensile strength [32]. On the other hand, elimination of the bleaching process could result in CED reduction of up to 1440 [MJ]. This is because manufacturing 1000 gliders would require approximately 4000 [kg] of paper pulp [Table 14.1] as bleaching requires 360 [MJ] of energy for every ton of pulp that is bleached [39].

In conclusion, the two aforementioned methods to reduce the CED do indicate that the EcoGlider glider has the potential to have an overall environmental impact, in terms of the GWP and CED, comparable to that of a reusable drone but this may need to be investigated further to arrive at a definitive way of reducing the CED.

14.3. Life-Cycle Costing

Life-cycle costing is an analysis of all the costs that are associated with the development of a product, accounting for all steps starting from initial concept design to the end-of-life of the product. In the case of the EcoGlider, the cost analysis will be focused primarily on the developmental stages of the glider, with a preliminary estimate of the costs associated with the manufacturing of the glider which will include costs stemming from electricity use, raw materials, transport of these materials and labour costs.

Chapter 16 already lists the cost breakdown of the materials that are used in the manufacturing of the glider. It is assumed that these costs include the labour costs associated with producing the processed product such as plywood from the raw material and also the cost associated with obtaining the raw material itself. The costs which are added to this are provided below:

- Based on the LCA conducted in section 14.2, the total energy required to produce a glider is 810.4 [MJ]. The industrial electricity price in the Netherlands, the place of production, is €0.0941/[kWh].¹² This results in a electricity cost of approximately 21.18£.
- In addition this, a total raw material transport distance of 100 [km] is assumed, which results in a price of approximately €80 for 20000 [kg] of material.¹³ This means for that a single glider, the associated transport costs is €0.08 assuming that for every glider, approximately 20 [kg]. of raw material is used, based on the empty weight of the glider (13 [kg] Table 14.1).
- The final cost that is included are the labour costs associated with the manufacturing of the glider. This is extremely difficult to estimate without actually manufacturing the glider but the number of hours is estimated based on ¹⁴ and the hourly wage estimate of factory workers in the Netherlands.¹⁵ The estimated number of hours is 12hours while the cost associated is €20 per hour. The labour costs associated with manufacturing then result in a cost of €240. The labour costs associated with assembly are not included since the glider will be shipped in 'kit' form meaning the glider is assembled at the launch location by the customers purchasing the glider.

¹¹<https://www.pulpandpapercanada.com/pulping-bleaching-1000143592/>

¹²<https://www.statista.com/statistics/596254/electricity-industry-price-netherlands/#:~:text=Dutch%20households%20on%20average%20paid%20around%2017.07%20cents%20per%20kWh%20for%20electricity.>

¹³<https://www.della-ua.com/cost/138/>

¹⁴<https://core.ac.uk/reader/19136956>

¹⁵[http://www.salaryexplorer.com/salary-survey.php?loc=152&loctype=1&job=33&jobtype=1#:~:text=The%20average%20hourly%20wage%20\(pay,in%20Netherlands%20is%20%20EUR.](http://www.salaryexplorer.com/salary-survey.php?loc=152&loctype=1&job=33&jobtype=1#:~:text=The%20average%20hourly%20wage%20(pay,in%20Netherlands%20is%20%20EUR.)

The aforementioned costs and the structure, payload costs from Table 16.1 are aggregated to estimate a total cost of manufacturing for a single glider (not an entire mission). The resulting final cost of producing one glider, in a disassembled form, is approximately €309. It should be kept in mind that this cost analysis is quite a preliminary estimate and excludes costs avoided through use of recycled materials.

15

Reliability, Availability, Maintainability & Safety

To further characterise the performance of the EcoGlide product, the RAMS characteristics can be assessed. RAMS is an acronym¹ for Reliability, Availability, Maintainability and Safety [40]. These points will be elaborated upon below. As Availability is mostly dependent on reliability and maintainability, this aspect will be discussed after reliability and maintainability (thus not strictly following the RAMS order).

- Reliability can be described as the probability that the mission is performed successfully. This probability is considered quite high. The gliders aerodynamic performance allows for leeway during the flight to account for conditions such as headwind and sinks while still reaching the intended destination. The control system also allows the glider to redirect itself towards the goal, should a gust of wind push it off track. Of course, during the worst of conditions the glider will not be able to reach its destination, but those occasions are rare. For example, as described in chapter 5, the glider is designed to reach 125km in case of headwind, with windspeeds that occur 78% of the time in Timbuktu and 99% of the time in Kabul.

Furthermore, the stakeholder has clarified that real time tracking of the glider is not required, and simply knowing the path and time of launch is enough. Given this information, it is safe to assume that collision accidents are very unlikely. In addition, the electronics and structural integrity are assumed to have a very small failure rate (after a few iterations of prototype testing).

Finally, the stakeholder stated that, if for whatever reason the glider does not reach its destination, they do not mind sending a second glider in order to deliver the payload. This means that even in case of failure, the mission can still be performed, further improving the reliability aspect of this system.

- Maintainability can be described as the probability that the system can be repaired within a specified time. Because of the single-use nature of the glider, maintainability doesn't apply here. However, it is important for the deployment system. As mentioned in chapter 10, the deployment balloon needs helium refills at regular intervals. Aside from that, the deployment system should also frequently be checked for leaks, creep and environmental/UV damage. To minimise time on this, this should be done during the refilling of the balloons with helium.

If damage is found on the deployment system, it should be repaired. However, the repair times are not yet known, and thus it is difficult to estimate the influence on availability. Nevertheless, it is safe to assume that minor repairs can be fixed without delaying the delivery. Since the deployment system is used only once per day, there is enough time to repair the system after the glider is deployed.

- Availability can be described as the probability that the system is functional at any given time. It is dependent on both reliability and maintainability. As described above, the reliability of the system is assumed to be quite good. The glider is capable of succeeding about 80% of the time. The maintainability is also quite good. The glider itself does not need maintenance, and the deployment system can be frequently checked for damage and repaired if necessary without causing delay. It can therefore be said that the system has a good availability as well. This is further supported by the fact that gliders are always available to the stakeholder, as 64 gliders are regularly shipped. This results in a product that is extremely unlikely to be unavailable for use.
- Safety can be described as the the ability not to harm people or the environment during a full life cycle. The life cycle costing is extensively analysed in chapter 14 and will not be repeated here. As for how safe the system is for humans to use, the system is considered quite safe. The system itself is not intended for harm, but quite the opposite, namely medical aid. It also lacks any means to actively harm people: the only way would be collision. However, the glider can only navigate itself to its predefined destination, so intended targeting of people is impossible.

¹URL https://www.sebokwiki.org/wiki/Reliability,_Availability,_and_Maintainability [cite 29 June 2020]

Despite intentional harm being nearly impossible, accidents can happen. The most probable accident is during landing, when someone is not paying attention, the glider can crash into them. However, given the size of the glider and the fact that the people at the landing site are expecting the glider to arrive, this is still quite unlikely. Another accident may be collision with other objects in the air, such as birds. Collision with human air traffic is not likely, as the air traffic operator is aware of the gliders location. If the glider collides with a bird, this of course harms the bird, but the glider itself may also break and crash. Fortunately, in the case of this mission the glider is unlikely to fly over densely populated area's, and as such the risk of it falling on someone is low. One final way accidents may occur is by failure of the deployment system. If the balloon quickly loses helium, it may crash down. The deployment system is likely built next to an encampment, and as such the risk of it crashing on someone is present. Caution should therefore be taken to eliminate this possibility.

16

Market Analysis

In this chapter the market position of the EcoGlide system is analysed. Several factors are included to provide a complete overview of the unique market position that the EcoGlide system has.

In section 16.1 the cost of the glider is analysed. This includes the price of a single glider as well as the cost for a full mission. In section 16.2 it is described how the EcoGlide system can be altered to suit other missions. section 16.3 describes the importance of aesthetics as well as the implementation in this mission. Finally, section 16.4 concludes this chapter with an overview of how the EcoGlide fits in the cargo delivery market.

16.1. Cost Estimation and Business Model

The total cost of the glider is comprised of many different aspects. The raw materials of each glider make up a significant portion of the cost of the glider, but the production, assembly, certification, code verification, shipping will likely make up a greater portion of the total price. These cost however are either one time costs, such as certification, or are costs, such as shipping, are dependent on the full production and logistics chains of the military and are dependent on components unrelated to the EcoGlide system. The raw material price will however be relatively constant with time as they will be purchased from third parties in bulk and then stored. For this reason, the materials are the only component of the total costs that can be priced with any degree of accuracy. In chapter 14, however, an initial estimate for these costs is provided, but this was excluded from this cost breakdown due to how this will likely change in the future.

The raw material costs of a single EcoGlide system can be split up over 5 subsystems, the glider structure^{1 2 3}, payload compartment^{4 5 6}, the guidance navigation and control system^{7 8 9}, the electrical power system^{10 11} and the deployment system. It is important to note that the deployment system^{12 13 14 15}, the battery from the electrical power system and various parts of the guidance, navigation and control system will be reused for multiple missions, but for the purposes of this cost breakdown it was assumed that only a single mission would be performed. The cost breakdown for the different components can be found in Table 16.1.

¹<https://www.eggcartons.com/Egg-Tray-Paper-Pulp-30-Cell-p/etp-30-1.htm>

²https://www.alibaba.com/product-detail/Biodegradable-PLA-Poly-Lactic-Acid-Shrink_62009336357.html

³<https://onlinelibrary.wiley.com/doi/pdf/10.1002/9780470259795.app1>

⁴<https://www.fishersci.com/shop/products/puretemp-phase-change-materials-pcm/p-8949003>

⁵<https://www.corklink.com/index.php/cork-granules-supplier/>

⁶<https://onlinelibrary.wiley.com/doi/pdf/10.1002/9780470259795.app1>

⁷https://shop.holybro.com/pixhawk4-mini_p1120.html

⁸https://www.amazon.com/ANNIMOS-Digital-Torque-Waterproof-Control/dp/B07GJ6ZCVY/ref=psdc_2234131011_t3_B073F92G2S

⁹<https://www.bambooimport.com/en/bamboo-beam-carbonized-60-x-60-mm-244-cm>

¹⁰https://hobbyking.com/en_us/zippy-compact-2700mah-2s-25c-lipo-pack.html

¹¹<https://www.amazon.com/JeTi-Voltage-Regulator-SBEC-2-10S/dp/B00L5QHxEE>

¹²<https://cbknot.com/samson-saturn-12-x-600ft-spool/>

¹³<https://www.boconline.co.uk/shop/en/uk/gas-a-z/speciality-gas/helium-cp-grade-cylinder>

¹⁴https://www.seattlefabrics.com/60-400-D-Packcloth-Nylon-Made-in-USA-1095-linear-yard_p_49.html

¹⁵<https://cbknot.com/samson-tech-12-x-600ft-spool/>

Table 16.1: EcoGlide cost breakdown

Subsystem	Component	Price [€]
Structure	Paper pulp	2.92
	PLA	0.01
	Plywood	3.52
Payload	PCM	40.25
	Cork	0.88
	Plywood	0.05
Deployment system	Tether	23063.64
	Helium	759.17
	Balloon envelope	371535.15
	Hoist rope	20049.23
GNC	<i>PixHawk 4 Mini + GPS</i>	160.33
	<i>2x ANNIMOS 25kg RC Digital Servos</i>	2x 23.05
	<i>2x Bamboo torque rods</i>	2x0.01
EPS	<i>ZIPPY Compact 2700mAh</i>	11.19
	<i>Jeti Voltage Regulator SBEC</i>	48.99

From the above table it can be seen that the raw materials for each glider are actually quite inexpensive. The majority of the price comes from the deployment system. The deployment system will however be reused for multiple missions only needing to be refilled with helium every so often. Similarly, all of the different components of the guidance, navigation and control subsystem, apart from the bamboo torque rods, will be retrieved from the glider and reused for multiple different missions. Doing this, and reusing the deployment system, will greatly decrease the price per mission. This leads to an overall high investment cost and low recurring costs. This makes it economically unfavourable for single case missions but for the military use case, where the system will be used over longer periods of time the low cost per glider could lead to the glider being an attractive option.

If one assumes that the structure and most of the payload compartment is replaced every mission, but the PCM can be reused for 1000 missions, a conservative estimate¹⁶, and that the robust GNC electronics and the voltage regulator are reused for 100 missions, while the torque rods are discarded after each mission and that finally that the battery is reused for 10 missions, the cost per mission can be calculated to be equal to £11.12. Add to this the roughly £23.07 per mission needed for helium the total price per mission can be found to equal less than £40. These costs and others are further elaborated on and estimated in chapter 14.

Since the price per glider structure is so low, an example of a business model that could work for the EcoGlide system would be to sell the expensive balloons at a initial loss and then make this money back by selling each individual glider at a profit. This is called the razor-razorblade business model¹⁷. This model gets it's name because razor handles are usually sold at a loss but razor companies make this money back through the recurring profits they make off of selling a dependent product, the razorblade. EcoGlide could mimic this business model by lowering the costs of the balloon by a certain amount to make it more attractive to consumers, and then raise the price of the much cheaper to produce glider bodies to eventually make a large profit over time. How much exactly could be charged for each product would have to be determined after a further market analysis and customer survey.

16.2. Adaptability

The EcoGlide system has been designed solely based on the military use case outlined in chapter 1. The glider could however be adapted to serve other market needs in the future. By adapting the landing method and reducing the impact forces, through the use of a parachute for example, the EcoGlide system could be used to deliver medicine to doctors in remote locations for humanitarian aid purposes. The flight controller could also be updated so that it can communicate with search and rescue drones so that the glider could be used to deliver survival supplies to survivors in search and rescue cases. By applying for extra certification the EcoGlide gliders could also be used for the delivery of small packages in rural areas. Once the glider is further along in the design process and the limitations of the glider are more clearly defined, another market analysis will be performed (see chapter 17) to check if it is worth pivoting the design of the glider to also fulfil one or multiple of these different market's needs. As a final note, in section 16.1 it became clear that the EcoGlide has high initial costs due to the investment into the deployment system, making the current system only viable for long term use with repeated deployment, which was deemed optimal for the current mission case. By considering other methods of deployment, the EcoGlide glider could also be interesting for single case missions.

¹⁶<https://www.puretemp.com/stories/puretemp-4-tds>

¹⁷<https://www.investopedia.com/terms/r/razor-razorblademodel.asp>

16.3. Reflection on Aesthetics

Aesthetics is an often ignored aspect in the technical design process. Engineers are often focused on performance over looks, but a beautiful design has certain benefits over a strictly functional one. The EcoGlide team recognises these benefits and plans to take the aesthetics into account throughout the design process such that it can influence design choices, Table 4.1 (R_DS_AEST_01). [25]

When choosing between two designs that are identical in every other aspect, the customer is likely to make their choice based on what they subjectively find more appealing. However, the advantages of aesthetics extend beyond just this. According to a study performed in 1995 on the effects of apparent usability vs inherent usability [31], when users determine if a system is easy to use, the beauty of the design plays a bigger role than the functional usability of the system. This means that users are more forgiving of slight flaws in an aesthetically pleasing design. [25]

There is of course a balance between beauty and functionality that needs to be found, since the aesthetics of the design should not be neglected. Finding the right balance will lead to a design where the aesthetics are appealing to customers and also add to the functionality. [25]

The first functional aspect of aesthetics flows from the quote "For an aircraft to fly well, it must be beautiful". These words are often attributed to Marcel Dassault, and it has to do with the streamlining of the aircraft. In the outline of the aircraft, sharp corners must be avoided as the flow is likely to separate there, leading to vortices, increasing the parasite drag of the aircraft. For this reason, smooth curves are preferred. [26]

In the specific mission profile considered for EcoGlide, the aesthetics fulfil two more functional roles. The glider should not be shot down and it should not scare civilians. There are also some required markings that impact the aesthetics. An aggressive look is generally considered appealing in an aircraft¹⁸, however this will make it more likely that the glider can be conceived as an attack drone instead of a cargo drone. This results in Marcus being scared by the glider more easily, which should be avoided. The EcoGlide team shall therefore not pursue an aggressive aesthetic. [26]

The livery, also known as the paint job of an airplane is one of its most striking characteristics. Due to the military nature of EcoGlide, the purpose of its livery is twofold: do not draw attention while flying, but allow for easy locating once it has reached its destination. Countershading is a concealment technique commonly used by animals, where the back of the animal is darker and the belly is lighter.¹⁹ This helps the animal blend in with its background, when seen from either above or below. When applying this idea to EcoGlide, the bottom of the glider can be painted to natural sky colour, such as light blue or grey, so that it is harder to spot from the ground while flying. A non-reflective, matte finish is preferred, in order to avoid glare. However, since it must be easy to find once landed, the top of the glider should then be painted to a striking colour, such as orange. These paintjobs do however increase manufacturing and ecological costs, and may therefore be decided against by the team. [26]

Finally, certain markings must be present on an aircraft for identification administrative reasons. Since the glider is designed to operate in a military environment, an insignia must be clearly visible in order to avoid friendly fire incidents with Bill Cortell. The roundel of the Dutch Air Force can be seen on Figure 16.1²⁰. Furthermore, for administrative purposes, the aircraft registration code or tail number must be present as well as the appropriate label prescribed by EU Regulations 2019/945[2]. The latter for class C4 unmanned aerial systems can be seen in Figure 16.6. [26]

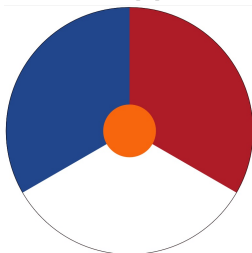


Figure 16.1: Royal Netherlands Airforce roundel

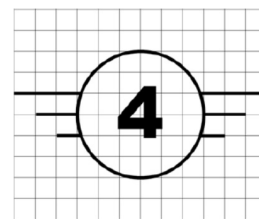


Figure 16.2: C4 UAS label [2]

Overall, the team decided not to settle for one specific livery yet. Rather, they allow the client to freely choose their own livery which they seem the best for their mission. The livery is very easily changed, as its applied by printing on the PLA skin that covers the skin of the glider. The process of printing on PLA film is very adaptable, allowing easy change of patterns as desired. To indicate the various liveries possible on the EcoGlide glider, the team made a collection of renders utilising different liveries, as shown in Figure 16.3

¹⁸URL <https://www.flyingmag.com/photo-gallery/photos/top-25-most-beautiful-airplanes/> [cite 20 May 2020]

¹⁹<https://www.thoughtco.com/what-is-countershading-2291704>

²⁰URL https://en.wikipedia.org/wiki/Royal_Netherlands_Air_Force/media/File:Roundel_of_the_Netherlands.svg [cited 19 May 2020]

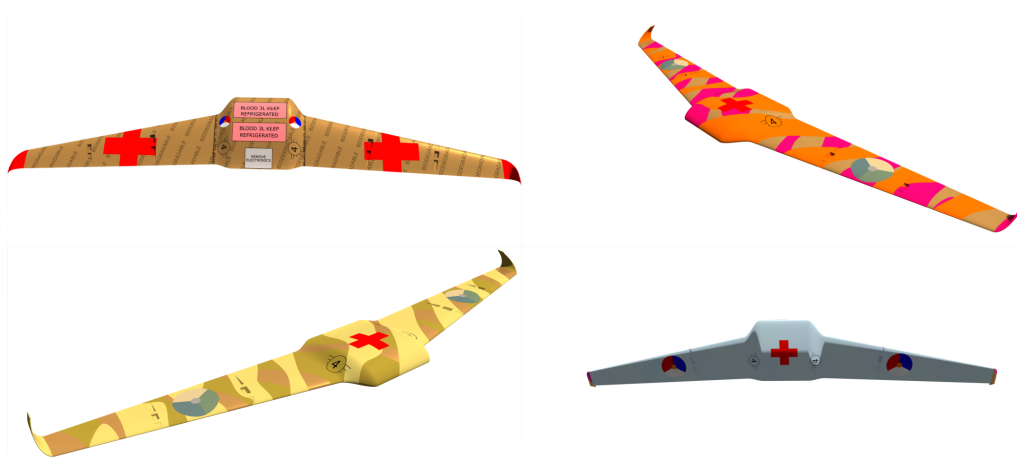


Figure 16.3: Artists impression of the various liveries possible on the glider

16.4. Market Competitiveness

The EcoGlide has an unique market position. Few comparable means of cargo transportation currently exist, meaning the competition is limited. However, a couple of comparable gliders exist. First, there is the APSARA glider²¹. This disposable glider is made entirely out of cardboard and serves a very similar mission profile. The APSARA however is meant to be deployed in swarms of several drones, rather than just a single delivery. Another comparable option is the TACAD glider²². This glider is being developed by the U.S. military and is meant to be discarded after use. Finally, the Zipline drone delivery also serves a similar purpose²³. These drones deliver a small payload and return to their base to be reused. They are currently being used by hospitals in Rwanda to deliver medicines and other medical cargo from hospitals.



Figure 16.4: APSARA glider^a



Figure 16.5: TACAD glider^a



Figure 16.6: Zipline drone^a

^a<https://spectrum.ieee.org/automaton/robotics/drones/otherlab-apsara-aerial-delivery-system>

^a<https://spectrum.ieee.org/automaton/robotics/drones/marines-testing-disposable-gliding-delivery-drones>

^a<https://www.flyzipline.com/how-it-works/>

The EcoGlide system has several key differences which places it in its own market spot. First off, the payload size: the EcoGlide can deliver payloads of 11 [kg], whereas the APSARA, Zipline and TACAD systems have payloads of 1, 1.7 and 317 [kg]. Second is its performance: the APSARA and TACAD glider have a glide ratio of 15, half of what the EcoGlide is designed for. For the Zipline drone, its range is 80 [km], meaning the EcoGlide still outperforms this drone on this regard. Finally, one could argue that it makes more sense to use the Zipline system for regular deliveries. However, the Zipline drones require a complex facility to be deployed. This would be unfeasible in the EcoGlide mission scenario, given the rapidly changing environment.

The EcoGlide does have a few drawbacks which limit its market position. Its main drawback is the fact that the initial cost is very high due to the deployment system. This limits the EcoGlide system in its current form to long term repeated missions. Second is the uncertainty of development. The EcoGlide is still in a relatively early stage, and it may not perform as well as expected. However, this is the case for any preliminary design, and is expected to be resolved with the use of prototypes and further design iterations.

²¹<https://spectrum.ieee.org/automaton/robotics/drones/otherlab-apsara-aerial-delivery-system>

²²<https://spectrum.ieee.org/automaton/robotics/drones/marines-testing-disposable-gliding-delivery-drones>

²³<https://www.flyzipline.com/how-it-works/>

Future Planning

This report concludes the Design Synthesis Exercise and with that, the design of the EcoGlide is likely to come to a halt. However, to allow the project to be continued, a planning was made. This chapter describes that planning using several tools. In section 17.1 a high level diagram is presented which shows all steps to be taken after the DSE. section 17.2 shows a Gantt chart which further explains this planning by showing dependencies and a more detailed timespan of all the tasks.

17.1. Project Design & Development Logic Diagram

Should the project be continued after the Design Synthesis Exercise, a proper planning is critical. To support this planning, a Project Design & Development Logic Diagram has been created. A preliminary version of this diagram was presented in the Midterm report [26]. The diagram gives a general overview of the steps to be taken and the timespan allocated for these tasks. In the first phase, a functional prototype will be built, alongside with a simplified glider code that includes basic functionalities. In the following phase a more detailed design will be worked out, while at the same time a logistics plan and cost analysis are made. During the next phase, the glider code is fully worked out, after which a test mission will be performed. Finally, the necessary certifications will be obtained, and the manufacturing will be set up. During this period, other customers can be contacted to gauge interest in the EcoGlide.

The diagram also shows several "go/no-go gates". These represent moment at which the feasibility of the project is reassessed. Failure to comply with the requirements at that point leads to reiteration of the design or abandoning of the project. The conditions for these gates are presented below in the form of questions. [26]

- **Gate 1:** Is the preliminary design indicative of a promising future product? Not only technically, but also within the current and future market.
- **Gate 2:** Does the glider fly and does the simplified code work?
- **Gate 3:** Do the flight and end-of-life performance meet the requirement?
- **Gate 4:** Can the glider successfully perform a test mission?

The Midterm report included a fifth go/no-go gate after the obtaining of certifications. However, since certifications are less significant in this mission than previously assumed, this is not considered a critical moment anymore.

An interesting addition to the diagram is the search for interest in other use cases. The EcoGlide system is currently designed with the military use case in mind. However, with few alterations, the EcoGlide could also be used in other situations. First, it could be checked whether or not the EcoGlide can perform the missions abandoned in the Baseline Report [25]. The mission profiles were abandoned to aid the design process and only aim at one goal, as this is much more manageable. This does not mean that the final product is incapable of performing these missions, and thus, checking whether or not this is possible could be the first step. The next step would be to search for other use cases not thought of before. As mentioned in chapter , the EcoGlide system provides a solution in a field where currently limited options are available. The EcoGlide thus has a relatively strong market position. Once the product is fully developed, other parties can be approached in a more effective manner; the capabilities and limitations of the product are even more defined at that stage.

17.2. Post-DSE Gantt chart

To further structure the design process after the DSE, another Gantt chart has been made. It includes the same tasks as the Project Design and Development Logic Diagram, and shows their assumed time to complete and dependencies. For ease of comparison, a similar colour scheme is used.

The structure of this Gantt chart is in many ways similar to the DSE Gantt chart presented in previous reports. However, there are of course also differences. The DSE Gantt chart was a living document, updated constantly. For this Gantt chart, that will not be possible (unless the project is continued after DSE). Another difference is the level of tasks

presented. In the DSE Gantt chart, tasks were divided until bitesize tasks remained, spanning only a couple of hours. The tasks in the Post-DSE Gantt chart are more high level and have work time in the order of weeks allocated to them. One limitation of this Gantt chart is the inability to show iterations. After DSE, iterations become more important for the design duration due to the presence of go/no-go gates and prototype tests. Despite being designed with the best intentions, the possibility exists that the glider will not pass these prototype tests and thus should be redesigned. This of course has a major impact on the planning. The workload and timespan presented in the Post-DSE Gantt chart (and also in the Project Design and Development Diagram) are therefore mere indications and not definitive.

Project Design & Development Logic Diagram

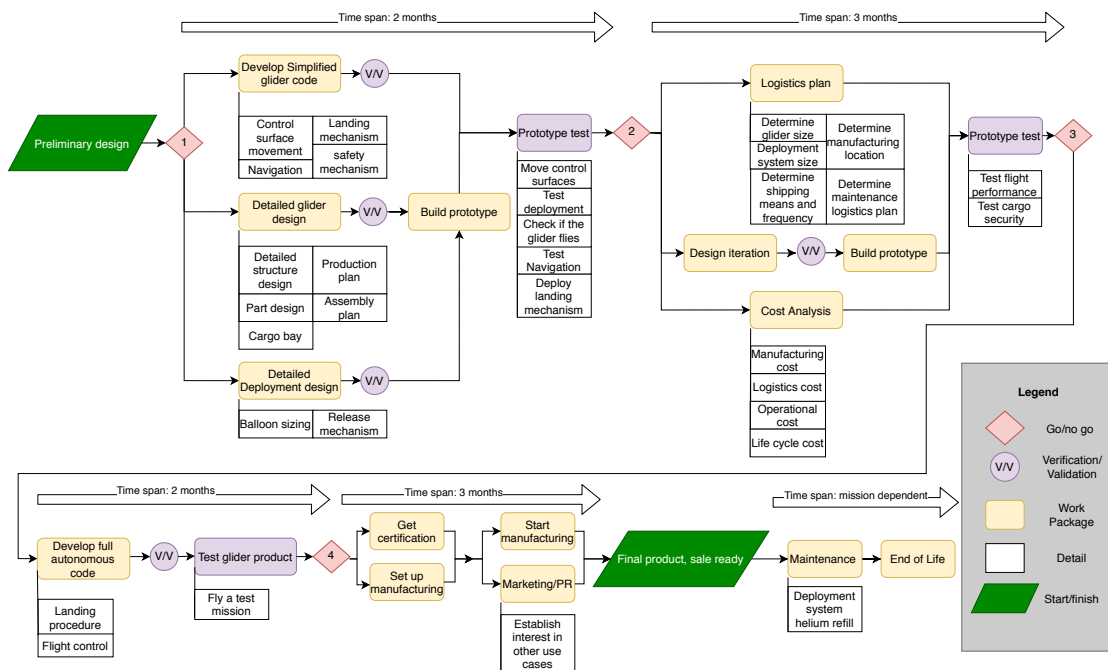
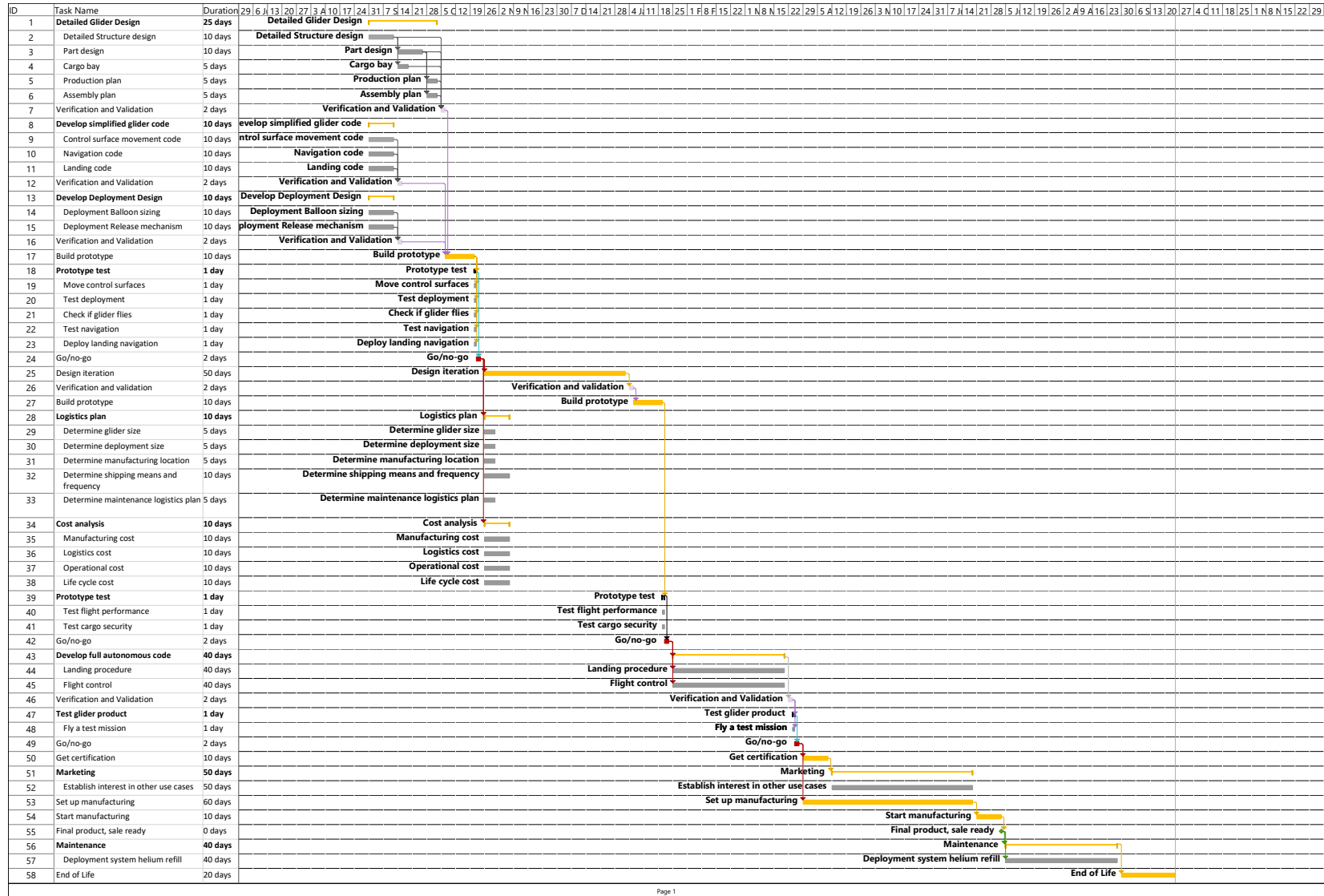


Figure 17.1: Project Design Development Logic Diagram



Conclusion & Recommendations

The EcoGlide design concepts, as chosen in the Midterm Report[26], were expanded in this report. This report will be the final report of the Design Synthesis Exercise and thus concludes this learning activity. Within this report, a preliminary design is presented for the blended wingbody glider configuration, the tethered balloon deployment system and the necessary operations and logistics.

The EcoGlide mission was designed for a specific use case as given by the Dutch military. In its mission, EcoGlide will offer a near-daily supply of up to 6 [L] of blood from the main hospital to a field hospital. By exploiting the capabilities of EcoGlide rather than the conventional on-ground supply chain of the military, the dangers of moving military personnel through an active combat zone can be avoided.

The design presented in this report provides a system capable of satisfying the needs and requirements of the mission as given above. Within this design, a trade-off between performance and simplicity had to be performed as the mission requires a high performance for a single-use glider. Although cost was not a driving design requirement initially, the project team was aware that a single-use product has to be cheap to be salable to potential customers.

To create a successful product, all different subsystems have to be fully integrated and up to requirements. This conclusion addresses compliance of the different subsystems with the requirements and recommendations for future development.

For aerodynamics & performance, an innovative approach for the stabilisation of a tailless glider was taken, with which the lifting capabilities of the wing could be improved to reach a high glide ratio. In this innovative approach, a stabilising body section was created that effectively generates no lift but provides a large stabilising contribution. To create such a body, the team created its own airfoil shape. The final aerodynamic design of the blended wingbody was analysed using XFLR5 and provided promising results. These results should, however, be validated in a future design step by performing test flights or wind tunnel experiments with a physical model.

For the structural design of the glider, it was challenging to find high-performance materials that are also biodegradable. Additionally, the use of these materials for an aerospace application had to be investigated as it was not done before. These materials were found to be suitable: plywood, paper pulp and PLA. The sizing of the structural elements was performed and a design with reasonable stresses and deformations could be created. The design of the ribs, which are integrated in the skin, was taken from an egg carton and resulted in a light yet strong design. This structural design should be tested in a future design stage to validate the load-bearing capabilities of the different components.

During the design of the guidance, navigation and control subsystem, it was chosen to use off-the-shelf components. This was done to lower cost and improve the reliability of the glider. The *PixHawk 4 Mini* running modified *PX4* code was chosen as the flight controller and 2 *ANNIMOS 25 [kg] RC Digital Servos* were chosen as actuators. An actuation mechanism for the two elevons was designed using biodegradable bamboo torque rods. Because the actuators and the control surfaces are so closely linked in terms of design, it was decided to design the elevons as part of the GNC. These elevons were sized to meet class I roll requirements and they were compared to other similar aircraft to validate the results. It is however recommended to perform extensive flight testing such that the entire GNC subsystem is verified and validated.

For the payload taken onboard the glider, a special container for the transportation of blood was designed. Two of these containers are placed in the glider. The main focus of the design was to create a casing that allows for maintaining the temperature of the payload while also shielding it from impact. The payload box is optimised for empty weight and made such that it is fully biodegradable, but it can also be reused multiple times. Preliminary validation provided promising results, however, it is still highly recommended to build a physical prototype to run additional validation tests.

The Electric Power system was sized for the power needs of the guidance, navigation and control electronics. The *ZIPPY Compact 2700 [mAh] 2S 25C Lipo Pack* battery was found sufficient for the energy provision of the full mission, including the time that the glider should be powered on, but is not flying. To ensure that the electronics receive their required 5.5 [V], the *Jeti Voltage Regulator SBEC 5-8V/12A* was found to be a good off-the-shelf component to regulate the power. It is however recommended to test these two electrical elements thoroughly, ensuring that the calculations performed in this report are correct.

The conceptual design of the deployment system resulted in a tethered balloon with a hoisting and launch mechanism as its payload. After multiple iterations of the preliminary sizing, a US Navy C-type shaped balloon was outlined. The C-type features a low lift and drag coefficient, which is desired for keeping the system lightweight and small. The tether

selected for the balloon is the *Saturn-12*, a *Dyneema SK78 High Modulus Polyethylene* rope. The tethered balloon was estimated to have a volume of 2760 [m³] and length of 37.6 [m]. It is capable to stay at its maximum altitude of 5000 [m] for an estimated 140 hours. Unfortunately, his design exceeds the size, weight, and above all cost expectations for the deployment method. Thus, alternative tethered balloon designs or even different deployment methods should be considered to reduce the price of the EcoGlide system.

The production and logistics of the EcoGlide system were designed to produce the glider's components off-site, i.e. in the Netherlands, at an EcoGlide plant. The production of these components will be executed by external suppliers. To maximise transport efficiency, the gliders are shipped in a kit form such that 64 gliders fit in one shipping container used by the military. This does, however, mean that the assembly of the system will have to occur on-site and needs to be executed by the military itself.

The main goal of carrying out the LCA was to determine the optimal method of disposal. Recycling was ruled as the optimal method of disposal as it had much lower emissions compared to incineration, 1.69 times lower. However, recycling was not deemed feasible by the military. Additionally, the conclusion drawn from the manufacturing LCA and the comparison with an existing, commercially used drone was that while the emissions were in an acceptable range, the energy demand has to be reduced. This high energy demand was created by the single-use nature of the product. A potential solution to reduce this energy demand is to increase the recycled content. Another solution could be to remove the bleaching step during the production of paper pulp. The removal of bleaching from the production does, however, have to be analysed in-depth in a future design phase to assess its influence on the mechanical properties of paper pulp. It is recommended for the life-cycle costing to first perform a comparative analysis after which an in-depth analysis of the glider's cost is executed. Additionally, it is required to find a more detailed estimate of labour cost required to manufacture the EcoGlide glider.

A RAMS analysis was performed to determine the reliability, availability, maintainability and safety of the EcoGlide system. It was found that the system is very likely to perform its mission as intended, needs little maintaining and is safe to use, both for people and for the environment. Finally, average availability of 80% could be reached based on wind data for the sample mission locations, Timbuktu and Kabul, which is in accordance with the requirement set by the principal tutor.

Although the design of EcoGlide was based on the military use case, the glider could be adapted to serve other market needs in the future through relatively minor adaptations. Potential future markets include humanitarian aid missions, search and rescue missions or the delivery of civilian cargo. This is currently limited to long term missions with repeated deployment due to the high initial cost of EcoGlide's deployment system. However, when other deployment methods become feasible from future studies, the glider also becomes interesting for single case missions.

Bibliography

- [1] Federal Aviation Administration. *Glider Flying Handbook*. Skyhorse Publishing, West 36th Street , New York, 2015.
- [2] European Aviation Safety Agency. Easy access rules for unmanned aircraft systems (regulations (eu) 2019/947 and (eu) 2019/945), March 2020.
- [3] European Environment Agency. *EEA Report No 21/2016 Part B 2.H.1 Pulp and paper industry 2016*. 2016.
- [4] Remei Aldrich Tomas. *Allocation of GHG emissions in a paper mill, an application tool to reduce emissions*. PhD thesis, Universitat de Girona, 2009.
- [5] Rahulan Thurai Alsahlan, Ahmad Abdulkarim. Aerofoil design for unmanned high-altitude aft-swept flying wings. 9(3), 09 2017.
- [6] *Storage and Handling of APA Trademarked Panels*. APA - The Engineering Wood Association, 2007. Form number U450E.
- [7] John J. Bertin and Russel M. Cummings. *Aerodynamics for Engineers*. Pearson, Edinburgh Gate , Essex, 2014.
- [8] R. Vos B.T.C. Zandbergen, J.A. Melkert. *AE1222-II: Aerospace Design Systems Engineering Elements I*. TU Delft, 2017.
- [9] Mustafa Cavcar. The international standard atmosphere (isa). *Anadolu University, Turkey*, 30(9):1–6, 2000.
- [10] CEN. Thermal bridges in building construction — linear thermal transmittance — simplified methods and default values (iso 14683:2007). 11 2017.
- [11] Russ C.Hibbeler. *Mechanics of Materials*. Pearson, Edinburgh Gate , Essex, 2014.
- [12] CIRRUS AIRCRAFT CORPORATION. Guide to the cirrus airframe parachute system (caps™), December 2013.
- [13] JARUS CS-LUAS. Recommendations for certification specification for light unmanned aeroplane systems, November 2016.
- [14] Sanquin bloodbank researcher D. de Korte. Online meeting with b. odinot.
- [15] Craig Damlo. Design Thinking for Aerospace Systems Innovations, April 2018.
- [16] Mattia Didone, Prateek Saxena, Ellen Brillhuis-Meijer, Guido Tosello, Giuliano Bissacco, Tim C McAloone, Daniela Cristina Antelmi Pigozzo, and Thomas J Howard. Moulded pulp manufacturing: Overview and prospects for the process technology. *Packaging Technology and Science*, 30(6):231–249, 2017.
- [17] F. Quagliotti E. Capello, G. Guglieri. A waypoint-based guidance algorithm for mini uavs. *IFAC Proceedings Volumes*, 46(30):120–125, 2013.
- [18] J.S.P. Peltola et al. Biodegradability and waste behavior of industrial wood-based construction materials. *Industrial Microbiology and Biotechnology*, March 2000.
- [19] R. Faragher. Understanding the basis of the kalman filter via a simple and intuitive derivation [lecture notes]. *IEEE Signal Processing Magazine*, 29(5):128–132, 2012.
- [20] R. Faragher et al. Understanding the basis of the kalman filter via a simple and intuitive derivation. *IEEE Signal processing magazine*, 29(5):128–132, 2012.
- [21] C A Featherston and C Ruiz. Buckling of flat plates under bending and shear. *Proceedings of the Institution of Mechanical Engineers, Part C: Journal of Mechanical Engineering Science*, 212(4):249–261, 1998. doi: 10.1177/095440629821200401.
- [22] Miguel A. Figliozzi. Lifecycle modeling and assessment of unmanned aerial vehicles (drones) co 2 e emissions. *Transportation Research Part D: Transport and Environment*, 57:251–261, 2017. doi: 10.1016/j.trd.2017.09.011.
- [23] Afval Energie Bedrijf Gemeente Amsterdam. Value from waste, the new standard for recovery of sustainable energy, metals and building materials from urban waste, March 2006.

- [24] M.S. Selig G.K. Ananda, P.P. Sukumar. Measured aerodynamic characteristics of wings at low reynolds numbers. *Aerospace Science and Technology*, 42(1):392–406, 2015.
- [25] G. den Butter A. Chatterjee V. Conings S. McGinley B. Odinet R. Smits D. Tóth D. van der Werff M. Verkammen J. Bertholdt, J. Bourgois. EcoGlide Baseline Report, May 2020.
- [26] G. den Butter A. Chatterjee V. Conings S. McGinley B. Odinet R. Smits D. Tóth D. van der Werff M. Verkammen J. Bertholdt, J. Bourgois. EcoGlide Midterm Report, May 2020.
- [27] Staff officer life sciences RNLA at Ministry of Defence Jack Koning. Online meeting with r. smits.
- [28] John D. Anderson Jr. *Introduction to flight*. McGraw-Hill Education, McGraw-Hill Education, 2 Penn Plaza, New York, NY10121, United States, 2016.
- [29] John D. Anderson Jr. *Fundamentals of aerodynamics*. McGraw-Hill Education, Penn Plaza, New York, 2017.
- [30] Inokuchi Y. Suzuki Y. et al. Kubojima, Y. Shear modulus of several kinds of japanese bamboo obtained by flexural vibration test. 56:64–70, 09 2010.
- [31] Masaaki Kurosu and Kaori Kashimura. Apparent usability vs. inherent usability experimental analysis on the determinants of the apparent usability. 2:292–293, 01 1995.
- [32] Lizi Li, Sanghoon Lee, Hak Lae Lee, and Hye Youn. Hydrogen peroxide bleaching of hardwood kraft pulp with adsorbed birch xylan and its effect on paper properties. *BioResources*, 6, 02 2011.
- [33] Dawei Vijn Aarohi Limpinsel, Moritz Kuo. SMARTS Modeling of Solar Spectra at Stratospheric Altitude and Influence on Performance of Selected III-V Solar Cells., November 2018.
- [34] J. S. Segmehl K. Casdorff T. Keplinger I. Burgert M. Frey, D. Widner. Delignified and densified cellulose bulk materials with excellent tensile properties for sustainable engineering, 2018.
- [35] James A. Menke. High-altitude tethered balloon systems study. *Goodyear Aerospace Corporation*, May 1967.
- [36] Philip F. Myers. *Tethered Balloon Handbook*. Goodyear Aerospace Corporation, Akron, Ohio, 1968.
- [37] Detlev Möller. *Chemistry for Environmental Scientists*. Walter de Gruyter GmbH Co KG, 2015.
- [38] NSAI. Building components and building elements - thermal resistance and thermal transmittance- calculation methods (iso 6946:2017). 07 2017.
- [39] Natural Resources Canada: Office of Energy Efficiency. *Energy cost reduction in the pulp and paper industry: an energy benchmarking perspective*. 2004.
- [40] Norwegian University of Science and Technology. System safety, July 2019.
- [41] Dr. F. Oliviero. *Aerospace Design and Systems Engineering Elements II*. TU Delft, 2018.
- [42] W. Pointner, G. Kotsis, P. Langthaler, and M. Naderhirn. Using formal methods to verify safe deep stall landing of a mav. In *2011 IEEE/AIAA 30th Digital Avionics Systems Conference*, pages 5D1–1–5D1–10, 2011.
- [43] Maureen Puettmann, Woodlife Environmental Consultants, and Elaine Oneil. Cradle to gate life cycle assessment of softwood plywood production from the southeast, 2012.
- [44] Raymond C. Rietz. *Storage of Lumber*. U.S. Department of Agriculture, Washington, D.C., 1978.
- [45] Dr. Jan Roskam. *Airplane Design*. DAR corporation, Lawrence, Kansas, 2003.
- [46] Ger J.J. Ruijgrok. *Elements of airplane performance*. Delft Academic Press, Leeghwaterstraat 42, Delft, 2 edition, 2009.
- [47] Mohammad H. Sadraey. *Aircraft Design - A Systems Engineering Approach*. John Wiley Sons, John Wiley Sons Ltd, The Atrium, Southern Gate, Chichester, West Sussex, PO19 8SQ, United Kingdom, 2013.
- [48] M. Nita J. Scholz. *Estimating the Oswald factor from basic aircraft geometrical properties*. Hamburg University of Applied Sciences, Berliner Tor, Hamburg, 2012.
- [49] Samuel Tabor, Iain Guilliard, and Andrey Kolobov. Arduoar: an open-source thermalling controller for resource-constrained autopilots, October 2018.
- [50] H. Taniguchi. Analysis of deepstall landing for uav. 2008.

- [51] E. Torenbeek. *Synthesis of Subsonic Airplane Design*. Delft University Press, Mijnbouwplein, Delft, 1982.
- [52] E. Trinklein and G. Parker. Combining multiple gps receivers to enhance relative distance measurements. pages 33–37, 2013.
- [53] Janice Trotter. *Standard conditioning and testing atmospheres for paper, board, pulp handsheets, and related products*. Technical Association of the Pulp and Paper Industry, April 2013. Draft No. 2.
- [54] u blox. Neo-m8 series product summary, January 2018.
- [55] Kos A. Umek, A. Validation of smartphone gyroscopes for mobile biofeedback applications. *Personal and Ubiquitous Computing volume*, 2016.
- [56] Joseph Robert Vanstrom. Mechanical characterization of commercial biodegradable plastic films. page 91, 01 2012.
- [57] Zero waste Europe. The impact of waste-to-energy incineration on climate, September 2019.